1984

The Effects of Steel Fibers on the Plastic Rotation Capacity and Properties of Reinforced Concrete Continuous Beams

Khani Sahebjam

THE EFFECT OF STEEL FIBERS ON THE PLASTIC ROTATION CAPACITY AND PROPERTIES OF REINFORCED CONCRETE CONTINUOUS BEAMS

by

KHANI SAHEBJAM

A thesis submitted
in partial fulfillment of the requirements for the
degree Master of Science
Major in Civil Engineering

South Dakota State University
1984

THE EFFECT OF STEEL FIBERS ON THE PLASTIC ROTATION CAPACITY AND PROPERTIES OF REINFORCED CONCRETE CONTINUOUS BEAMS

This thesis is approved as a creditable and independent investigation by a candidate for the degree, Master of Science, and is acceptable for meeting the thesis requirements for this degree. Acceptance of this thesis does not imply that the conclusions reached by the candidate are necessarily the conclusions of the major department.

Dr. M. Nadim Hassoun
Major Advisor

Date

Dr. Dwayne A. Rollag
Head, Civil Engineering Department

Date

DEDICATIONS

I wish to dedicate this thesis to my mother for her support, and to my wife, Barb for her continual encouragement, assistance and patience throughout this study.

ACKNOWLEDGMENTS

The author would like to express sincere appreciation to Dr. M. Nadim Hassoun for his assistance and guidance throughout the course of this study.

Acknowledgments are extended to Dr. Dwayne A. Rollag, Head of the Civil Engineering Department for his encouragement and support, Dr. Robert J. Lacher for his assistance with the statistical analysis of the data, Cheryl Havrevold for expertly typing the totality of this thesis, and to Thomas A. Biggar, Laboratory Technician, for his help in fabricating the forms and constructing the necessary laboratory equipment.

Special thanks to the faculty and students for their suggestions and assistance during testing.

TABLE OF CONTENTS

LIST OF TABLES

Tables | Page

Tables Page

Tables Page

APPENDIX B

Tables Page

APPENDIX C

LIST OF FIGURES

NOTATIONS

A	Cross section of standard cylinder
A_c	The effective tension area of concrete around the main reinforcing (having the same reinforcement centroid, divided by the number of bars)
A_s	Area of main steel
ASTM	American Society for Testing Materials
A_v	Cross section area of one stirrup
a	$\frac{A_s f_y}{0.85 f_c' b}$
a_1, a_2	The length over which curvature is measured at middle support
b	width of the beams
C	Compression force on a concrete compression block
c	Distance from extreme compression fiber to neutral axis
D	Diameter of standard cylinder
d	Effective depth of the beams
d_c	The cover of the outermost bar measured from the steel centroid
d_f	Diameter of steel fiber
E_c	Modulus of elasticity of concrete = $w^{1.5}\ 33\sqrt{f_c'}$
E_{ca}	Actual modulus of elasticity from testing
E_{cc}	Calculated modulus of elasticity of fibrous concrete
E_s	Modulus of elasticity of steel = 29,000,000 psi
f	flexure stress = $\frac{Mc}{I}$
f_c	Concrete stresses at working load
f_{ct}	Split cylinder strength = $6.7\sqrt{f_c'}$

f_{cta}	Actual split cylinder strength
f_{cs}	Split cylinder strength of fibrous concrete $= (6.7 + 2.3\ \rho_s)\ \sqrt{f_c'}$
f_c'	Compressive strength of concrete for standard size cylinders
f_r	Modulus of rupture of concrete $= 7.5\sqrt{f_c'}$
f_{rl}	First modulus of rupture of fibrous concrete $= (7.5 + 2.6\ \rho_s)\ \sqrt{f_c'}$
f_{ru}	Ultimate modulus of rupture of fibrous concrete $= (7.5 + 4.35\ \rho_s)\ \sqrt{f_c'}$
f_s	Steel stress
f_y	Yield strength of steel reinforcement
H_L	Plastic hinge length
h	Total height of the section
I	Moment of inertia
I_{cr}	Moment of inertia of a cracted section transformed to concrete
I'_{cr}	Moment of inertia of a cracked fibrous concrete section
I_e	Effective moment of inertia for plain concrete
I_c'	Effective moment of inertia for fibrous concrete
I_g	gross moment of inertia of the section neglecting the steel
j	$1 - \frac{K}{3}$
K	Ratio of the depth of the neutral axis measured from the extreme compressive fibers to the effective depth
K_u	K at ultimate load
K_1	K at limit state 1
k	$(1 + 0.5\ \rho_s)$
k_1	$(1 + 0.35\ \rho_s)$

k_2	$(1 + 0.58\ \rho_s)$
kips	Kilo pounds (1000 pounds)
L	Span length or length of the cylinders
L_f	Length of steel fibers
L_1	Limit state when steel yields
l_d	Development length
M	Moment
M_a	Moment at service load at midspan
M_A, M_B	Plastic moments at A and B
M_{AF}, M_{BF}	Fixed end moment at A and B
M_{cr}	Cracking moment
M_p	Plastic Moment
M_u	Ultimate moment capacity of a section
M_{y1}	Yield moment at section 1
M_{y2}	Yield moment at section 2
M_1	Moment at stage L_1
m	$1 - 0.23\ \rho_s$
n	Modular ratio = E_s/E_c
P	Applied load
P_c'	Actual load at collapse
P_u	Ultimate load
P_y	Yield load
P_{y1}	Yield load of section 1
P_{y2}	Yield load of section 2

P_y'	Actual yield load
P_u'	Actual ultimate load
psi	Pounds per square inch
pcf	Pounds per cubic foot
R	Radius of curvature
r	Load redistribution factor P_u/P_y
r'	Experimental load redistribution factor P_u'/P_y'
S_{min}	Minimum distance between stirrups
S.F.	Steel Fiber
T	Tension force in main steel reinforcement
V_u	Maximum shearing force
v_c	Concrete shear strength $2\sqrt{f_c'}$
v_s	Shear stress taken by stirrups
v_u	Ultimate shear stress $\frac{V_u}{b.d}$
w	Unit weight of concrete
W	Maximum crack width
W_E	External work
W_I	Internal work
w/c	Water cement ratio
X	The distance from the load to outside supports
y_t	Distance from centroidal axis of gross section to extreme fiber in tension
Z	The distance from point of zero moment to the middle support
z	$f_s\sqrt[3]{A_c d_c}$
α	$1.06 + 0.13\ \rho\rho_s$

β	Curvature distribution factor
β_1	A factor equal to 0.85 for $f_c' \leq 4000$ psi which decreases by 0.05 for every increase in strength of 1000 psi
β_h	Ratio of the distance to the neutral axis from the extreme tension concrete fiber, to the distance from the neutral axis to the centroid of the tensile steel
Δa_1	Change in length a_1 due to rotation
Δa_2	Change in length a_2 due to rotation
ΔL	Axial deformation
Δ	Deflection at assumed service load
Δ_p	Plastic deflection
ε	Strain $\frac{\Delta L}{L}$
ε_c	Concrete strain
ε_s	Steel strain
ε_p	Plastic strain = $\varepsilon_{cu} - \varepsilon_{cy}$
ε_{cu}	Ultimate concrete strain
ε_{cy}	Concrete strain when steel yields
ε_{c1}	Concrete strain at limit state L_1
ε_{s1}	Steel strain at limit state L_1 (yield strain of steel)
σ	Stress = $\frac{\text{load}}{\text{area}}$
ρ	Tension steel percentage = $\frac{A_s}{bd} \times 100$
ρ_b	Main steel percentage for a balanced section
ρ_s	Percentage of steel fibers
ρ_{max}	0.75 ρ_b
ρ_{min}	Minimum steel percentage in section

γ	$(1.27 + 0.38\ \rho + 5.42\ \rho\rho_s)$
ϕ	Curvature $\frac{\varepsilon_d}{Kd}$
ϕ_e	Elastic curvature
ϕ_p	Plastic curvature
ϕ_u	Ultimate curvature
ϕ_y	Curvature at yield
μ	$\frac{\phi_u}{\phi_y}$ ductility index
μ'	Ductility index for fibrous concrete $(1 + 3.1\ \rho_s)\ \mu$
θ	Rotation
θ_e	Elastic rotation
θ_p	Plastic rotation
θ_{pu}	Plastic rotation at failure
θ_{pl}	$\frac{\varepsilon_{cu}}{K_u} - \frac{f_y}{E_s(1-K_u)}$
θ_{pc}	Angle of the tangent drawn to the middle support at failure
λ	$(1 + 0.14\ \rho_s)$

CHAPTER I

INTRODUCTION

1.1 A General Overview

During the development of structural engineering, many ideas and concepts were considered and tested. A great deal of research has been done on reinforced concrete, which plays a significant role in current structural construction. Over the past decades there has been a competition between concrete and steel structures. Both concrete and steel structures have some advantages and disadvantages. Obviously, depending on the type of structure, choosing the right alternative is important.

Reinforced concrete structures, unlike steel structures, tend to fail in a relatively brittle manner because the deformation capacity of reinforced concrete is limited. When dynamic loadings are involved, concrete structures are not suitable because they cannot absorb strain energy as efficiently as steel.[20] Structural steel has the ability to take a great deal of inelastic rotation at the so-called "plastic-hinges" where the highest moment is applied. This occurs because of the strain-hardening effect of steel that takes place long after the yield strength of steel is reached.

There is a very important difference in the plastic design of steel structures and reinforced concrete structures. In steel structures the most important consideration is that the structure is able to develop enough plastic hinges to create a mechanism in the

structures to cause a collapse. There is little attention paid to the strains developed in the critical sections during the redistribution of moments. The reason for this is that steel has a significantly high strain energy absorption capacity and is able to take the inelastic deformation. On the other hand, the strains in reinforced concrete are far less than those in the regular mild steel; therefore, it is possible that the strain capacity of reinforced concrete plastic hinges reaches its maximum value before full redistribution of moments. If reinforced concrete is capable of absorbing the strain energy at the critical sections, and is able to undergo considerable deformation without a reduction in its load carrying capacity, sudden and catastrophic failures can be avoided.[20]

1.2 Concept of Limit-State Design

Concrete is a complex and heterogeneous material. In the past, the theory of reinforced concrete design has been influenced by a philosophy of design associated with steel structures. The theories for the behavior of reinforced concrete, in which it was considered as a combination of two elastic materials, have proven to be inadequate.[6] When a reinforced concrete structural member is loaded in low stresses it behaves very nearly elastically. When loads are increased to higher stages it is far from an elastically linear stress-strain relationship. This is caused by the spread of small microcracks that result in internal displacements which are nonrecoverable.[6] Because of these complexities and the differing

test results on the strength and deformation of reinforced concrete, it is beneficial to establish simple, reliable and realistic methods and calculations for the design of concrete structures.

It was A. L. L. Baker's[6] idea that, "Although generally given permissible values for working load conditions, but actually had fictitious values based on the results of tests to determine the ultimate resistance of reinforced concrete member". The theory of elasticity often gave different results than the actual stresses that developed in structures imply because of the inelastic effects that influenced the stress distribution.

Plastic design, or the so called limit-state design of concrete, is the most realistic method used because it considers the ultimate resistance of the constituent materials. The structure is designed on the basis of its ultimate strength or limit-states; in other words, a limit-state may be defined as "a condition of a structure at which it ceases to function in the manner for which it was designed".[6]

1.3 Inelastic Behavior of Reinforced Concrete

When a reinforced concrete structure is subjected to an earthquake or to blast loading, its ability to deform inelastically together with its ability to carry load is important.[11] Sufficient ductility is required at the critical sections for the redistribution of the internal moments in order to have a flexible or

ductile collapse. In an under-reinforced section, after the steel has yielded, the compression side of that section has to be able to take enough rotation in order to reach a mechanism and develop the ultimate load capacity of the structure. In the limit-design method of reinforced concrete structures, the distribution of moments at failure when a mechanism occurs are different than the distribution of the elastic moments at working loads. This is because of the moment redistribution. The limit design method is a correct method, if the following conditions are satisfied:

1) mechanism condition: Sufficient plastic hinges must be formed to develop a mechanism in the whole or part of the structure.
2) limit equilibrium condition: The bending moment distribution must be in equilibrium with the applied loads.
3) yield condition: The plastic or the ultimate moment can not be exceeded at any part of the structure.
4) rotation compatibility condition: There has to be sufficient inelastic rotation capacity at the plastic hinges to allow the structure to develop a mechanism.

To prevent a brittle failure of reinforced concrete, it must have a high ultimate strain capacity. When concrete has a low ultimate strain, plastic hinge rotations depending primarily on concrete compression are small. In critical cases, this reduces the degree of moment redistribution unless the ultimate strain can be increased.[15]

The ultimate compressive strain of concrete can be increased simply by adding secondary steel reinforcement in the concrete member. Research has been done on this idea and positive results have been obtained. Researchers[11,13,17] have concluded that the addition of secondary steel, in addition to the main reinforcement, adds sufficient ductility to concrete in order to develop its required plastic rotation. Secondary steel is considered to be double reinforcement, closely spaced binding (stirrups), and fibers, etc. Secondary reinforcement has appreciable effect on ductility in over-reinforced members.[40] Under-reinforced members appear to have more ability to rotate than the balanced or over-reinforced concrete members.[9,15,40] Stirrups and steel fibers increase the ductility of concrete; therefore, they increase the compressive strain by reducing the internal crack growth.[40]

1.4 Definition of Steel Fibers and Fibrous Concrete

Steel fibers are small and thin materials that have different standard sizes and shapes. They can be straight, hooked at the ends, or deformed. Steel fibers are specified by their aspect ration, which is the ratio of their length to diameter (L_f/d_f).

Fibrous concrete is a composite material consisting of concrete matrix and steel fibers. Steel fibers are added to the wet concrete mix, and it is porportioned to the concrete on the basis of volume percentage; it normally varies from 0% - 1.5% of concrete volume. The main purpose behind the addition of steel fibers is

the improvement found in ductility and crack arrest. After the fibrous concrete has cracked, the steel fibers will have the characteristics of tensile steel and take the tensile forces.

1.5 Historical Background

The subject of limit design of concrete is relatively new. Through the past 3-4 decades it has been preferred over the so-called classical elastic theory. The turning point occured in the 1940's when Professor A. L. L. Baker, Professor of Concrete Structures and Technology at the Imperial College of Science and Technology in London, developed the idea of inelastic behavior of reinforced concrete. Professor Baker proved by theory and experimental work that reinforced concrete, especially under-reinforced concrete, could be a very ductile material. Baker showed that under-reinforced concrete could withstand additional loads and deformation after the yield point of the main reinforcement was reached.

Many researchers have realized the efficiency and importance of plastic analysis in reinforced concrete. Since the 1950's there has been research done on inelastic behavior of reinforced concrete in England, Germany, France, Canada, U.S. and India.

In 1955, W. W. L. Chan[15] concluded that lateral binding increases the rotation capability of reinforced concrete. Chan also concluded that under-reinforced sections develop high ductility and plastic rotations.

M. Z. Cohn[17], in 1963, established a test program on redundant reinforced concrete beams and concluded that as long as the main steel percentage (ρ) is less than 2 and the distribution factor P_u/P_y does not exceed 1.6, full moment redistribution can be obtained. In 1980, Kauskik, Ramamurthy[27] and Kokeuja[27] had the same result concerning percentage of main steel to be less than 2% at critical hinges. They also mention that if the ratio of test and calculated ultimate loads is greater than 1.25 enough moment redistribution will occur in order to achieve a desirable collapse.

Alan Mattock, in 1964,[33] concluded that the compressive strain of concrete is much greater than the theoretical value of .003. Therefore, the ultimate curvature can also be much greater than the value calculated by assuming .003 for compressive strain; as a result of this, the inelastic rotation occuring in the hinging region at maximum moment is considerably greater than might be expected. The British Code CP110[13] suggests a value of 0.0035 for the crushing strain of concrete. Bishara, Londot, Au and Sastry[12] concluded in 1979 that the plastic rotations calculated were very close to the measured values. But, there are many tedious calculations and assumptions involved with rotation capacity. Many researchers have concluded that these calculations are not necessary. Beckett, in 1967,[9] mentions the difficulty of the rotation calculation and the controversy that exists.

In 1975, the importance of confining the compression zone of concrete was proven in a test program designed by Desayi, Iyengar

and Reddy,[20] and the result was as expected; the ductility of a confined compression zone is considerably greater than unconfined members.

A very important part of limit-state design is the calculation of the plastic hinge length. It is usually drawn and analyzed as if it was a point, but actually it develops over a finite length that can be measured and also calculated. A. L. L. Baker[6] recommended a safe value equal to the effective depth d, which many researchers have used and agreed upon. In 1955, Chan[15] concluded that in a uniformly distributed loading in continuous beams, the plastic hinge length does not exceed one tenth of the clear span (L/10). He also mentioned in 1962,[14] that the hinge length could range from about 0.40d to 2.4d on a general basis. The Institution of Civil Engineering research committee (ICE)[26] recommended a widely used equation to calculate H_L. $H_L = K_1 K_2 K_3 (Z/d)^{1/4} (d)$

where: $K_1 = 0.7$ mild steel

$K_1 = 0.9$ coldworked steel

$K_2 = 1$ influence of axial load

$K_3 = 0.6$ $f_c' = 6$ Ksi

$K_3 = 0.75$ $f_c' = 4$ Ksi

$K_3 = 0.9$ $f_c' = 2$ Ksi

Z = distance from critical section to point of contraflexure.

Wright and Berwanger[51], in 1960, also recommended a hinge length equal to the effective depth, (H_L=d). In 1962, Berwanger[10]

stated that in a case of elastic-strain hardening materials like reinforced concrete the hinge length can be determined from the moment diagram at the actual ultimate load, when M_u of the critical section has been reached. The hinge forms at midspan M_Y and sections with greater moments than M_Y. He also said that this length is normally greater than the effective depth, and therefore, the required rotation is less when H_L=d is assumed.

In 1963, Cohn and Petca[17] came up with a value ranging from .30d to 0.9d, which is a safe and conservative value that reduces the required rotation leading to a safer safety factor. They also recommend a value of .5 to .6 for β the shape factor or curvature distribution factor. The preceding research was conducted on plain reinforced concrete, and no investigation was done on the inelastic behavior of fibrous concrete.

The effects of steel fiber on reinforced concrete properties and behavior has been tested and analyzed in past years. These effects will be divided into different categories as follows:

A. Compressive strength of fibrous concrete

The effect of steel fibers on the compressive strength of concrete has been tested by many researchers during the past two decades. In June, 1979, Halvorsen and Kesler[22] concluded that the compressive strength remains practically unchanged by fiber content or even the type of fibers. Swamy,[48] in 1982, reported that compressive strength of fibrous concrete increased by only 12-15%. Jitrendra-Anil[28]

in 1972, also concluded that compressive strength increase of fibrous concrete was not appreciable.

B. Deflection

Deflection control is a very important aspect of concrete structures because high deflections in concrete structures at service loads could lead to large cracks and other problems which have to be controlled. Therefore, researchers tried to test the effect of fibers on the deflections of concrete structural members. In 1975, Swamy, Alnoori[48] concluded that at maximum load, deflection of fibrous concrete is twice as much as in the plain concrete beams. Swamy[49] also states, in a paper in 1979, that the fibers increase the stiffness of the beam and consequently, reduce the deflections at working load. In 1982, a research experiment on the effect of steel fibers on concrete,[34] concluded that beams containing steel fibers are very effective in resisting deflections in all stages of loading. The most effective results were obtained when lower percent of main steel was used.

C. Strains and ductility

Ductility, an important issue in design of reinforced concrete, has been considered and tested in previous research. Steel fibers have proven to be very effective in increasing concrete ductility. In August, 1979, Swamy reported that steel reinforcement with yield stress of 88 Ksi can be used

in fibrous concrete, and such beams control both cracks and deflections. More importantly, this improves plastic deformation appreciably at failure. In September, 1981, Swamy-AlTaan[47] showed that the presence of fibers allows the use of high strength steel bars up to 100 Ksi, so crack widths and deflections can be controlled. Concrete is known to have an ultimate strain of around 0.003-0.0035, which is used in theoretical computations. This could be unsatisfactory in some cases where high inelastic deformation is required. Tests[49] have shown that concrete strains on the compressive face of the beams at loads prior to failure varied from 5240 to 6620 x 10^{-6} (in/in) for beams reinforced with steel fibers. This shows that the ultimate strains could be almost doubled by the use of steel fibers.

D. Stiffness (flexural rigidity)

Stiffness or flexural rigidity is probably one of the most controversial and important issues surrounding reinforced concrete. The reason for that being the variable effective moment of inertia (I_e) . During the stages of loading the moment of inertia of the member is not constant, and it varies from one section to the other. Therefore, an average value is used for I_e which is adopted by the ACI Code. Inclusion of steel fibers increases the flexural rigidity and decreases the deflections of the structural member.[50]

1.6 Applications of Steel Fiber

The use of steel fibers in actual construction is limited because it is not well known among contractors, and it is also a fairly new concept being introduced to the world of reinforced concrete. Recent extensive research proves the superiority of fibrous concrete over plain concrete. This has encouraged engineers and contractors to use steel fibers. Steel fibers are used for different projects and purposes.

1) Bridges and deck overlays: for better performance and repair.
2) Highways, streets and airport runways: where impact loads are significant, steel fibers help the fatigue life and ductility of the overlays. Another advantage is that it could be poured in thin sections which would be economical.
3) Pipes: the benefit of using thinner pipes with increasing strength on the outside edges for protection against accidents during handling is appreciable.
4) Industrial floors: by reducing the amount of concrete used and increasing allowable working stresses and reduction in maintenance and repair costs. (35)
5) Structural units: the advantages in this application includes reduction in thickness of deck slabs, therefore, reducing the weight and ease of handling and increasing crack resistance and ductility at failure along with higher load capacity. (35)

1.7 Objective and Scope of Investigation

The main objective of this experimental investigation is to study the effect of steel fibers on the plastic rotation of reinforced concrete in continuous beams. This research also studies the effect of steel fibers on the behavior and some of the properties of reinforced concrete. The emphasis will mainly be on: the modulus of elasticity, effective moment of inertia, deflections, crack width and distribution, compressive strength, ductility, tensile strength, (modulus of rupture test and split cylinder test).

For the purpose of this research, ten beams with different main reinforcement and percentage of steel fibers will be made. The effect of the variables (main steel and % steel fibers) on the length of the plastic hinge, curvature distribution factor, ductility and plastic rotation capacity of reinforced conrete will be closely analyzed. In addition, concrete cylinders will be used to determine the tensile strength, compressive strength and modulus of elasticity of plain and fibrous concrete.

CHAPTER II

ROTATION CAPACITY OF REINFORCED CONCRETE

2.1 Rotation Capacity

The calculation of rotation capacity of reinforced concrete has proven to be very tedious and complex. There are some reasonable assumptions made in order to get satisfactory results that could be compared to the actual rotations. In general, rotation is the integral of curvature. The curvature can be evaluated at any stage of loading and be integrated over a finite length to give the rotation occured over a desired length (more on curvature later in this chapter).

The total rotation up to failure that occurs at a critical section consists of two major parts.

1) Elastic rotation "θ_e" which is the rotation up to first yield of main reinforcement.
2) Plastic rotation "θ_p" from first yield up to failure. The plastic rotation θ_p is a much larger amount compared to elastic rotation θ_e simply because the section is not taking any extra moment, and therefore, the low restraint causes excessive rotation. The calculation of elastic rotation could be performed without any problem. The elastic rotation at a support can be evaluated at any stage from the following equation:

$$\theta_e = \phi_e \cdot \ell \qquad (2.1)$$

where ϕ_e = is the elastic curvature $(\frac{M}{EI})$ or $\frac{\varepsilon_c}{Kd}$ (Figure 2.1)

ℓ = desired length

ε_c = concrete strain

Kd = distance from neutral axis to extreme compression fiber

EI = flexural rigidity assumed constant throughout the elastic range.

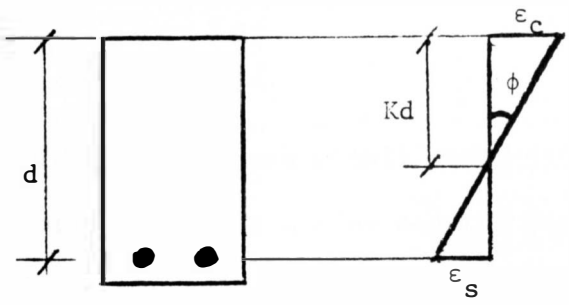

Figure 2.1
Strain-Curvature relationship

The plastic rotation θ_p can be expressed as the total rotation accumulated along a short region (H_L), which is the plastic hinge length (more on hinge length later in this chapter). Equation (2.2) shows a general form of this value.

$$\theta_p = \int_o^{H_L} (\phi_u - \phi_y)\, d\ell = \phi_p . H_L \qquad (2.2)$$

where ϕ_u = ultimate curvature

ϕ_y = curvature at yield

ϕ_p = plastic curvature (figure 2.10)

The plastic rotation is equal to the dashed area in figure (2.10) and as it is apparent this value is not exact because the

curvature is not constant along the hinge. In some literature[17,18] the value of $\phi_p.H_L$ is multiplied by a shape factor or curvature distribution factor (β).

Therefore equation (2.2) becomes:

$$\theta_p = \beta(\phi_u-\phi_y)\ H_L = \beta.\phi_p.H_L \qquad (2.3)$$

This distribution factor "β" accepts an average constant value of the curvature instead of the actual distribution along the plastic hinge and can be calculated from experimental values of ϕ_p, H_L, θ_p.

$$\beta = \frac{\theta_p}{\phi_p.H_L} \qquad (2.4)$$

In order to have a full redistribution of the forces, the actual rotation should not exceed the rotation capacity of the section. Also, the calculated rotation capacity or the provided rotation capacity of the section has to be higher than the required rotation of plastic hinges. The required rotation for a plastic hinge in an indeterminate structure to allow other plastic hinges to develop, and the structure to reach a mechanism can be calculated as follows:[24]

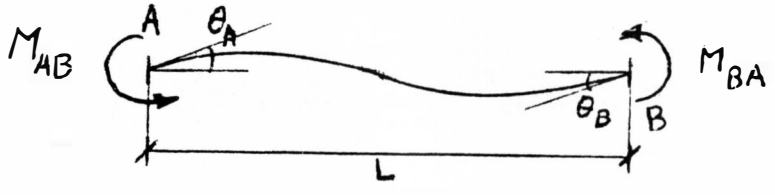

Figure (2.2)

$$\theta_{AB} = \frac{L}{6EI}\ [2(M_A-M_{AF})+(M_B-M_{BF})] \qquad (2.5)$$

where M_A, M_B = plastic moments at A and B respectively

M_{AF}, M_{BF} = fixed end moments at A and B as calculated by the elastic theory.

E = modulus of elasticity of concrete.

I = moment of inertia of a cracked section

$= \frac{1}{3} b(Kd)^3 + n A_s (d-Kd)^2$

$n = \frac{E_s}{E_c}$ = modular ratio

Kd = distance from the compressive fibers to the neutral axis

Equation (2.5) is the elastic slope-deflection method which is used to calculate the rotation or change of slope at a support with the existing moments. If an estimated numerical value of the rotation capacity is desired, it can be obtained as follows:[6,24]

angle of plastic rotation $\theta_{pl} = \phi_p . H_L$

$\phi_p = \frac{\varepsilon_p}{K_u . d}$ and $\theta_{pl} = \frac{\varepsilon_p H_L}{K_u . d}$

assuming $H_L = d$ then $\theta_{pl} \simeq \frac{\varepsilon_p}{k_u} = \frac{\varepsilon_{cu} - \varepsilon_{cy}}{k_u}$

$\varepsilon_{cy} = \varepsilon_{sy} \frac{k_u}{1-k_u} = \frac{f_y}{E_s} \cdot \frac{k_u}{(1-k_u)}$ from fig (2.3)

Therefore: $\theta_{pl} = \frac{\varepsilon_{cu}}{k_u} - \frac{f_y}{E_s(1-k_u)}$ (2.6)

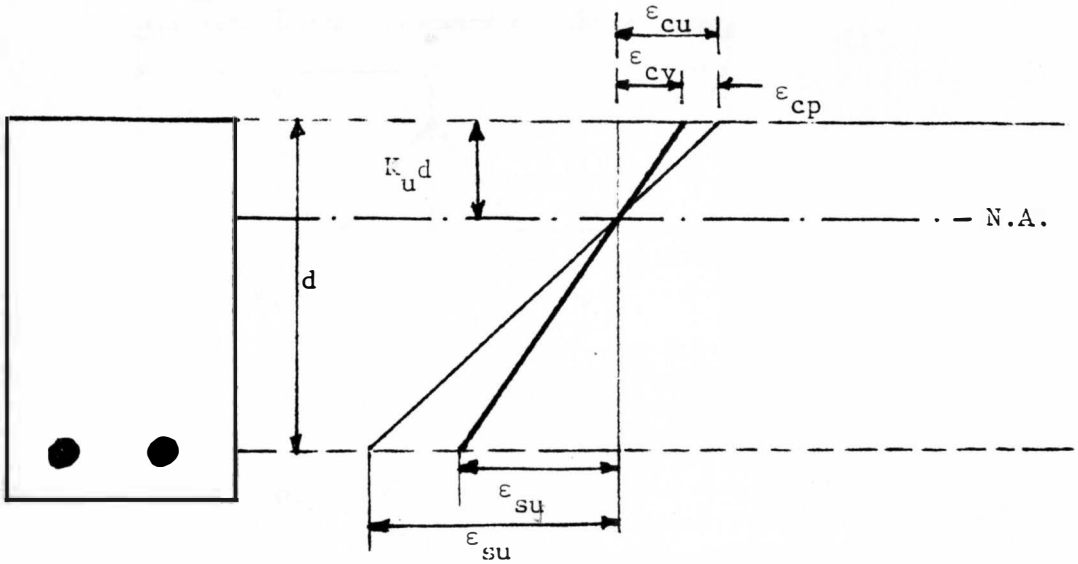

Figure 2.3 Ultimate Strain Diagram

The preceding value of θ_{pl} has to be greater than the required rotation obtained by equation (2.5) and the actual rotation should not have to exceed the rotation capacity of the section. If extra rotations are required, the ultimate strain capacity of concrete has to be improved by adding secondary reinforcement.

2.2 Rotation Compatibility

The rotation compatibility of reinforced concrete can be best analyzed in an indeterminate structure where a complete moment redistribution should take place before the complete collapse of the structure. Consider the two span, continuous beam of figure (2.4).

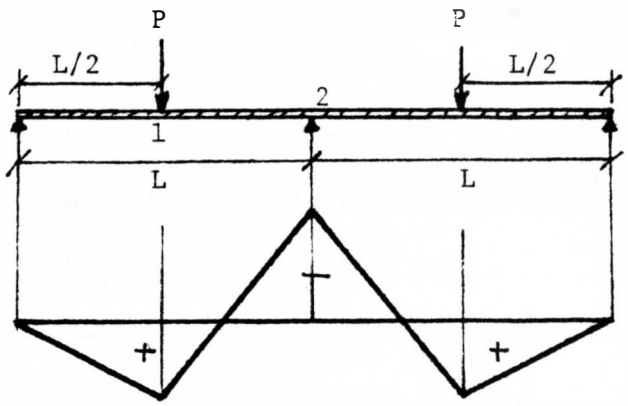

Figure 2.4 Continuous beam

The beam is loaded with two concentrated loads at midspans. As the load is applied, the negative moment that develops at section (2) is higher than the positive moment that develops at section (1) and consequently, higher stresses are applied at section (2). Figure (2.5.1) shows a completely elastic behavior. As the load is increased the yield moment of section (2) will be reached (My_2) and the corresponding load is (Py_2). From this point on, section (2) is in a plastic zone and this section undergoes excessive deformation under nearly constant moment Mp. Thus Mp is higher than My_2 and less than Mu_2 the ultimate moment of the section. The redistribution of moment occurs after the steel in the middle support section has yielded and some of the moment is transferred to section (1). Each of the two portions of the beam is now acting as a determinate simply supported beam where there is a known moment acting at the end (Mp).

Before the ultimate moment of section (2) is reached the middle support has to be able to have enough rotation in order to develop a mechanism in the structure; in other words, a full redistribution of moment has to take place so that the yield point of section (1) at midspan is reached (My_1).

To be able to achieve this, the actual plastic rotation θp_u at failure has to be less than or equal to the available plastic rotation capacity of the section θ_p; $\theta_{pu} \leq \theta_p$. This is considered a full and complete failure (fig. 2.5a). Section 2 has to have enough ductility in order to develop a mechanism. A partial collapse is possible when the actual plastic rotation exceeds the calculated or available rotation capacity $\theta_{pu} > \theta_p$. In this case the member is not able to redistribute enough forces to reach a mechanism and develop the yield point at midspan figure (2.5b). It is obvious when a partial failure occurs the mid support undergoes local fracture and that would be the ultimate load (P_u) the structure can support which is less than the P_u when a full redistribution of moments occurs.

One can see from the above discussion, that the most important and general condition of rotation compatibility is:

$$\theta_{P_u} \leq \theta_p \qquad (2.7)$$

An illustrative discussion is shown in figure (2.5) for both cases at full and partial moment redistribution of the structure.

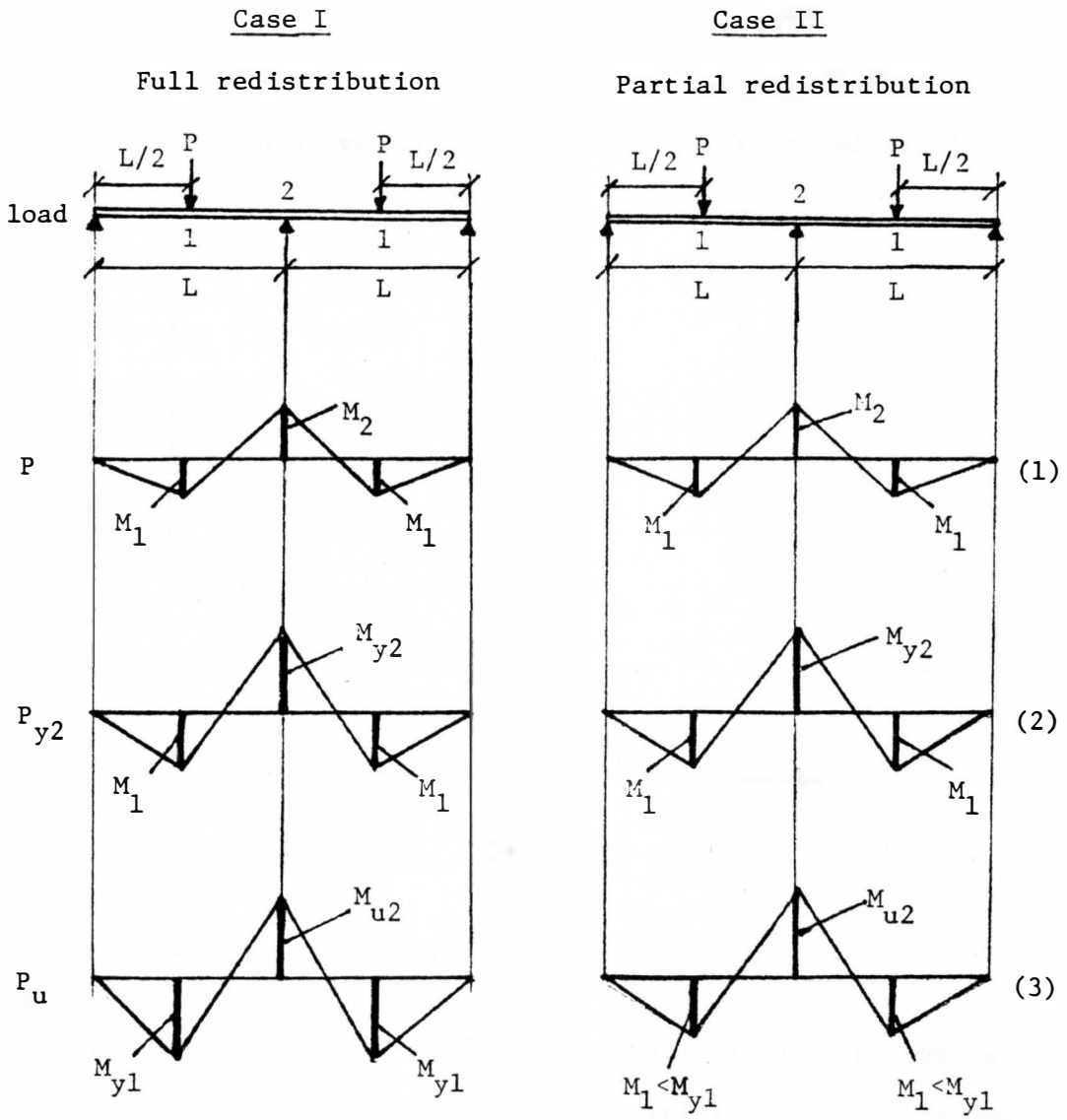

Figure 2.5 Rotation Compatibility

2.3 Moment-Curvature relationship

One of the basic and important aspects necessary for a theoretical and experimental study of inelastic behavior and moment redistribution of reinforced concrete in determinate or indeterminate structures is the moment-curvature (M-ϕ) relations.

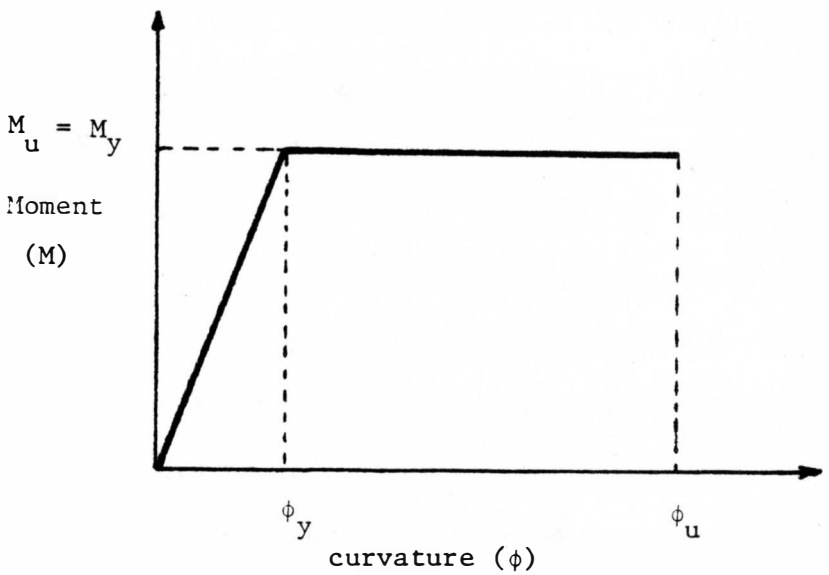

Figure 2.6 Idealized moment-curvature relationship

The moment curvature relation is usually assumed to have a bi-linear relation (figure 2.6). This theoritical assumption assumes a totally elastic behavior up to the first yield and a completely plastic behavior after first yield with excessive deformation at constant moment (M_p) applied at the critical section. This assumption is very uncharacteristic for concrete because reinforced concrete does not even have a complete elastic and linear (M-ϕ) relation in the elastic range.

A tri-segmental (M-ϕ) relation has been preferred over the bi-linear (M-ϕ) because the tri-segmental (M-ϕ) considers a progressive cracking. Also, the bi-linear (M-ϕ) relation over-estimates the deformations of a given section, which is believed to be safe.(7) But in continuous members, the internal force distribution is dependent upon the interaction of the stiffness of the different critical sections and over-estimation of deformations which could even result in unsafe predictions.(43)

A bi-linear relationship has also been reported to give satisfactory results.(43) It is obvious that there are contradictions over (M-ϕ) relationship. Figure (2.7) compares an ideal elastoplastic bi-linear (M-ϕ) to the actual (M-ϕ) relationship of reinforced concrete which is obtained from test results.

Curvature or the unit rotation (figure 2.8) at any stage of loading can be calculated from the equation, $\phi = \frac{M}{EI}$. It can also be experimentally calculated from figure (2.1).

It is obvious that the value of 'ϕ' increases as loading is increased to ultimate load and consequently the compressive strain of concrete increases.

The flexural rigidity of concrete decreases while excessive cracks are developing beyond the yield point of steel. Flexural rigidity or stiffness of the member can be calculated for cracked or uncracked (elastic) sections. In some experiments the value of EI was assumed to be constant through the elastic and plastic stages.

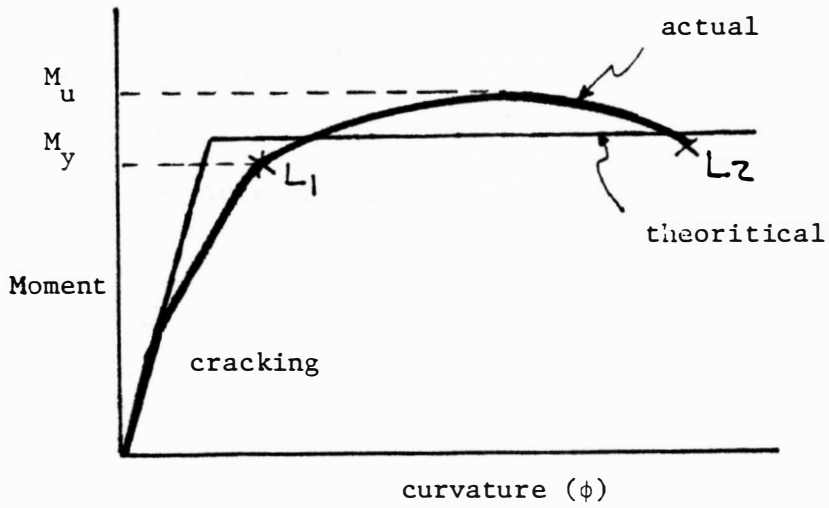

Figure 2.7 Actual and Theoritical Moment-curvature

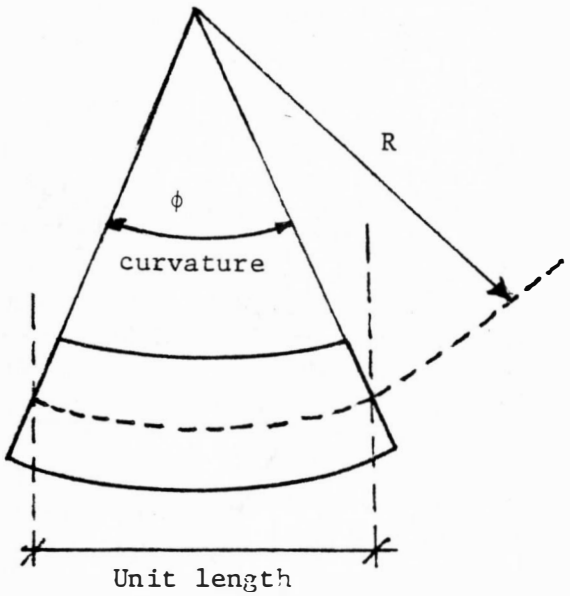

Figure 2.8 Unit rotation

where $\phi = \frac{1}{R}$

For a rectangular section:

$$EI = E_c \left(\frac{bd^3}{12}\right)$$

where: b = width of section

d = effective depth

E_c = modulus of elasticity of concrete

which is a conservative and over-estimating value especially for rotation calculations.

A. L. L. Baker[6] defines EI for a cracked rectangular section as in equation (2.9), which is not just based on properties of the material and the geometry of the section, but on the curvature at a particular limit-state L_1 (figure 2.7), and therefore, depends on the stress in concrete and the corresponding accumulated strain values.

$$\frac{M_1}{EI} = \frac{1}{R} = \phi$$

$$\phi = \frac{\varepsilon_{c1}}{K_1 d} = \frac{\varepsilon_{s1}}{d - K_1 d} \qquad \text{(Figure 2.9)}$$

$$\text{or } EI = \frac{M_1 K_1 d}{\varepsilon_{c1}} \text{ and } EI = \frac{M_1 (1-K_1) d}{\varepsilon_{s1}} \qquad (2.9)$$

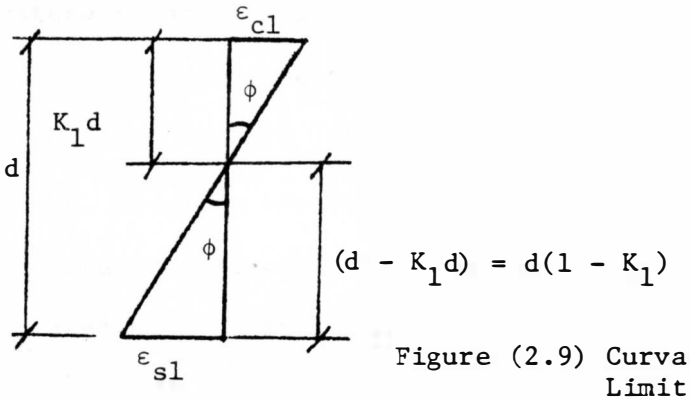

Figure (2.9) Curvature at Limit State L_1

where K_1 = ratio of the neutral axis depth to the effective depth.

M_1 = Moment at stage L_1

2.4 Plastic Hinge

The assumption that the inelastic rotation of concrete occurs at the point of maximum moment, which means that it occurs at one point and other portions of the member act elastically, is a theoritical assumption which is not true. The plastic rotation actually occurs on both sides of the maximum moment section over a finite length. This length which is called the hinge length H_L can be calculated with acceptable accuracy. The calculation of the hinge length can be done relative to the effective depth and also to the distance from the section of highest moment to the point of contra flexure (zero moment). One of the most common methods to calculate H_L is from moment-curvature and bending moment diagram which is shown in figure (2.10).

The value "H_L" on figure (2.10) represents the plastic hinge length which can be easily calculated. This shows another importance of the moment-curvature relationship.

It has been shown by testing that usually in reinforced concrete continuous structural members, the calculated rotation capacity is less than the actual rotation that is developed at the supports. Therefore, the calculated rotation capacity is a conservative value which could be increased by a limited safe value.[21]

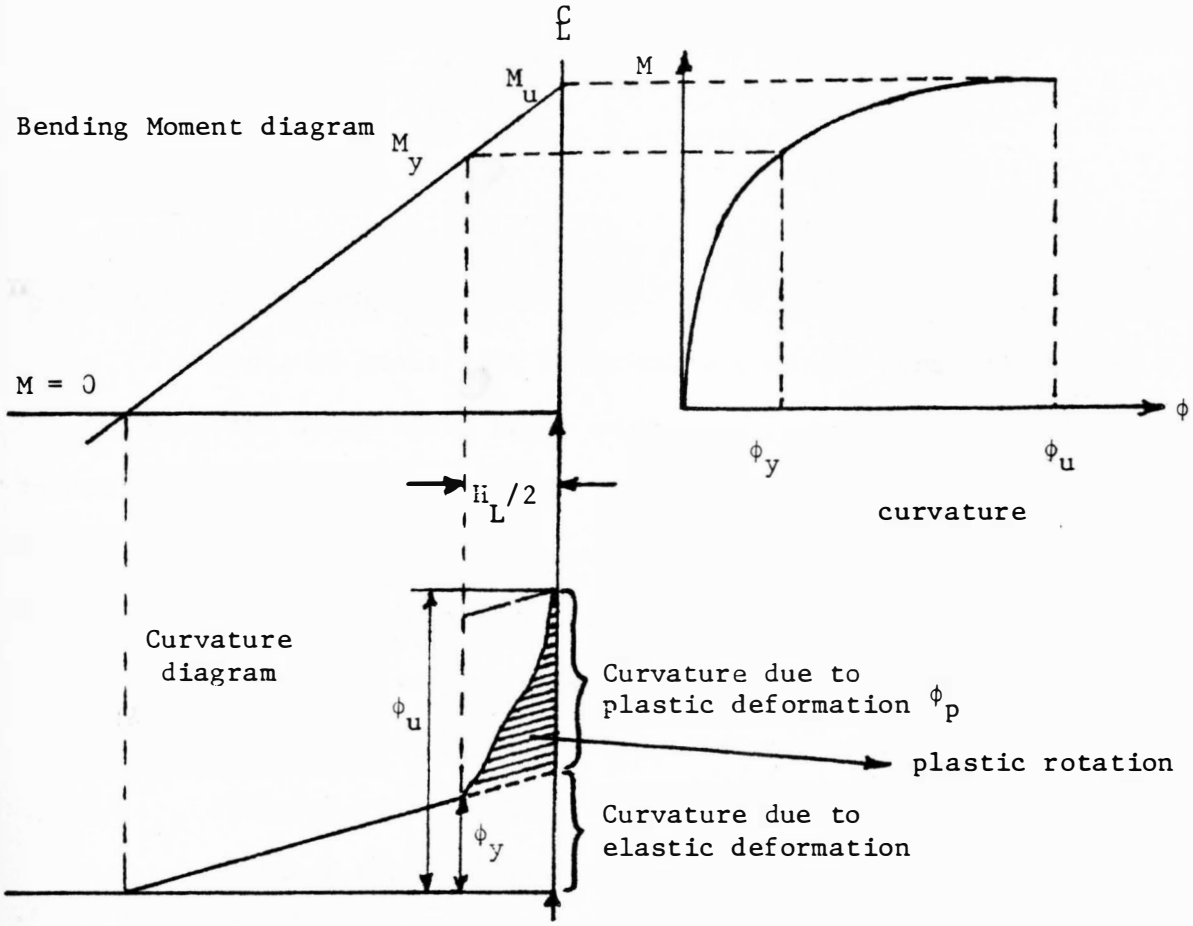

Figure 2.10 Plastic Rotation from Moment-curvature and Moment Gradient

CHAPTER III

MATERIAL AND TESTING PROCEDURE

3.1 Materials

3.1.1 Beam Arrangement

Ten concrete beams with identical dimensions were used in the experiment. The beams had a total depth of 8 inches, a width of 5 inches and a length of 11 feet (8"x5"x132"). The beams had variable main steel reinforcement and also varied in steel fiber percentage. The beams were divided into four different groups:

1. Three beams without steel fibers were used, each consisting of different main steel reinforcement.

   0% Steel Fibers main steel 2#3

   0% Steel Fibers main steel 2#4

   0% Steel Fibers main steel 2#5

2. Three beams with 0.8% steel fibers with different main steel reinforcement.

   0.8% Steel Fibers main steel 2#3

   0.8% Steel Fibers main steel 2#4

   0.8% Steel Fibers main steel 2#5

3. Three beams with 1.2% steel fibers with different main steel reinforcement.

   1.2% Steel Fibers main steel 2#3

   1.2% Steel Fibers main steel 2#4

   1.2% Steel Fibers main steel 2#5

4. One beam with 0.8% steel fibers and compression steel was used.

   0.8% Steel Fibers-Tension Steel 2#6-Compression Steel 2#3

The summary of beam arrangements is shown in Table 3.1.

Table 3.1

Beam Arrangement

Beam No.	Main Steel	% of Main Steel (ρ)	% of Steel Fibers (ρ_s)
B1			0
B4	2#3	0.67	0.8
B7			1.2
B2			0
B5	2#4	1.21	0.8
B8			1.2
B3			0
B6	2#5	1.89	0.8
B9			1.2
B10	2#6 tension 2#3 compression	ρ = 2.07 tension ρ' = 0.67 compression	0.8

A two span continuous simply supported beam setup was chosen with two concentrated loads on each span. The main steel reinforcements were placed at the top over the middle support where a negative moment exists while steel bras were placed at the bottom of the beam where a positive moment exists.

3.1.2 Steel Reinforcements

Two types of main reinforcement were used to resist the tensile forces in the beams. Flexure and shear are the two main stresses to be resisted by adequate reinforcement. A complete illustrative diagram is shown in figure (3.1).

The flexure tensile forces were resisted by 2#3, 2#4 or 2#5 at each critical section on the tension side. Figure (3.2) shows the moment diagram and the steel arrangement in the beams, showing the necessary development length to ensure enough bond between concrete and steel. The development length "ℓ_d" for each bar was calculated from equation 3.1 of the ACI Code, $\ell_d = 0.04\ A_b F_y / \sqrt{f_c'}$ but not less than $0.4\ D\ F_y \times 10^{-3}$.

The main bars were marked and cut off with an acetylene torch at the proper points. A one inch cover was allowed between the end of the bars and the end of the concrete beam (figure 3.1). The bars on the positive moment region were not extended all the way through the middle support to the other end. They were cut at a distance of about 4" to 12" depending on the bar diameter. The reason for this was to allow the concrete compression zone to take the inelastic

deformation alone after the yield of steel, with no contribution by any compression steel (except in beam B10).

For shear reinforcements #2 bars were used spaced at 3 inch intervals to ensure sufficient shear reinforcement. The stirrups were cut at 17 inch lengths and bent manually on a specially designed and fabricated equipment. There was a total of 44 stirrups in each beam. Figure (3.1) shows typical stirrup arrangement and beam cross section (same arrangement for beam B10).

The main steel reinforcement and stirrups were tied manually using 5.5 inch long tie wires. The surface of the main steel bars was filed and smoothed at the points of maximum moments for the purpose of attaching strain gages on each bar at each critical section. Special care was taken not to change the characteristic of of the steel bars at that point. After smoothening the surface, it was cleaned and degreased (figure 3.3).

3.1.3 Strain Gages

Three different types of SR-4 strain gages were used.

1. A-8 strain gages with a resistance of 120 $\pm$ 0.3 ohms and a gage factor of 1.73 $\pm$ 2%, were used for positive and negative steel reinforcement bars (figure 3.4).
2. A-1-S6 strain gages with resistance of 120 $\pm$ 2% ohms and a gage factor of 2.03 $\pm$ 1%, were used for concrete compression strains.

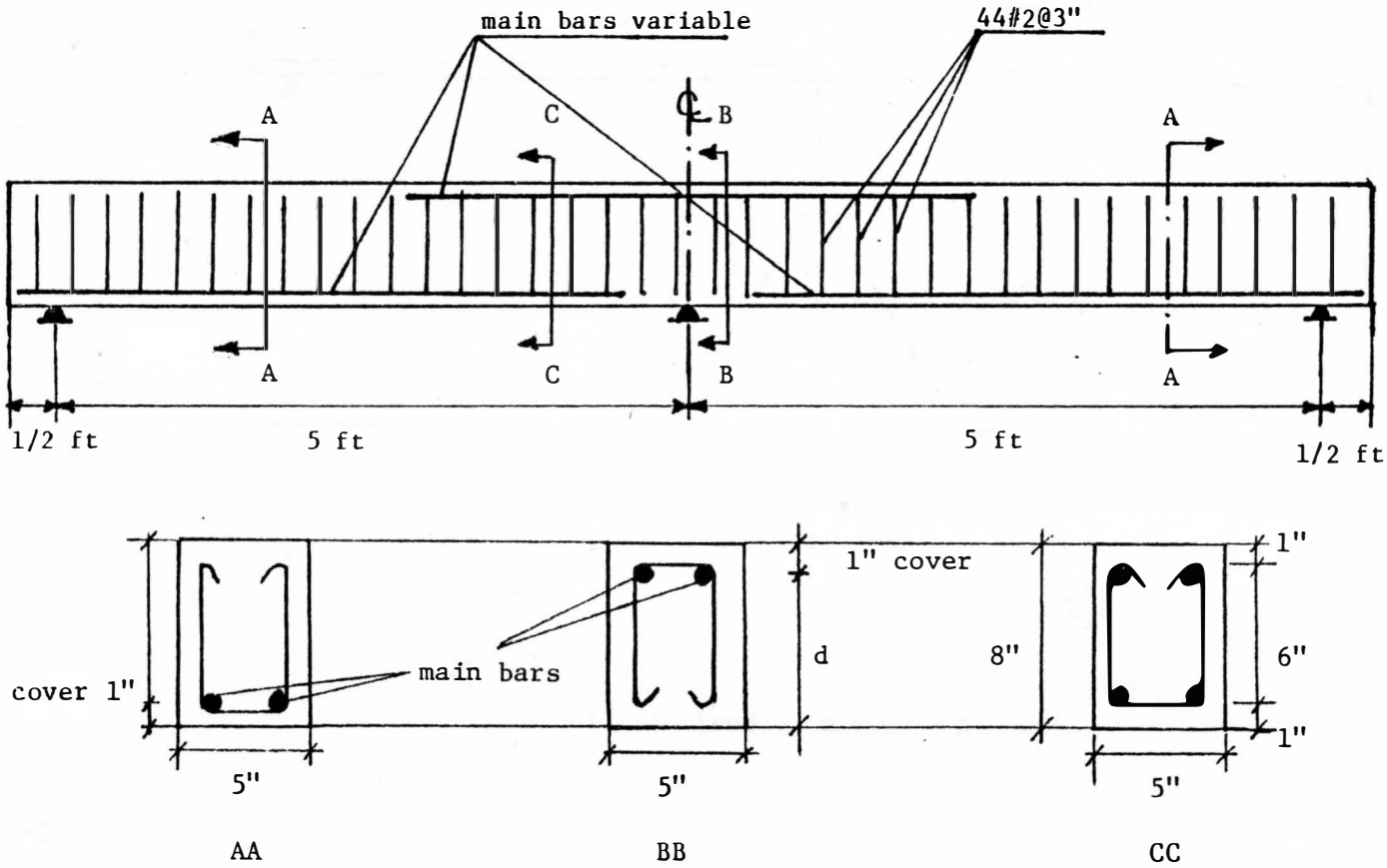

Figure 3.1 Steel arrangement of beams

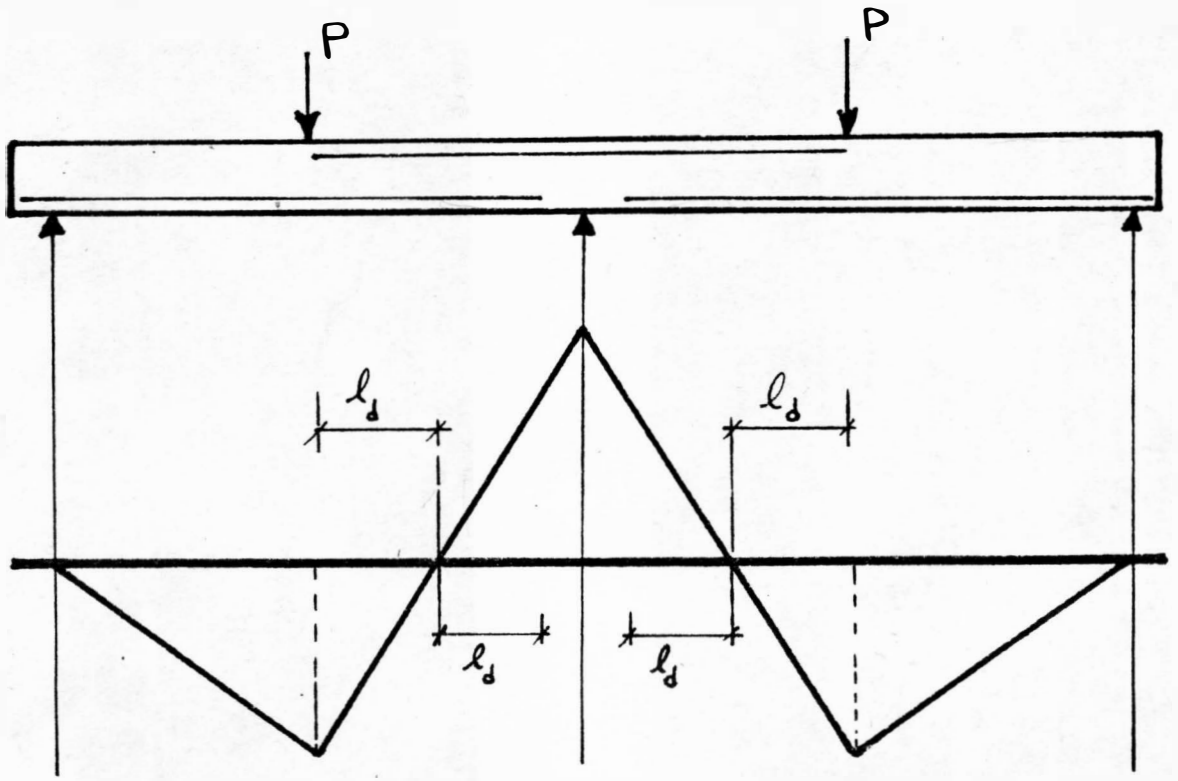

Figure 3.2 Development length of positive and neagive steel bars

Figure 3.3 Polished steel surface

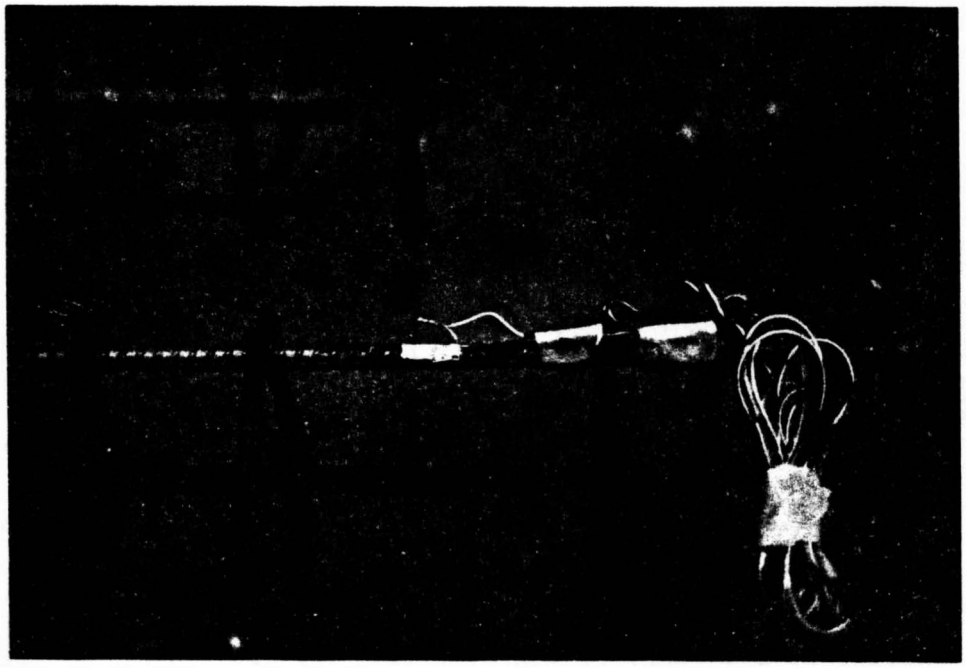

Figure 3.4 Attached strain gage

3. PA-7 post-yield strain gages with resistance of 120 ± 1.0 ohms and a gage factor of 1.92 ± 1% were used only for the negative section for strain readings after the yield of steel.

The steel strain gages were glued at the polished points (figure 3.5) and left for 24 hours, then covered with a special material SR-4 Carrier E to prevent the moisture penetration to the strain gages. A hot melt glue was used to seal and protect this carrier and the strain gage from any damage or moisture seepage (figure 3.6). Special stranded #22 wires were soldered to the strain gage leads. The following diagram shows a simplified example of the wiring from the strain gage to the digital strain indicator.

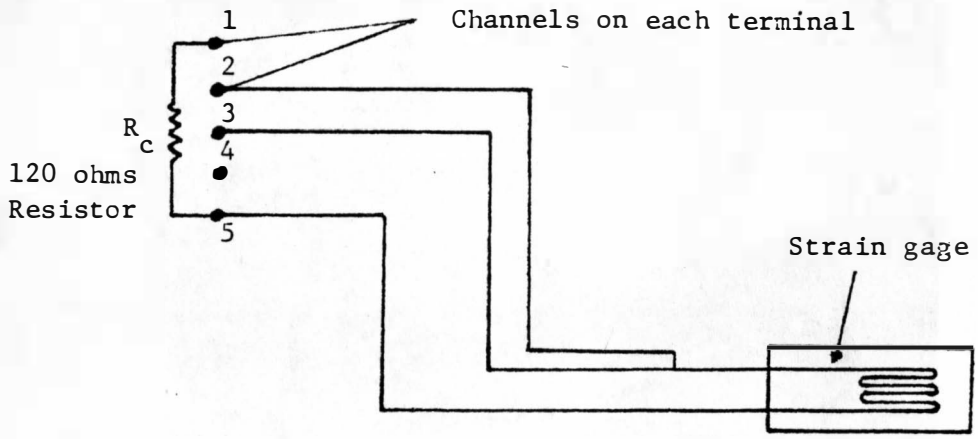

Figure 3.7 Wiring System

A resistor was used on each terminal for temperature change compensation. (More on Digital Strain Indicator in Section 3.2.4).

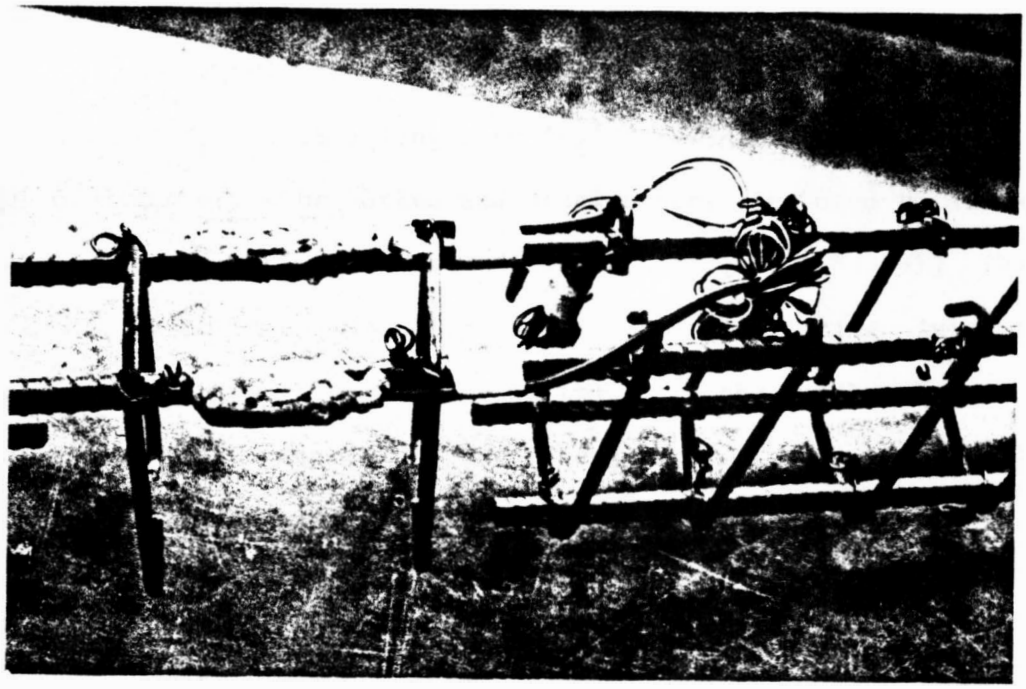

Figure 3.5 Covered strain gage at negative moment section

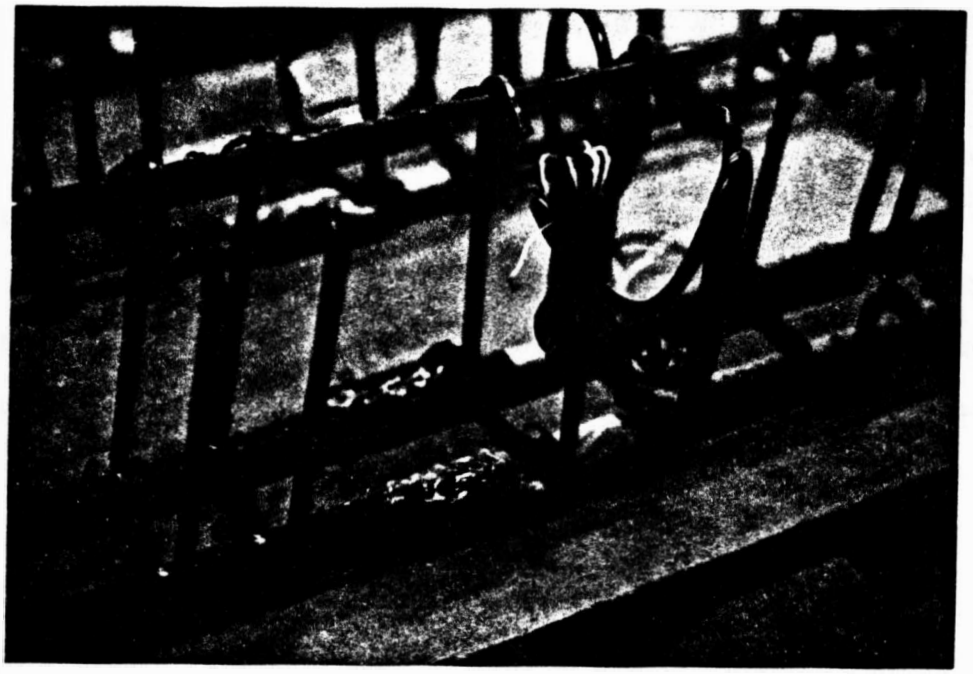

Figure 3.6 Covered strain gage at positive moment section

3.1.4 Steel Fibers

The steel fibers used in this experiment had an aspect ratio of 100 (L_f/d_f), with a length of 'L_f' of 2 inches and diameter 'd_f' of 0.02 inches. The hooked end steel fibers were used to allow anchorage between the fiber and concrete (figure 3.8,3.9). The fibers, which come in bundles of 25, were added during mixing of concrete. The water soluble glue that held the bundles togther dissolved in the water, and the fibers were released from each other and distributed uniformly throughout the concrete mix.

3.1.5 Concrete Components and Mixing

Concrete mix consisted of the following:

1 - Type I Portland Cement

2 - Fine aggregate with a fineness modulus of 2.90

3 - Coarse aggregate, maximum size of 3/8 inch

4 - Water

A 3.0 cubic foot capacity mixer (figure 3.10) was used for mixing the concrete needed for: three (5x8x132 in) main beams, six (6x12 in) cylinders for the compressive strength and split cylinder test, and two (6x6x21 in) small beams for the modulus of rupture test. A total of approximately 12 cubic foot of concrete was needed each time and it was divided into four equal 3 cubic foot batches.

A mixing time of about 4 minutes allowed the concrete to mix thoroughly. Steel fibers were added to the mix at equal intervals in a period of 6 to 8 minutes mixing time. The steel fibers were

Figure 3.8 Steel fibers

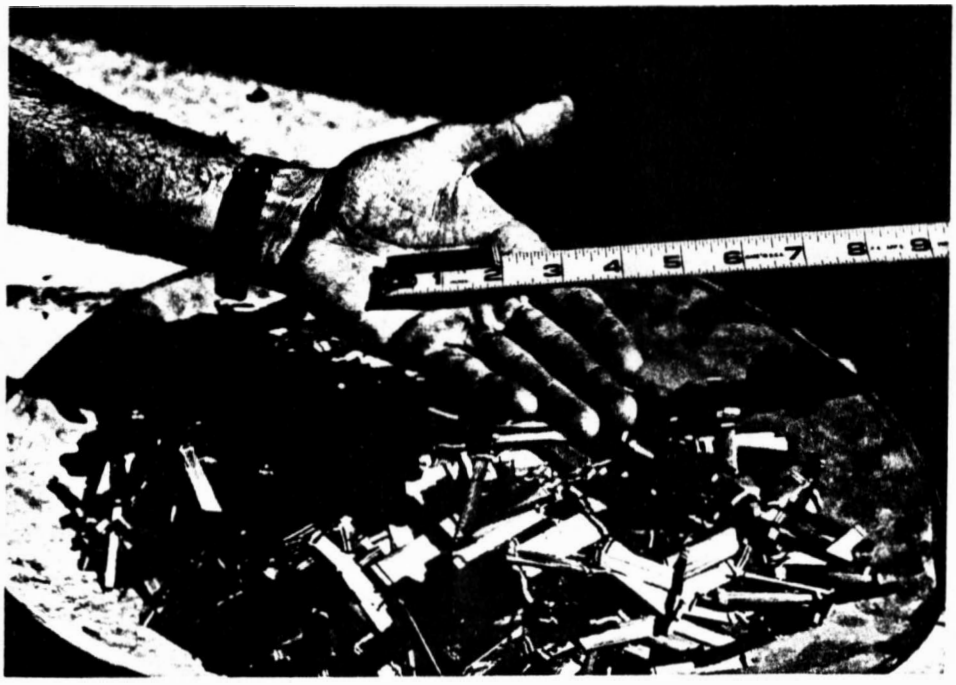

Figure 3.9 Steel fiber length

allowed to disperse and mix uniformly throughout the concrete mix. Each batch was controlled by the slump test according to ASTM standards (C-143). The concrete mix was scooped into the forms and molds. The use of a vibrator was necessary to ensure dispersion and penetration of the aggregate and steel fibers within the steel work (figure 3.11). A three-fourths inch cover on the sides was provided and the excess concrete was scraped off the surface and it was smoothed by using a wooden trowel (figure 3.12).

3.1.6 Formwork

A specially designed wooden formwork was fabricated for this experiment. The forms were designed for variable uniform width and length (up to 11 feet) and maximun depth of 10 inches for future use. The wooden forms were supported by steel brackets for lateral support due to concrete pressure (figure 3.14).

3.1.7 Beam Preparation

After 24 hours the beams and cylinders were stripped, and covered with wet burlap (figure 3.15). The burlap was moistened every day for one week so complete hydration of cement took place. The beams were handled with care so cracks would not occur in the beams. After placing the beams in the testing frame, the supports were leveled (more on the testing frame in section 3.2).

The concrete surface was scraped and smoothed for strain gage attachments. The A-1 concrete strain gages were attached at

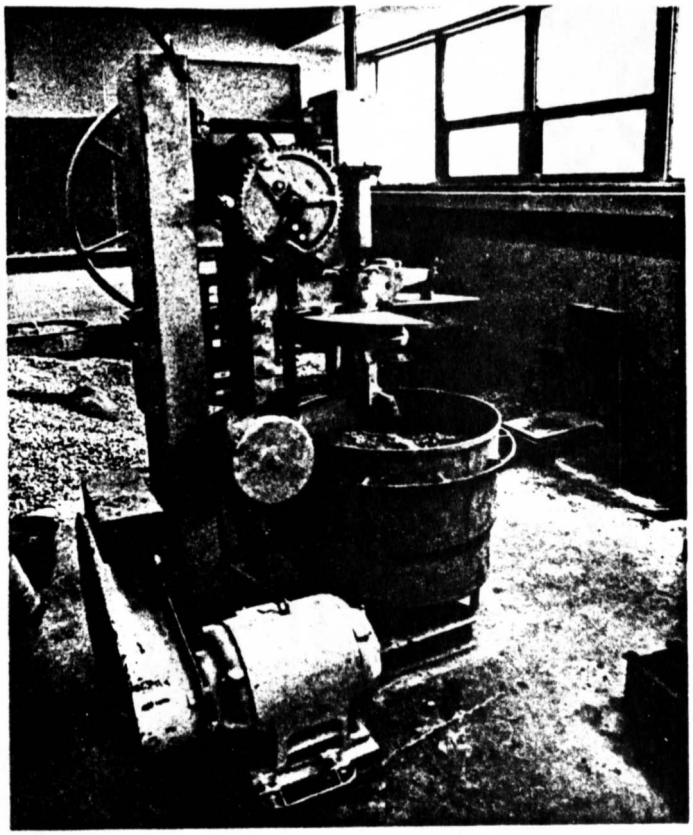

Figure 3.10 3.0 Cubic foot mixer

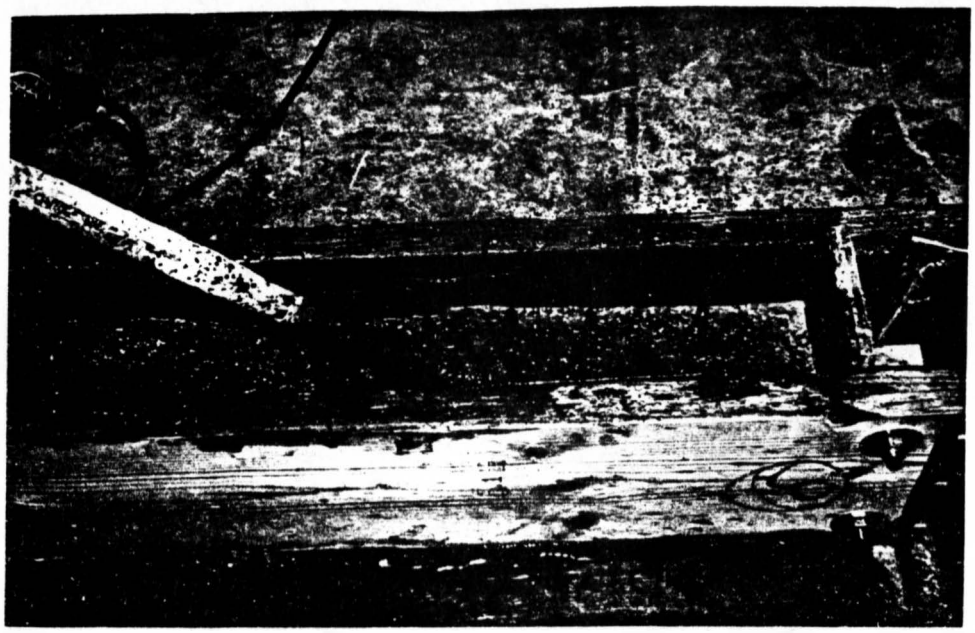

Figure 3.11 Fibrous Concrete Vibration

Figure 3.12 Concrete finishing

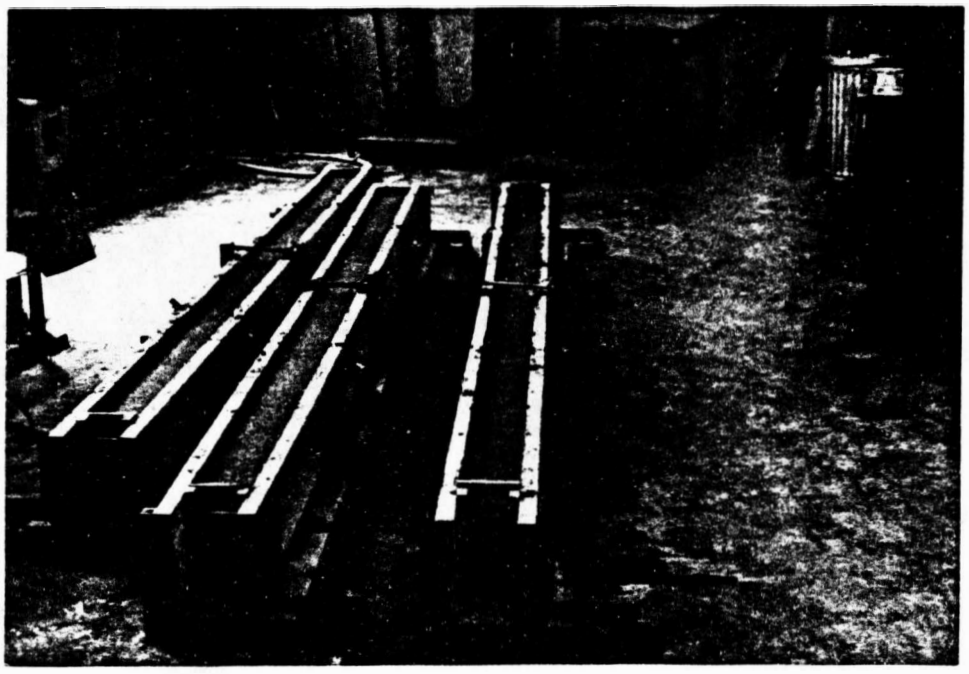

Figure 3.13 Completed work

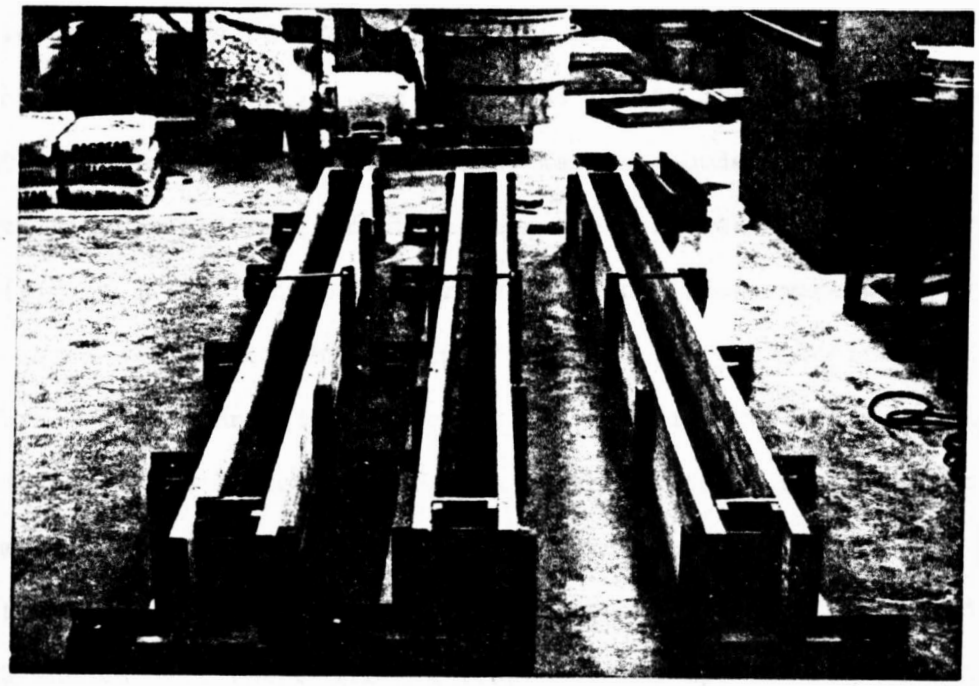

Figure 3.14 Formwork

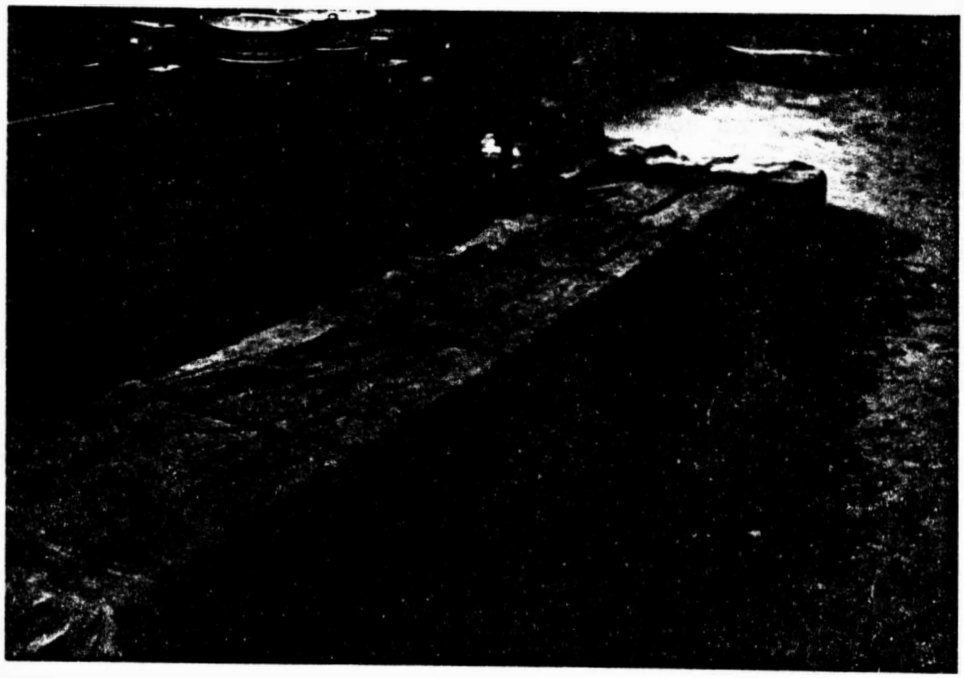

Figure 3.15 Concrete curing

least 24 hours before testing, the necessary wires were soldered onto the strain gages and connected to the digital strain indicator. Dental plaster of paris (gypsum) was used under the loading plates to ensure uniform contact between the plate and concrete surface (figure 3.16). Crack measurements on the beams were done by the use of cylindrical brass studs (3/8x3/8 in) with conical holes. The brass studs were glued at every one inch interval on a straightline drawn on the center of the beam at the critical section over the middle support. At the positive moment sections (under the load), the studs were glued every one inch over a 14 in. length and every 2 inches over the remaining length of the span. (Figure 3.17) shows a complete illustration of the brass studs arrangement. The brass studs were also glued at the middle support on the side for curvature measurement (figure 3.18).

The beams were marked at seven points for level readings. A scale with an accuracy of one hundredth of an inch was used to read the actual elastic curves and, more importantly, the plastic deformations of the critical section up to failure.

3.2 Testing Apparatus

3.2.1 Testing Frame

A steel girder frame with a capacity of 120 tons, twenty feet in length, five feet in width and three feet in depth was used. In this project a maximum load of 15 tons per jack was applied (figure 3.19).

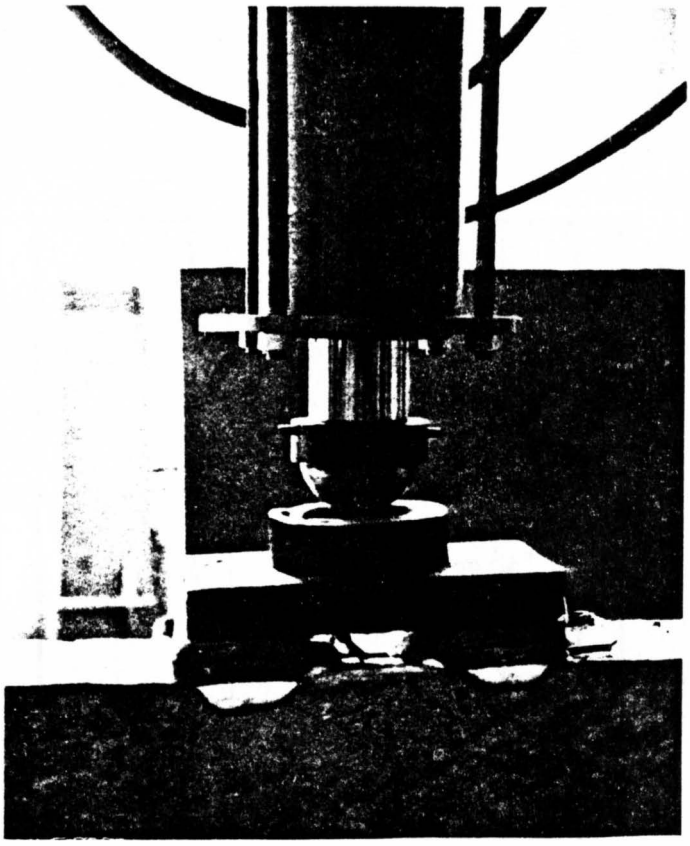

Figure 3.16 30 Ton loading jack

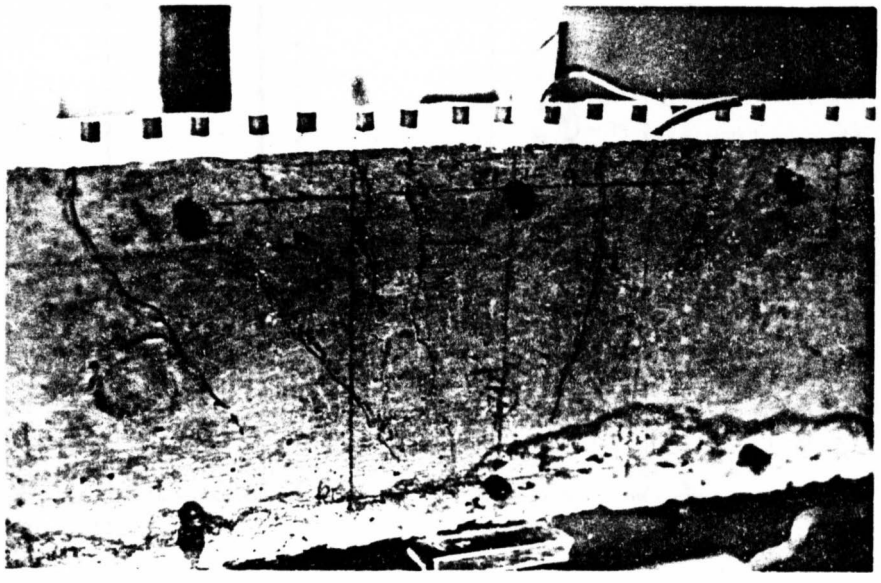

Figure 3.18 Brass stud arrangement for curvature and cracks

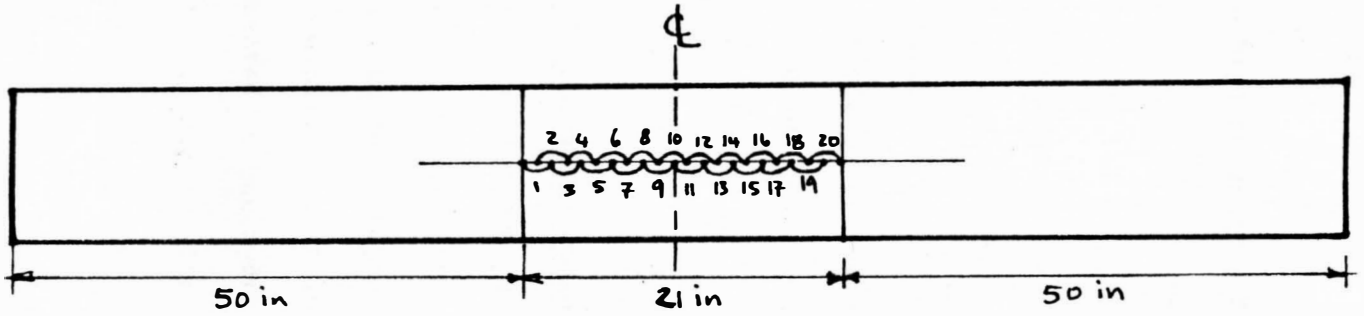

Top view

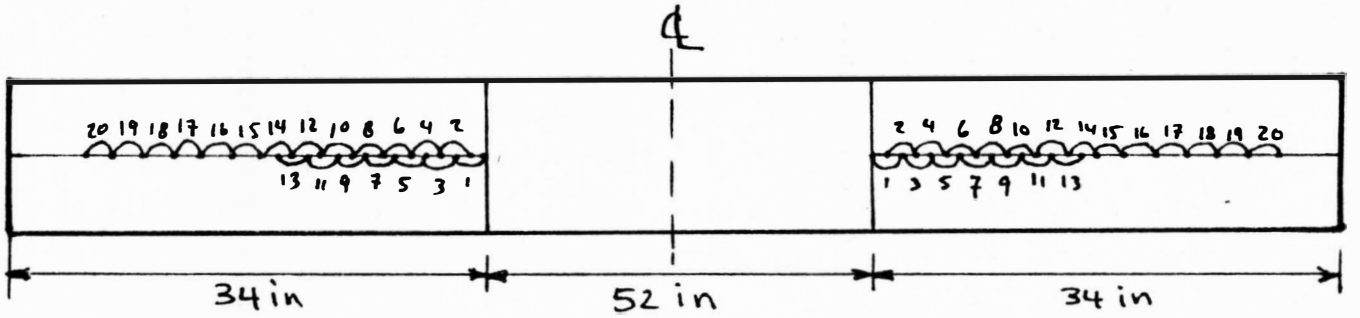

Bottom view

Figure 3.17 Brass studs arrangement for crack reading

3.2.2 Hydraulic Jacks

Two thirty ton hydraulic jacks were used for concentrated loading on the two spans (figure 3.16). The jacks were connected with high pressure hydraulic hoses by self-sealing couplers to the outlets on the loading frame. The oil was pumped manually into the jacks from the main hydraulic control console. The jacks were calibrated before testing using a Tinius Olsen testing machine, and they proved to behave identically. Maximum difference between the two jacks was at the pressure of 500 psi, with an error of 2.5%, but at higher pressures the error remained under 1%. Testing the Tinius Olsen testing machine against a proving ring showed an accuracy of about 0.1%. The calibration chart of the jacks vs. the testing machine is shown in Appendix E.

3.2.3 Hydraulic Console

The 10,000 psi capacity dual range hydraulic console consists of a low and high range. The low range is from zero to 2000 psi, with an increment of 20 psi. The high range is from zero to 10,000 psi, with an increment of 100 psi. An air pressure system is connected to the hydraulic console which is energized by the building's air supply with air pressure of about 120 pounds per square inch. This was used to release the loads from beams (figure 3.20).

3.2.4 Portable Digital Strain Indicator

An Electronic Digital Strain Indicator was used for the necessary strain gage readings. The strain indicator consists of four main components:

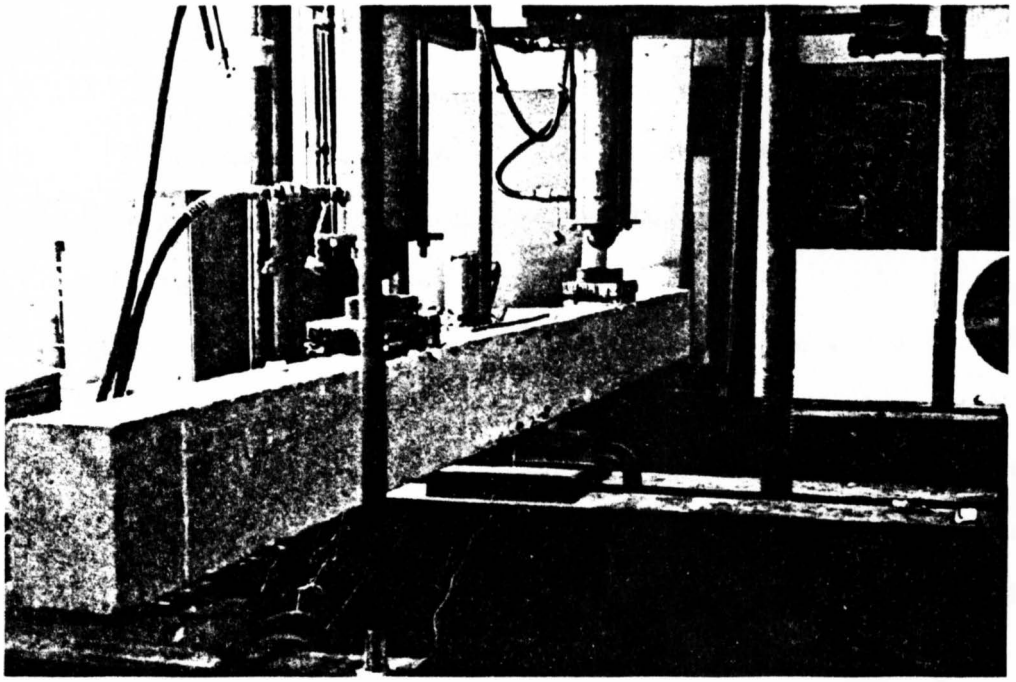

Figure 3.19 Testing frame

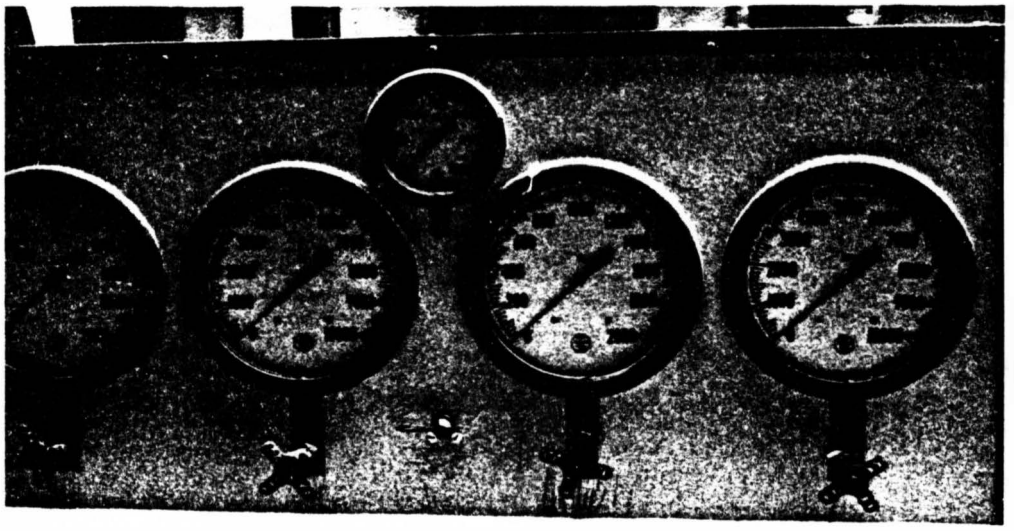

Figure 3.20 Hydraulic console

1 - Digital strain indicator which gives direct strain readings from the channel being used. The corresponding gage factor is also set on this unit.

2 - A printer which could be set to print the strain readings.

3 - Scanning module is the unit to which the wires from the strain gages are hooked up. The channel selection button and the adjusting buttons for each channel are also on this unit.

4 - Controller which has a three-way position mode switch and four push button switches for manual step, stop, reset and start. The three scanning modes are: a - manual mode is used for individual readings, b - single scan mode cycles through every channel and stops after the last reading has been printed out, c - continuous scan mode cycles the system until a stop function is initiated (figure 3.21).

3.2.5 Dial Gages

A total of three dial gages were used in the beam testing. Two were used for deflection readings under the beam with an accuracy of one thousandth of an inch, figure (3.22). The third was used for crack width measurements with an accuracy of ten thousandth of an inch.

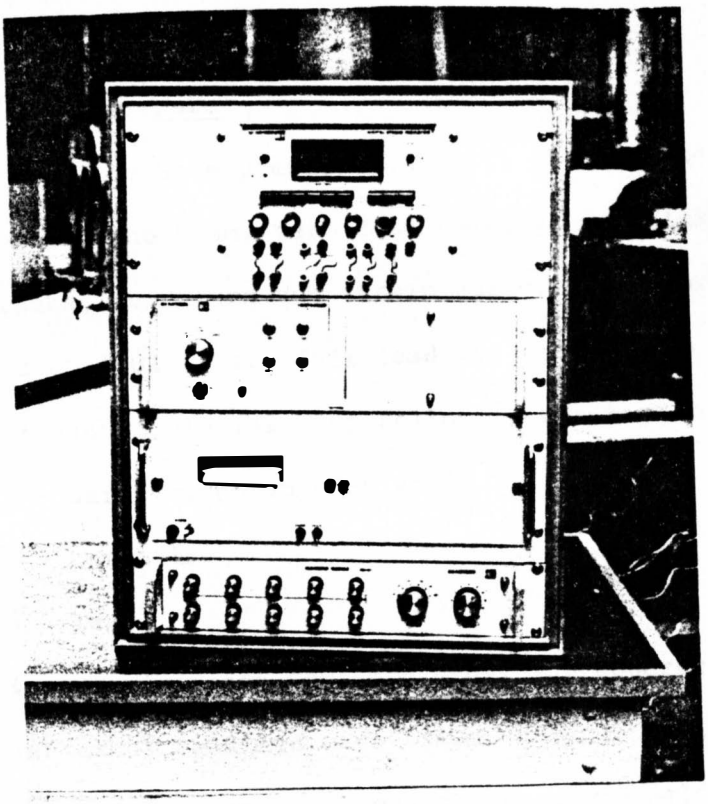

Figure 3.21 Portable digital strain indicator

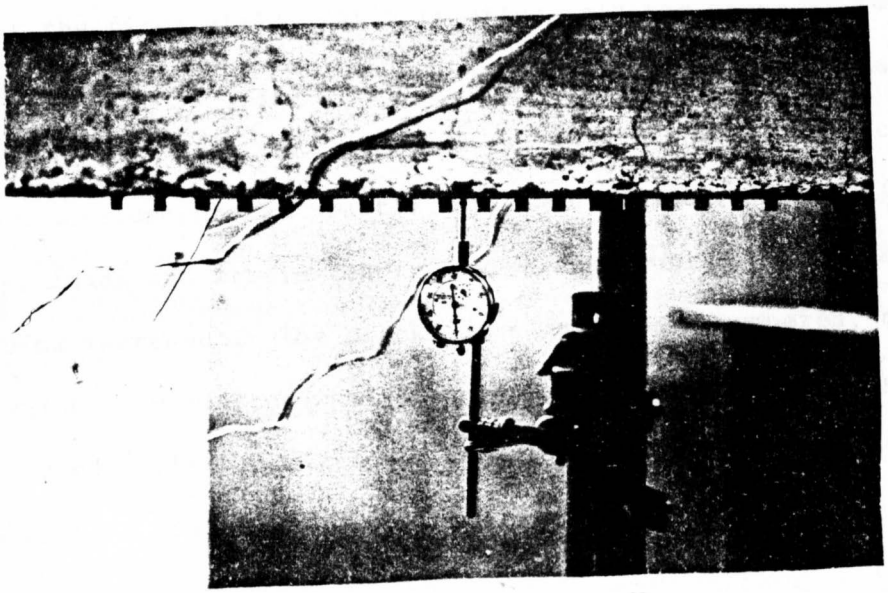

Figure 3.22 Deflection dial gage

3.3 Testing Procedure

After the beam preparations, all the equipment was rechecked. Before loading the beam, zero load readings were taken for deflections, level, cracks, curvature and strain gages. The load was applied in increments of 1,010 lbs. This load was the same in both manifolded jacks. At each 1,010 lbs. the following readings were taken:

1 - deflections on each span

2 - curvature

3 - level

4 - strain gages for both steel and concrete

The crack readings were taken every 2,020 lbs. During the time of measurements and readings the load was held constant and then increased manually and the same procedure was followed until the first yield of steel occured at the middle support. Large cracks developed after the first yield. At this stage only the critical readings, especially for cracks, were taken because the cracks that had developed were the only ones that propagated. In other words, the chances of new crack developments in plastic range was minimal. Deflections, curvature, level and strain readings were taken up to failure at each loading increment. The cracks were marked and numbered, and the load at which they started was also recorded. The data was recorded and tabulated. The calculations, comparison and interpretation of the results are given in Chapters V and VI.

CHAPTER IV

BEAM DESIGN

4.1 Concrete Mix Design

The method used for the concrete mix design was the absolute volumetric method. The calculation will be based on a cubic yards basis and then converted to pounds per cubic feet depending on the volume required. The calculations are as follows:

Specific Gravity (from testing ASTM C-127, 128)

Portland Cement Type I	= 3.15
Coarse Aggregate	= 2.65
Fine Aggregate	= 2.61

Aggregate Absorption (from testing ASTM C-127, 128)

Fine Aggregate	= 1.25%
Coarse Aggregate	= 1.61%

Moisture Content of Aggregates and Known Parameters

Fine Aggregate	= 2.2%
Coarse Aggregate	= 0.34%
Water Content	= 285 lbs/yd^3
W/C	= 0.55
% Fine Aggregates	= 45

Calculations

Volume of water = Unit Weight/Unit Weight of Water

$$= \frac{285\ lbs/yd^3}{62.4\ lb/ft^3} = 4.57\ ft^3/yd^3$$

Weight and Volume of Cement:

$$C = \frac{W}{0.55} = \frac{285}{0.55} = 518.18 \text{ lbs/yd}^3$$

$$\text{Volume of Cement} = \frac{\text{Weight}}{\text{Sp. Gr. x } 62.4 \text{ lbs/ft}^3} = \frac{518.18}{3.15 \text{ x } 62.4}$$

$$= 2.64 \text{ ft}^3/\text{yd}^3$$

$$\text{Volume of Aggregate} = 27 \text{ ft}^3/\text{yd}^3 - V_{water} - V_{cement}$$

$$= 27 - 4.57 - 2.64 = 19.79 \text{ ft}^3/\text{yd}^3$$

Weight of Aggregate = (V_{agg}) x (62.4 lbs/ft^3) x (Sp. Gr. of Aggregate) x (% Aggregate)

Weight of Fine = 19.79 ft^3/yd^3 x 62.4 lbs/ft^3 x 2.61 x 0.45

= 1450.39 lbs/yd^3

Weight of Coarse = 19.79 ft^3/yd^3 x 62.4 lbs/ft^3 x 2.65 x 0.55

= 1799.86 lbs/yd^3

Moisture Corrections:

Correction Weight = (moisture content-absorption) $(\frac{\text{weight of aggregate}}{1 + \text{absorption}})$

$$\text{Fine Correction} = (0.022 - 0.0125)(\frac{1450.39}{1 + 0.0125}) = 13.6 \text{ lbs/yd}^3$$

$$\text{Coarse Correction} = (0.0034 - 0.0161)\ (\frac{1799.86}{1 + 0.0161})$$

$$= -22.5 \text{ lbs/yd}^3$$

Component	Weight lbs/yd^3	Correction lbs/yd^3	Corrected Weight lbs/yd^3
Cement	518.18	-	518.18
Water	285.00	+ 8.9	293.9
Fine Aggregate	1,450.39	+13.6	1,464.0
Coarse Aggregate	1,799.86	-22.5	1,777.36

Total batch weight used in the experiment:

1.5 cubic yards of concrete was used, therefore the total component weights are as follows:

Component	Total Weight (lbs)
Cement	778
Water	441
Fine Aggregate	2,196
Coarse Aggregate	2,666

Calculations for Steel Fiber Quantities:

Specific Gravity of Steel Fibers = 7.8

Unit weight of fibers = specific gravity x 62.4 lbs/ft^3

= 7.8 x 62.4 = 486.72 lbs/ft^3

Volume of each concrete mix = 12 ft^3

Weight of Steel Fibers used in each mix:

Weight of fibers when 0.8% is used

Weight of fiber: 486.72 lbs/ft^3 x 12 ft^3 = 5840.64 lbs

$$5840.64 \times \frac{0.8}{100} = 47 \text{ lbs}$$

Weight of fibers when 1.2% is used

$486.72 \text{ lbs/ft}^3 \times 12 \text{ ft}^3 = 5840.64 \text{ lbs}$

$5840.64 \times \frac{1.2}{100} = 70 \text{ lbs}$

% Steel Fibers	Weight of Steel Fibers (lbs)
0	0
0.8	47
1.2	70
	Total weight = 117 lbs

4.2 Loading System

The loading system used in this project is shown in figure (4.1) where two concentrated loads are applied at midspan on a two span simply supported continuous beam. Three different loading possibilities were considered before choosing the optimum case:

1 - load at X = 0.45L when maximum positive moment is obtained.

2 - Load at X = 0.55L when maximum negative moment at support is obtained.

3 - Load at midspan (X = 0.50L).

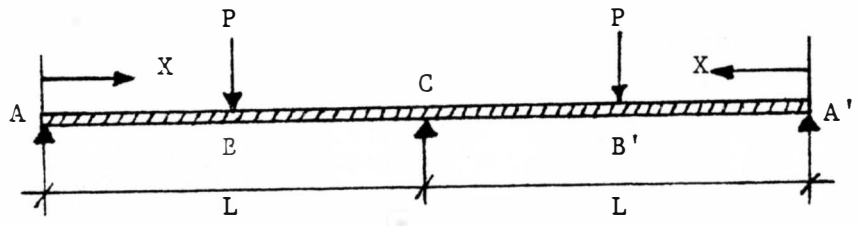

Figure 4.1 Loading System

The moments at 'B' and 'C' are computed and tabulated in terms of P, where L = 60 inches

Table 4.1

X	0.45L	0.55L	0.50L
M_B	10P	8.53P	9.4P
M_C	10.76P	11.5P	11.25P
r	1.07	1.35	1.19

The redistribution factor "r" was determined for each case. As it is obvious when X = 0.45L, r = 1.07 where there is not enough redistribution of moments to discuss the plastic rotation capacity of the critical section. When X = 0.55L the value of r = 1.35 meaning 35 percent moment redistribution is required for the critical section to develop a collapse mechanism which is relatively high.

Therefore an optimum "X" value of 0.5L was chosen to result in a reasonable 19% moment redistribution, so the rotation capacity of the middle support can be determined without a premature failure.

4.3 Beam Analysis

4.3.1 Analysis of the Beams (Elastic Theory)

The three-moment theorem was used for the elastic analysis of the beams.

The general equation used for this analysis is as follows:

$$M_A + 4M_C + M_E = - \Sigma P_1 L(K_1 - K_1^3) - \Sigma P_2 L(K_2 - K_2^3)$$

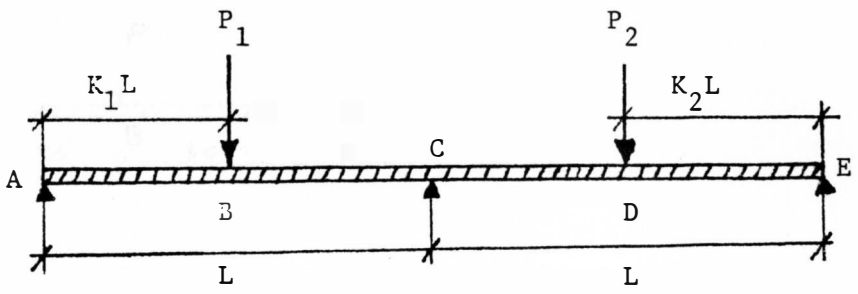

Figure 4.2 Beam Loading

In this case where equal concentrated loads exist and equal spans and the load being at the center of the span (K_1=K_2=0.5) the equations becomes as follows:

$$M_A + 4M_C + M_E = -2P(0.375L) = -0.75\ PL$$

$M_A = M_E = 0$ $\qquad$ $4M_C = -0.75\ PL$

where L = 60"

$M_C = -11.25P$

The reactions and shear and moment diagrams are shown in figure (4.3). Flexure and shear reinforcement design were based on these values.

4.3.2 Plastic Analysis

The virtual displacement principle is used to analyze the two span continuous beam with concentrated loads at the center of the spans. This principle is based on the equilibrium condition which can be

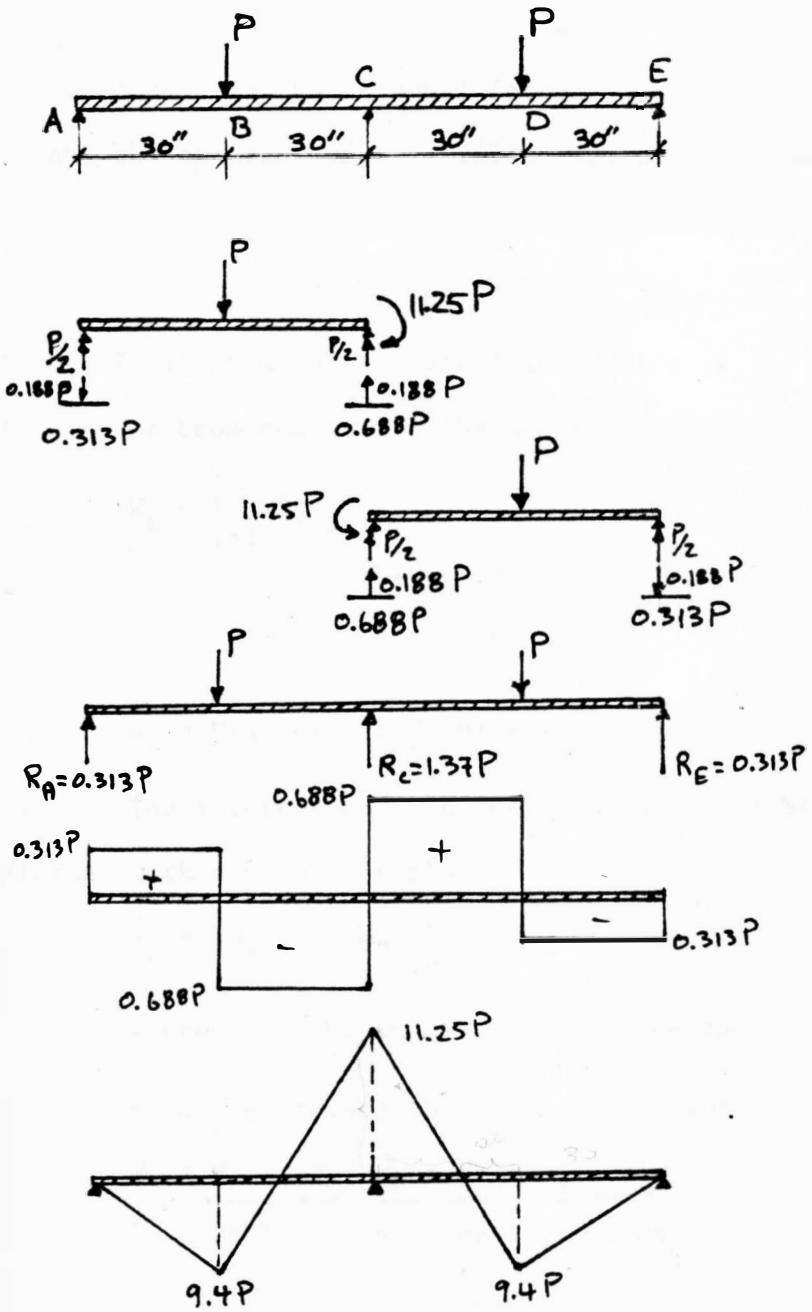

Reactions

Shear Diagram

Bending moment diagram

Figure 4.3 Elastic analysis

stated as follows: "If a system of forces in equilibrium is subjected to a virtual displacement, the work done by the external forces equals the work done by the internal forces.[8] The internal work is called W_I and the external work is called W_E, therefore the preceding principle is expressed as:

$$W_E = W_I$$

Figure (4.4) shows a complete illustration of the virtual displacement method for beam analysis. The necessary calculations are as follows:

$$W_E = \sum_{i=1}^{k} P_i \Delta_i$$

where Δ = vertical displacement of hinges

$$\Delta_2 = \Delta_4 = \frac{L}{2} \cdot \theta$$

$$W_E = P(\frac{L}{2} \cdot \theta) + P(\frac{L}{2} \cdot \theta) = 2\ P\ \frac{L}{2}\ \theta$$

The internal work in the structure will be the sum of the virtual work done at the plastic hinges.

$$W_I = \Sigma M_P\ \theta_i = M_P \sum_{i=1}^{k} \theta_i$$

where θ_i = the angle through which the hinges rotate.

From fig. (4.4b) the following is obtained:

$$W_I = \underbrace{M_P \times 2\theta}_{\text{section 2}} + \underbrace{M_P \times 2\theta}_{\text{section 3}} + \underbrace{M_P \times 2\theta}_{\text{section 4}}$$

$$W_I = 3\ M_P . 2\theta$$

$$W_I = W_E$$

$$2P\frac{L}{2}\ \theta = 3\ M_P . 2\theta$$

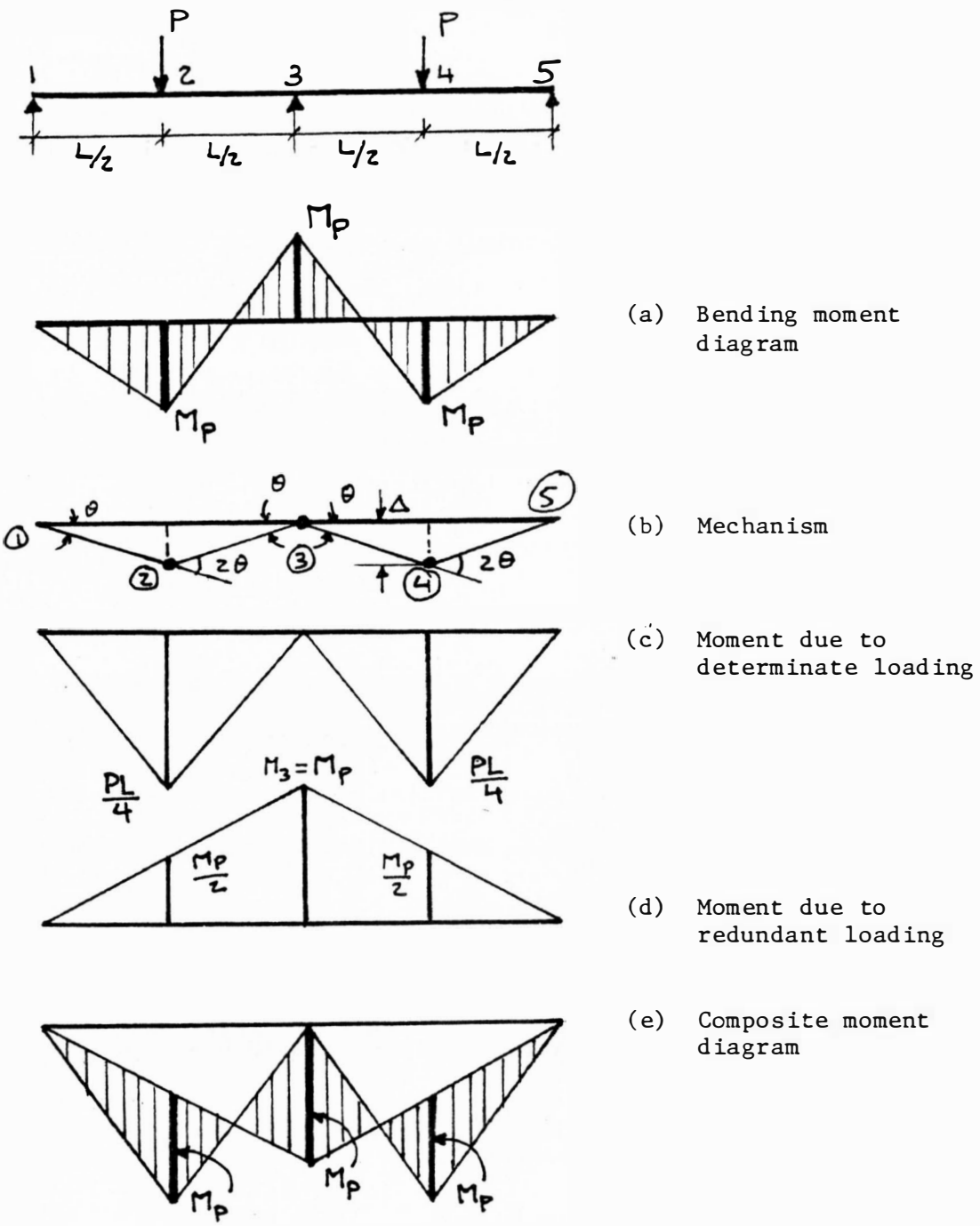

(a) Bending moment diagram

(b) Mechanism

(c) Moment due to determinate loading

(d) Moment due to redundant loading

(e) Composite moment diagram

Figure 4.4 Plastic analysis

$$P_u = \frac{6M_P}{L}$$

where: L = 60 in.

Thus: $M_P = 10\ P_u$

This result can be checked by the equilibrium equation by adding the moments at section 2 on figure (4.4c,d,e)

$$\frac{P_u L}{4} = M_P + \frac{M_P}{2}$$

$$P_u = \frac{6M_P}{L}$$

where L = 60 in

$$M_P = 10\ P_u$$

4.4 Flexure Design of the Beams

The method used for design of the moment for the beams is based on the ultimate strength theory of reinforced concrete according to the ACI Code (318-83). In the following calculations the contribution of steel fibers to the ultimate moment capacity of the beam is neglected.

1 - Beams with 2#3 tension steel

$$\rho_b = 0.85\ \beta_1\ \frac{f_c'}{f_y}\ \left(\frac{87}{87 + f_y}\right)$$

$$\rho_{max} = 0.75\ \rho_b = 0.64\ \beta_1\ \frac{f_c'}{f_y}\ \left(\frac{87}{87 + f_y}\right)$$

f_c' = 4,584 psi f_y = 66.8 Ksi $A_s = 0.22\ in^2$

d = 6.56 in

$$\rho = \frac{A_s}{bd} = \frac{0.22}{5x6.56} = 0.0067$$

$$\rho_{max} = 0.64 \times 0.825 \times \frac{4.584}{66.8} \left(\frac{87}{87 + 66.8}\right) = 0.0205$$

$$\rho_{min} = \frac{200}{f_y} = 0.003$$

For singly reinforced concrete sections:

$$M_u = A_s.f_y\left(d - \frac{A_s\ f_y}{1.7\ f_c'.b}\right)$$

$$= 0.22 \times 66.8 \left(6.56 - \frac{0.22 \times 66.8}{1.7 \times 4.584 \times 5}\right) = 90.86 \text{ K-in}$$

2 - Beams with 2#4 tension steel

$f_c' = 4584$ psi, $f_y = 70.8$ Ksi, $d = 6.5$ in., $A_s = 0.393$ in^2

$$\rho_{max} = 0.0205$$

$$\rho_{min} = \frac{200}{70,800} = 0.0028$$

$$P = \frac{0.393}{5 \times 6.5} = 0.0121$$

$$M_u = 0.393 \times 70.8 \left(6.5 - \frac{0.393 \times 70.8}{1.7 \times 4.584 \times 5}\right) = 161 \text{ K-in}$$

3 - Beams with 2#5 tension steel

$f_c' = 4584$ psi, $f_y = 52.0$ Ksi, $d = 6.44$ in., $A_s = 0.61$ in^2

$$\rho_{max} = 0.0205$$

$$\rho_{min} = \frac{200}{52,000} = 0.00385$$

$$\rho = \frac{0.61}{5 \times 6.44} = 0.0189$$

$$M_u = 0.61 \times 52 \left(6.44 - \frac{0.61 \times 52}{1.7 \times 4.584 \times 5}\right) = 178.5 \text{ K-in}$$

4 - Beam with double reinforcement 2#6 tension steel and 2#3 compression steel:

$f_c' = 5438$ psi, $f_y = 63.1$ Ksi, $A_s = 0.88$ in^2

$d = 6.375$ in $\qquad A_s' = 0.22$ in^2

$d' = 1.44$ in.

$$\rho = \frac{A_s - A_s'}{bd} = \frac{0.88 - 0.22}{6.375 \times 5} = 0.0207$$

$$M_u = [(A_s - A_s')\, f_y\, (d - \tfrac{a}{2}) + A_s'\, f_y\, (d - d')]$$

$$a = \frac{(A_s - A_s')\, f_y}{0.85\, f_c'\, b} = \frac{(0.88 - 0.22)(63.1)}{0.85 \times 5.438 \times 5} = 1.8 \text{ in.}$$

$$M_u = [(0.88 - 0.22)(63.1)(6.375 - \tfrac{1.8}{2}) + (0.22)(63.1)$$
$$(6.375 - 14.4)]$$

$M_u = 296.52$ K-in

If the increase in compressive strength of concrete due to steel fibers is considered in the preceding calculations, the moment capacity changes by a very small percentage (less than 1%). Results are shown in Table 4.2

4.5 Shear Check

The following shear check calculation is done for the most critical case when 2#5 reinforcement bars are used, where higher loads and higher shear stresses are used.

2#5: $P_u = 21.0$ Kips

$V_u = 0.688\, P_u$ (from shear diagram)

$$v_u = \frac{V_u}{b.d}$$

$$v_u = \frac{0.688 \times 21{,}000}{5 \times 6.44} = 448.7 \text{ psi}$$

$$v_c = 2\sqrt{f_c'} = 2\sqrt{4584} = 135.4 \text{ psi}$$

$$v_s = 448.7 - 135.4 = 313.3 \text{ psi}$$

$$S_{min} = \frac{A_v f_y}{v_s b} = \frac{0.10 \times 62{,}000}{313.3 \times 5} = 3.95 \text{ in}$$

The spacing used was 3 inches for all beams, therefore the shear reinforcement is adequate. The same calculations were done for 2#4 and 2#3 bars and the corresponding S_{min} was 4.6 in. and 14 in. respectively which is less than 3".

Table 4.2

Ultimate Moment Capacity

	% Fibers	A_s (in^2)	A_s' in^2	b_{in}	d_{in}	ρ	M_u K-in	P_y Kips	P_u Kips
	0.0	0.22	-	5	6.56	.0067	90.86	8.16	10.7
Case 1	0.8	0.22	-	5	6.56	.0067	91.10	8.10	10.7
2#3	1.2	0.22	-	5	6.56	.0067	91.20	8.20	11.0
	0.0	0.39	-	5	6.5	.0121	161.0	14.46	19.0
Case 2	0.8	0.39	-	5	6.5	.0121	162.0	14.55	19.1
2#4	1.2	0.39	-	5	6.5	.0121	162.4	14.6	19.15
	0.0	0.61	-	5	6.44	.0189	178.5	16.03	21.05
Case 3	0.8	0.61	-	5	6.44	.0189	179.6	16.14	21.20
2#5	1.2	0.61	-	5	6.44	.0189	180.3	16.20	21.25
Case 4	0.8	0.88	0.22	5	6.375	.0276	296.0	26.60	35.00
2#6									
2#3									

CHAPTER V

TEST RESULTS

5.1 Compressive Strength

Reinforced concrete is used to resist compressive forces, its ability to take compression is much higher than its tensile strength. Compressive strength of concrete is determined by testing 28 day standard size cylinders. The 6"x12" cylinders are tested in a specially manufactored loading machine at a specified loading rate. The 28 day compressive strength of concrete ranges from about 2,500 psi to as high as 14,000 psi, normally the strength ranges from 3,000 to 7,000 psi. For ordinary applications, 3,000 to 4,000 psi concrete is used, while for prestressed concrete it ranges from 5,000 to 7,000 psi. The compressive strength is mainly affected by the water-cement ratio and curing condition.

In this research the strength of plain concrete and also fibrous concrete with different percentage of steel fibers were determined and compared. The results of the compressive strength of the cylinders are shown in table 5.1.

5.2 Modulus of Elasticity

Reinforced concrete does not have an exact, clear cut modulus of elasticity. Its value varies with different strength, age, loading type, cement and aggregate characteristics. There are different definitions for modulus of elasticity of concrete:

1) Initial modulus which is the slope of stress-strain diagram at the origin.

Table 5.1

Compressive Strengths

Case	Cylinder	% Steel Fiber	For Beams	f_c' psi	Average f_c' psi	% increase from 0% steel fibers
I	C1	0.0	B1,B2,B3	4,421	4,584	-
	C2			4,719		
	C3			4,457		
	C4			4,740		
II	C1	0.8	B7,B8,B9	4,757	4,805	4.8
	C2			4,828		
	C3			4,792		
	C4			4,846		
III	C1	1.2	B4,B5,B6	5,043	4,927	7.5
	C2			4,863		
	C3			4,873		

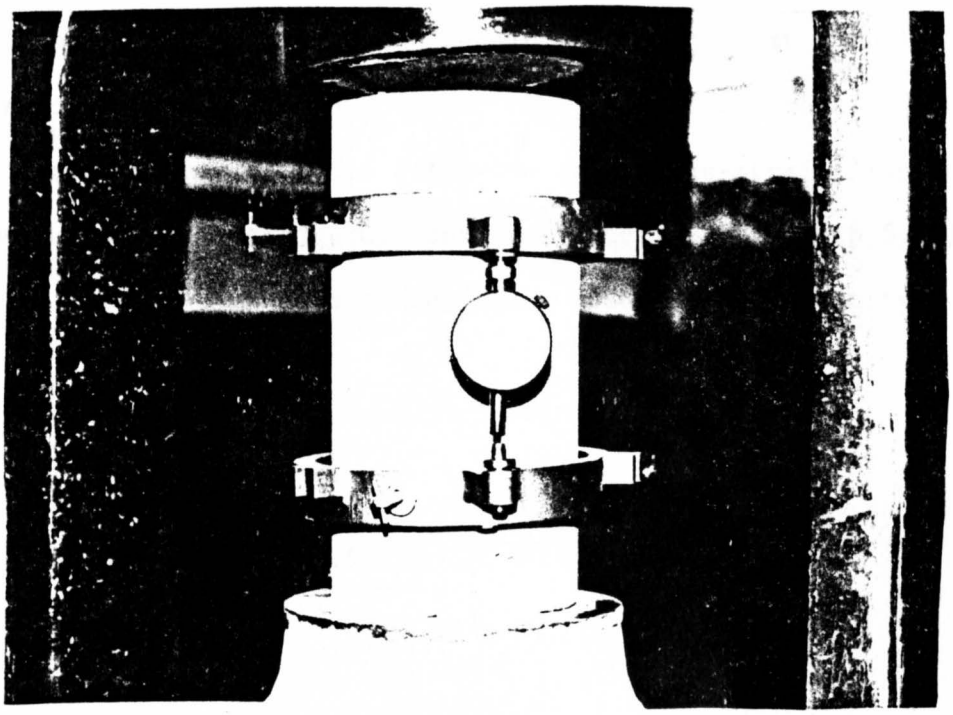

Figure 5.1 Compressometer to determine modulus of elasticity

length marked (6 inches). The readings were taken at 5000 lbs. load intervals up to about 135,000 lbs. The resulting stress and strain coordinates were plotted to determine the stress-strain diagram and the modulus of elasticity of conrete (Figures 5.2 through 5.11).

The formulae used to determine modulus of elasticity were:

$$\sigma = \frac{P}{A}$$

$$\varepsilon = \frac{\Delta L}{L}$$

$$E_{ca} = \frac{0.5\ f_c'}{\varepsilon}$$

where:

σ = stress (psi)

P = applied load (lbs)

A = cross section area (28.27 in^2)

ε = average strain of cylinder (in/in)

ΔL = deformation (in)

L = gage length (6 inches)

E_{ca} = secant modulus of elasticity (psi)

The results of modulus of elasticity are shown in a tabulated form in table 5.2. The effect of steel fibers on the modulus of elasticity is shown in table 5.3.

5.3 Split Cylinder

Reinforced concrete has a low tensile strength, it ranges from 10% to 15% of its compressive strength. Tensile stresses in

Figure 5.2

Modulus of elasticity of concrete
Cylinder C1
%Steel Fibers=0.0 fc'=4421 psi

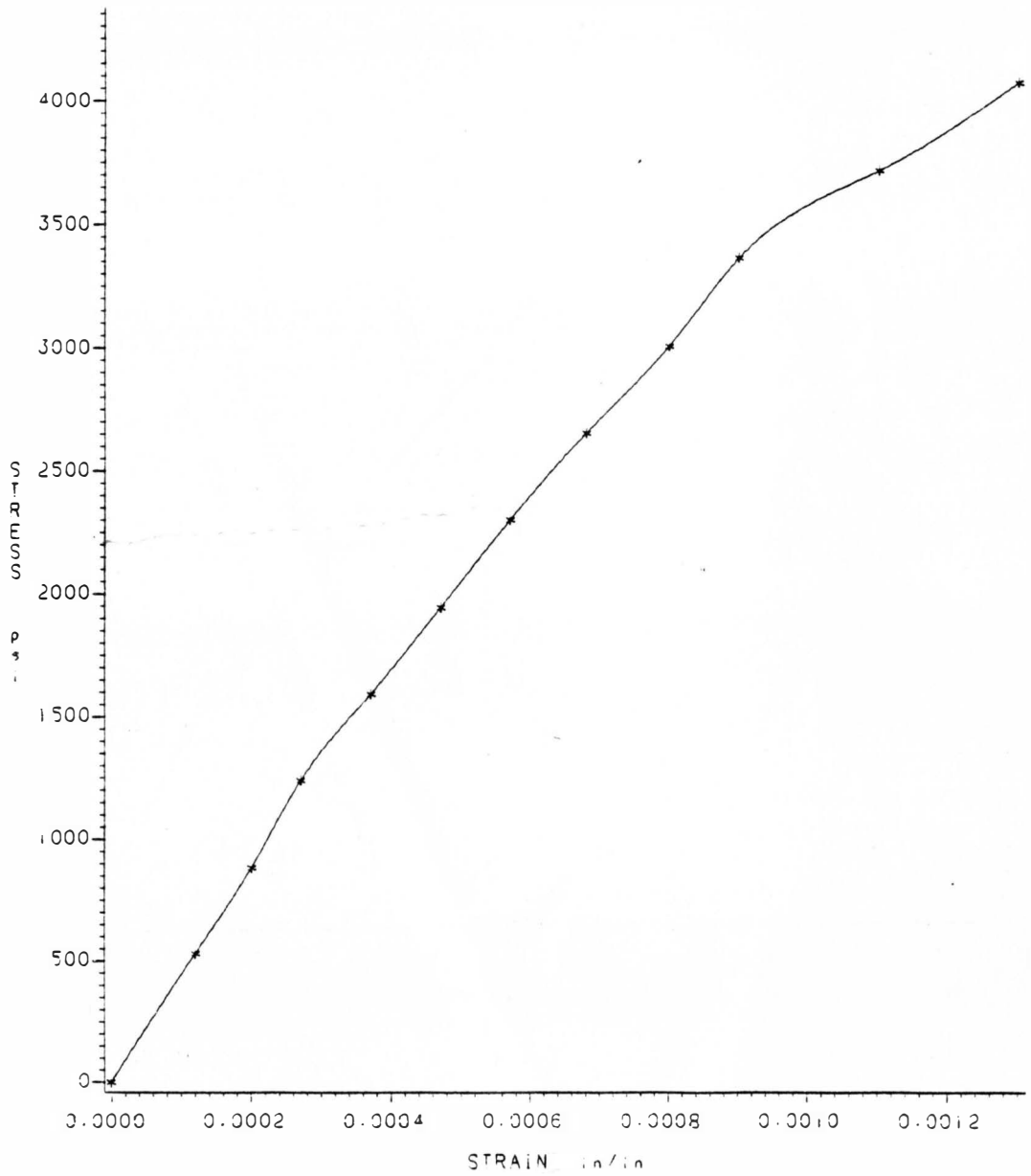

Figure 5.2 Stress vs. Strain

Figure 5.3

Modulus of elasticity of concrete
Cylinder C2
% Steel Fibers=0.0 fc'=4719 psi

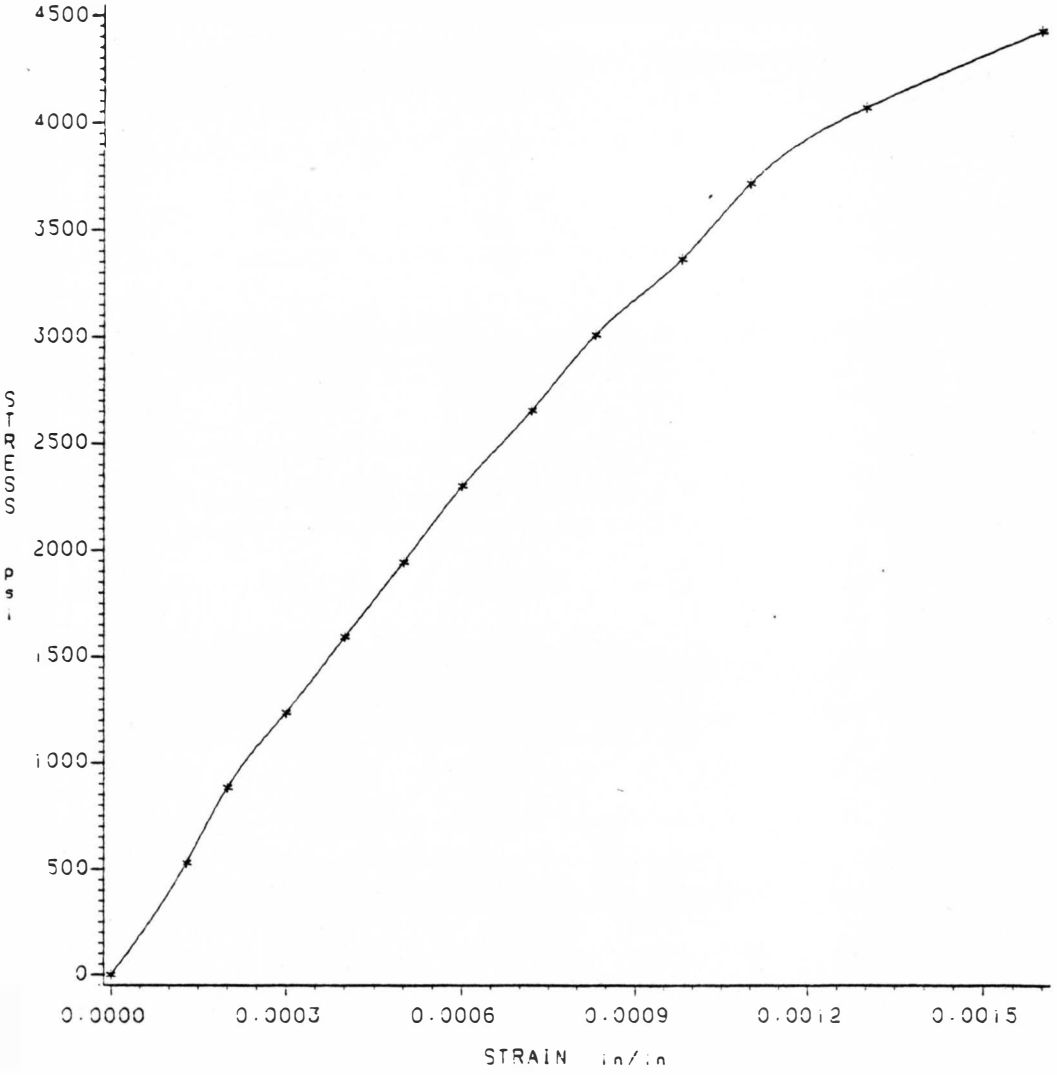

Figure 5.3 Stress vs. Strain

Figure 5.4

Modulus of elasticity of concrete
Cylinder C3
% Steel Fibers=0.0 fc=4457 psi

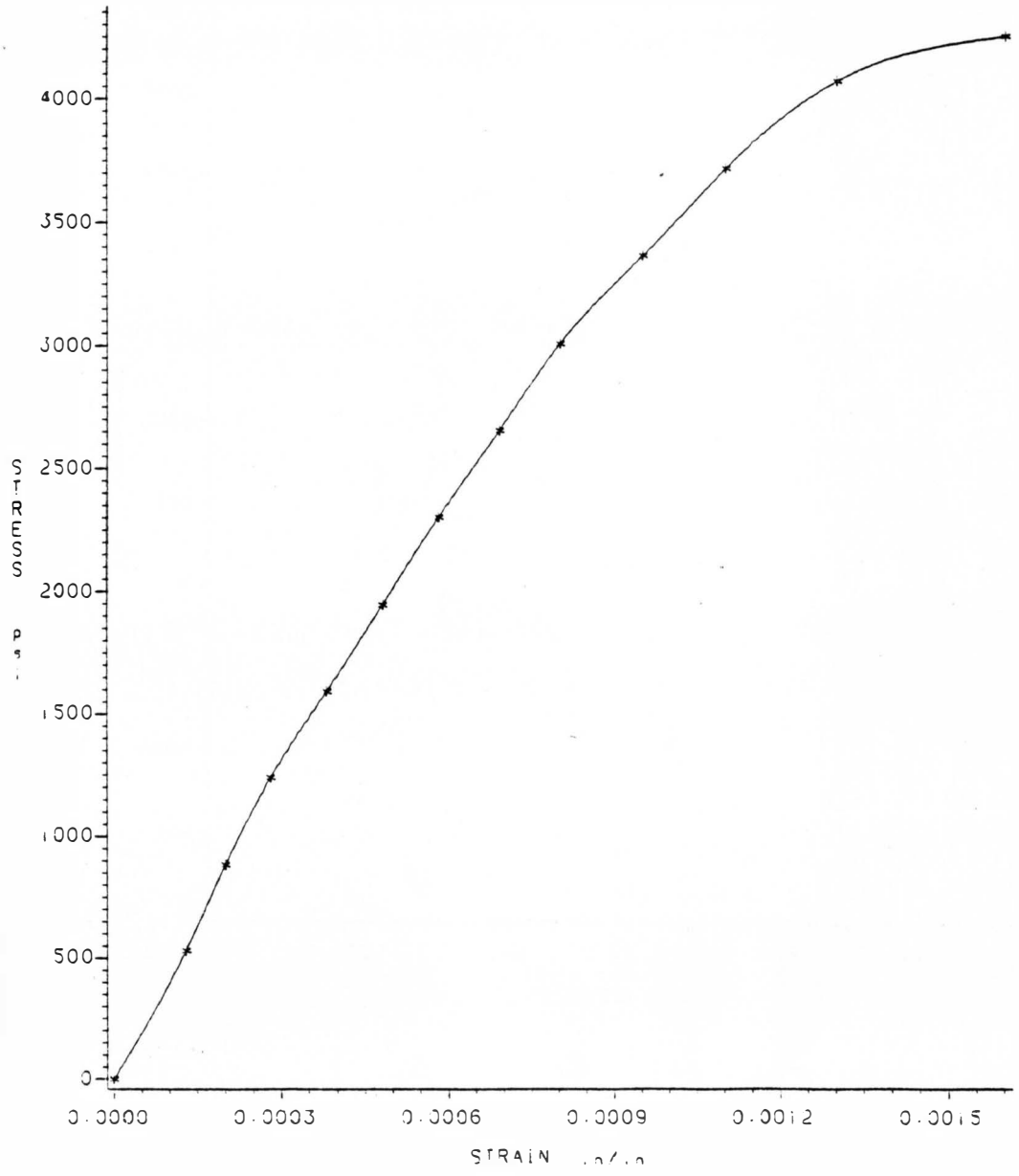

Figure 5.4 Stress vs. Strain

Figure 5.5

Modulus of elasticity of concrete
Cylinder C1
% Steel Fibers=0.8 fc'=5482 psi

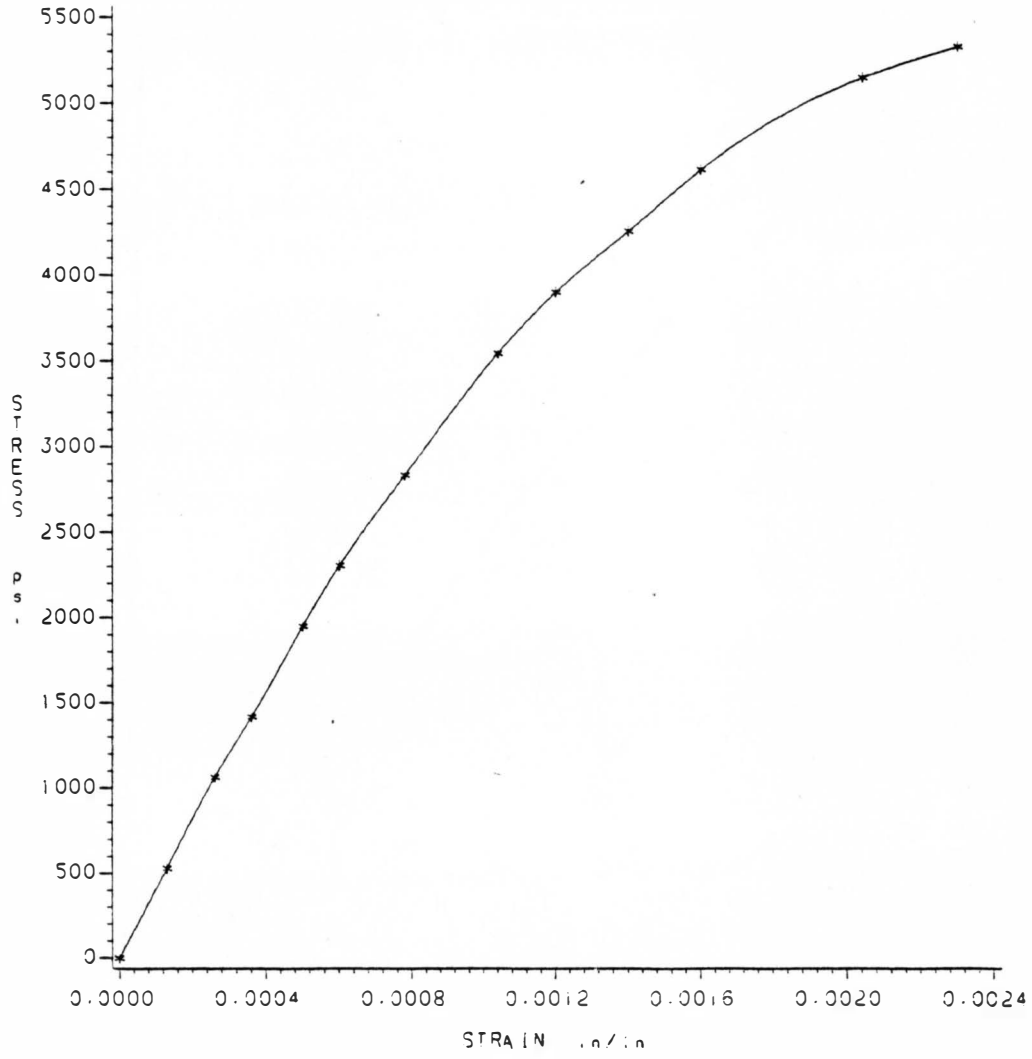

Figure 5.5 Stress vs. Strain

Figure 5.6

Modulus of elasticity of concrete
Cylinder C2,
% Steel Fibers=0.8 fc=5393 psi

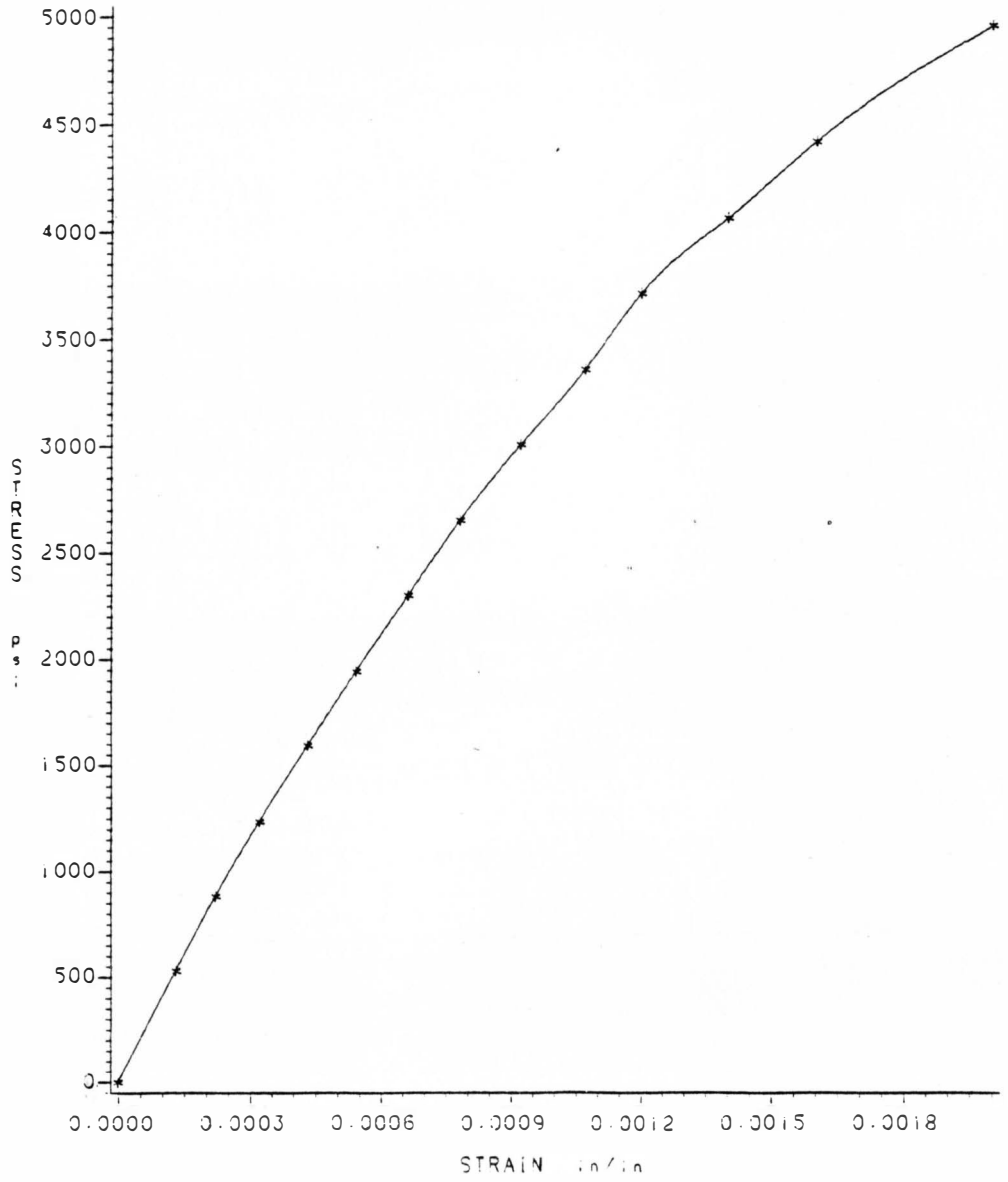

Figure 5.6 Stress vs. Strain

FIGURE 5.7

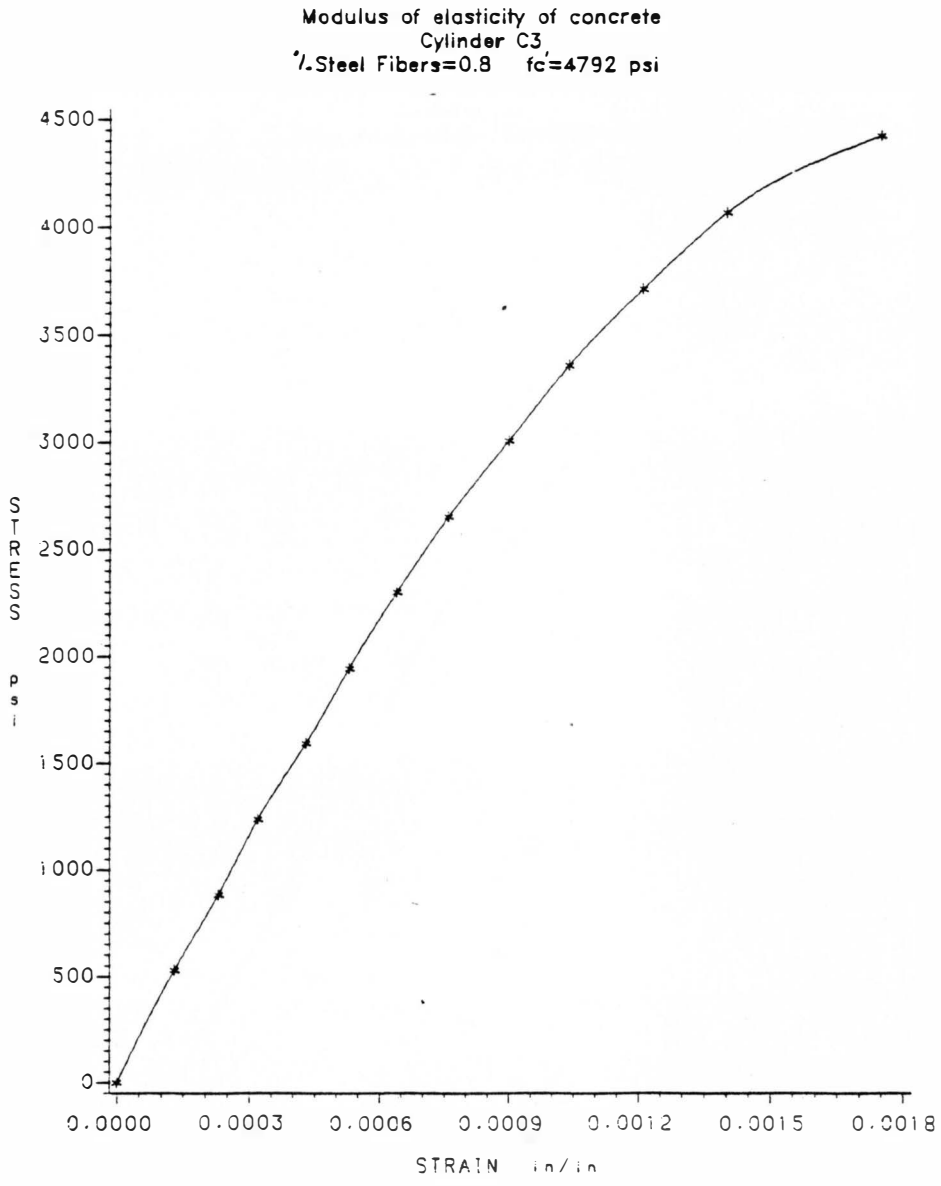

FIGURE 5.7 STRESS VS. STRAIN

Figure 5.8

Modulus of elasticity of concrete
Cylinder C4
% Steel Fibers=0.8 fc=4828 psi

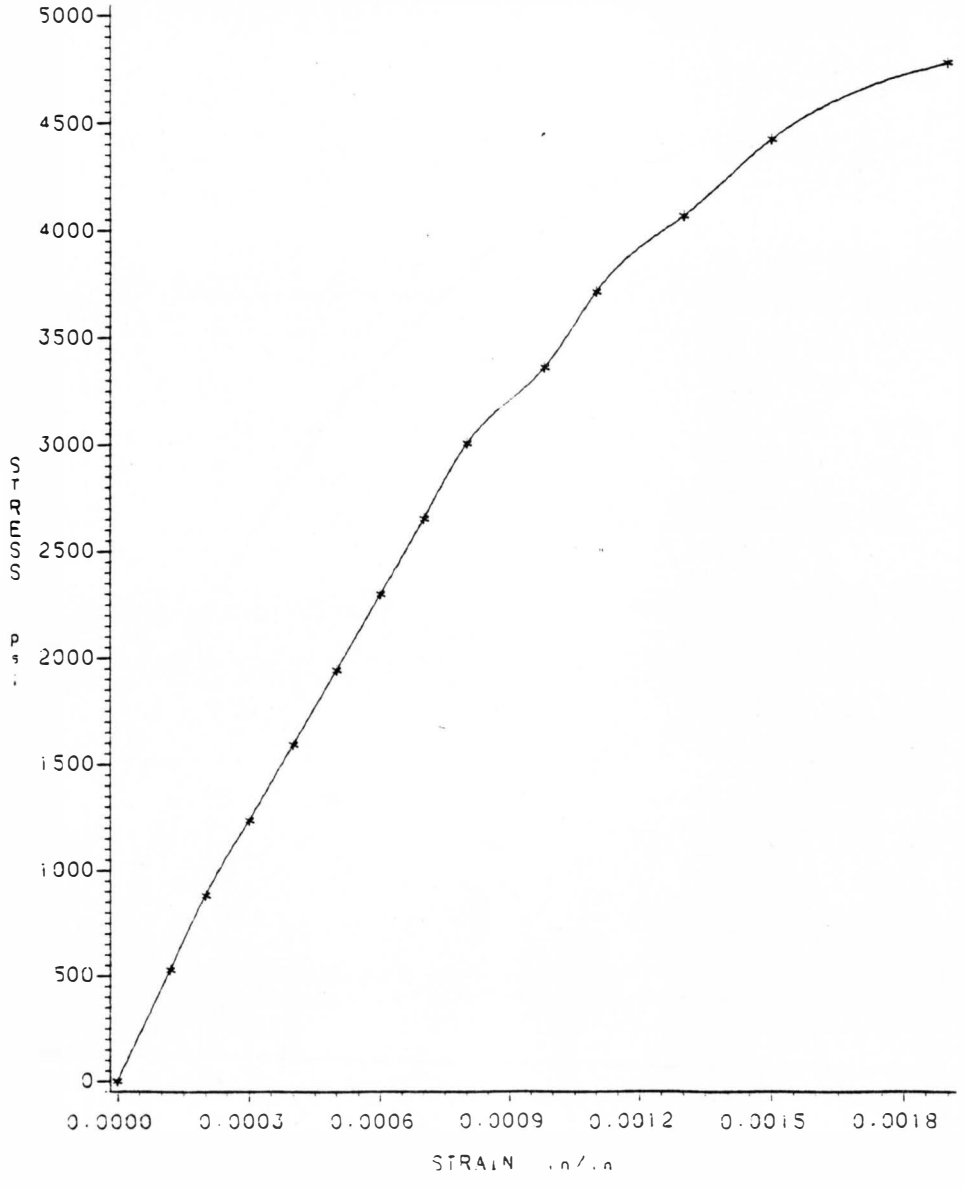

Figure 5.8 Stress vs. Strain

Figure 5.9

Modulus of elasticity of concrete
Cylinder C1
% Steel Fibers=1.2 fc'=5043 psi

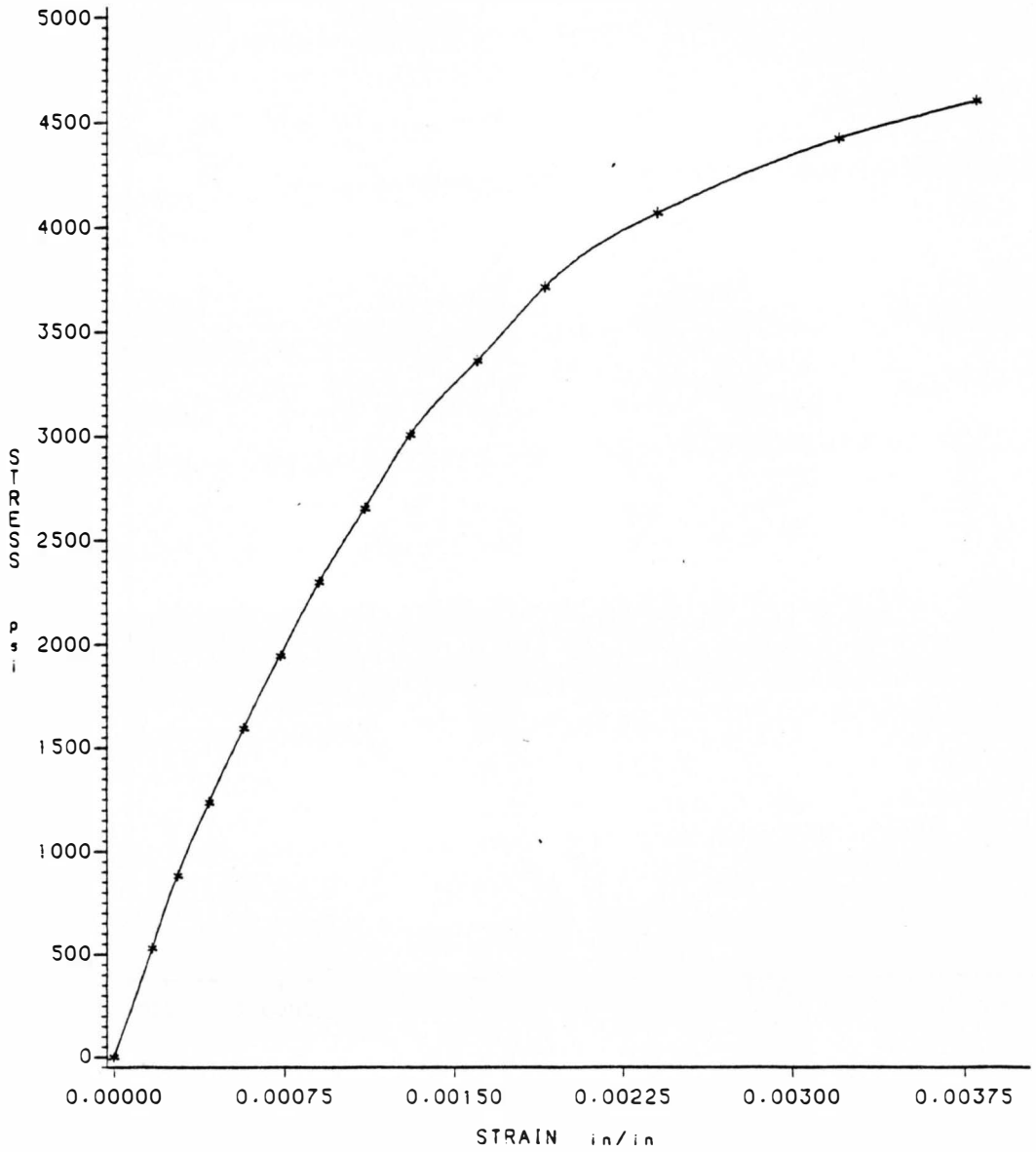

Figure 5.9 Stress vs. Strain

Figure 5.10

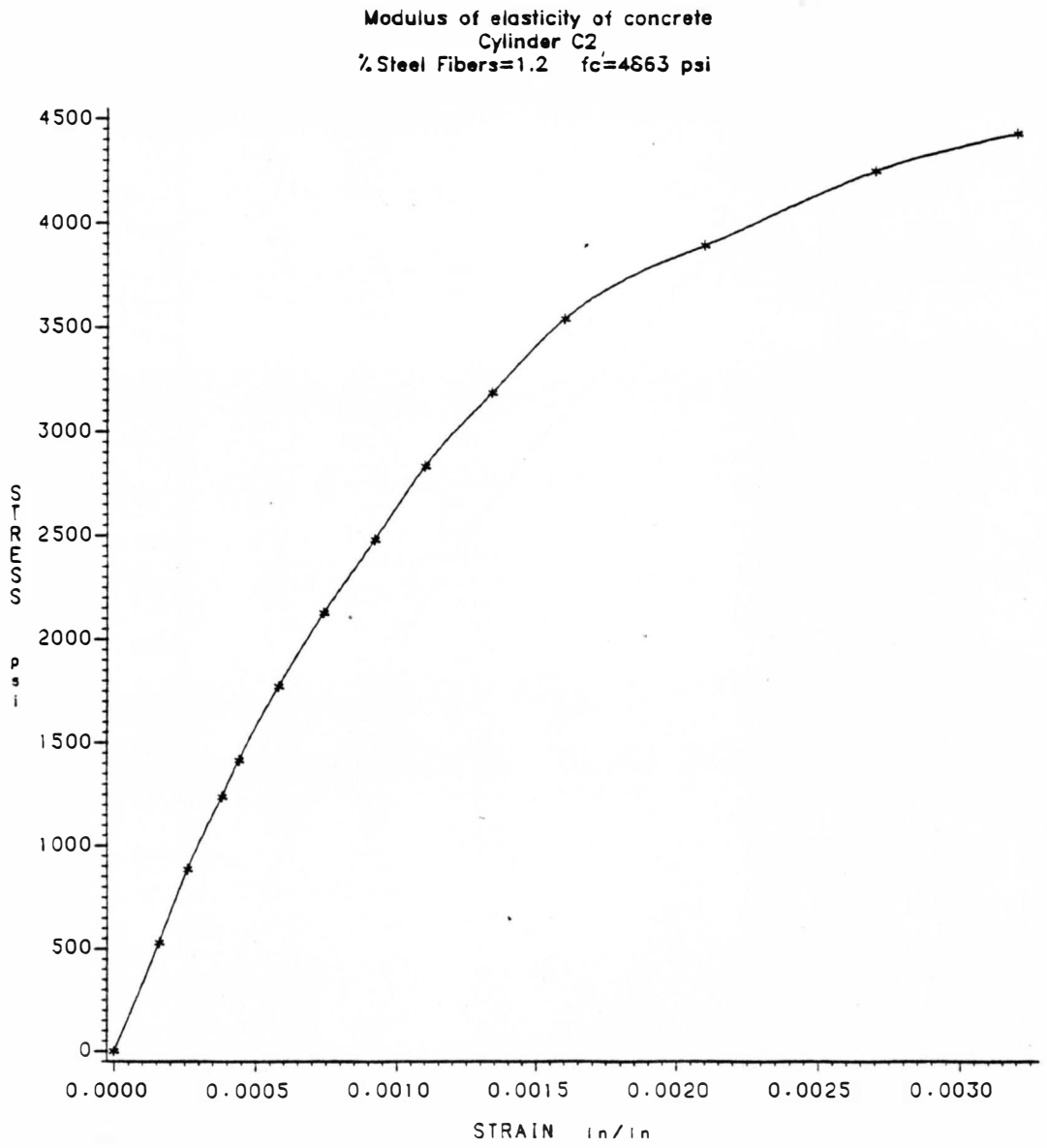

Figure 5.10 Stress vs. Strain

Figure 5.11

Modulus of elasticity of concrete
Cylinder C3
% Steel Fibers=1.2 fc'=4573 psi

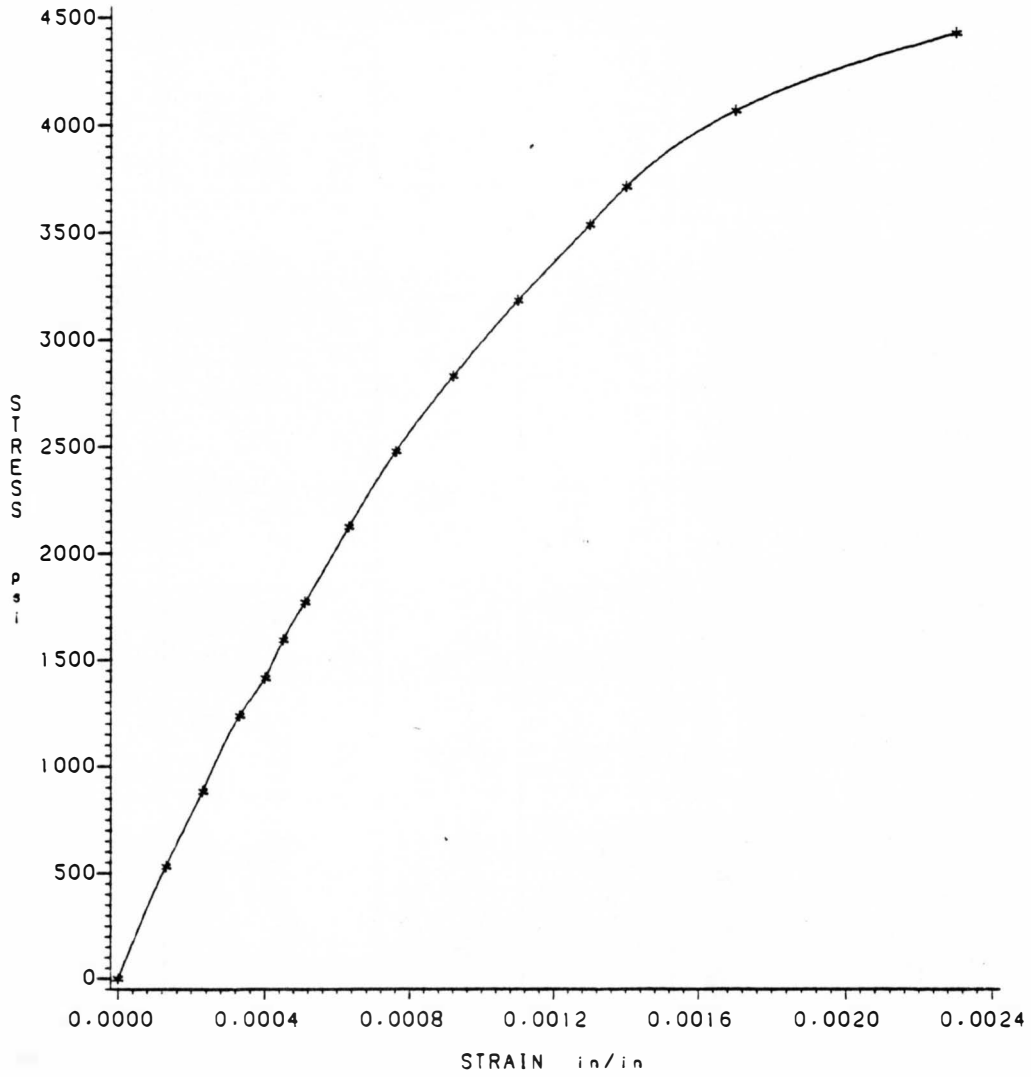

Figure 5.11 Stress vs. Strain

Table 5.2

Modulus of Elasticity of Concrete

Case	Cylinder	% Steel Fibers	Beams	f_c' (psi)	unit weight	$E_{ca} \times 10^6$ (psi)	$E_{cc} \times 10^6$ (psi) $=33w^{1.5}\sqrt{f_c'}$	% deviation from ACI *Code	average % deviation
I	C1	0	B1,B2,B3	4421	148.5	4.06	3.97	2.2	-0.33
	C2			4719	147.6	4.05	4.01	1.0	
	C3			4457	148.0	3.85	3.97	-3.1	
II	C1	0.8	B7,B8,B9	4828	152.6	3.83	4.32	-11.4	-14.00
	C2			4792	151.5	3.50	4.26	-17.8	
III	C2	1.2	B4,B5,B6	4863	151.8	2.71	4.30	-37.0	-30.00
	C3			4873	152.1	3.32	4.32	-23.0	

*% deviation $= \frac{E_{cc} - E_{ca}}{E_{ca}} \times 100$

Table 5.3

Effect of Steel Fiber on Modulus of Elasticity of Concrete

Case	Cylinder	% Steel Fiber	$E_{ca} \times 10^6$ psi	Average $E_{ca} \times 10^6$ (psi)	% decrease from 0% Fiber
I	C1	0	4.06	3.97	-
	C2		4.05		
	C3		3.80		
II	C1	0.8	3.83	3.67	- 7.6
	C2		3.50		
III	C2	1.2	2.71	3.02	-23.9
	C3		3.25		

reinforced concrete are of great importance because of crack control. The size and extent of cracks have to be limited to a maximum value because of possible deterioration of main steel from moisture seepage. The tensile strength of concrete is normally neglected in design calculations, nevertheless, the tensile strength of concrete members have a positive effect on deflections.

Split Cylinder Test (ASTM C-78) is a method used to determine the strength of concrete in tension. A 6x12 (in) cylinder similar to the ones for compression tests were used. The cylinder was placed in a compression-testing machine on its side and loaded uniformly along the two sides. The cylinders were loaded until failure occured and the results are shown in table 5.4. Plywood pads were placed between the loading plates and cylinders to ensure uniform pressure on specimens. The tensile stress existing in the cylinder is nearly uniform (Figure 5.12).

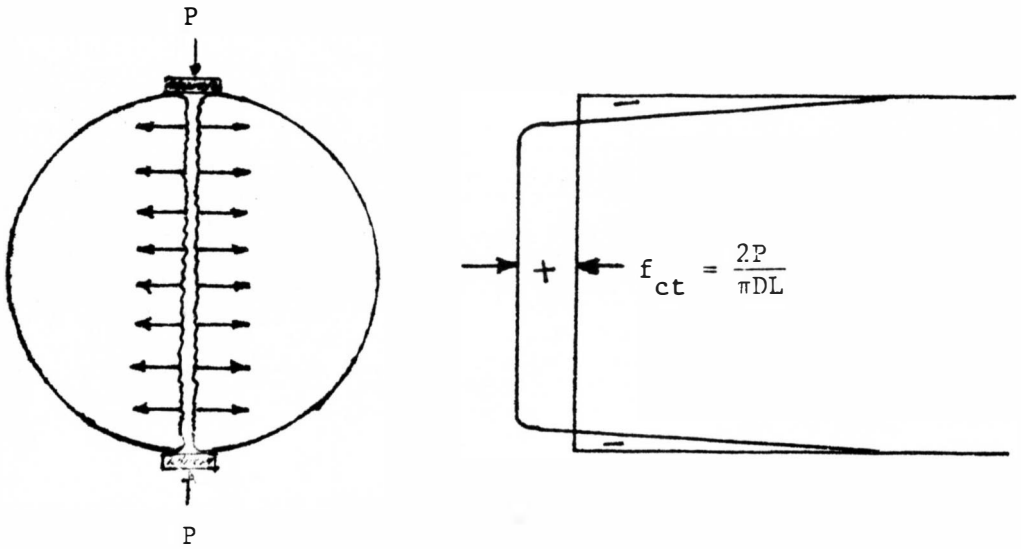

Figure 5.12 Stresses in Split Cylinder Test

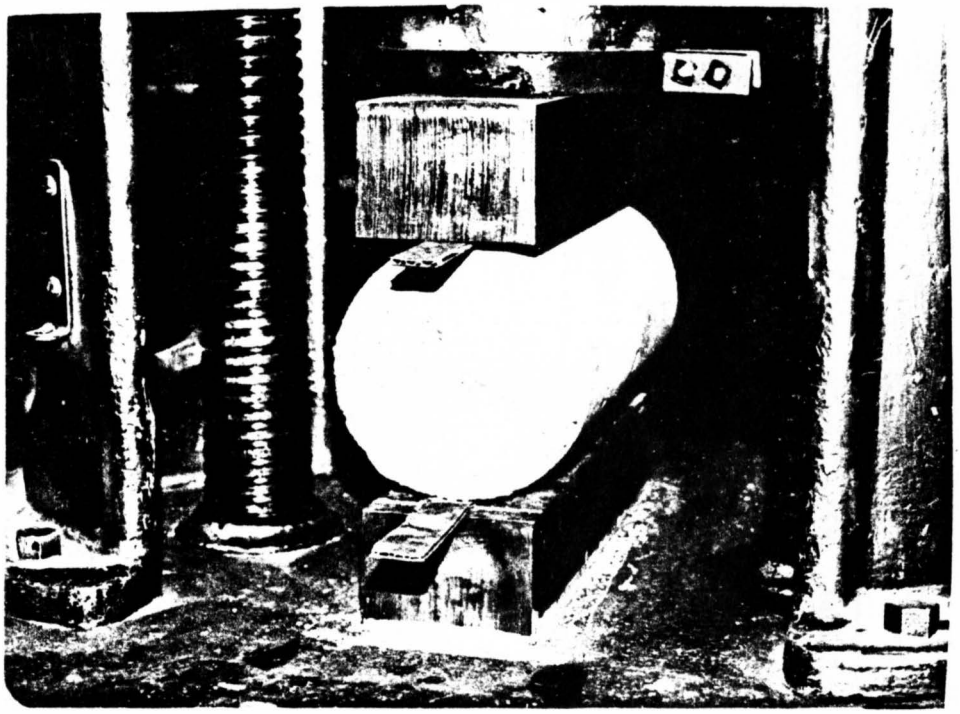

Figure 5.13 Split cylinder test set up

Table 5.4

Split Cylinder Test Results

Group	Cylinder	For Beams	% of Steel Fibers	unit weight (pcf)	f_c' (psi)	P_u (lbs)	$f_{cta} = \frac{2P}{\pi DL}$ (psi)	average f_{cta} (psi)	$f_{ct} = 6.7\sqrt{f_c'}$ (psi) from Code	% deviation from $6.7\sqrt{f_c'}$
I	C5	B1,B2,B3	0.0	147.5	4,584	49,390	436	433	454	- 4.6
	C6			147.0		48,400	428			
	C7			149.0		49,190	435			
II	C5	B7,B8,B9	0.8	151.6	4,805	63,200	559	555	465	+19.4
	C6			151.9		62,300	550			
III	C4	B4,B5,B6	1.2	155.2	4,927	71,540	632	635	470	+35.1
	C5			152.0		72,000	637			

As it is shown on Figure (5.12) the tensile stress is calculated by the following formula:

$$f_{cta} = \frac{2P}{\pi DL}$$

where:

P = applied load at failure

D = diameter of cylinder (in)

L = length of cylinder (in)

The experimental results can be compared to the following empirical equation:

$f_{ct} = 6\sqrt{f_c'}$ to $f_{ct} = 7\sqrt{f_c'}$ for normal weight concrete

The ACI Code suggests an average value of

$f_{ct} = 6.7\sqrt{f_c'}$ at an age of 28 days.

where:

f_{ct} = the split-cylinder tensile strength (psi)

f_c' = 28-day compressive strength (psi)

The effect of steel fibers on tensile strength of concrete is shown in table 5.5.

5.4 Modulus of Rupture

The modulus of rupture is the tensile strength of concrete in bending. This is used especially in deflection and crack control of reinforced concrete beams. The modulus of rupture f_r is computed from the general flexure formula $f = \frac{Mc}{I}$.

Table 5.5

Split Cylinder Test

(Effect of Steel Fiber on Tensile Strength)

Group	For Beams	% Steel Fibers	Average f_{cta} (psi)	% Increase From 0% Fibers
I	B1,B2,B3	0.0	433	-
II	B7,B8,B9	0.8	555	+28.2
III	B4,B5,B6	1.2	635	+46.7

In this experiment one 6x6x21 inch beam was prepared for each mix and tested in model S6 beam tester. A clear span of 18 inches was required according to ASTM Standards C78. The S6 model testing machine gave direct readings (psi) and the results were recorded and are shown in table 5.6 and the effects of steel fibers on modulus of rupture are shown in table 5.7.

The ACI Code section 9.5.2.3 accepts an average value for modulus of rupture $f_r = 7.5\sqrt{f_c'}$ where f_c' is the compressive strength of concrete.

5.5 Rotations

The concept of rotation capacity of reinforced concrete beams or frames is explained in chapter II. The methods used for measurement of actual rotations from testing are presented in this chapter and Appendix A.

Three methods were used for rotation measurements:

1) Brass studs were glued on the side of the beam as shown in figure (5.14).

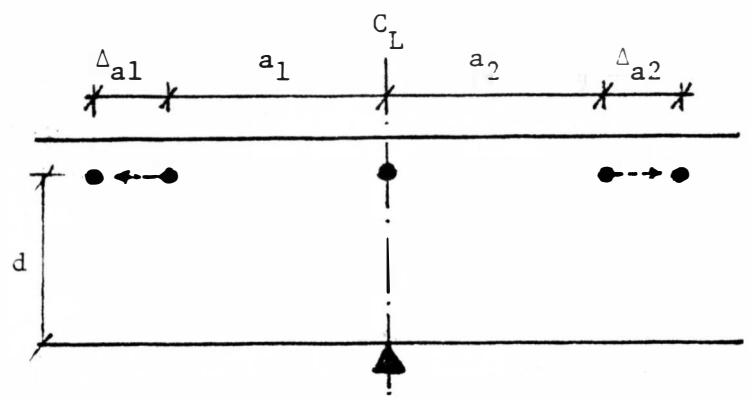

Figure 5.14 Curvature Measurement

Table 5.6

Modulus of Rupture (f_r) for Beams (6x6x21 in)

Group	Beams	For Beams	% Steel Fiber	unit weight (pcf)	f_c' (psi)	ACI Code $f_r=7.5\sqrt{f_c'}$	First Crack f_{rl} (psi)	First Crack % deviation from Code	Ultimate f_{ru} (psi)	Ultimate % deviation from Code
	BF1			149.8			525	+3	525	+3
I		B1,B2,B3	0.0		4,584	508				
	BF2			149.7			500	+2	500	+2
II	BF1	B7,B8,B9	0.8	150.8	4,805	520	670	+28.9	760	+46.2
III	BF1	B4,B5,B6	1.2	151.2	4,927	527	750	+42.3	900	+70.8

Table 5.7

Effect of Steel Fibers on Modulus of Rupture

Group	For Beams	% Steel Fibers	First Crack		Ultimate	
			f_{rl} (psi) average	% increase from 0% Fiber	f_{ru} (psi) average	% increase from 0% Fiber
I	B1,B2,B3	0.0	513	-	513	-
II	B7,B8,B9	0.8	670	+31	760	+48
III	B4,B5,B6	1.2	750	+46	900	+75

In this method the curvature is calculated by measuring the strain using the dial gage as discussed in chapter III. The curvature was calculated as follows:

$$\phi = \sum_{i=1}^{2} \frac{\Delta a_i}{a_i} \cdot \frac{1}{d} = \frac{1}{d} \sum_{i=1}^{2} \frac{\Delta a}{a} = \frac{1}{d} \left(\frac{\Delta a_1}{a_1} + \frac{\Delta a_2}{a_2}\right)$$

where: $\frac{\Delta a_i}{a_i}$ is the strain at the section. Δa was measured in 10^{-4} inches and "a" chosen to be 8 inches in this experiment.

d = effective depth of the section.

The rotation is the total curvature over a finite length. After the first yield of the main steel at the middle support, a plastic hinge is developed, figure (5.15). The approximate length of the hinge was measured 0.25 inches from the outside edge of the end cracks at the plastic hinge (figure 5.15).

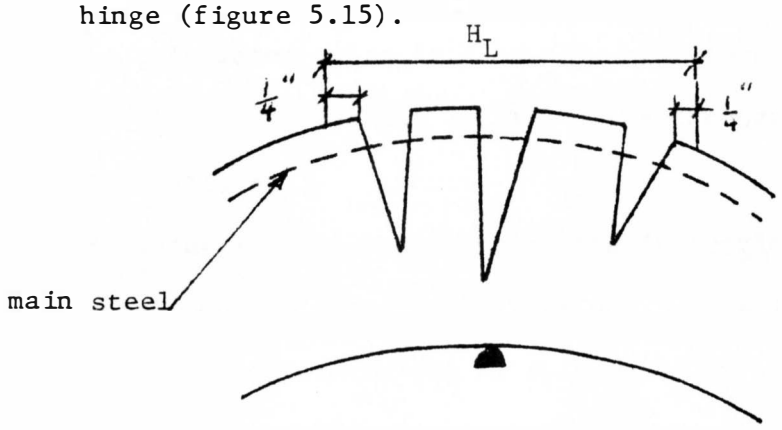

Figure 5.15 Plastic Hinge Length at Middle Support.

Therefore "θ" the total rotation over the hinge length is $\theta = \phi.H_L$. Results are in Appendix A Tables A.1 through A.8.

2) This method is theoretically the same as the previous method. The strains in steel and concrete were used to calculate the curvature as follows:

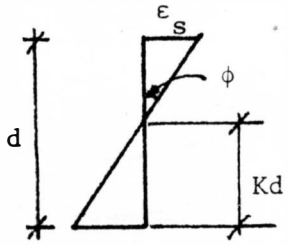

Strain Diagram

where $\phi = \frac{\varepsilon_c}{kd} = \frac{\varepsilon_s}{d(1-k)} = \frac{\varepsilon_c+\varepsilon_s}{d}$

This method is not used for measuring plastic rotations after the first yield of steel, because the strain gages on the steel do not function after the yield of steel, therefore the plastic rotation would be impossible to be calculated using this method. The results up to the first yield are shown in tables A.9 through A. 18 (Appendix A).

3) By using a level and a scale, the deflections at different points on the beams was determined. This is an approriate method to determine the elastic curve. The most important advantage of this procedure was that the plastic deformation (hinge angle) was directly calculated. Figure (5.16) shows the different stages that the beams went through.

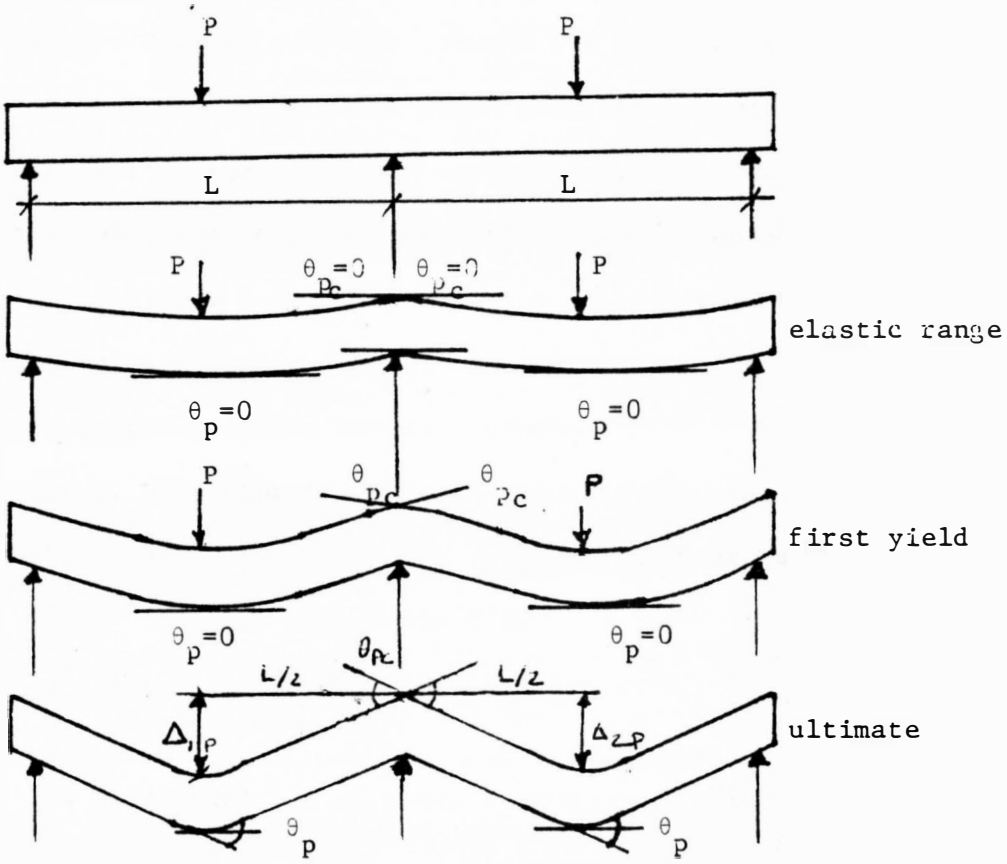

where:

$$\theta_{pc} = \frac{\Delta_{1p}}{L/2} + \frac{\Delta_{2p}}{L/2} \quad (\Delta_{1p} + \Delta_{2p} \text{ are plastic deflections})$$

Δ_1 and Δ_2 are obtained from Appendix B tables B.1 through B.3.

Figure 5.16 Loading Stages

From figure 5.16, it can be seen that by using the differences between the level readings, the elastic curve of the beam and also the inelastic deformation and finally the plastic rotation can be determined. The level readings are shown in Appendix B tables B.1 to B.3. The tangent line drawn to the curve at the critical section shows "θ" the angle of rotation at each section.

The elastic portion of the beam between the plastic hinges is assumed to be a straight line, in other words these portions are not taking any stresses after plastic hinge development. The calculated experimental and required plastic rotations are presented in table 5.9.

As mentioned before, there is no exact method for the calculation of plastic hinge length. An estimated value of 0.5d - 1.3d is suggested from previous research studies.[10,17] In this research project actual hinge lengths were measured to the nearest one half inch as shown in figure 5.15. The results are recorded in table 5.8.

Table 5.8

Plastic Hinge Lengths

Beam	% Main Steel	% Steel Fibers	Plastic Hinge Length H_L (inches
		0.0	8.0
2#3	0.67	0.8	6.5
		1.2	7.5
		0.0	7.0
2#4	1.21	0.8	8.0
		1.2	-
		0.0	6.5
2#5	1.89	0.8	8.0
		1.2	9.0

Sample Calculation for table 5.9

Beam with 2#3 main steel and 0.0% steel fibers:

Plastic moment = 10 P_u (P_u is from table 4.2)

= 10 x 10.7 = 107 Kip-in

Fixed-end moment = $\frac{P_u.L}{8} = \frac{10.7 \times 60}{8}$ = 80.3 Kip-in

$$K = \frac{Kd}{d}$$

where:

$\overline{Kd}$ is calculated from the following:

$$\frac{b\overline{Kd}^2}{2} - n A_s (d-\overline{Kd}) = 0$$

$$2.5 (\overline{Kd})^2 + 1.66 \overline{Kd} - 10.89 = 0$$

$$Kd = 1.78 \text{ in}$$

$$K = \frac{1.78}{6.56} = 0.271$$

$$K_u = \frac{K_u d}{d}$$

where $K_u d = \frac{a}{0.85}$

and $\frac{A_s f_y}{0.85 f_c' b} = \frac{0.22 \times 66.8}{0.85 \times 4.58 \times 5} = 0.755$ in

$$K_u d = \frac{0.755}{0.85} = 0.888 \text{ in}$$

$$K_u = \frac{0.888}{6.56} = 0.135$$

$$I = \frac{b\overline{Kd}^3}{3} + n A_s (d-\overline{Kd})^2$$

$$= \frac{5(1.78)^3}{3} + 7.55 \times 0.22\ (6.56 - 1.78)^2 = 47.35\ in^4$$

$$I_p = \frac{b\overline{K_u d}^3}{3} + n\ A_s\ (d - K_u d)^2$$

$$= 5 \times \frac{(0.888)^3}{3} + (7.55)(0.22)(6.56 - 0.888)^2 = 54.60\ in^4$$

To calculate the required rotation using equation (2.5), the smaller value of moment of inertia is used to require higher rotations.

$$\theta = \frac{L}{6EI}\ [2(M_A - M_{AF}) + (M_B - M_{BF})]$$

$$\theta = \frac{60}{6 \times 3.97 \times 10^3 \times 47.35}\ [2(-107+80.3)+(0+80.3)] = 14.31 \times 10^{-4} \text{ radians}$$

Rotation capacity using equation 2.6:

$$\theta_{P1} = \frac{\varepsilon_{cu}}{K_u} - \frac{f_y}{E_s(1-K_u)}$$

$$\theta_{P1} = \frac{0.0035}{0.135} - \frac{66.8}{30 \times 10^3 (1-0.135)} = 232 \times 10^{-4} \text{ radians}$$

Actual rotations were obtained from tables A.1 through A.8 in Appendix A.

Table 5.9

Required and Available Rotation Capacity

Beam	% Main Steel	% Steel Fibers	f_y Ksi	f_c' Ksi	Plastic Moment Kip in	Fixed End Moment Kip-in	I in^4	Ip in^4	K	K_u	Required Rotation Using Equation (2.5) (radians)$\times 10^{-4}$	Rotation Capacity Using Equation (2.6) (radians)$\times 10^{-4}$	Actual Rotation At Ultimate From Testing (radians)$\times 10^{-4}$
		0.0	66.8	4.58	107	80.3	47.35	54.6	0.271	0.135	14.31	232	298
2#3	0.67	0.8	66.8	4.81	107	80.3	50.4	59.7	0.280	0.129	14.54	245	1277
		1.2	66.8	4.93	110	82.5	62.0	77.9	0.312	0.126	15.73	251	1924
		0.0	70.8	4.58	190	142.5	74.2	76.4	0.313	0.257	16.10	102	145
2#4	1.21	0.8	70.8	4.81	191	143.3	77.9	83.6	0.358	0.244	16.75	111	781
		1.2	70.8	4.93	192	144.0	94.0	107.8	0.400	0.239	18.10	114	-*
		0.0	51.9	4.58	211	157.9	97.2	106.1	0.410	0.297	13.4	93	238
2#5	1.89	0.8	51.9	4.81	212	159.0	102.5	116.4	0.424	0.283	14.1	98	876
		1.2	51.9	4.93	213	159.4	121.8	150.0	0.466	0.276	15.2	102	1495

*premature failure

Another important factor involving the calculation of plastic rotations is the curvature distribution factor 'β'. The curvature along the plastic hinge varies significantly and in most rotation estimations this factor is ignored which leads to over-estimation of the plastic rotations. Therefore the rotation capacity of a section is less than what expected (chapter II). The curvature distribution factor was calculated for each beam in this experiment and recorded in table 5.10. θ_{Pc} calculation is shown in figure 5.16 which is the slope of the tangent to the beam at the middle support at failure.

Table 5.10

Curvature Distribution Factor

Beam	% Main Steel	% Steel Fiber	θ_{Pc} x10^{-4} radians	ϕ_P	H_L (in)	$\phi_P . H_L$ x10^{-4} radians	$\beta = \frac{\theta_{Pc}}{\phi . H_L}$
		0.0	175	37.32	8.0	298	0.59
2#3	0.67	0.8	559	196.50	6.5	1277	0.44
		1.2	616	256.60	7.5	1924	0.32
		0.0	78	20.60	7.0	145	0.54
2#4	1.21	0.8	352	97.60	8.0	781	0.45
		1.2	-	-	-	-	-
		0.0	127	36.60	6.5	238	0.53
2#5	1.89	0.8	385	109.00	8.0	876	0.44
		1.2	554	166.00	9.0	1495	0.37

The actual Moment-Curvature diagrams are shown in figures (5.17) through (5.24) for different main steel and steel fiber reinforcements. The curvature was measured using actual strains using method 1 in figure 5.14 and the moment was determined from the actual load applied on the beams from Tables A.1 through A.8.

5.6 Deflection

5.6.1 Discussion

Deflections of reinforced concrete structures have to be limited for the following reasons:

1) Control of cracking: high deflections could lead to excessive large cracks at service loads.
2) Structural appearance: if slabs and beams are subjected to high deflections the appearance of the structure is damaged and could frighten the occupants although the structure is safe.
3) Poor fitting of door frames, windows and partitions.
4) Excessive vibrations: any structure has to be free of excessive vibration to ensure trust in the building and a sense of security.

In order to have a serviceable structure with small deflections, it has to have adequate rigidity or stiffness to minimize the preceding problems. The flexural rigidity of reinforced concrete consists of modulus of elasticity and moment of inertia of the section. However, there is a problem calculating the moment of inertia of reinforced

Figure 5.17

Moment–Curvature relationship
Main Steel=2#3 %Steel Fibers=0.0
Beam B1

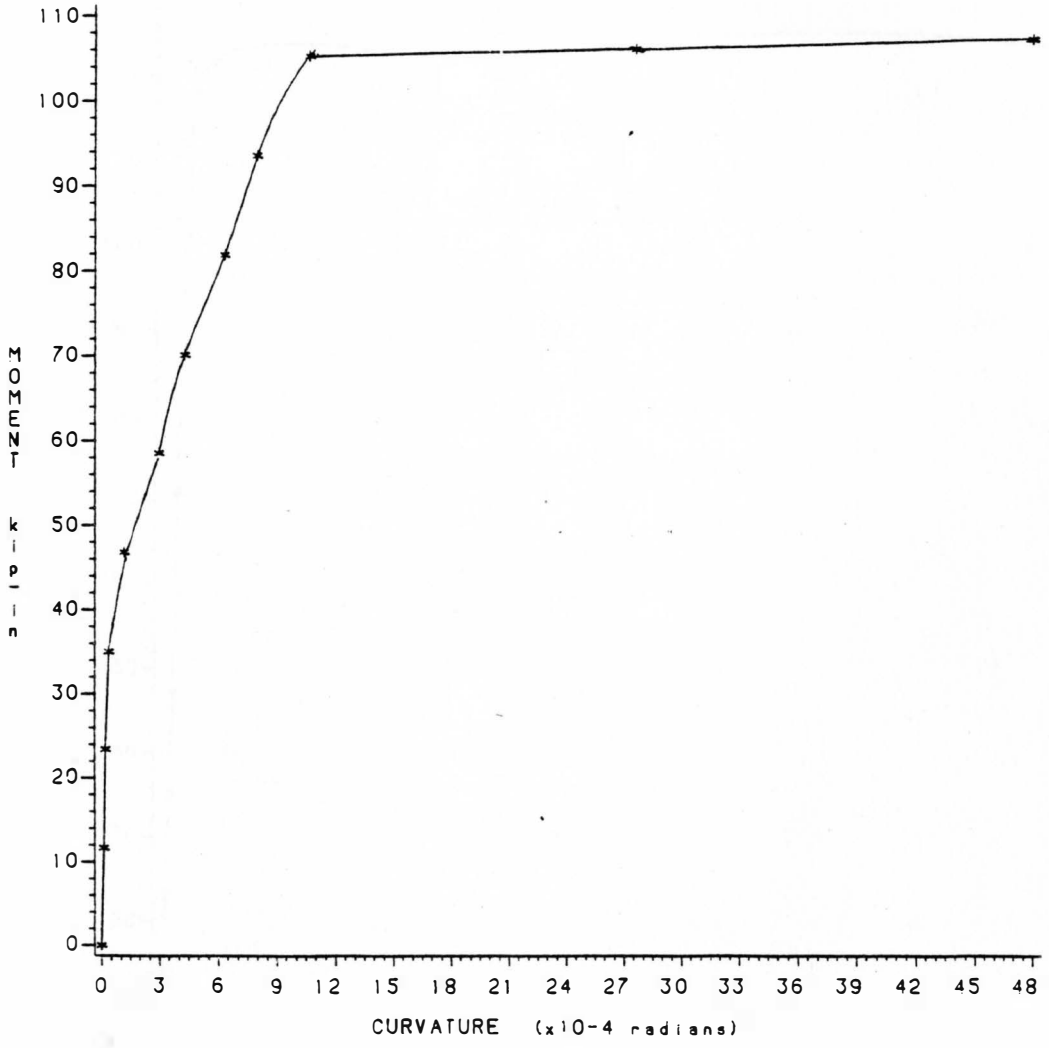

Figure 5.17 Moment–Curvature

Figure 5.18

Moment–Curvature relationship
Main Steel=2#3 %Steel Fibers=0.8
Beam B7

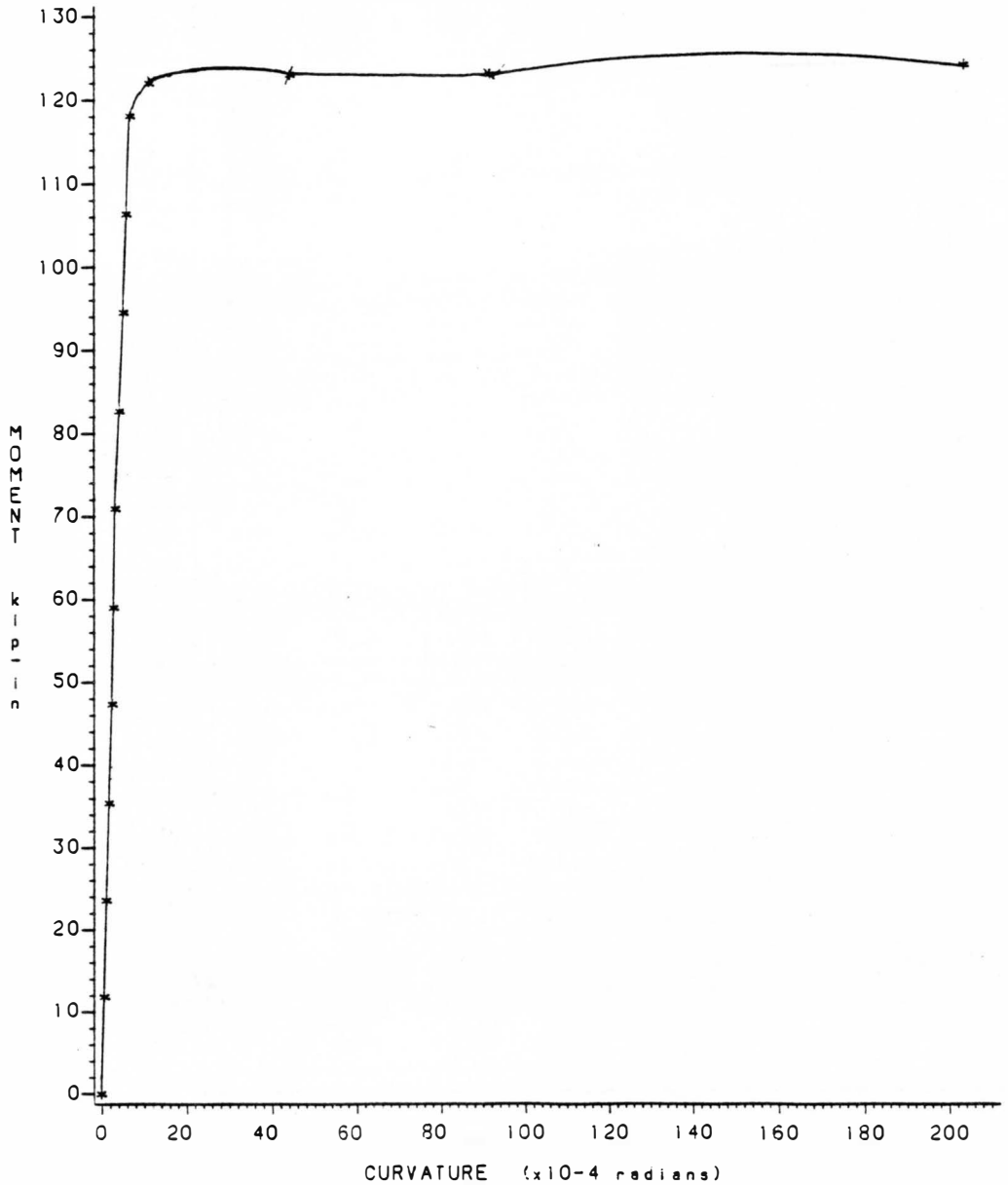

Figure 5.18 Moment–Curvature

Figure 5.19

Moment–Curvature relationship
Main Steel=2#3 %Steel Fibers=1.2
Beam B4

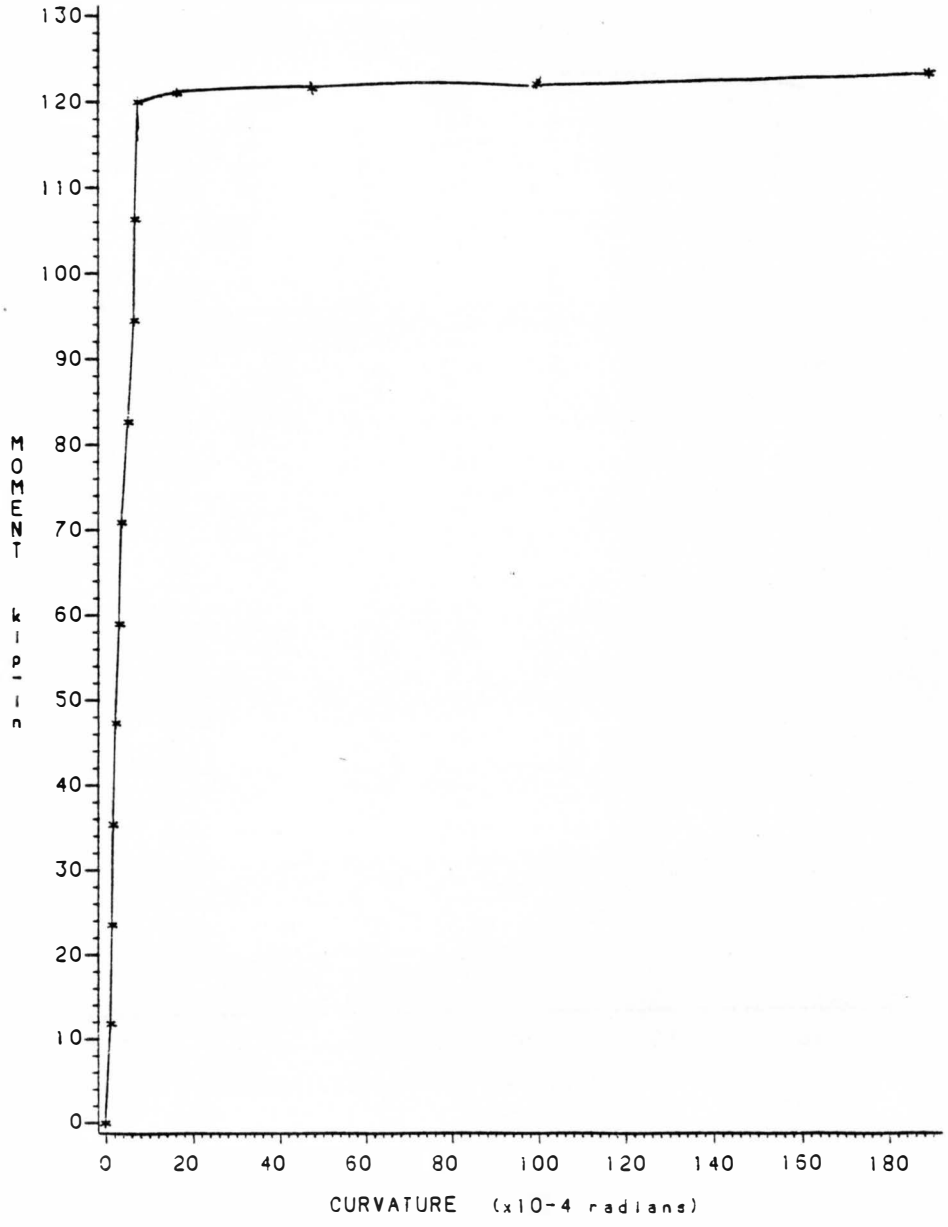

Figure 5.19 Moment–Curvature

Figure 5.20

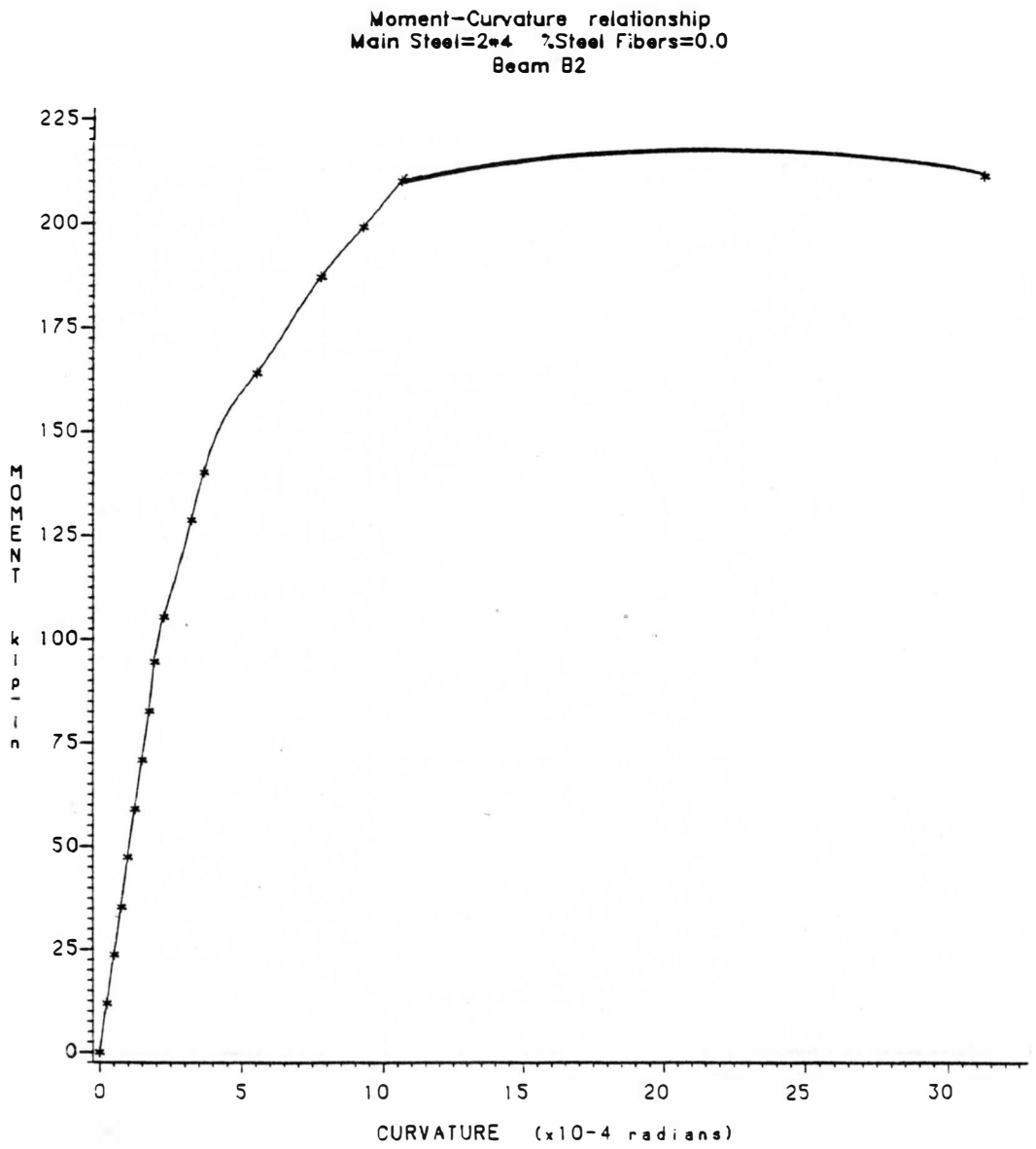

Figure 5.20 Moment-Curvature

Figure 5.21

Moment–Curvature relationship
Main Steel=2#4 %Steel Fibers=0.8
Beam B8

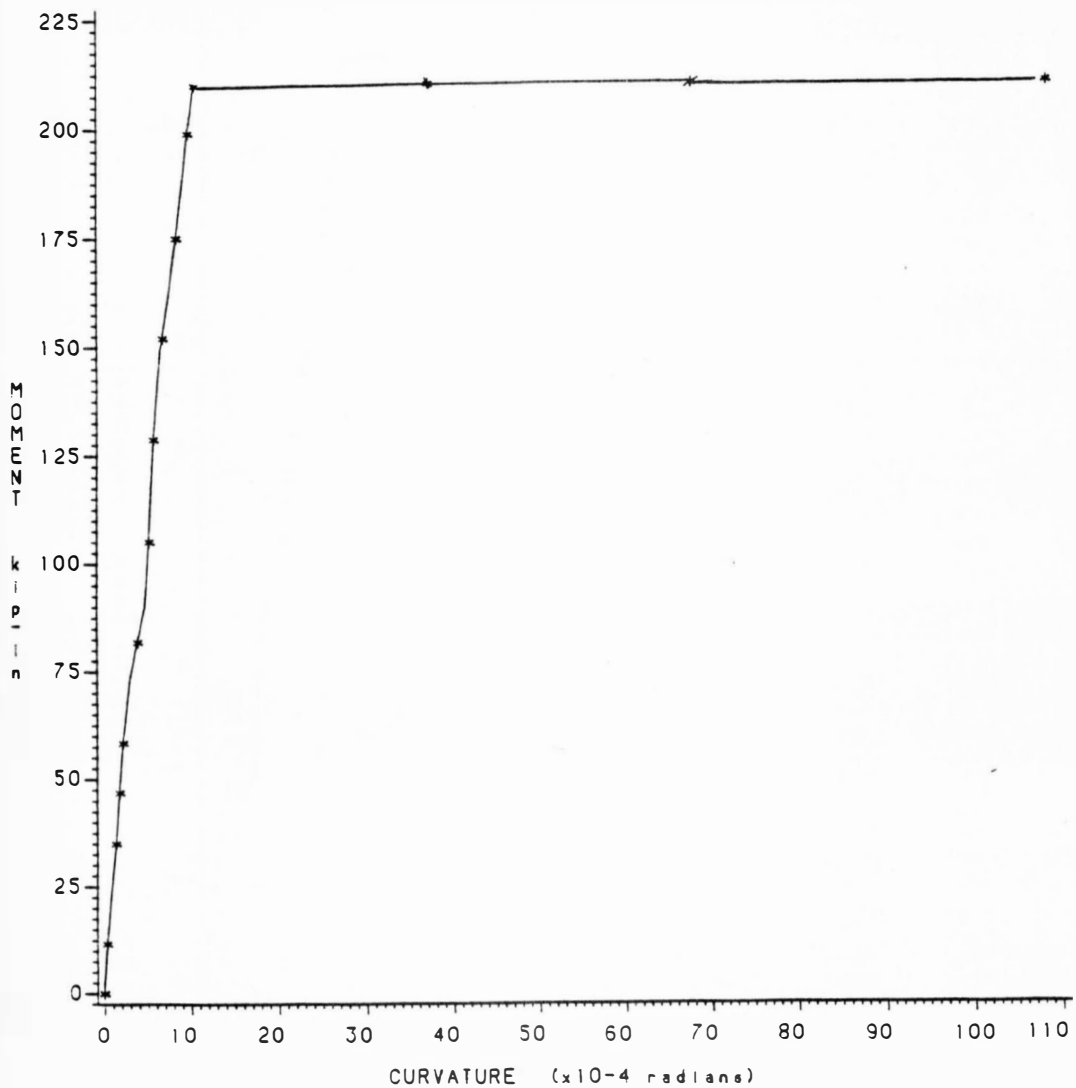

Figure 5.21 Moment–Curvature

Figure 5.22

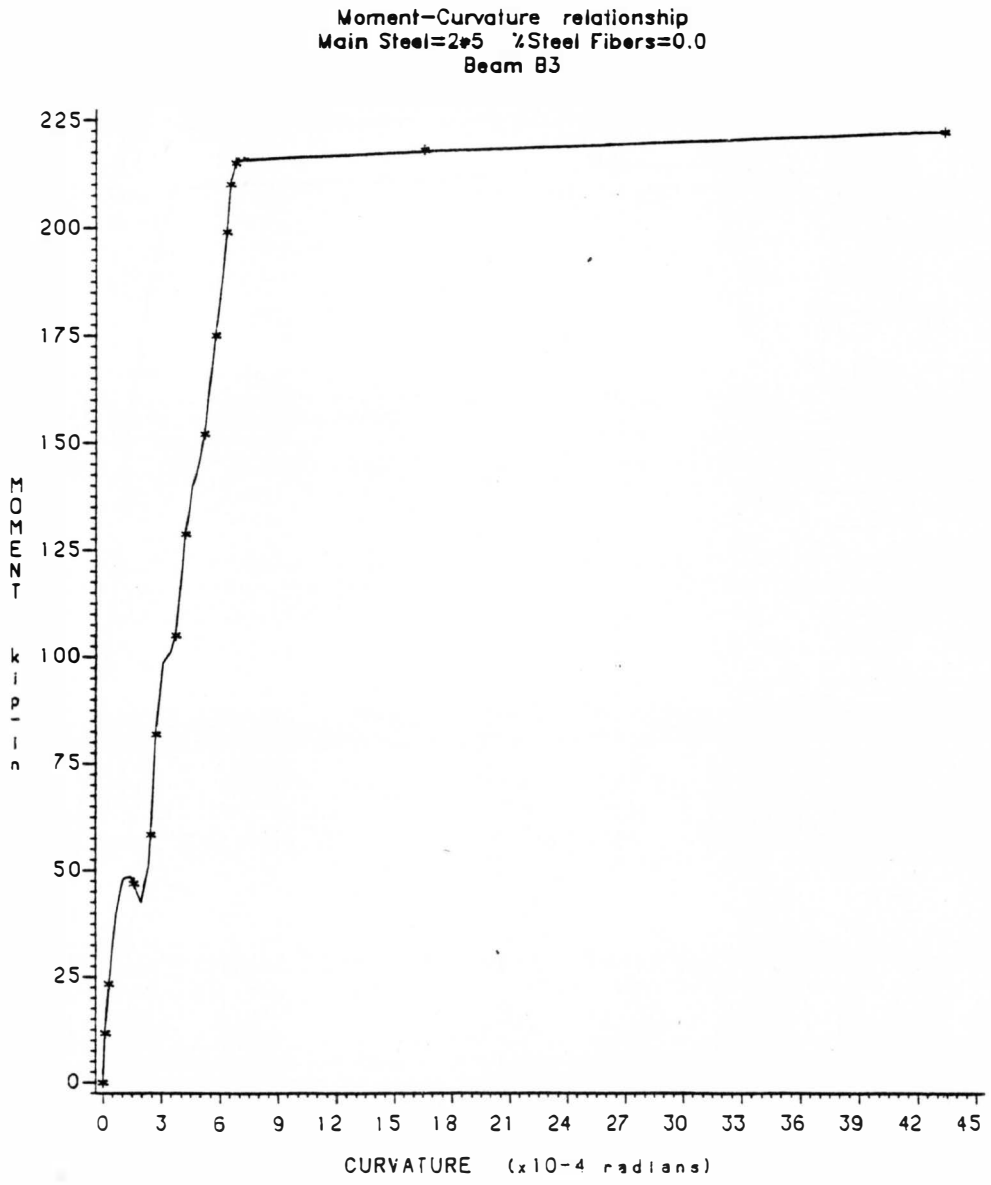

Figure 5.22 Moment-Curvature

Figure 5.23

Moment–Curvature relationship
Main Steel=2#5 %Steel Fibers=0.8
Beam B9

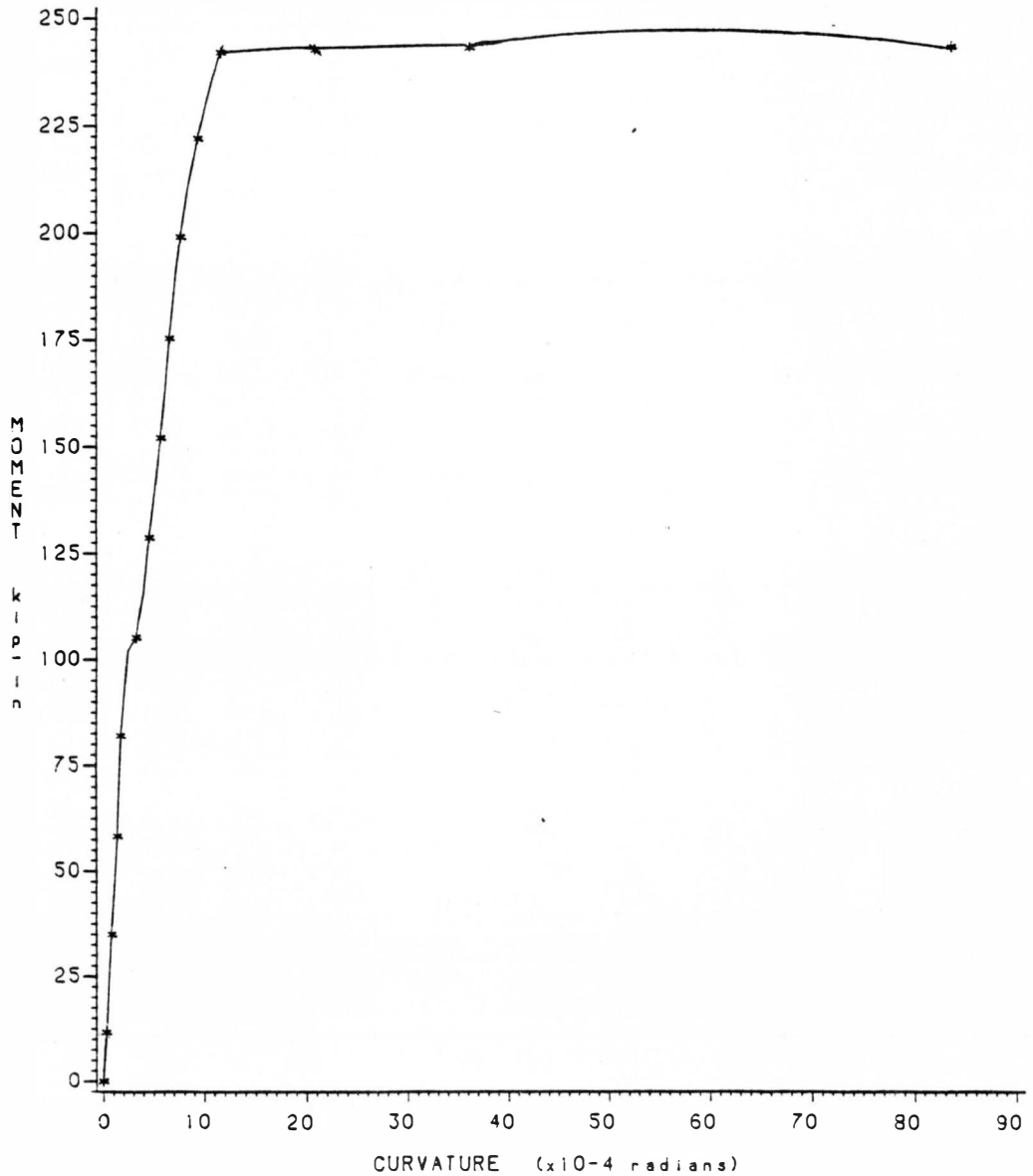

Figure 5.23 Moment–Curvature

Figure 5.24

Moment–Curvature relationship
Main Steel=2#5 %Steel Fibers=1.2
Beam B6

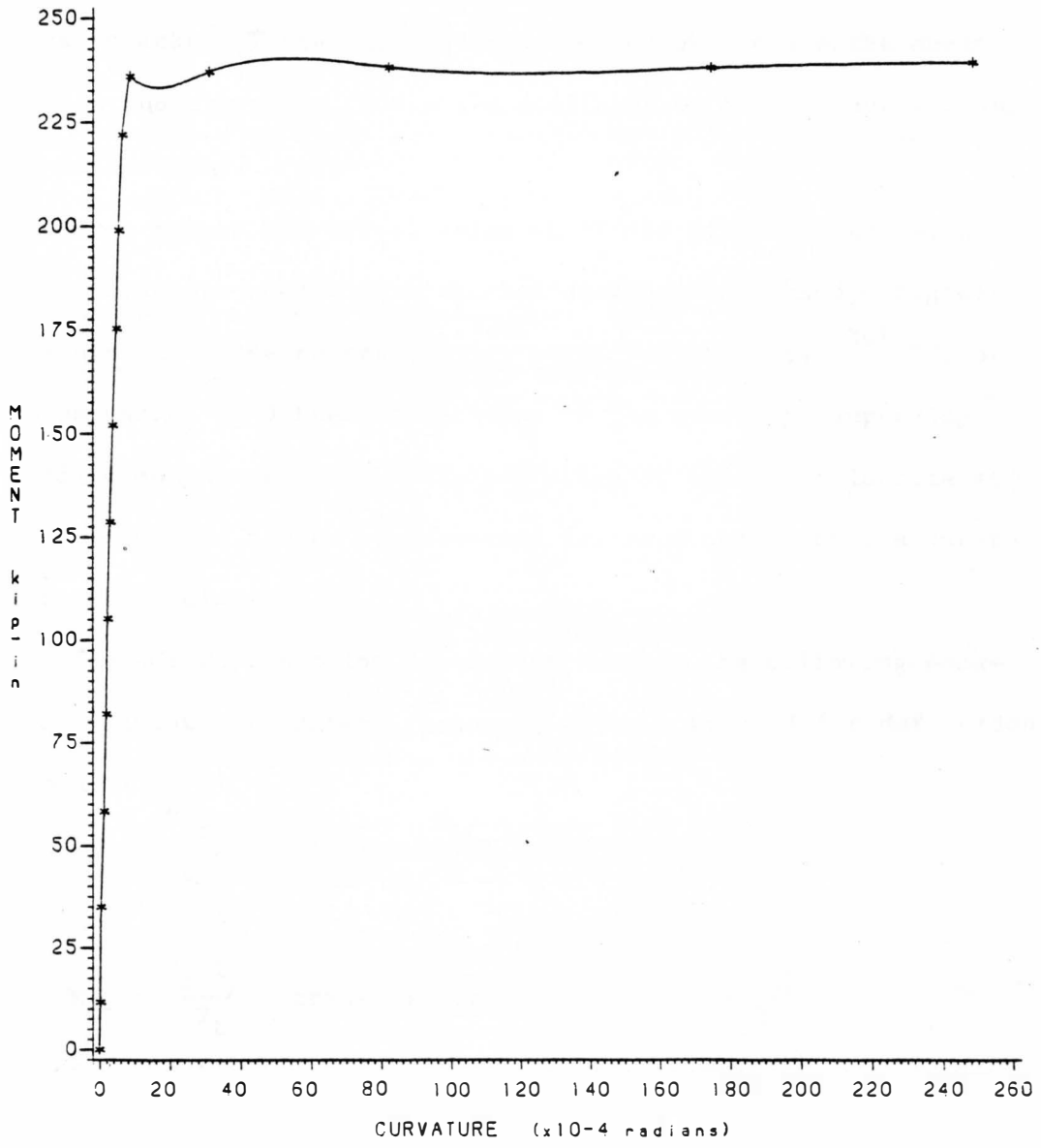

Figure 5.24 Moment–Curvature

concrete section. If the bending moment at the section is less than cracking moment (M_{cr}), the gross moment of inertia (I_g) is used. The problem exists when the bending moment exceed the cracking moment and cause cracks. These unknown amount of cracks reduce the moment of inertia and therefore reduce the stiffness of the section causing higher deflections.

As a result the actual value of 'I' is difficult to calculate. Usually a concrete member in a cracked section would have a rigidity of one-third to three fourths of its uncracked rigidity.(30) Flexural stiffness varies in different sections of the structure depending on the bending moment present. This variation of moment of inertia at different sections has to be accounted for in order to have accurate deflection calculations.

The ACI Code section 9.5.2.3 recommends the following equation to calculate the effective moment of inertia used for deflection calculations.

$$I_e = \left(\frac{M_{cr}}{M_a}\right)^3 I_g + \left[1 - \left(\frac{M_{cr}}{M_a}\right)^3\right] I_{cr}$$

where:

$M_{cr} = \frac{f_r I_g}{y_t}$ cracking moment

$f_r = 7.5\sqrt{f_c'}$ modulus of rupture (for normal weight concrete)

I_g = gross moment of inertia neglecting steel

I_{cr} = transformed moment of inertia for cracked section

The maximum permissible computed deflections by the ACI Code are shown in table 9.5(b) of the ACI Code. In this case $\frac{L}{360}$ is used for members not supporting or attached to nonstructural elements likely to be damaged by large deflections.

5.6.2 Theoritical Deflection Calculations

The theoritical deflection is calculated using the following method.

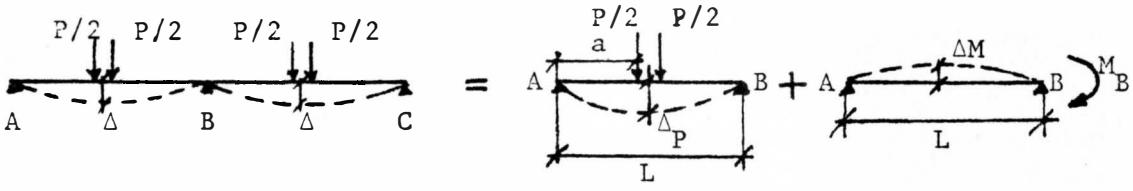

By using superposition the algebraic summation of the two deflections is the correct value.

$$\Delta_P = \frac{\frac{P}{2}\ L^3}{48\ EI_e}\ \left[\frac{3a}{L} - 4\left(\frac{a}{L}\right)^3\right]$$

where a = 0.45L

$$\Delta_{P_{max}} = 2\ \frac{\frac{P}{2}\ L^3}{48\ EI_e}\ \left[\frac{3x0.45L}{L} - 4\left(\frac{0.45L}{L}\right)^3\right]$$

$$= 2 \times 0.9855\ \frac{\frac{P}{2}\ L^3}{48\ EI_e} = 0.020\ \frac{PL^3}{EI_e}$$

$$\Delta_M = \frac{ML^2}{16\ EI_e}$$

where M_B = 11.25 P = 0.1875 PL

$$\Delta_M = -\frac{0.1875\ PL^3}{16\ EI_e} = -0.01\ \frac{PL^3}{EI_e}$$

$$\Delta_{max} = \Delta_{P_{max}} + \Delta_{M_{max}} = 0.01\ \frac{PL^3}{EI_e}$$

Calculation of deflections at service load:

For Beam 1 2#3 main bars and 0% steel fibers

$A_s = 0.22\ in^2$

$d = 6.56\ in$

$$n = \frac{E_s}{E_c} = \frac{30 \times 10^6}{3.97 \times 10^6} = 7.55$$

$b = 5\ in$

$$\frac{b\ \overline{Kd}^2}{2} - n\ A_s\ (d - \overline{Kd}) = 0$$

$$2.5\ \overline{Kd}^2 + 1.66\ \overline{Kd} - 10.89 = 0$$

$Kd = 1.78\ in$

$$I_{cr} = \frac{b\ \overline{Kd}^3}{3} + n\ A_s\ (d - Kd)^2$$

$$I_{cr} = \frac{5 \times (1.78)^3}{3} + 7.55 \times 0.22\ (6.56 - 1.78)^2 = 47.35\ in^4$$

$$I_g = \frac{1}{12}.b.h^3 = \frac{1}{12} \times 5 \times (8)^3 = 213.33\ in^4$$

$$M_{cr} = \frac{f_r.I_g}{y_t} = \frac{513 \times 213.33}{4} = 27.36\ Kip\text{-}in$$

$$M_a = 9.4\ P = 9.4 \times (0.6\ P_u) = 9.4 \times 7.0 = 65.8\ K\text{-}in$$

$$(\frac{M_{cr}}{M_a})^3 = (\frac{27.36}{65.8})^3 = 0.072$$

$$I_e = \left(\frac{M_{cr}}{M_a}\right)^3 I_g + \left[1 - \left(\frac{M_{cr}}{M_a}\right)^3\right] I_{cr}$$

$$I_e = 0.072 \times 213.23 + (1 - 0.072) \times 47.35 = 59.28 \text{ in}^4$$

$$\Delta = \frac{PL^3}{100\ EI_e}$$

$$= \frac{7{,}000 \times (60)^3 \times 1000}{100 \times 3.97 \times 10^6 \times 59.28} = 64.2 \times 10^{-3} \text{ in}$$

The actual deflection results are shown in Appendix B, tables B.4 to B.7. The values of the modular ratios are shown in tables 5.11 and the results of the deflections at service load are shown in table 5.12. Figures 5.25 thru 5.33 show the load and deflection relationship for different beams.

Table 5.11

Modular Ratio for Varying Percentage of Steel Fibers

% Steel Fiber	$E_{ca} \times 10^6$ psi	$E_{steel} \times 10^6$ psi	$n = \frac{E_s}{E_{ca}}$
0.0	3.97	29	7.55
0.8	3.67	29	8.17
1.2	3.02	29	9.60

5.7 Load Carrying Capacity

5.7.1 Ultimate Load Capacity

In order to serve its main purpose, a structure has to be safe and serviceable under actual loads. Usually structures are not

Figure 5.25

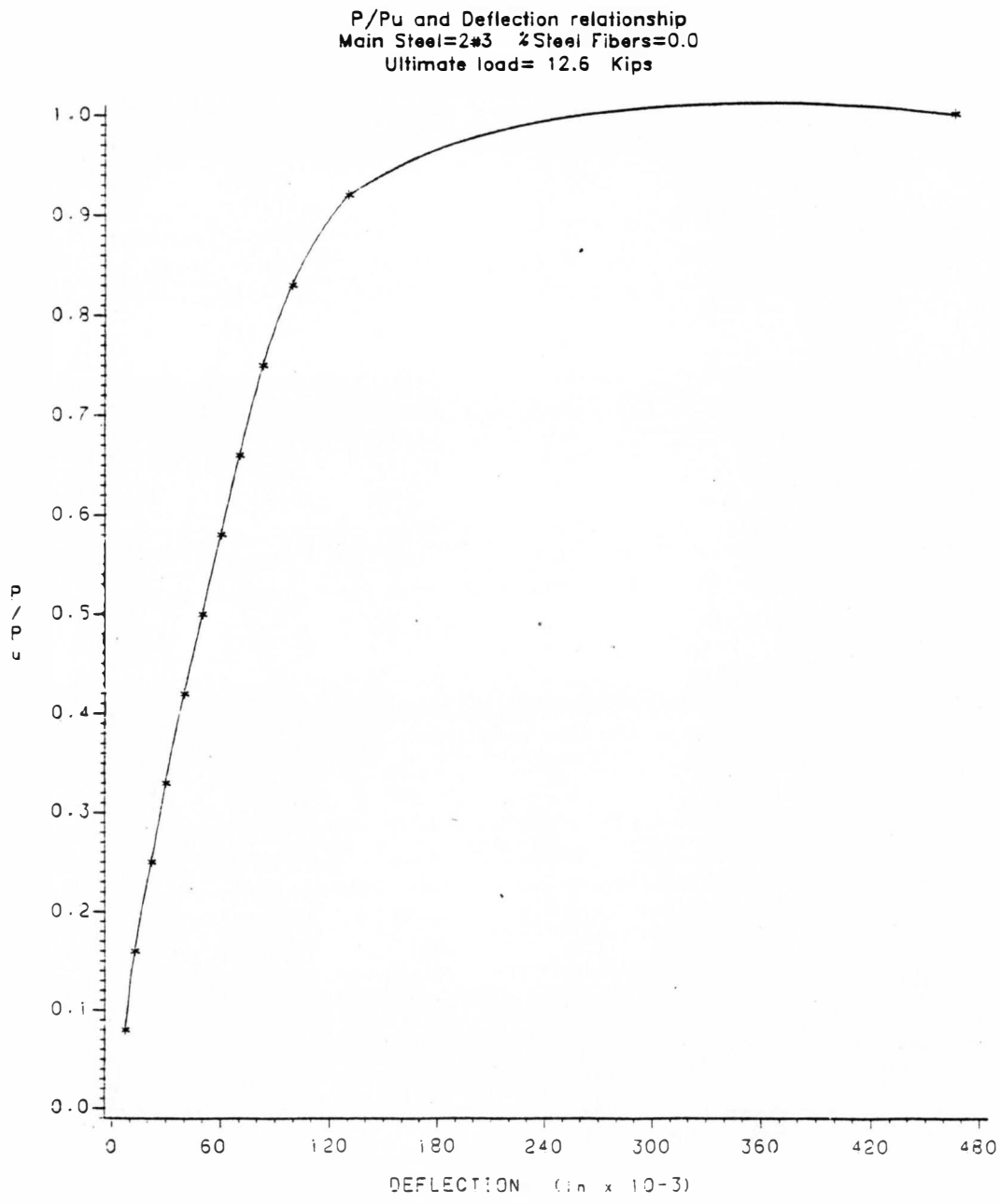

Figure 5.25 Load vs. Deflection

Figure 5.26

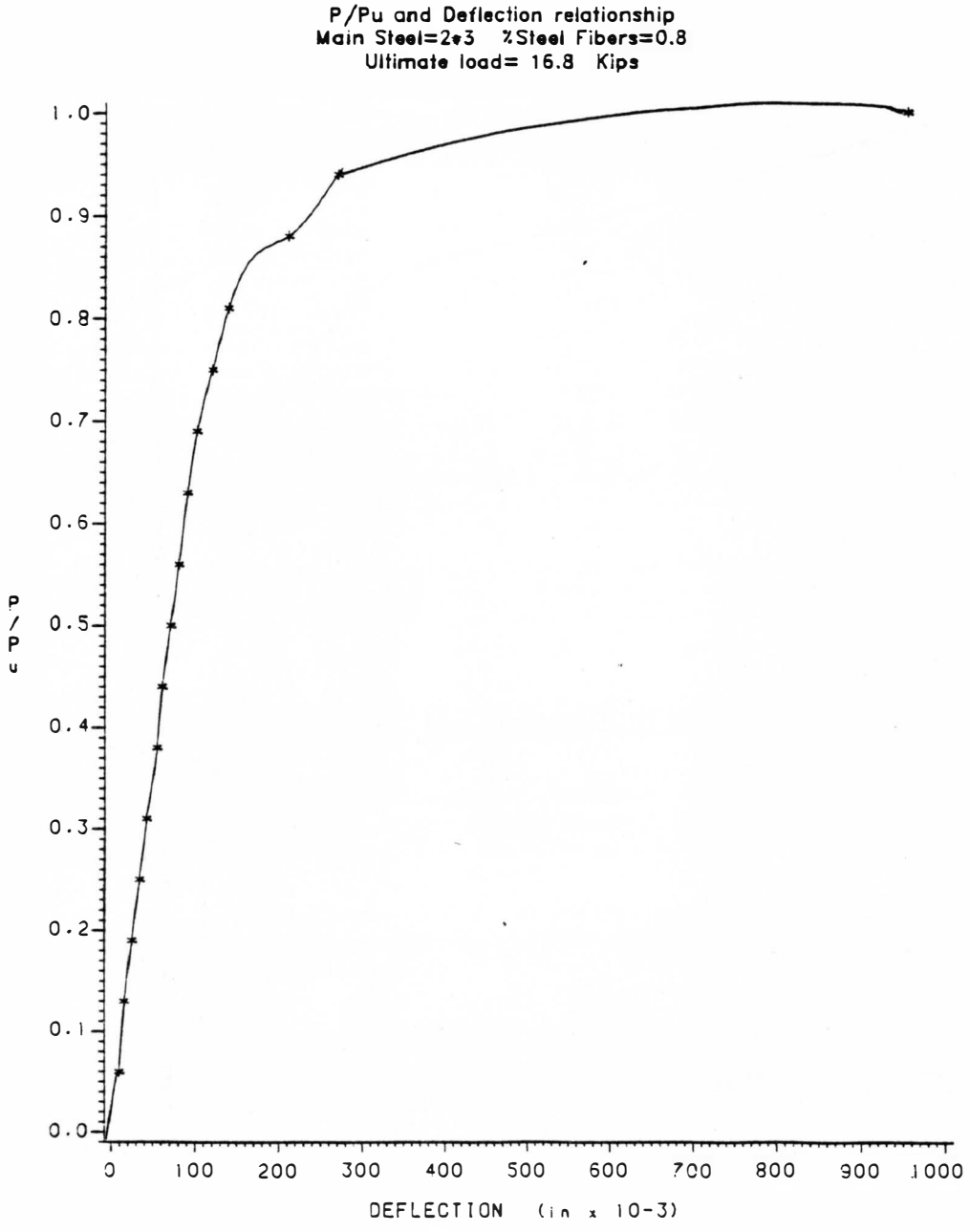

Figure 5.26 Load vs. Deflection

Figure 5.27

P/Pu and Deflection relationship
Main Steel=2*3 % Steel Fibers=1.2
Ultimate load= 16.8 Kips

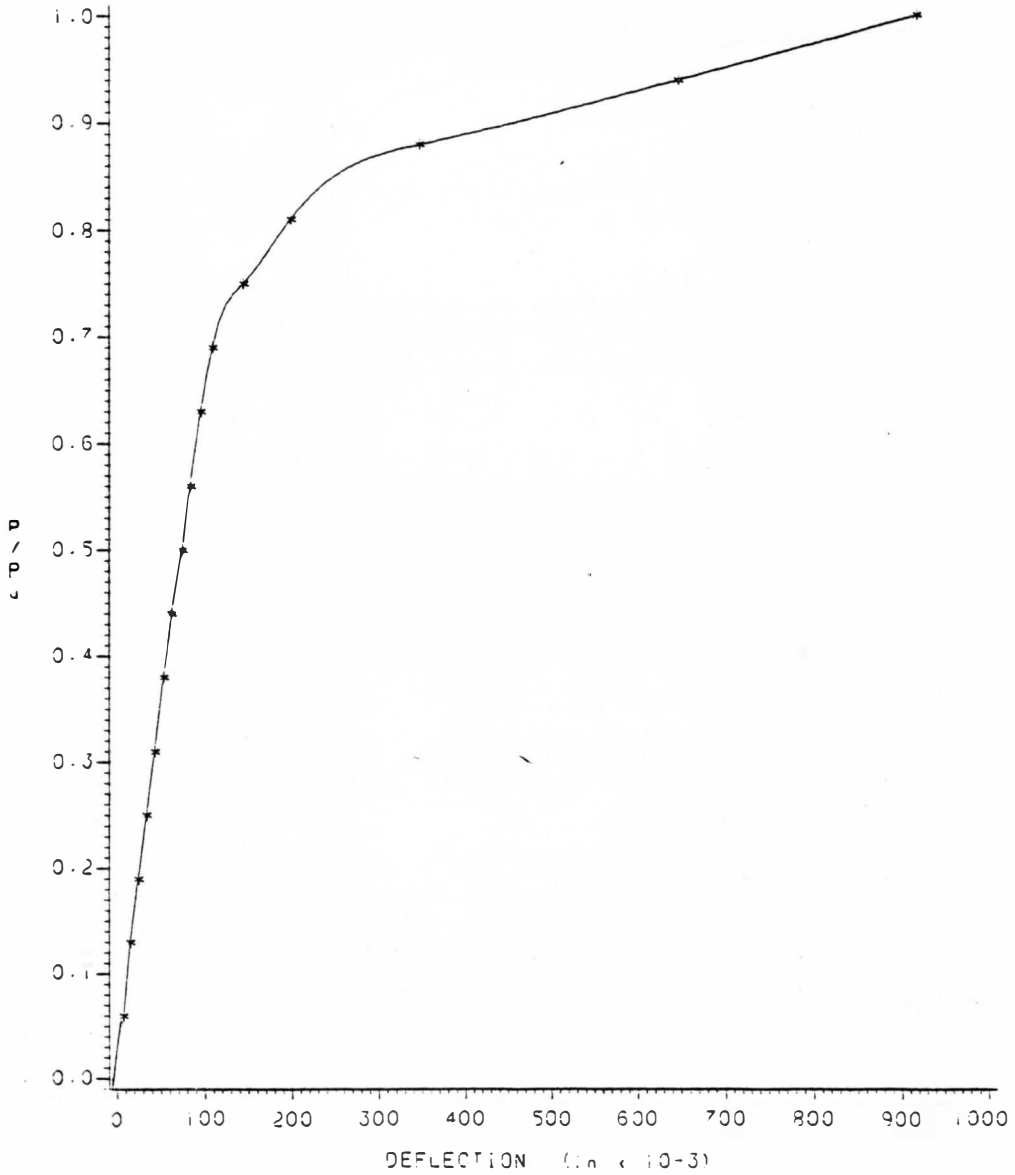

Figure 5.27 Load vs. Deflection

Figure 5.28

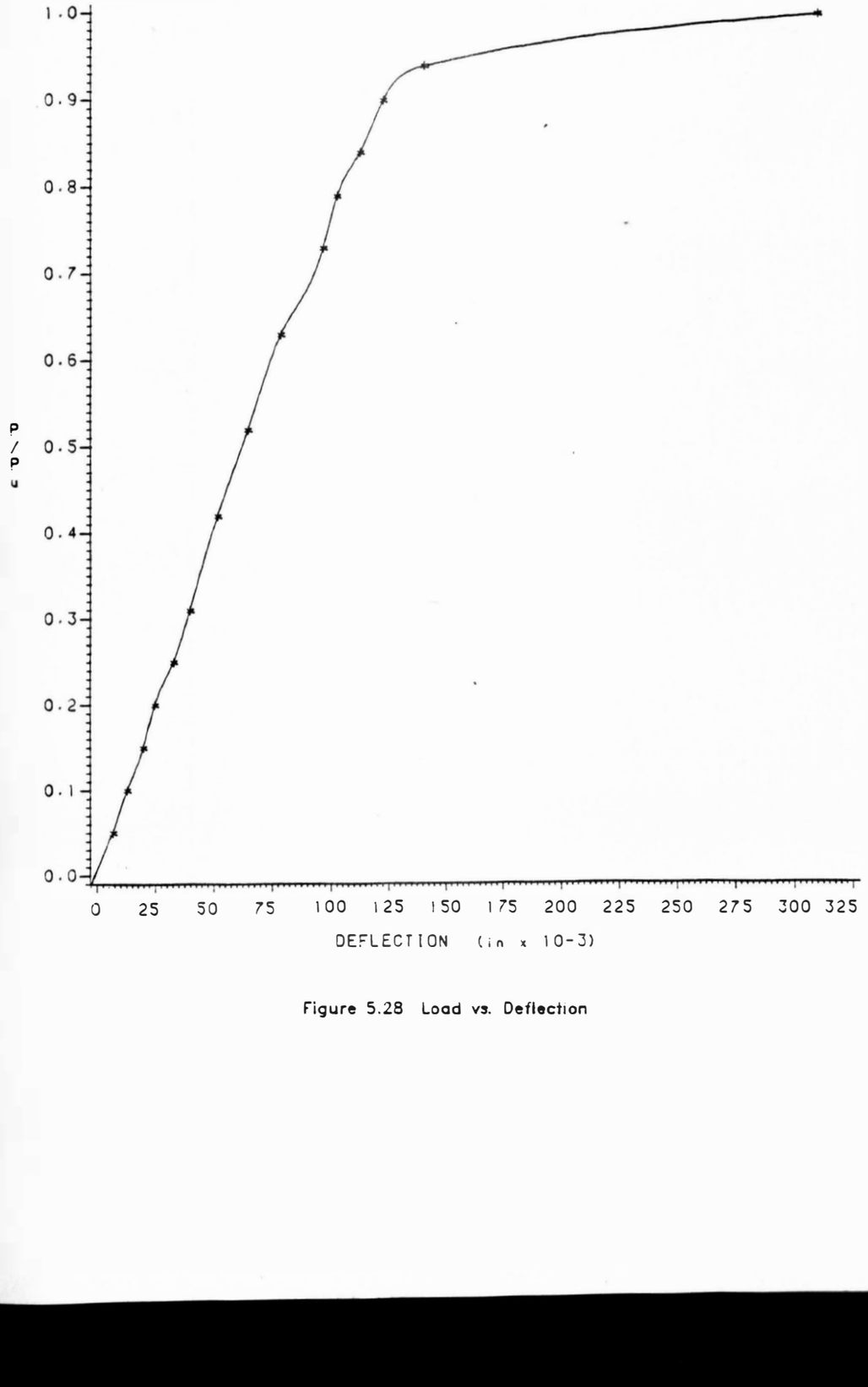

Figure 5.28 Load vs. Deflection

Figure 5.29

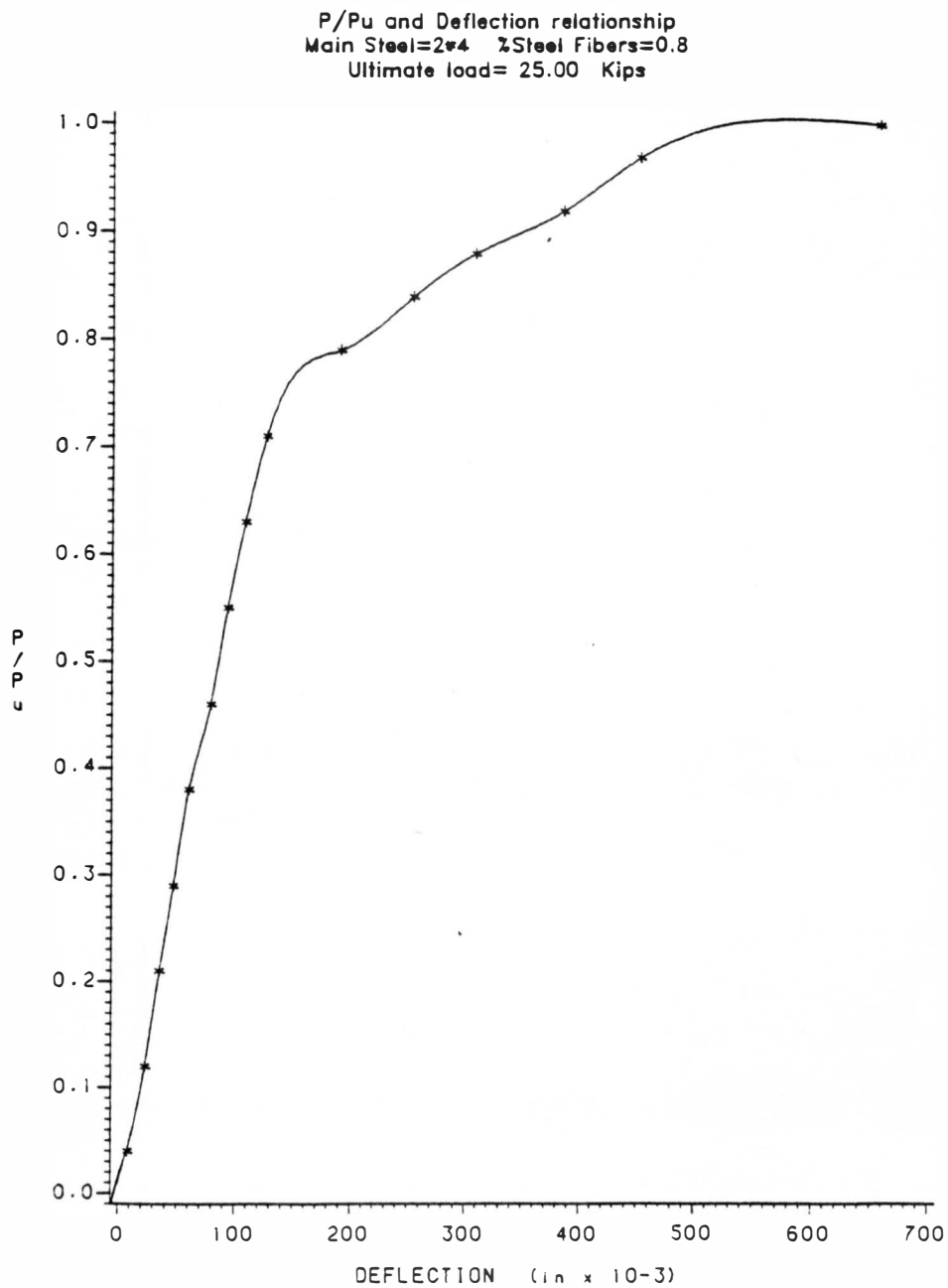

Figure 5.29 Load vs. Deflection

Figure 5.30

P/Pu and Deflection relationship
Main Steel=2#4 %Steel Fibers=1.2
Ultimate load= 12.0 Kips

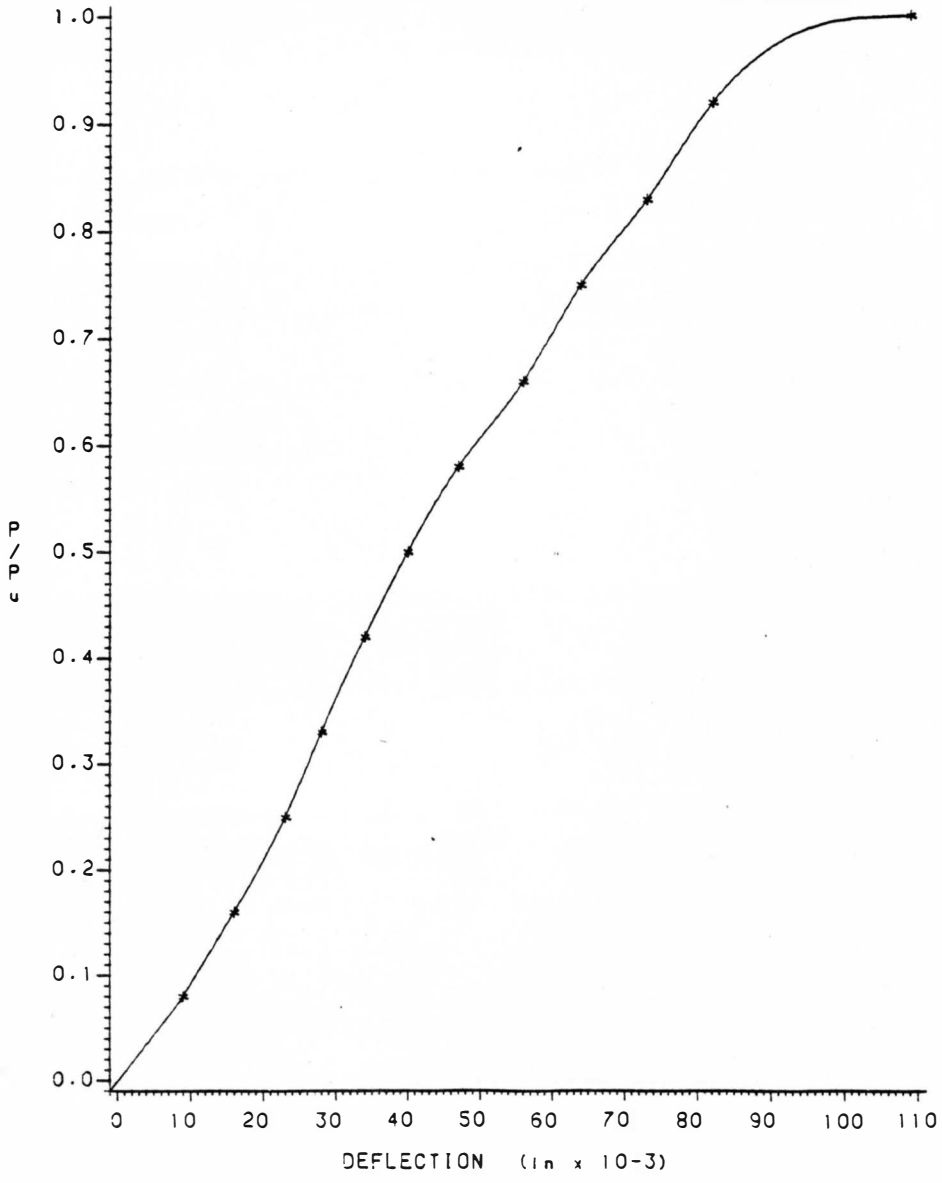

Figure 5.30 Load vs. Deflection

Figure 5.31

P/Pu and Deflection relationship
Main Steel=2#5 % Steel Fibers=0.0
Ultimate load= 23.1 Kips

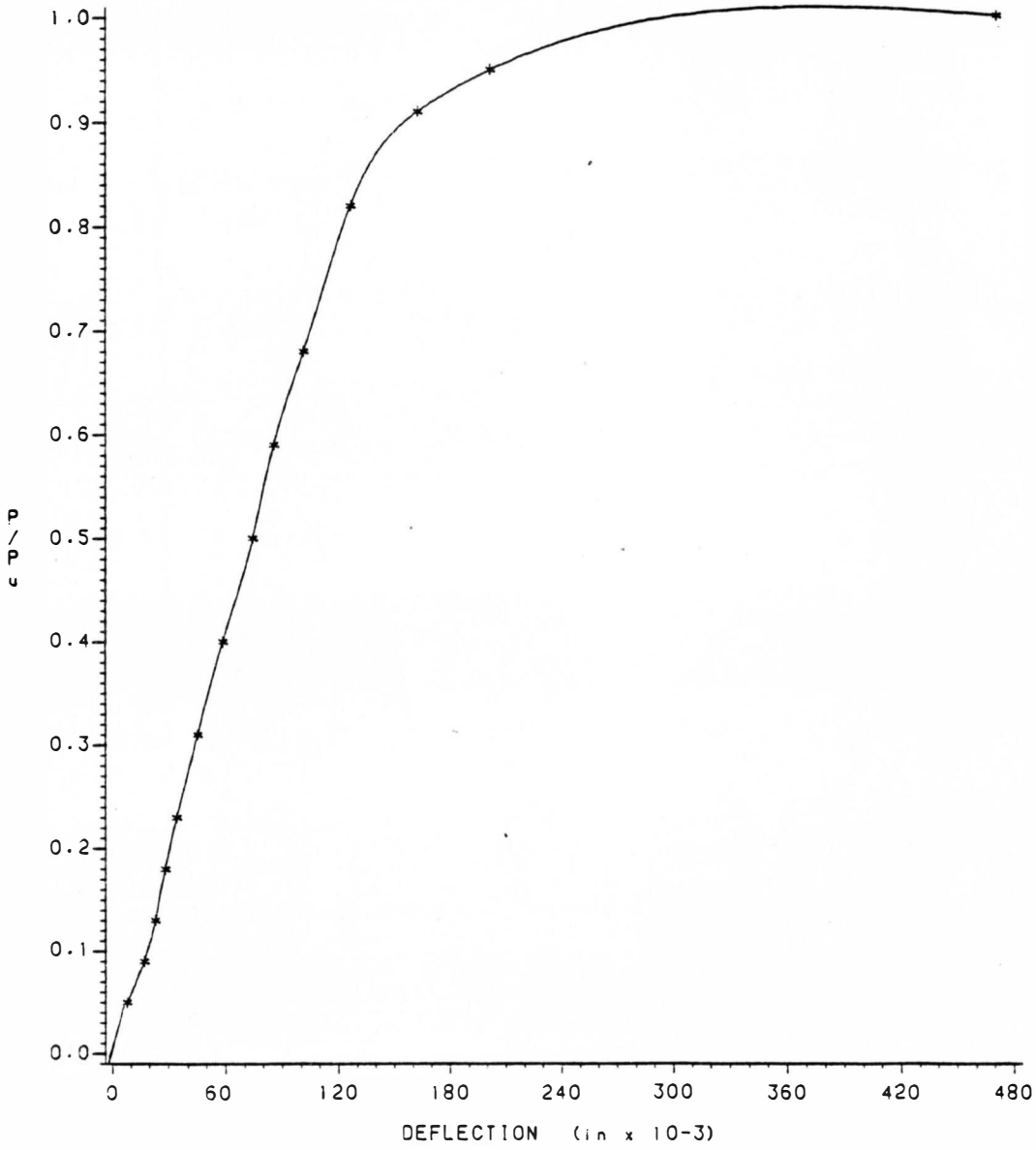

Figure 5.31 Load vs. Deflection

Figure 5.32

P/Pu and Deflection relationship
Main Steel=2-#5 % Steel Fibers=0.8
Ultimate load= 25.2 Kips

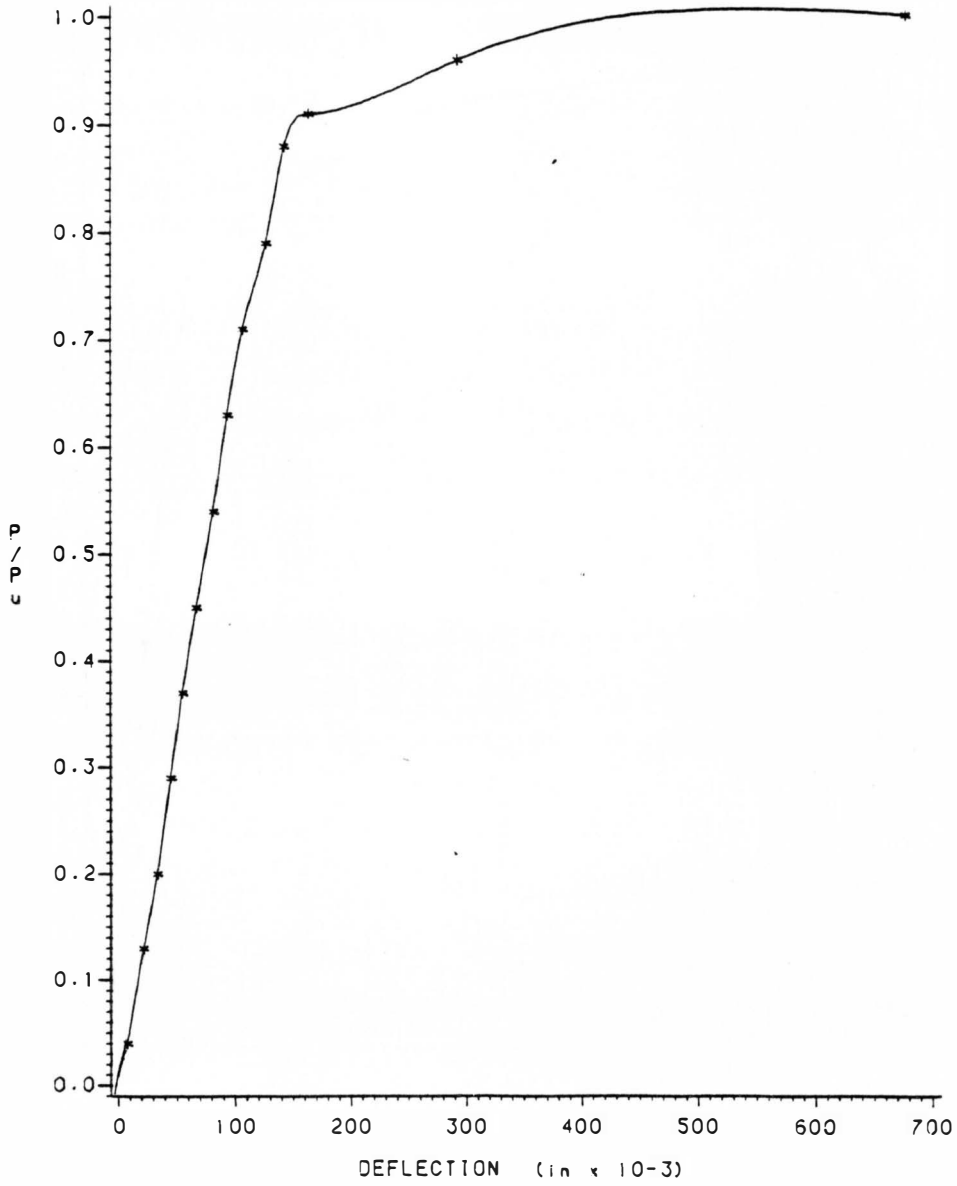

Figure 5.32 Load vs. Deflection

Figure 5.33

P/Pu and Deflection relationship
Main Steel=2#5 % Steel Fibers=1.2
Ultimate load= 25.2 Kips

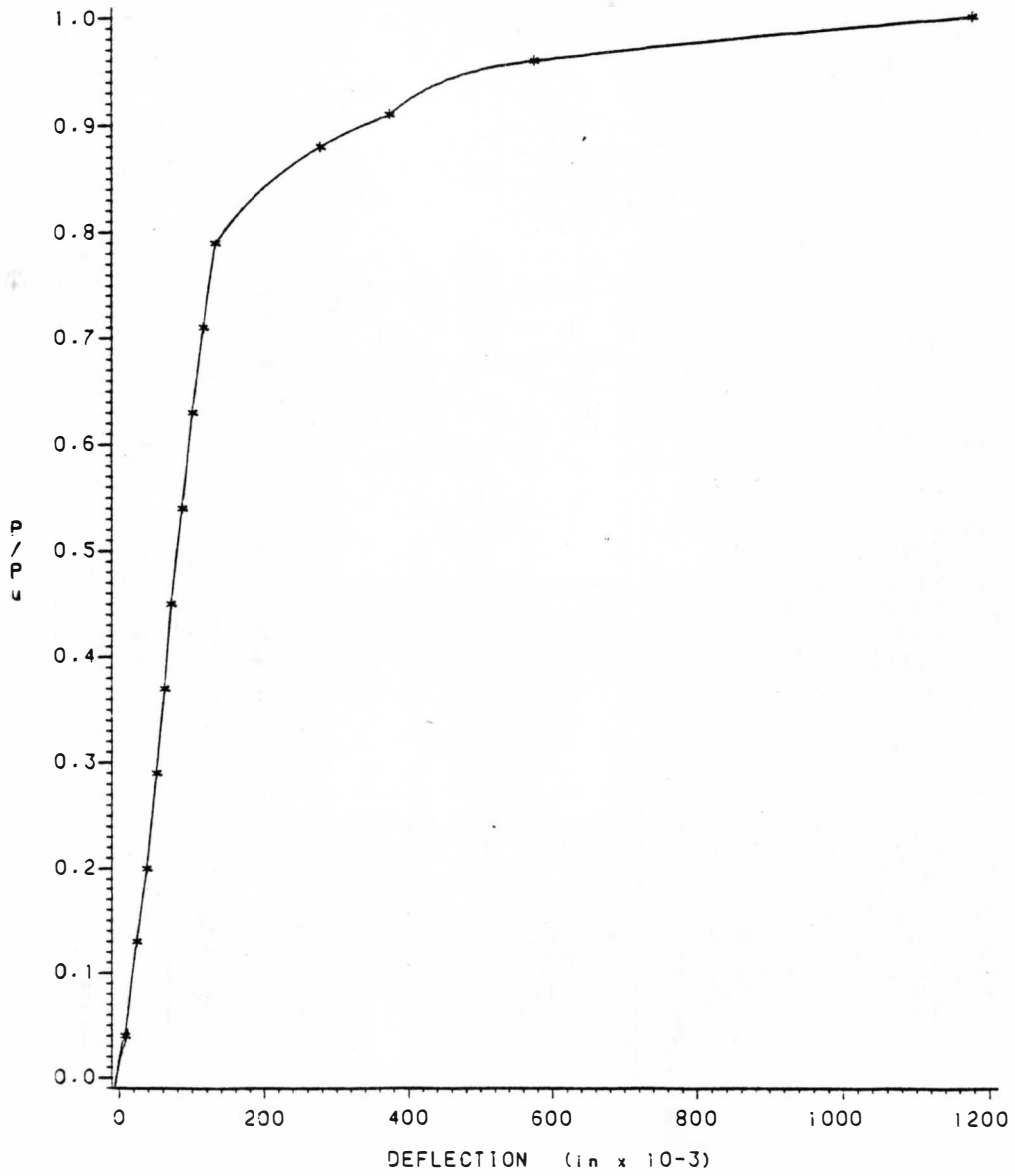

Figure 5.33 Load vs. Deflection

Table 5.12

Calculated and Actual Deflection at Service Load

Beam	% Fibers	Service load $P=0.6P_u$	Kd (in)	I_g in^4	f_{rl} (psi)	M_{cr} K-in	M_a K-in	$(\frac{M_{cr}}{M_a})^3$	I_{cr} (in^4)	I_e* (in^4)	$E_{ca} \times 10^6$ psi	$\Delta \times 10^{-3}$ actual (in)	$\Delta \times 10^{-3}$ calculated (in)	% deviation
	0.0	7.00	1.78	213.33	513	27.36	65.8	.0720	47.35	59.28	3.97	55	64	-14.0
2#3	0.8	7.00	1.84	213.33	670	35.70	65.8	.1590	50.40	76.30	3.67	54	55	- 1.9
	1.2	7.00	1.95	213.33	750	40.00	65.8	.2250	57.30	92.40	3.02	53	55	- 3.6
	0.0	11.34	2.04	213.33	513	27.36	106.6	.0170	74.20	76.56	3.97	71	77	- 8.0
2#4	0.8	11.34	2.33	213.33	670	35.70	106.6	.0376	77.90	83.00	3.67	72	81	-12.5
	1.2	11.34	2.49	213.33	750	40.00	106.6	.0528	87.70	94.30	3.02	-	87	-
	0.0	12.00	2.65	213.33	513	27.36	112.8	.0143	97.20	98.85	3.97	73	66	+ 9.6
2#5	0.8	12.00	2.73	213.33	670	35.70	112.8	.0317	102.50	106.00	3.67	66	67	- 1.5
	1.2	12.00	2.88	213.33	750	40.00	112.8	.0446	114.30	118.70	3.02	71	73	- 2.8

*I_e calculated from ACI Code's equation

designed only to take the service loads that occur in its lifetime. In construction there are always some uncertainties of actual strength of the material or workmanship which have to be considered in the design of the structure. A so-called reduction factor is introduced to the design of the members to compensate for the uncertainties. In this research the reduction factor is not considered due to extreme caution of the mix design and placement of the reinforcement and other factors.

As explained in chapter IV the ultimate load capacity was calculated by equating the external moments due to existing load on the beam, to the internal moment capacity of the section. The calculated yield and ultimate load of the beams are shown in table 4.2, where P_y is the load at which the steel in the critical section (at the middle support) yielded and P_u is the load when the steel in the positive section (at midspan) yielded. In the beams reinforced with steel fibers there was an effective strength reserved in the section even after the yield of the positive steel, meaning the load increases slightly to a magnitude of P_c' before collapse. Table 5.13 shows the calculated yield and ultimate loads (P_y and P_u) and actual yield, ultimate and collapse loads (P_y', P_u', P_c' respectively) and their ratios. In table 5.13 the ratio of ultimate to yield load $\frac{P_u}{P_y} = r$ called the redistribution factor is computed both theoritically and experimentally. The effective strength reserved in the beams are shown in the last column of table 5.13.

Table 5.13

Load Carrying Capacity of Beams

Beam	% Steel Fibers (1)	P_y (Kips) (2)	P_u (Kips) (3)	P_y' (Kips) (4)	P_u' (Kips) (5)	P_c' (Kips) (6)	$r=\frac{P_u}{P_y}$ (7)	$r'=\frac{P_u'}{P_y'}$ (8)	$\frac{P_u'}{P_u}$ (9)	$\frac{P_y'}{P_y}$ (10)	$\frac{P_c'}{P_u'}$ (11)
	0.0	8.16	10.70	9.45	12.60	13.00	1.31	1.33	1.17	1.16	1.03
2#3	0.8	8.18	10.7	10.5	12.60	16.80	1.31	1.20	1.17	1.28	1.33
	1.2	8.20	11.0	10.80	12.80	16.60	1.33	1.19	1.16	1.31	1.29
	0.0	14.46	19.0	17.9	19.95	19.95	1.31	1.11	1.05	1.23	1.00
2#4	0.8	14.55	19.1	18.9	22.00	23.50	1.31	1.16	1.15	1.30	1.07
	1.2	14.60	19.15	-	-	-	1.31	-	-	-	-
	0.0	16.03	21.05	19.95	21.50	21.50	1.31	1.08	1.02	1.24	1.00
2#5	0.8	16.14	21.20	21.00	22.00	24.00	1.31	1.05	1.03	1.30	1.09
	1.2	16.20	21.25	21.10	22.00	24.00	1.31	1.02	1.03	1.30	1.09

Using the yield and ultimate loads obtained from testing the actual moment capacity of the sections can be determined. The actual and calculated moment capacity of the beams are tabulated in table 5.14. The last column in table 5.14 represents the percent increase of the ultimate moment capacity when steel fibers are used. This increase in strength is most effective when the least percentage of main steel is used ($\rho<1\%$).

5.7.2 Strains in Main Steel and Concrete

The main reason that the ultimate moment capacity of a section increases when steel fibers are used, is the reduction in strains in the main steel. The presence of steel fibers causes a reduction in strains of main steel because fibrous concrete is more effective in tension than plain concrete, so part of the tensile stresses are taken by the fibers, leading to a reduction in strains and stresses of main steel. The main advantage of this reduction is that the yield load of fibrous concrete increases slightly so the moment capacity increases without changing the amount of main steel or cross section. As it was discussed in section 5.7.1, the increase in strength is most effective when low steel percentage is used. In this experiment a maximum increase of about 11 percent was found.

The strain in steel or concrete at each section at any load can be found knowing the stresses at the desired part of the cross section. Figure (5.34) shows a typical cross section of the beams.

Table 5.14

Ultimate Moment Capacity of the Middle Support

Beam	% Main Steel	% Steel Fibers	Calculated Ultimate Negative Moment (K-in)	Actual Ultimate Negative Moment (K-in)	% Deviation of Actual From Calculated	Ratio of Actual to Calculated Negative Moment	% Increase of Actual Ultimate Moment From 0% S.F.
		0.0	91.8	106.3	15.8	1.15	-
2#3	0.67	0.8	92.1	118.1	28.2	1.28	11.10
		1.2	92.3	121.5	76.0	1.31	14.30
		0.0	162.7	201.3	23.7	1.23	-
2#4	1.21	0.8	163.7	212.7	30.9	1.30	5.66
		1.2	164.3	-	-	-	-
		0.0	180.3	224.4	24.4	1.24	-
2#5	1.90	0.8	181.6	236.3	30.1	1.30	5.30
		1.2	182.3	237.4	30.2	1.30	5.80

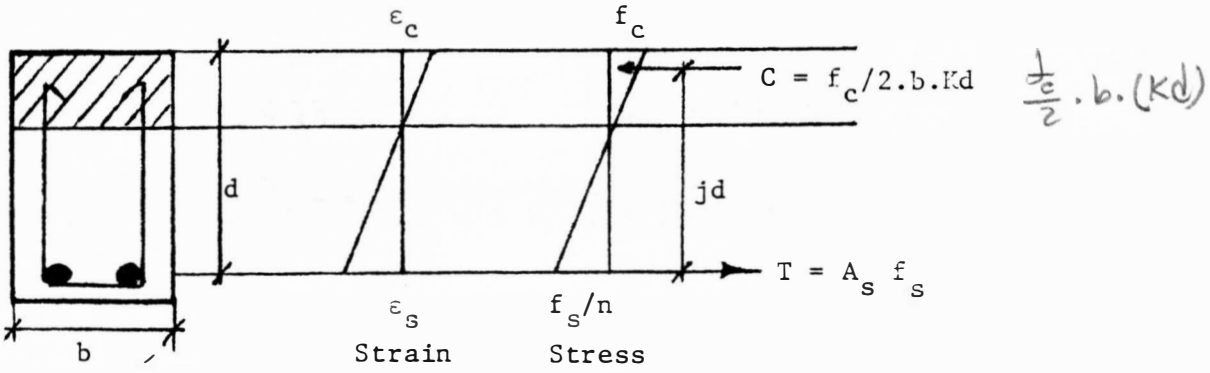

Figure 5.34 Stress and Strain Diagram of a Rectangular Cross Section

From the stress diagram shown in figure 5.34 the stresses at tension steel and extreme compressive fiber can be calculated and dividing the stress by the corresponding modulus of elasticity the strains can be found.

Calculation of strains in concrete compression zone and steel at service load.

The following calculation is for Beam 1 with 2#3 main bars and 0% steel fibers:

a) At middle support

$\rho = .0067$ $\quad n = 7.55$

$M = Cjd$ $\quad A_s = 0.22\ in^2$

$$C = \frac{f_c}{2}\, b.Kd.jd = 0.5\, f_c\, bd^2\, Kj$$

$$f_c = \frac{2M}{bd^2\, Kj}$$

$$M = (0.6\, P_u)(11.25) = 0.6 \times 11.7 \times 11.25 = 79\ K\text{-in}$$

$$K = \sqrt{(\rho n)^2 + 2\rho n} - \rho n = 0.271$$

$$j = 1 - \frac{K}{3} = 0.909$$

$$f_c = \frac{2 \times 79 \times 1000}{5 \times (6.56)^2 \times 0.271 \times 0.909} = 2981 \text{ psi}$$

$$f_s = \frac{M}{A_s.J.d} = \frac{79 \times 1000}{0.22 \times 0.909 \times 6.56} = 60,220 \text{ psi}$$

$$\text{Concrete strain} \times 10^{-6} \text{ (in/in)} = \frac{2981}{3.97 \times 10^6} = 751$$

$$\text{Steel strain} \times 10^{-6} \text{ (in/in)} = \frac{60,220}{30 \times 10^6} = 2007$$

b) At midspan

All parameter are the same as above except the bending moment is different.

$M = 65.8$ K-in

$$f_c = \frac{2 \times 65.8 \times 1000}{5 \times (6.56)^2 \times 0.271 \times 0.909} = 2483 \text{ psi}$$

$$f_s = \frac{65.8 \times 1000}{0.22 \times 0.909 \times 6.56} = 50,157.5 \text{ psi}$$

$$\text{Concrete strain} \times 10^{-6} \text{ (in/in)} = \frac{2483}{3.97 \times 10^6} = 625$$

$$\text{Steel strain} \times 10^{-6} \text{ (in/in)} = \frac{50,157.5}{30 \times 10^6} = 1673$$

The calculated and actual steel and concrete strains are shown in tables 5.15 and 5.16 respectively for both positive and negative moment sections.

Table 5.15

Calculated and Actual Strains in Main Steel at Service Load

Beam	% Main Steel	% Steel	n	K	j	Negative Moment Section					Positive Moment Section				
						M_a (K-in)	f_s Ksi	Calculated Strain x 10^{-6} in/in	Actual Strain x 10^{-6} in/in	% deviation	M_a (K-in)	f_s (Ksi)	Calculated Strain x 10^{-6} in/in	Actual Strain x 10^{-6} in/in	% deviation
		0.0	7.55	0.271	0.909	79.0	60.22	2007	1500	-25	6.58	50.20	1673	1300	-22
2#3	0.67	0.8	8.17	0.280	0.906	79.0	60.41	2013	1100	-45	65.8	50.30	1676	1100	-34
		1.2	9.60	0.312	0.896	79.0	61.10	2036	1240	-39	65.8	50.90	1697	1612	-5
		0.0	7.55	0.313	0.895	127.6	54.80	1827	1820	-0.4	106.6	45.80	1527	1800	+17
2#4	1.21	0.8	8.17	0.358	0.880	127.6	55.77	1859	1560	-16	106.6	46.60	1553	1355	-12
		1.2	9.60	0.400	0.861	127.6	57.00	1900	-	-	106.6	47.60	1586	-	-
		0.0	7.55	0.410	0.863	135.0	39.80	1327	1300	-2.0	112.8	33.27	1110	1336	+20
2#5	1.98	0.8	8.17	0.424	0.858	135.0	40.00	1333	1000	-25	112.8	33.46	1115	1009	-10
		1.2	9.60	0.466	0.844	135.0	40.71	1357	1030	-24	112.8	34.0	1133	1025	-9.5

Table 5.16

Calculated and Actual Strains on Concrete Compression Zone at Service Load

Beam	% Main Steel	% Steel Fiber	n	K	j	E_{ca} x10^6 psi	Negative Moment Section					Postive Moment Section				
							M_a (K-in)	f_c (psi)	Calculated Strain x 10^{-6} in/in	Actual Strain x 10^{-6} in/in	% deviation	M_a (K-in)	f_c (psi)	Calculated Strain x 10^{-6} in/in	Actual Strain x 10^{-6} in/in	% deviation
		0.0	7.55	0.271	0.909	3.97	79.0	2981	751	700	-6.8	65.8	2483	626	630	+0.6
2#3	0.67	0.8	8.17	0.280	0.906	3.67	79.0	2895	789	685	-13.0	65.8	2411	657	623	-5.0
		1.2	9.60	0.312	0.896	3.02	79.0	2627	931	1001	+7.5	65.8	2188	776	640	-17.0
		0.0	7.55	0.313	0.895	3.97	127.6	4312	1086	884	-18.0	106.6	3592	905	810	-10.0
2#4	1.21	0.8	8.17	0.358	0.880	3.67	127.6	3835	1045	950	-9.0	106.6	3194	870	930	+7.0
		1.2	9.60	0.400	0.861	3.02	127.6	3508	1244	-	-	106.6	2922	1036	-	-
		0.0	7.55	0.410	0.863	3.97	135.0	3680	927	1002	+8.0	112.8	3065	772	765	-1.0
2#5	1.98	0.8	8.17	0.424	0.858	3.67	135.0	3579	975	1100	+3.0	112.8	2981	812	760	-6.4
		1.2	9.60	0.466	0.844	3.02	135.0	3311	1174	1180	+0.5	112.8	2758	978	1008	+3.0

5.8 Crack Widths

Due to the low tensile strength of concrete, cracks will develop in members where tensile forces exist. Development of large cracks has to be prevented mainly because it leads to deterioration of the main reinforcement, and changes the characteristics of the steel due to weathering causing unexpected and premature failure.

Cracks are least present when low tensile strength steel is used. Low stresses reduce the chance of development of large cracks at service loads. High strength steel developes high stresses at service load which could cause visible large cracks. Therefore, the maximum allowable crack width must be limited to a limited value.

In 1968 Gergely and Lutz developed the following equation to estimate the crack width for steel stresses up to 60 percent of yield stress of the steel.

$$w = 0.076.\beta_h.f_s \sqrt[3]{d_c.A_c}$$

where: β_h = ratio of the distance from neutral axis to the extreme tension fiber, to the distance from neutral axis to steel centroid.

f_s = steel stress (ksi)

d_c = thickness of concrete cover measured from extreme tension fiber to center of bar located closest thereto. (in)

A_c = the effective tension area of concrete around the main reinforcing (having the same reinforcement centroid, divided by the number of bars). in^2

The ACI Code adopted the preceding equation and used a value of $\beta_h = 1.2$ with the cross section so proportioned that the formula $z = f_s \sqrt[3]{d_c . A_c}$ is limited to a maximum value of 175 Kips per inch for interior members and 145 Kips per inch for exterior members. These limiting values allow maximum crack widths of 0.016 inches and 0.013 inches for interior and exterior members respectively.

Crack Width and Crack Spacing Measurements

As explained in Chapter III the crack widths were measured at different loads by the use of a mechanical dial gage with an accuracy of ten thousandth of an inch. The crack widths were determined at both negative (over the middle support) and positive section (under the load). Calculated and experimental crack widths are shown in tables 5.17 and 5.18. The differential of all readings were the crack widths measurements which are recorded in tables C.1 through C.18 in Appendix C.

The spacing of the cracks were also measured at service load and ultimate. The maximum and minimum crack spacing along with the number of cracks at each critical section at service load and ultimate are shown in tables 5.19 and 5.20.

Table 5.17

Maximum Calculated and Actual Crack Widths at the Middle Support

Beam	% Main Steel	% Steel Fiber	Service load Kips	$f_s=0.6\ f_y$ Ksi	Kd in	d_c in	A_c in^2	β_h	Calculated crack width 10^{-4} in	Maximum Actual crack 10^{-4} width	% deviation
		0.0		40.0	1.78	1.44	7.2	1.30	86	82	-5
2#3	0.67	0.8	5.0	40.0	1.83	1.44	7.2	1.30	86	60	+43
		1.2		40.0	2.04	1.44	7.2	1.31	87	55	-37
		0.0		42.0	2.03	1.50	7.5	1.33	95	105	+10
2#4	1.21	0.8	9.0	42.0	2.32	1.50	7.5	1.35	97	80	-17
		1.2		42.0	2.60	1.50	7.5	1.38	98	-	-
		0.0		39.0	2.64	1.56	7.8	1.41	95	117	+23
2#5	1.89	0.8	9.3	39.0	2.73	1.56	7.8	1.42	97	107	+10
		1.2		39.0	3.00	1.56	7.8	1.45	99	68	-31
2#6 and 2#3	2.76	0.8	16.8	37.8	2.96	1.60	8.0	1.46	98	103	+ 5

Table 5.18

Maximum Calculated and Actual Crack Widths at Midspan

Beam	% Main Steel	% Steel Fiber	Service load Kips	$f_s=0.6\ f_y$ Ksi	Kd in	d_c in	A_c in	β_h	Calculated max. crack width 10^{-4} inch	Actual max. crack width 10^{-4} inch	% deviation
		0.0		34	1.78	1.44	7.2	1.30	73	87	+19
2#3	0.67	0.8	5.0	34	1.83	1.44	7.2	1.30	73	57	-22
		1.2		34	2.04	1.44	7.2	1.31	74	49	-34
		0.0		35	2.03	1.50	7.5	1.33	79	83	+ 5
2#4	1.21	0.8	9.0	35	2.32	1.50	7.5	1.35	81	65	-19
		1.2		35	2.60	1.50	7.5	1.38	82	-	-
		0.0		33	2.64	1.56	7.8	1.41	80	75	- 6
2#5	1.89	0.8	9.3	33	2.73	1.56	7.8	1.42	82	57	-30
		1.2		33	3.00	1.56	7.8	1.45	84	46	-45
2#6 and 2#3	2.76	0.8	16.8	32	2.96	1.60	8.0	1.46	83	98	+18

Table 5.19

Maximum and Minimum Crack Spacings at the Middle Support (negative region)

Beam	% Main Steel	% Steel Fibers	Maximum Spacing (inches)	Minimum Spacing (inches)	Average Spacing (inches)	Ratio*	Number of Cracks at service load	Number of Cracks at failure
		0.0	8	2.0	5.5	1.00	4	6
2#3	0.67	0.8	5	2.0	3.5	0.65	3	5
		1.2	6	1.5	3.1	0.55	4	7
		0.0	5	2.0	3.5	1.00	3	4
2#4	1.21	0.8	4	2.0	2.8	0.8	3	7
		1.2	-	-	-	-	-	-
		0.0	6	3.0	4.5	1.00	3	4
2#5	1.89	0.8	3	1.0	3.6	0.80	4	7
		1.2	5	2.0	3.0	0.67	3	5
2#6 and 2#3	2.76	0.8	4	2.0	3.0	-	3	5

* Ratio = $\frac{\text{Average spacing no fibers}}{\text{Average spacing with fibers}}$

Table 5.20

Maximum and Minimum Crack Spacings at Midspans (Positive Region)

Beam	% Main Steel	% Steel Fibers	Maximum Spacing (inches)	Minimum Spacing (inches)	Average Spacing (inches)	Ratio*	Number of Cracks at service load	Number of Cracks at failure
		0.0	7.0	3.0	5.30	1.00	5	6
2#3	0.67	0.8	4.5	2.0	2.75	0.52	6	9
		1.2	4.0	2.0	2.50	0.47	4	8
		0.0	5.0	4.0	4.50	1.00	4	5
2#4	1.21	0.8	3.5	1.0	2.30	0.51	5	11
		1.2	-	-	-	-	-	-
		0.0	5.5	2.0	3.9	1.00	4	5
2#5	1.89	0.8	4.0	1.0	3.7	0.94	3	6
		1.2	5.0	2.0	3.2	0.82	4	7
2#6 and 2#3	2.76	0.8	3.0	2.0	2.2	-	4	6

*Ratio = $\frac{\text{Average Spacing no fibers}}{\text{Average Spacing with fibers}}$

CHAPTER VI

DISCUSSION OF RESULTS

6.1 Compressive Strength

Standard size concrete cylinders (6"x12") were used to test the 28 day compressive strength of plain and fibrous concrete. The percentage of steel fibers used were 0.0, 0.8 and 1.2

Four cylinders were tested for each mix. There was a little increase in compressive strength as the percentage of steel fibers increased. Table 6.1 shows a summary of the results.

Table 6.1

% Steel Fibers	Compressive Strength (psi)	% increase from 0% Steel Fibers
0.0	4,584	-
0.8	4,805	4.8
1.2	4,927	7.5

It is obvious that the increase in strength is not significant compared to the increase of fibers. A maximum 7.5 percent increase of strength was obtained by using 1.2 percent steel fibers and 4.8 percent increase with 0.8 percent steel fibers in the concrete. This shows that the use of steel fibers is not an efficient method to increase compressive strength of concrete. This result was also obtained by other researchers[30,48] where an insignificant or no increase in compressive strength using steel fibers was concluded.

Figures 6.1 and 6.2 show the difference in the modes of failure between plain and fibrous concrete cylinders.

6.2 Modulus of Elasticity

The modulus of elasticity of plain and fibrous concrete was determined by testing eight standard size cylinders. Using the secant modulus, the actual moduli of elasticity of plain and fibrous concrete were determined and a summary of the results is shown in table 6.2.

Table 6.2

Modulus of Elasticity of Fibrous Concrete

% Steel Fiber	$E_c x 10^6$ psi	% decrease from 0% Steel Fibers
0.0	3.97	-
0.8	3.67	-7.6
1.2	3.02	-24.0

It is apparent from table (6.2) that the modulus of elasticity of concrete decreases when steel fibers are used. The decrease is 7.6 percent for 0.8 percent steel fibers and 24.0 percent for 1.2 percent steel fibers. The summary of calculated and actual moduli of elasticity are shown in table 6.3.

In table 6.3 for plain concrete, a deviation of 0.25 percent shows an agreement between this experiment and the ACI formula for modulus of elasticity calculation. As the amount of steel fibers

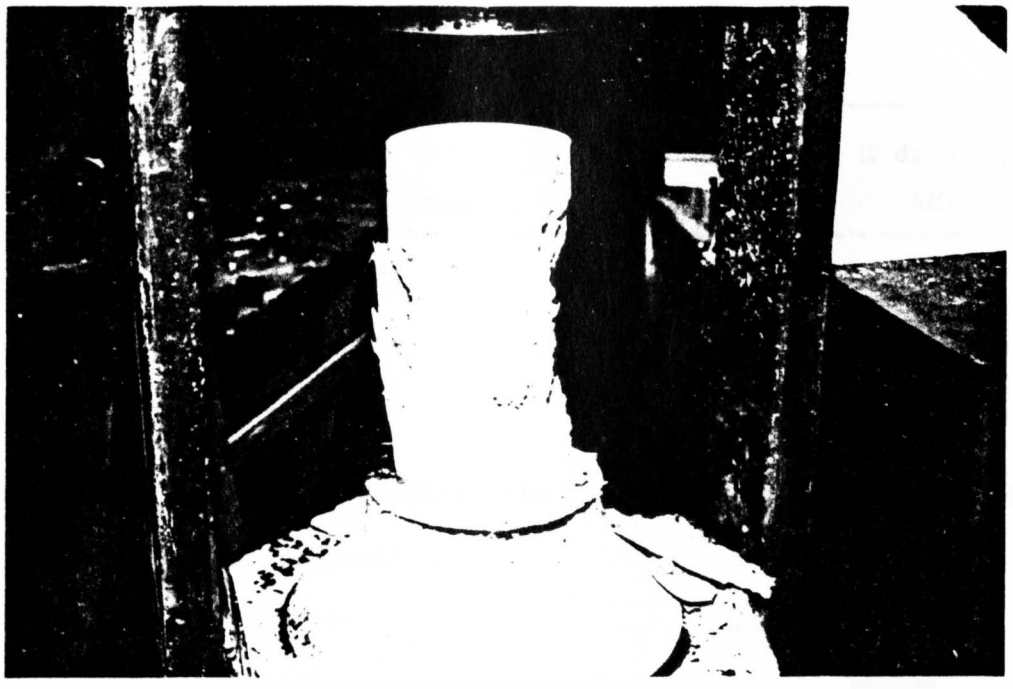

Figure 6.1 Failure of plain concrete in compression

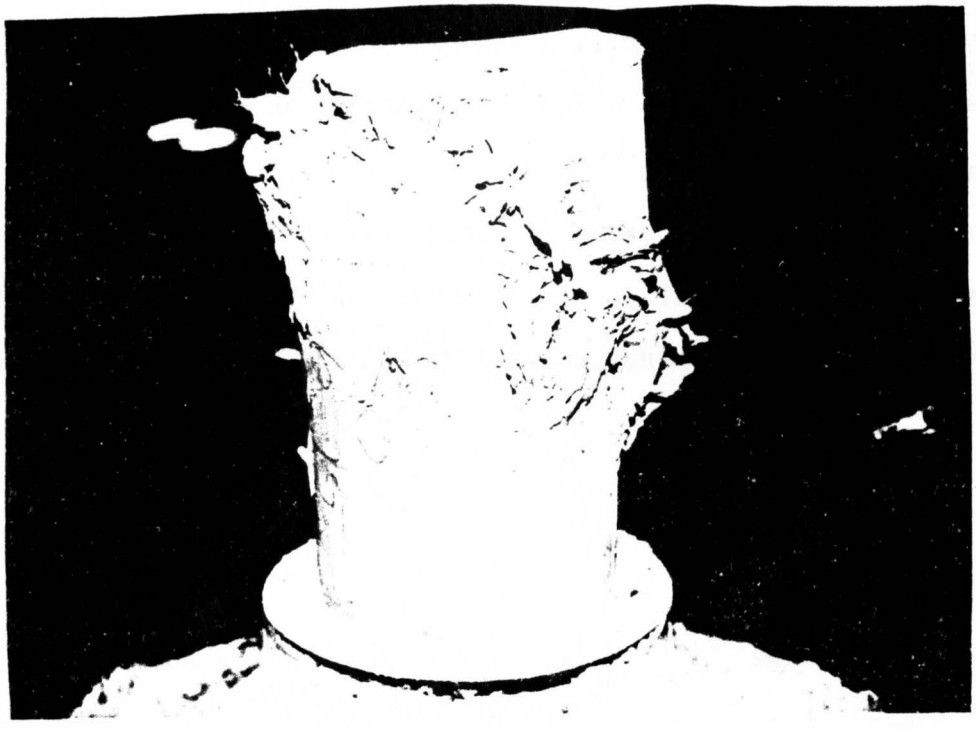

Figure 6.2 Failure of fibrous concrete incompression

Table 6.3

% Steel Fibers	$E_{ca} \times 10^6$ (psi) from testing	$E_{cc} \times 10^6$ (psi) ACI Code	% deviation from ACI Code
0.0	3.97	3.98	- 0.25
0.8	3.67	4.29	+14.50
1.2	3.02	4.31	+30.00

increase to 0.8 and 1.2 percent the deviation increases to 14.50 and 30.00 percent respectively.

The ACI formula ($E_c = 33\ w^{1.5}\ \sqrt{f_c'}$) cannot be used to calculate the modulus of elasticity of fibrous concrete because the ACI formula over-estimates the 'E_c' where the actual values are much smaller.

A statistical analysis of the data was done using simple regression and the best fitting line through the data points was evaluated and shown in figure (6.3). $m = E_{cc}/33w^{1.5}\sqrt{f_c'}$ versus percentage of steel fibers in the concrete mix. The best fitting line thru the data had a slope of (-0.23) and an intercept of (1) $m = 1 - 0.23\rho_s$. Applying this coefficient to the ACI formula, then the following is obtained:

$$E_{cc} = m\ 33w^{1.5}\sqrt{f_c'}$$

$$\text{or}\quad E_{cc} = (33 - 7.6\rho_s)\ w^{1.5}\sqrt{f_c'} \qquad (6.1)$$

The correlation coefficient between 'm' and 'ρ' was 0.920 which means about 85% ($r^2 = 0.85$) of the variations is accounted for and an 'F'

Figure 6.3

Modulus of elasticity coefficient vs.
Steel Fibers
$m = 1 - 0.23\rho_s$
Correlation Coefficient=0.920

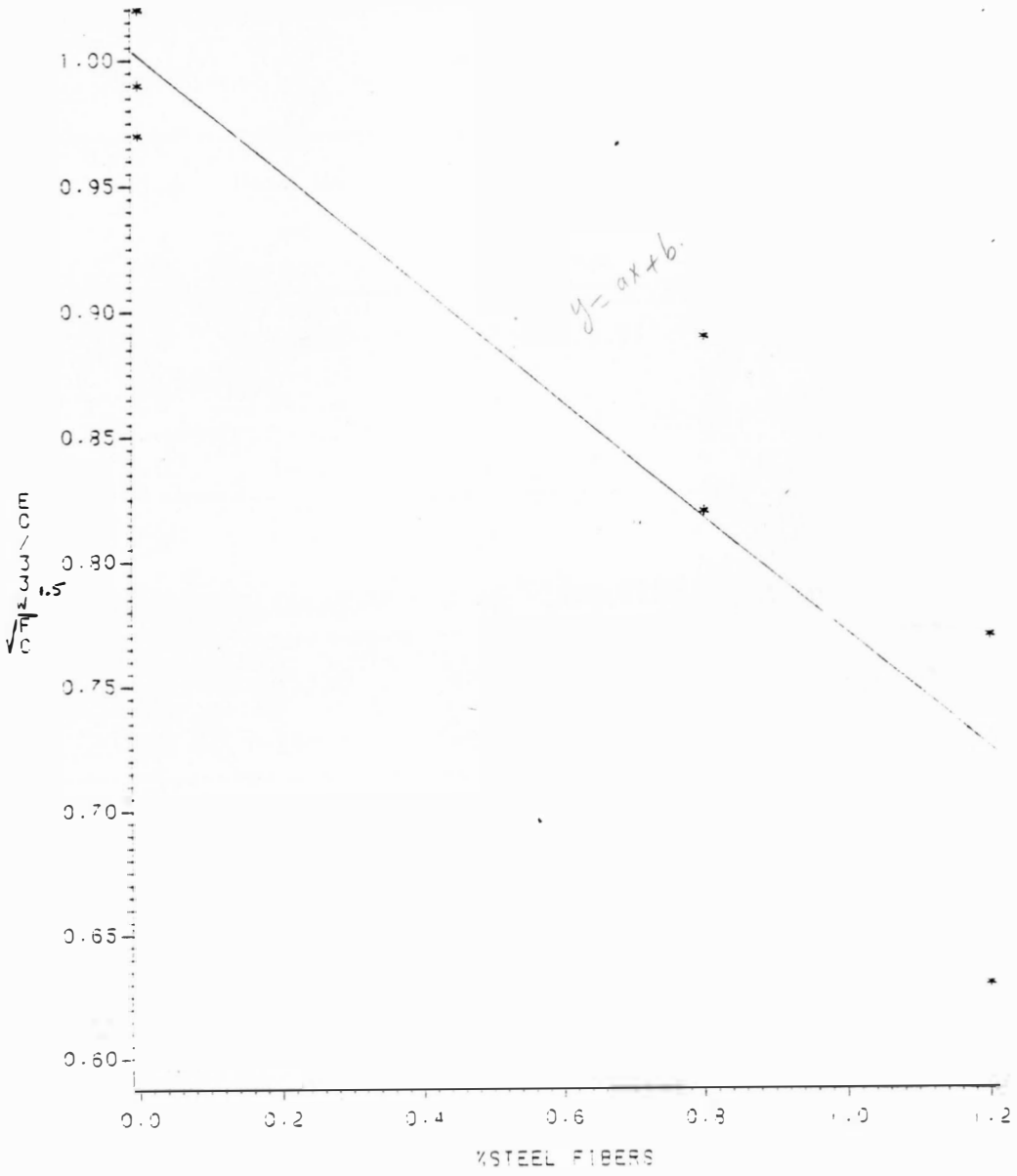

Figure 6.3 m vs. Steel Fibers

value of 28 which is highly significant (Table D.1). Using equation 6.1 to estimate the modulus of elasticity of fibrous concrete, provides table 6.4 where calculated values using equation 6.1 and actual values are compared.

Table 6.4

Cylinder	% S.F.	Unit Weight pcf	f_c' (psi)	$E_{cc} \times 10^6$ psi equ. 6.1	$E_{ca} \times 10^6$ psi	% deviation
C1	0.0	148.5	4421	3.97	4.06	-2.2
C2	0.0	147.6	4719	4.01	4.05	-1.0
C3	0.0	148.0	4457	3.97	3.85	+3.0
C1	0.8	152.6	4828	3.53	3.83	-7.8
C2	0.8	151.5	4792	3.47	3.50	-1.0
C2	1.2	151.8	4863	3.11	2.70	+15.0
C3	1.2	152.1	4873	3.13	3.25	- 4.0

Equation 6.1 applies to concrete with strengths ranging from 4000 to 5000 psi. The results could vary with f_c' less than 4000 psi or for high strength concrete. The discrepancy in reduction of modulus of elasticity when percent steel fibers are increased is that, addition of steel fibers slightly increases the "f_c'" and there is a positive relationship between compressive strength and modulus of elasticity, therefore modulus of elasticity should increase theoritically.

The results obtained in this research shows that at a given stress level, the strains of fibrous concrete cylinders are much higher than that of plain concrete cylinders. This increase of strain when fibers are used, proves that the deformation of fibrous concrete at a given level of stress is higher than plain concrete due to more ductility. The main reason for this, is the difference between the bond characteristics of fibrous concrete and plain concrete.

In plain concrete, the bond is only between the aggregate and cement paste but in fibrous concrete the bond is between: a) fiber and cement and b) aggregate and cement and it is apparent that the bond strength of steel fibers with cement in compression is weaker than aggregate with cement. The unusual point here is that this weakness of bond stress between fiber and cement not only adds to the strength but improves the concrete ductility as well. There are higher deformation in more ductile materials, therefore higher strains are expected in fibrous concrete.

6.3 Split Cylinder

One of the methods used to test the tensile strength of plain and fibrous concrete was the split cylinder test according to ASTM standards C78.

Seven cylinders were tested with percentage of steel fibers varying from zero to 1.2 percent. The summary of the results are shown in table 5.4 and 5.5.

As it is obvious the percentage of deviation of actual values from the ACI Code formula for normal weight concrete ($f_{ct} = 6.7\sqrt{f_c'}$) increases by 20 and 35 percent for 0.8 and 1.2 percent steel fiber respectively. This indicates that the ACI Code formula is not applicable to fibrous concrete. Table 5.5 shows an increase in tensile strength of 28 and 47 percent for 0.8 and 1.2 percent steel fiber used in the mixes.

A linear regression statistical analysis was done, and a best fitting line through the data was found with an intercept of 6.7 and a slope of 2.3 (figure 6.4). The correlation coefficient between ($f_{ct}/\sqrt{f_c'}$) and (ρ_s) is 0.9979 which means 99.6 percent of the variations is accounted for and an 'F' value of 246 was obtained (Table D.2).

Therefore the split cylinder strength of fibrous concrete with compressive strength between 4000 to 5000 psi can be calculated by equation 6.2.

$$f_{cs} = (6.7 + 2.3\ \rho_s)\ \sqrt{f_c'} \qquad (6.2)$$

where: f_{cs} = split cylinder strength of fibrous concrete (psi)

ρ_s = % steel fibers

f_c' = compressive strength (psi)

The calculated values for split cylinder strength of fibrous concrete are shown in table 6.5.

The modes of failure of plain and fibrous concrete are shown in figure 6.5 and 6.6. Cylinders without steel fibers had a sudden

Figure 6.4

Split Cylinder Test of Concrete
$FCS=(6.7+2.3\rho S)\sqrt{FC'}$
Correlation coefficient=0.998

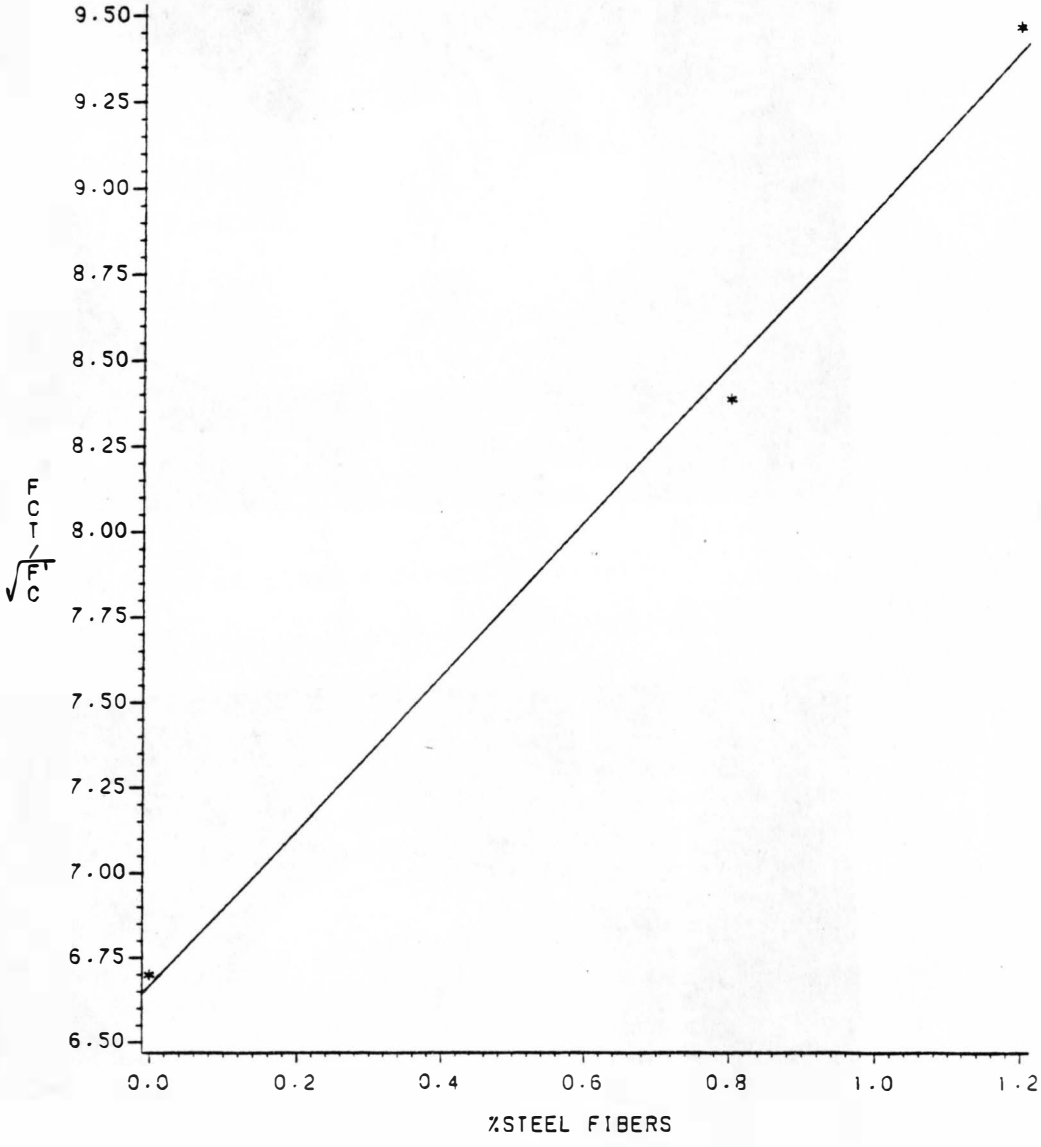

Figure 6.4 $FCT/\sqrt{FC'}$ vs. % Steel Fibers

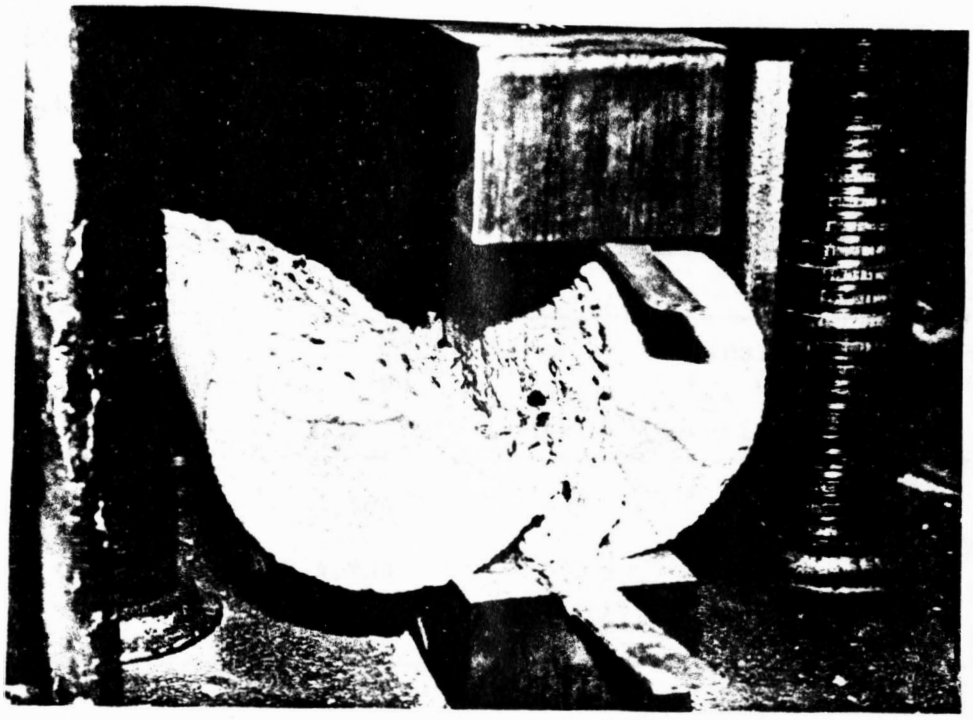

Figure 6.5 Failure of plain concrete in tension

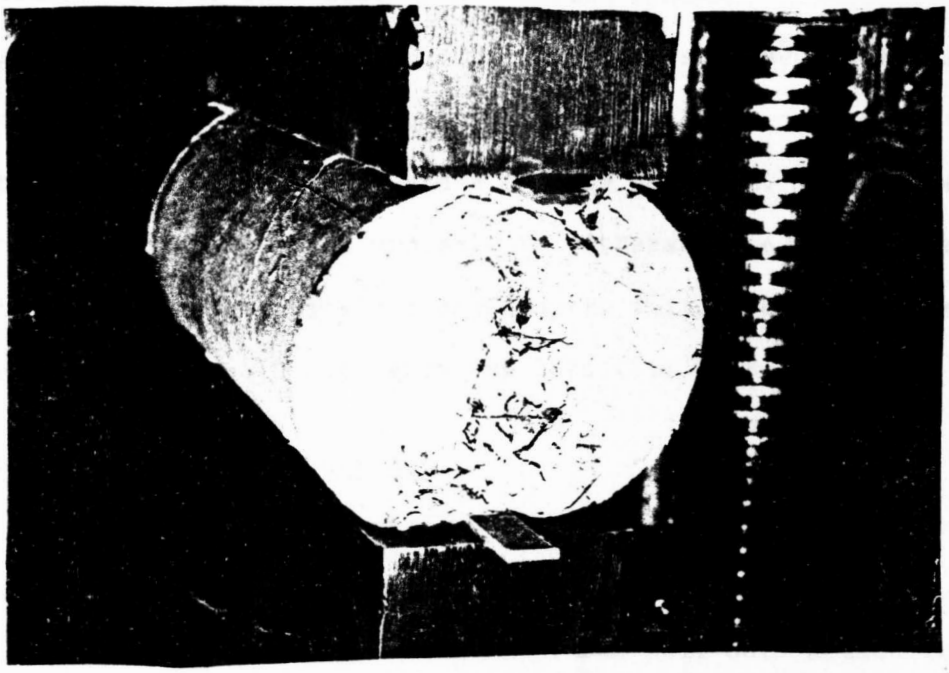

Figure 6.6 Failure of fibrous concrete in tension

failure with a single crack. Fibrous concrete cylinders failed at higher stresses and in a ductile manner with no sudden failure.

Table 6.5

Actual and Calculated Split Cylinder Strengths

% Steel Fiber	f_c' (psi)	f_{cta} (psi)	Calculated f_{cs} (psi) equation 6.2	% deviation from actual value
0.0	4,584	433	454	+4.8
0.8	4,805	555	592	+6.6
1.2	4,927	635	664	+4.6

6.4 Modulus of Rupture

The modulus of rupture of plain and fibrous concrete was determined for four standard size beam 6"x6"x21" using ASTM standard C78. The failure of plain concrete was sudden with a single crack, on the other hand the failure of fibrous concrete beams had two stages a first crack and a ductile collapse. After the first crack started the beam was able to withstand the load and even its load carrying capacity increased up to failure when the beams were exhausted and could not carry any load (figure 6.7, 6.8).

6.4.1 First Crack Strength

First crack started when the debonding of the fibers from the cement mortar began. When the bond shear strength between the two material was exceeded, a so called "fiber pull-out" action took place.

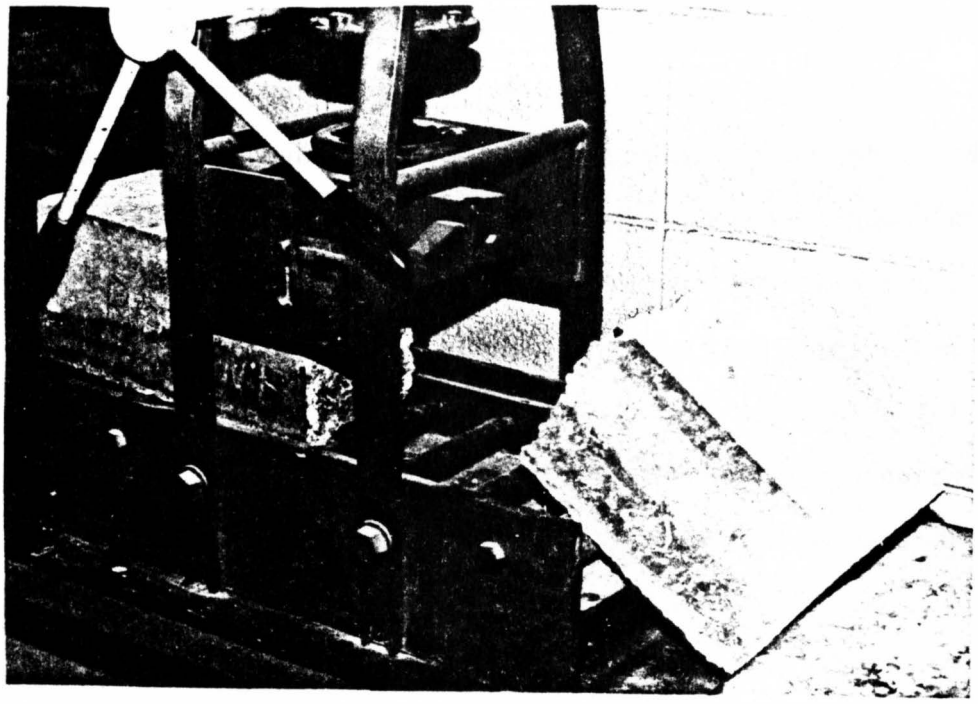

Figure 6.7 Failure of plain concrete in flexure

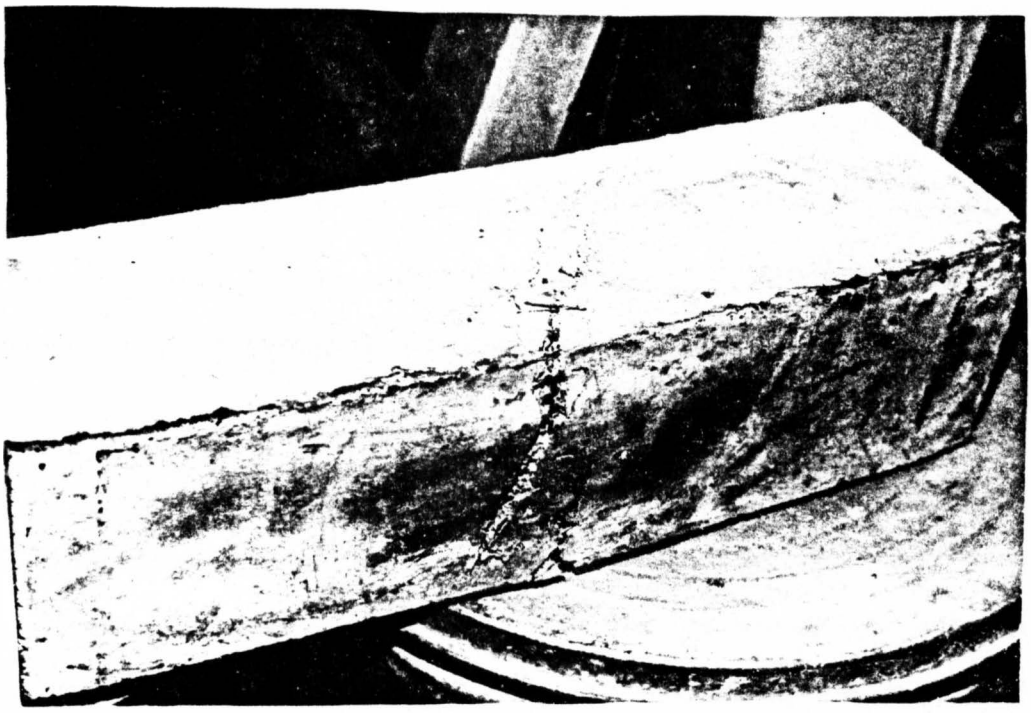

Figure 6.8 Failure of fibrous concrete in flexure

page 88

The results of the first crack strength are shown in table 5.6. The actual values were compared with ACI Code formula $f_r = 7.5\sqrt{f_c'}$ for normal weight concrete, and the percentage of deviation ranged from 2 to 42 percent. The ACI Code formula cannot be used for fibrous concrete, therefore a regression analysis was performed for the data and the ratio ($f_{rl}/\sqrt{f_c'}$) and volume percentage of steel fiber were plotted (figure 6.9). An intercept of 7.5 and a slope of 2.6 was obtained with F = 213 which is highly significant and a correlation coefficient of 0.9967 (Table D.3) meaning about 99 percent of the $f_{rl}/\sqrt{f_c'}$ variation due to increase of steel fibers is accounted for and the following equation can be used to calculate the first modulus of rupture of fibrous concrete.

$$f_{rl} = (7.5 + 2.6\ \rho_s)\ \sqrt{f_c'} \qquad (6.3)$$

where f_{rl} = first modulus of rupture psi

ρ_s = % steel fibers by volume

f_c' = compressive strength at 28 days (psi)

Table 6.6 compares the actual and calcualted values for first modulus of rupture using equation 6.3.

6.4.2 Ultimate Modulus of Rupture

After pull-out of fibers started to take place, the load carrying capacity increased slowly until the ultimate bond shear strength of fiber and cement was reached. Then the load decreased and the failure occured, but the failed specimen did not disintegrate because

Figure 6.9

First Modulus of rupture vs.
% Steel Fibers
$FR1=(7.5+2.6(\%S)\sqrt{FC'}$
Correlation coefficient=0.9967

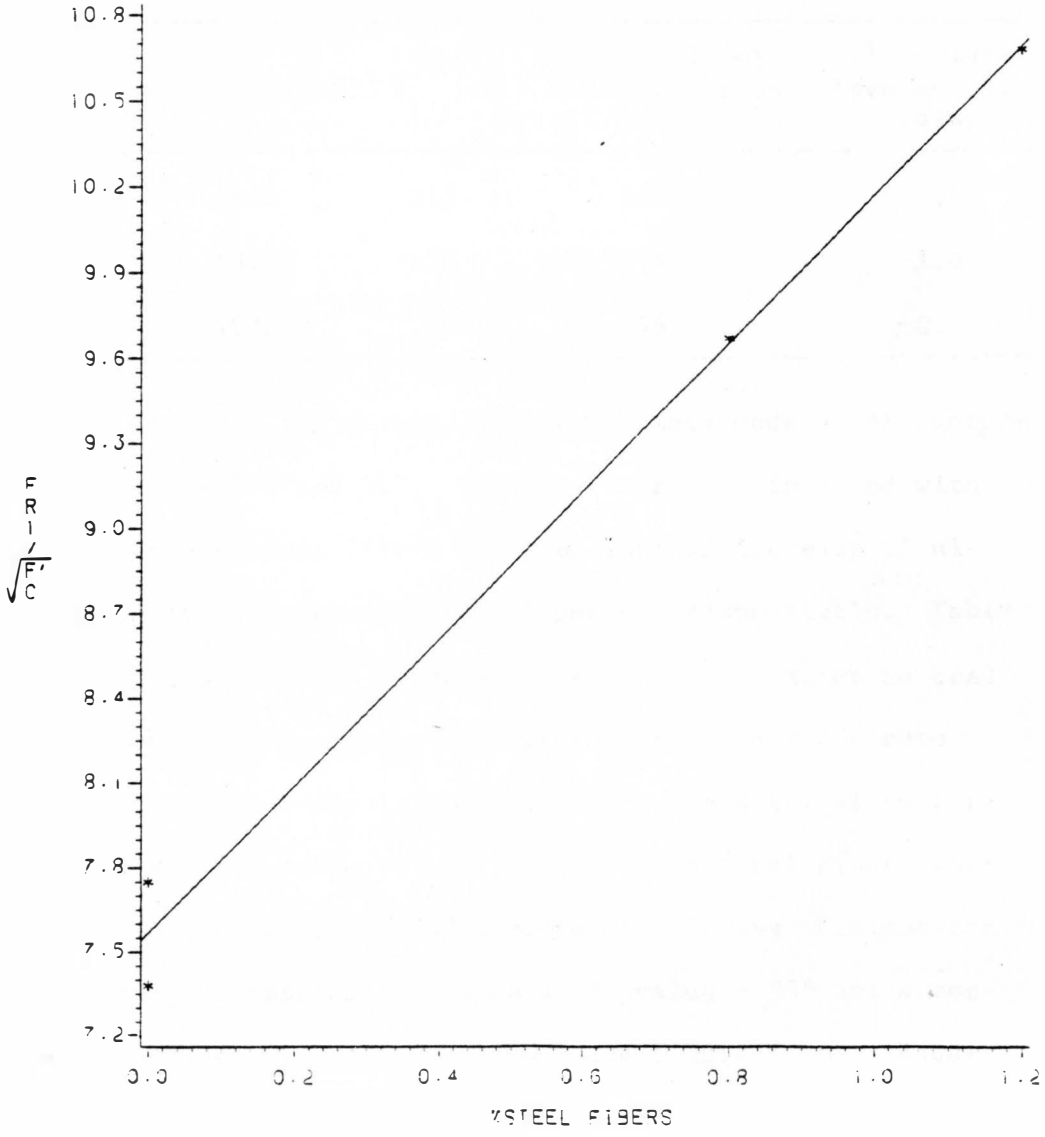

Figure 6.9 $FR1/\sqrt{FC'}$ vs. % Steel Fibers

Table 6.6

Actual and Calculated Values of First Modulus of Rupture Using Equation 6.3

% Steel Fibers	f_c' (psi)	f_{rl} psi	Calculated f_{rl} using equation 6.3 (psi)	% deviation from actual value
0.0	4584	513	508	+1.0
0.8	4805	670	664	-1.0
1.2	4927	750	745	-0.7

of the steel fibers. The results of the ultimate modulus of rupture is shown in tables 5.6 and 5.7. Fibrous concrete reinforced with 0.8 and 1.2 percent steel fibers resulted into an increase of ultimate modulus of rupture of 48 and 75 percent respectively. Table 5.6 also shows that the ACI formula ($f_r = 7.5\sqrt{f_c'}$) cannot be used to calculate the ultimate modulus of rupture for fibrous concrete.

A statistical analysis similar to first modulus of rupture was performed and the ratio ($f_{ru}/\sqrt{f_c'}$) versus % steel fibers were plotted. An intercept of 7.5 and a slope of 4.35 was obtained for the best fitting regression line with a 'F' value = 535 and a correlation coefficient of 0.994 (Table D.4 and figure 6.10). Equation 6.4 can be used to calculate the ultimate modulus of rupture of fibrous concrete with volume of steel fibers ranging from 0.0 to 1.2 percent.

$$f_{ru} = (7.5 + 4.35\ \rho_s)\ \sqrt{f_c'} \qquad (6.4)$$

Figure 6.10

Ultimate Modulus of rupture vs.
% Steel Fibers
FRU=(7.5+4.35ρ_s)$\sqrt{FC'}$
Correlation coefficient=0.994

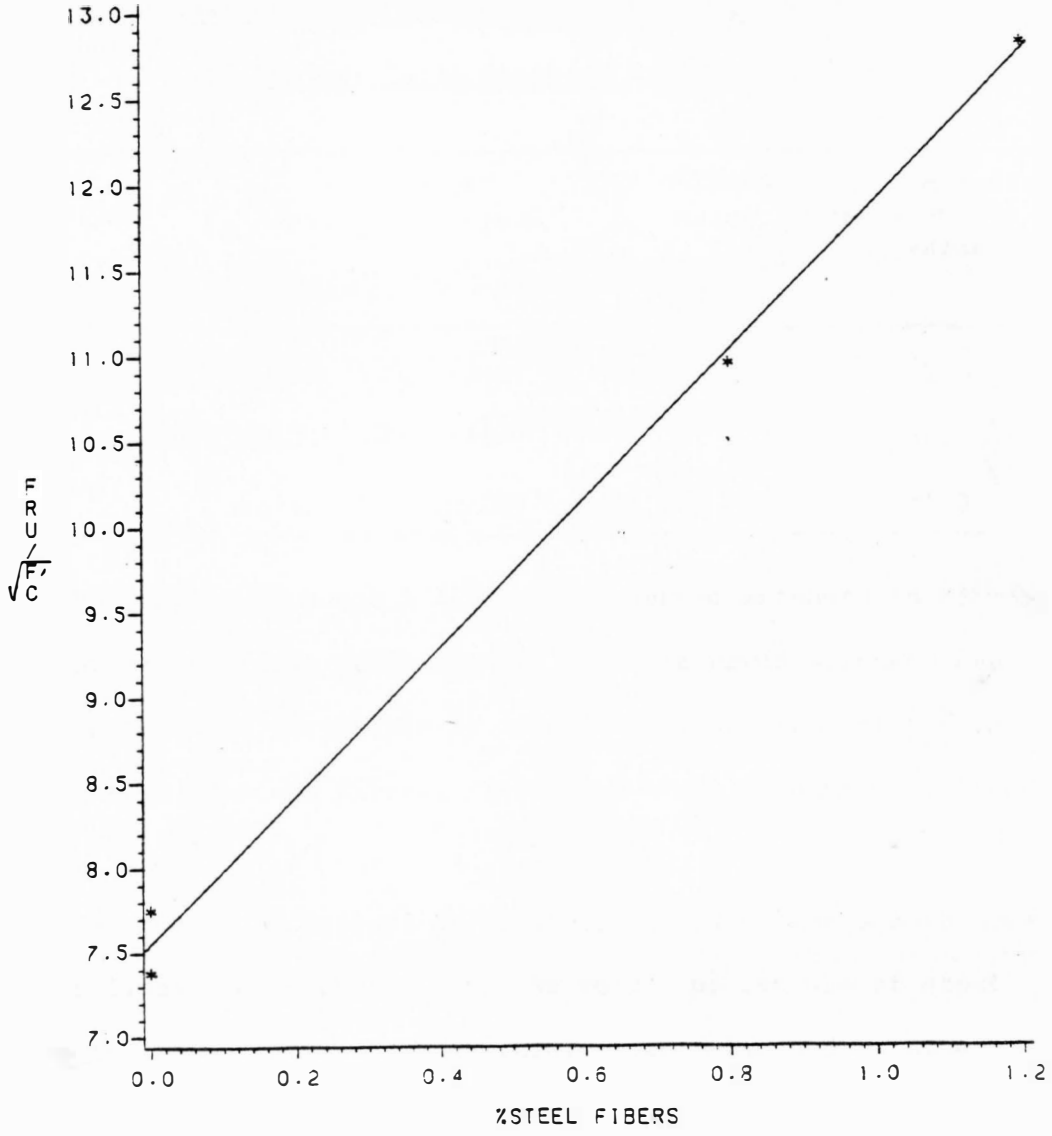

Figure 6.10 FRU/$\sqrt{FC'}$ vs. % Steel Fibers

Table 6.7 shows the actual and calculated ultimate modulus of rupture for plain and fibrous concrete using equation 6.4.

Table 6.7

Actual and Calculated Ultimate Modulus of Rupture Using Equation 6.4

% Steel Fibers	f_c' (psi)	Actual f_{ru} (psi)	Calculated f_{ru} using equation 6.4 (psi)	% deviation from actual value
0.0	4,584	513	508	-1.0
0.8	4,805	760	761	+0.2
1.2	4,927	900	892	-1.0

The results of table 5.7 shows a reserved strength in fibrous concrete after the first crack occurs. This reserved strength can be shown in terms of percentage by calculating the ratio of $\frac{f_{ru}}{f_{rl}}$ for each percentage of steel fibers. Table 6.8 shows a summary of these results.

The modulus of rupture at first crack and ultimate both have a positive linear relationship with the volume percentage of steel fibers up to 1.2 percent. Similar results were obtained by other researchers[34,47] where they concluded a positive linear relationship between flexural strength of concrete with the percentage of steel fibers.

Table 6.8

% Steel Fiber	f_{ru} (psi)	f_{rl} (psi)	$\frac{f_{ru}}{f_{rl}}$	% strength reserved	% strength reserved from suggested equations
0.0	513	513	1.00	0.0	0.0
0.8	760	670	1.13	13.0	14.0
1.2	900	750	1.20	20.0	19.0

6.5 Rotations

Rotation capacity of reinforced concrete continuous beams was determined and the results are shown in table 5.9. Important factors affecting the prediction of actual rotation capacity of reinforced concrete are the plastic hinge length, and the curvature distribution factor. Equation 2.3 ($\theta_p = \beta.\phi_p.H_L$) shows the importance of the correct assumption of (H_L) and (β), where in most calculations (β) is taken as unity and (H_L) = d (effective depth). In this section the results obtained from actual testing will be statistically analyzed and also the effect of steel fibers on plastic rotation of reinforced concrete will be discussed.

6.5.1 Plastic Hinges

The plastic hinges were measured as explained in section 5.5 and the results are shown in table 5.8. Actual plastic hinges are shown in figures 6.11 and 6.12.

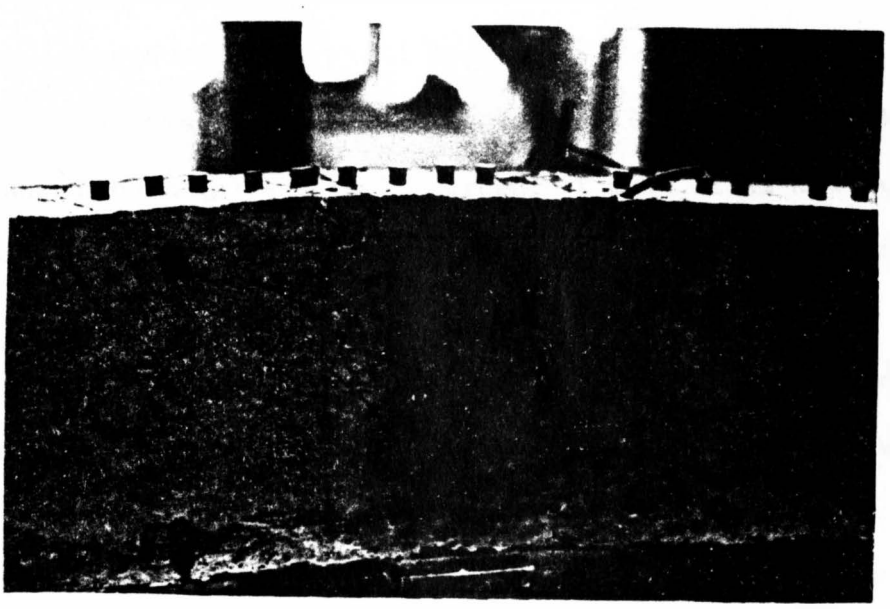

Figure 6.11 First plastic hinge at middle support

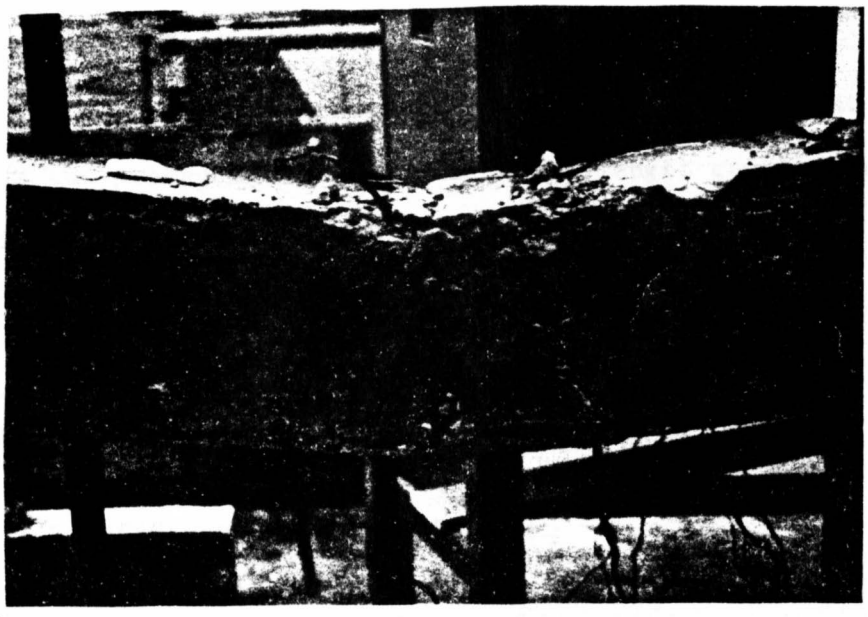

Figure 6.12 Second plastic hinge at positive section

A multiple regression analysis was done on the effect of steel fibers and main steel percentage on the length of the plastic hinge. Statistical analysis shows that (H_L), the plastic hinge depends on both (ρ) and (ρ_s), percent of main steel and percent of steel fibers. As mentioned in section 1.5 the length of the plastic hinge is related to the effective depth of the section, the most common assumption is $H_L = d$. In this research it was found that, the length of the plastic hinge can be written as $H_L = \alpha.d$ where $\alpha = f(\rho, \rho_s)$. Different statistical models were tested, one, two or three variables and the best was decided to be a one variable quadratic model with (F = 9) because R^2 for two or three variable model is not significantly higher than that of one variable (Table D.5), therefore:

$$\alpha = 1.06 + 0.13 \rho_s$$

where ρ = % of main steel ($\rho_{min} \leq \rho \leq \rho_{max}$)

ρ = % steel fibers between 0.0 and 1.2 percent

From the preceding, the plastic hinge length can be predicted by using equation 6.5.

$$H_L = (1.06 + 0.13 \rho\rho_s).d \qquad (6.5)$$

Table 6.9 compares the actual and estimated values using equation 6.5

6.5.2 Curvature Distribution Factor

The actual results of $\beta = \frac{\theta_{pc}}{\theta_p H_L}$ the curvature distributon factor are presented in table 5.10. A multiple regression analysis was

Table 6.9

Actual and Calculated Plastic Hinge Length

% main Steel	% steel fibers	Actual Plastic hinge (in)	Calculated Plastic Hinge	% deviation from actual value
	0.0	8.0	7.0	-12
0.67	0.8	6.5	7.4	+14
	1.2	7.5	7.6	+ 1
	0.0	7.0	6.9	- 1
1.21	0.8	8.0	7.7	- 4
	0.0	6.5	6.8	+ 4
1.89	0.8	8.0	8.0	0
	1.2	9.0	8.7	- 3

performed for the data obtained and the best fitting model for the data was a straight line relationship between (β) and (ρ_s) the percent of steel fibers figure 6.13. The effect of main steel was neglegible and also no interaction between (ρ) and (ρ_s) was present. An intercept of (0.56) and a slope of (-0.16) with (F = 65) and a correlation coefficient of 0.056 was obtained (Table D.6). Equation 6.6 can be used to predict the curvature distribution factor.

$$\beta = 0.56 - 0.16\,\rho_s \qquad (6.6)$$

where ρ_s = % steel fiber ($0 \leq \rho_s \leq 1.2$)

Figure 6.13

Curvature distribution factor vs.
Steel Fibers
$\beta = 0.56 - 0.16\rho_s$
Correlation coefficient=0.956

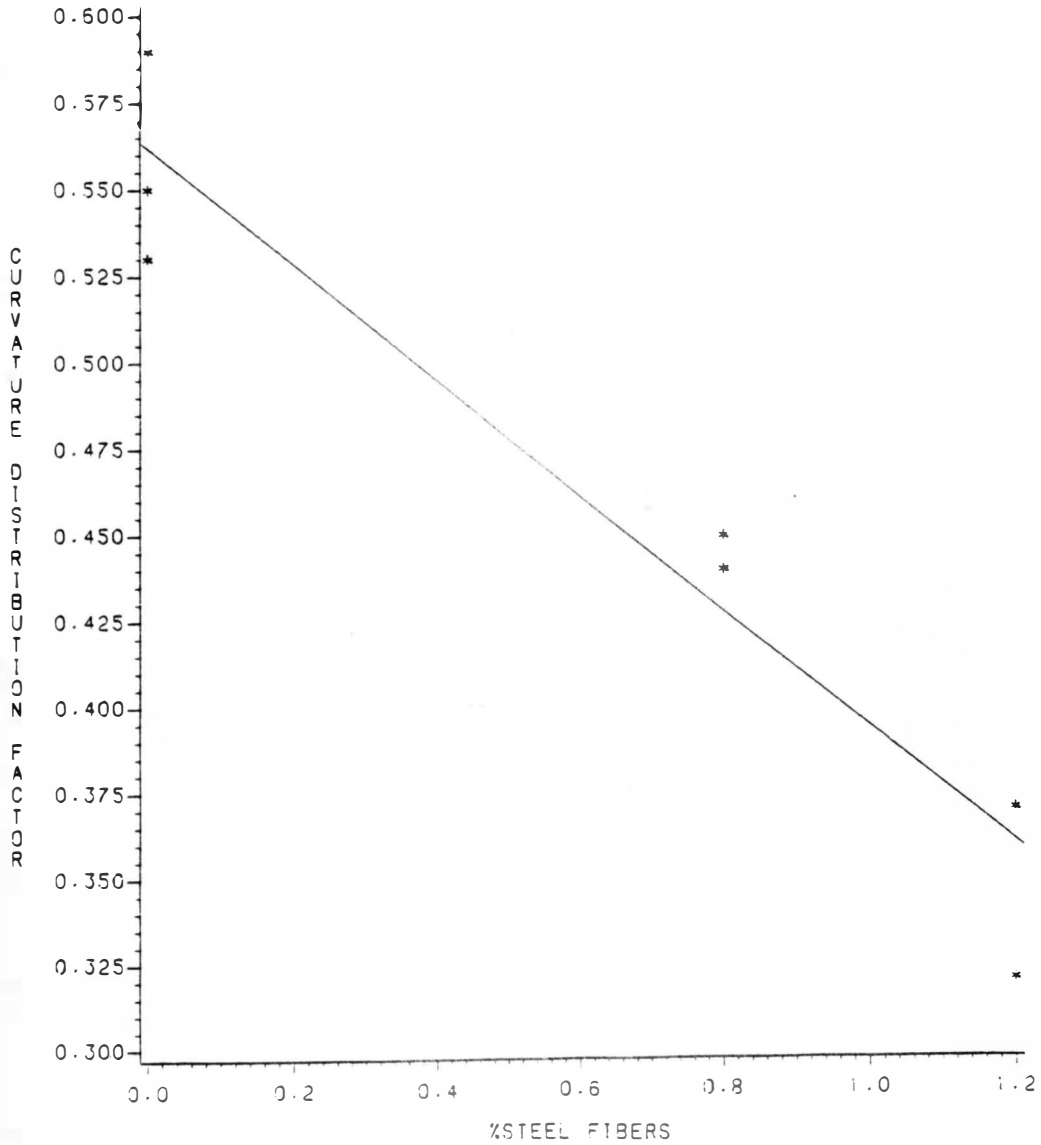

Figure 6.13 β vs. Steel Fibers

From equation 6.6 a (β) value of 0.56 is suggested for plain concrete and as steel fibers are added to the mix 'β' is reduced. Table 6.10 compares the actual and calculated curvature distribution factors using equation 6.6.

Table 6.10

Actual and Calculated 'β' Using Equation 6.6

% main Steel	% steel Fibers	Actual 'β'	Calculated β by equation 6.6	% deviation from actual value
	0.0	0.59	0.56	- 5
0.67	0.8	0.44	0.43	- 2
	1.2	0.32	0.37	+ 4
	0.0	0.54	0.56	+ 3
1.21	0.8	0.45	0.43	- 4
	1.2	-	0.37	-
	0.0	0.53	0.56	+ 5
1.89	0.8	0.44	0.43	- 2
	1.2	0.37	0.37	0

When steel fibers were used, the curvature distribution factor decreased especially for 1.2% steel fibers, 'β' was approximately cut in half. Chan[15] also reported a 34% reduction in 'β' when secondary reinforcement was used in concrete. He also concluded that longitudinal steel ratios have only a small influence

on (β), this was also concluded in this research. Kaushik and Ramamurthy and Kukreja[27] recommended a (β) of 0.5 for plain concrete. Cohn and Petcu[17] concluded that (β) ranges between 0.34 and 0.97 and a value of 0.5 to 0.6 seems to be satisfactory.

The distribution of the cracks at the negative moment region is shown in figure (6.14a). The actual and idealized curvature distribution along the members are shown in figure (6.14b), where the dashed area represents the total plastic rotation over the support.

The reduction of curvature distribution factor of fibrous concrete does not imply that the rotation capacity of fibrous concrete is lower than plain concrete. If two fibrous and plain reinforced concrete beams with identical geometry and main bars have the same plastic curvature at failure, then the use of steel fibers would be of a disadvantage because of the reduction of β. It is apparent from this research that the plastic curvature of fibrous concrete is substantially higher than that of plain concrete; therefore, the effect of the reduction of curvature distribution factor on the plastic rotation capacity of fibrous concrete is minimal. Table 6.11 shows the actual rotations after curvature distribution factor has been applied. Figure 6.15 shows the distribution of the curvature along the plastic hinges. The curvature distribution of each beam is plotted according to the results in table 5.10. β represents the ratio of the area under each curve to the area of the rectangle $(\phi_p . H_L)$.

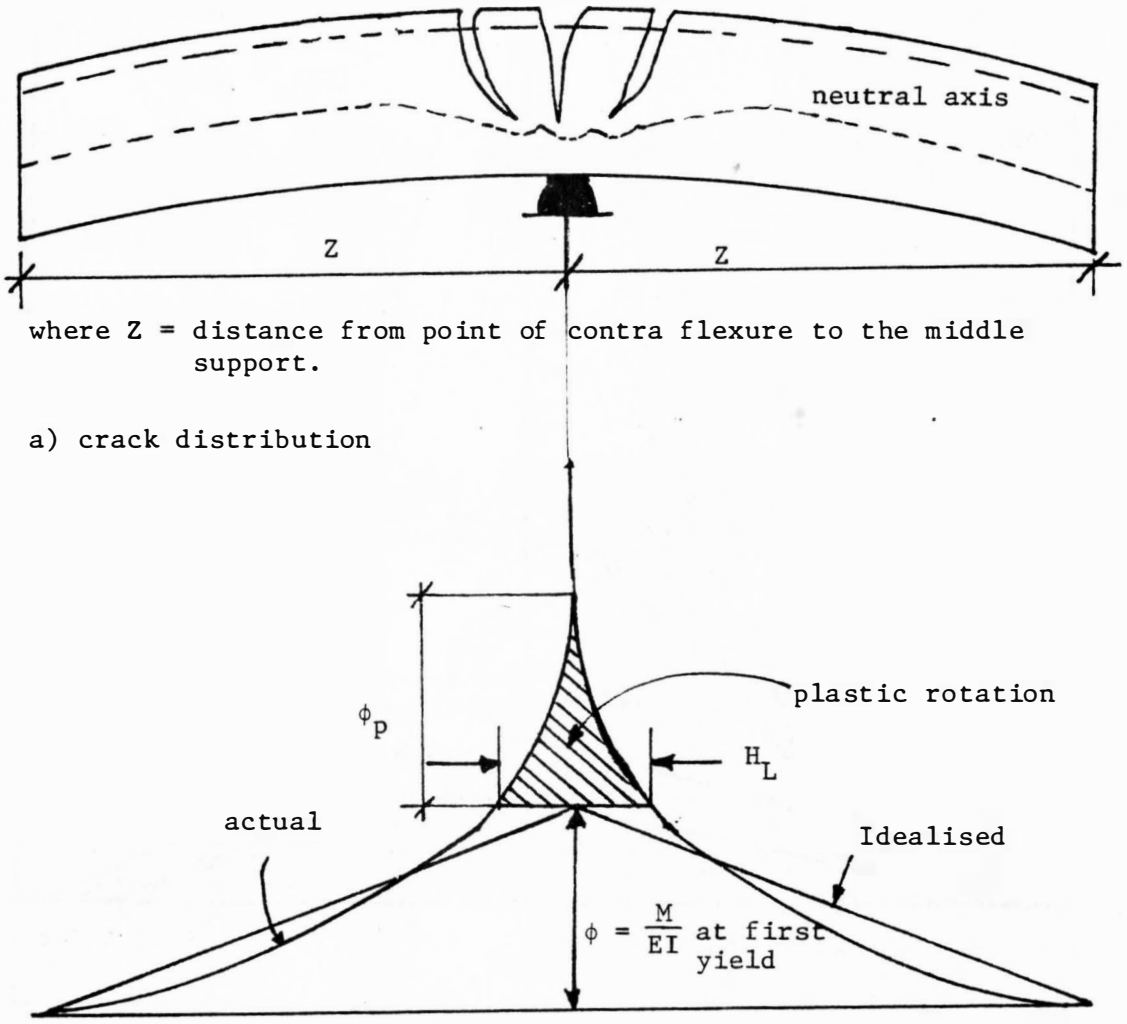

Figure 6.14 Typical deformation of a member

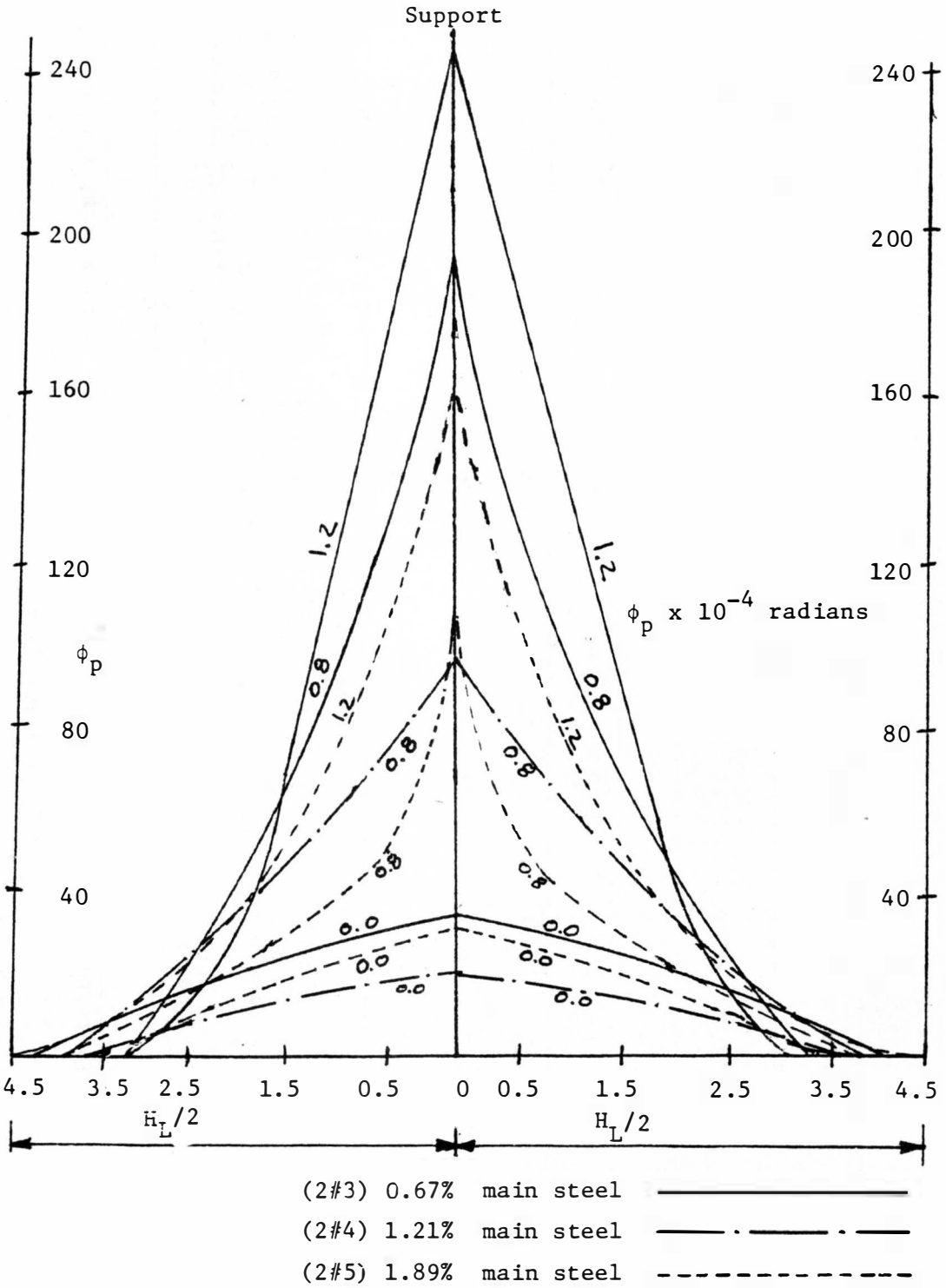

Note: The numbers labeled on curve are the percentage of steel fibers

Figure 6.15 Actual curvature distribution along the plastic hinge

Table 6.11

Effect of Curvature Distribution Factor on Plastic Rotation Capacity of Fibrous Reinforced Concrete

% main steel ρ	f_y ksi	% Steel Fibers ρ_s	ϕ_p	$\phi_p . H_L$ from table 5.9 x 10^{-4} radians	β using equation 6.6	Actual rotation $\theta_p = \beta . \phi_p . H_L$ x 10^{-4} radians from testing	θ_{pc} x 10^{-4} radians from testing	% deviation from θ_{pc}	% increase of plastic rotation from 0% steel fibers
		0.0	37	298	0.56	167	175	-4.5	-
0.67	66	0.8	196	1277	0.43	549	559	-1.8	+230
		1.2	257	1924	0.37	712	616	+1.5	+326
		0.0	21	145	0.56	81	78	+4.0	-
1.21	72	0.8	98	781	0.43	336	352	-4.5	+310
		0.0	37	238	0.56	133	127	+4.7	-
1.89	52	0.8	110	876	0.43	376	385	-2.3	+182
		1.2	166	1495	0.37	553	554	-0.2	+315

It is concluded from figure 6.15 that the curvature distribution for a plain concrete plastic hinge is close to a first degree curve, and the plastic hinges with 0.8% steel fibers have a second degree parabola curvature distribution, and the plastichinges that consist of 1.2% steel fibers have a third or higher degree curve representing the curvature distribution.

6.5.3 Plastic Rotation Capacity

As explained in Chapter I the calculation of plastic rotation of reinforced concrete is a very tedious process. There are many factors involved which could change the outcome of the calculations tremendously. Therefore the necessary assumptions have to be made with extreme caution.

The following can be stated as a general idea on plastic rotation of reinforced concrete.

$$\theta_p = f(\phi_p, \beta, H_L)$$

This experimental research project was done to suggest a formula so the rotation capacity of reinforced concrete and especially fibrous concrete could be calculated.

A statistical analysis was done on the ratio of actual rotations (based on strains) to the calculated rotations, with percentage of steel fibers, percentage of main steel and yield strength of steel bars. A three variable model with F = 78 and a correlation coefficient of 0.99 was found (Table D.7). Equation 6.7 can be used to estimate the plastic rotation of fibrous concrete.

$$\theta_p = \gamma.\beta.\theta_{pl} \qquad (6.7)$$

where $\gamma = 4.3 + 2.24\ \rho_s - 0.043\ f_y + 4.17\ \rho\rho_s$

$\beta = 0.56 - 0.16\ \rho_s$

$$\theta_{pl} = \frac{0.0035}{K_u} - \frac{f_y}{E_s(1-K_u)} \qquad (2.6)$$

Therefore:

$$\theta_p = \gamma.\beta\ \left(\frac{0.0035}{K_u} - \frac{f_y}{E_s(1-K_u)}\right) \qquad (6.8)$$

where: f_y = yield strength of steel (Ksi)

E_s = modulus of elasticity of steel (Ksi)

K_u = ratio of the depth of neutral axis to the effective depth.

Equation (6.8) is an empirical equation based on actual testing. It is of evidence that the plastic rotation estimation of fibrous reinforced concrete is dependent upon the percentage of steel fibers, percentage main steel and the yield strength of the main bar where an increase in yield strength of steel, reduces the plastic rotations.

Equation (6.8) includes the effect of plastic hinge length change on the rotation, therefore no adjustment is required.

Equation (6.8) can be simplified and reduced conservatively to the following equation (6.9)

$$\theta_p = \gamma.\beta.\ \frac{0.003}{K_u} \qquad (6.9)$$

where: $K_u = \frac{A_s f_y}{0.72 f_c' b}$

$\gamma = 4.3 + 2.24 \rho_s - 0.043 f_y + 4.17 \rho\rho_s$

$\beta = 0.56 - 0.16 \rho_s$

ρ_s = % steel fibers

ρ = % main steel

The CEB-FIP (Comite Euro-International du Beton) of 1978 suggested $\theta_p = \frac{0.004}{K_u}$ which seems to over-estimate the rotation capacity of reinforced concrete.

Table 6.12 shows a comparison between actual plastic rotation from testing and plastic rotation capacity calculated from equations 6.8 and 6.9. The percent deviation of the results obtained from equations 6.8 and 6.9 are in the last columns of table 6.12. The maximum and minimum deviations of equations 6.8 and 6.9 are between 4 and 14 percent. The results of the calculated rotations using equation 6.8 are within 15 percent of the actual values, and using equation 6.9 gives deviation of less than 8 percent except when 2#5 main bars with 0.8 steel fibers were used.

The plastic rotation capacity of fibrous concrete was between 200 and 320 percent, higher than plain concrete which shows the superiority of fibrous concrete over plain concrete in plastic deformation.

6.5.4 Ductility Index

The ratio of ultimate to yield curvature is called the ductility index ($\mu = \frac{\phi_u}{\phi_y}$). This is another method to evaluate the ductility of a material in flexure.

Table 6.12

Comparison of Actual and Calculated Plastic Rotation Capacities Using Equations 6.8 and 6.9

% main Steel ρ	% Steel Fibers ρ_s	Actual Plastic Rotation Capacity from Testing x 10^{-4} radians	Plastic Rotation Capacity Using Equation 6.8 x 10^{-4} radians	% Deviation from Actual θ_{pc}	Plastic Rotation Capacity Using Equation 6.9 x 10^{-4} radians	% Deviation from Actual θ_{pc}	% Deviation Between Equation 6.8 and 6.9
	0.0	176	189	+ 7	181	+ 3	- 4
0.67	0.8	559	580	+ 4	550	- 2	- 5
	1.2	616	693	+12	657	+ 6	- 5
	0.0	78	71	- 9	81	+ 4	+14
1.21	0.8	352	339	- 3	375	+ 6	+10
	0.0	127	107	-15	116	- 8	+ 8
1.89	0.8	385	430	+11	461	+19	+ 7
	1.2	554	533	- 4	568	+ 2	+ 6

Cohn[19] recommended that a ductility index of at least 5 is required for plastic analysis. The ductility index for this experiment is shown in table 6.13.

Table 6.13

Ductility Index

Beam	% Steel Fibers	ϕ_y x 10^{-4} rad	ϕ_u x 10^{-4} rad	$\mu = \frac{\phi_u}{\phi_y}$
	0.0	10.60	48.0	4.5
2#3	0.8	6.67	203.0	31.0
	1.2	7.30	264.3	36.0
	0.0	10.60	31.2	3.0
2#4	0.8	10.50	108.0	10.3
	0.0	6.76	43.0	6.4
2#5	0.8	11.50	121.0	10.5
	1.2	8.35	174.0	20.8

Table 6.13 shows that when steel fibers are used the ductility index increases significantly, especially when 0.8 to 1.2 percent of steel fibers were used.

Therefore the inclusion of steel fibers added to the ductility. On average, when 0.8% steel fibers were used, the ductility index increased by a factor of about 4 from that of plain concrete and when 1.2 percent steel fibers were used, it increased by a factor of 5 .

A simple regression analysis using the ratios of the ductility index of fibrous to plain concrete ($\frac{\mu'}{\mu}$) and percent steel fibers, results into the following equation to estimate the ductility of fibrous concrete (Table D.8).

$$\mu' = (1 - 3.8\ \rho_s)\mu \qquad (6.10)$$

where: μ = the ratio of ultimate to yield curvature for plain concrete

ρ_s = % steel fibers

μ' = ductility of fibrous concrete

Figure 6.16, 6.17, 6.18 show the rotation of plain and fibrous concrete.

6.6 Deflections

The deflection calculations and actual measurements at service load are shown in table 5.12. The deviation of actual measurements from the calculated deflection had a maximum value of 14 percent and a minimum of 1.5 percent.

The effect of steel fibers on deflections has been tested in previous research works[34,47]. These researchers concluded that in simply supported beams, because of the increase in (I_e) the stiffness increased so the deflections decreased, when steel fibers were used. In this research it is concluded from table 5.12 that the effect of steel fibers on deflections in continuous reinforced concrete beams with an f_c' of 4000 to 5000 psi is minor. The maximum decrease of deflection was 10% when 2#5 bars with yield strength of

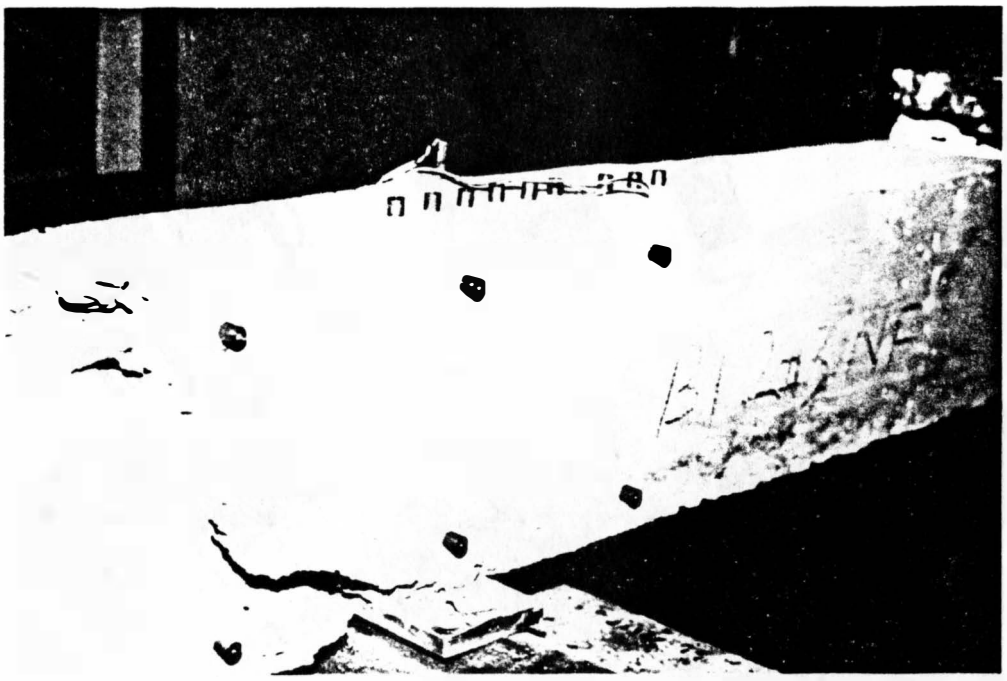

Figure 6.16 Rotation of plain concrete (0% fibers)

Figure 6.17 Rotation of fibrous concrete (2#5, 1.2% fibers)

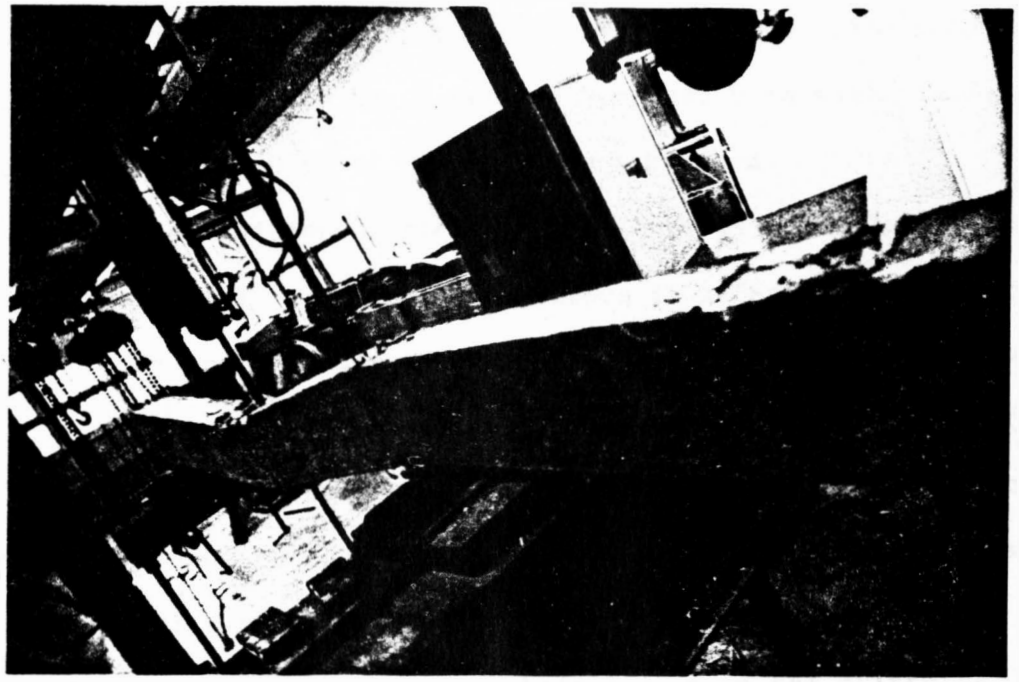

Figure 6.18 Rotation of fibrous concrete (2#3, 1.2% fibers)

51 Ksi and 0.8 percent of steel fibers were used. The maximum increase of deflection was 8 percent when 2#3 bars with yield strength of 66.8 Ksi and 0.8% of steel fibers were used.

The addition of steel fibers, creates a double effect on the stiffness (EI_e) of concrete, therefore it affects the deflections.

1) The increase of effective moment of inertia due to the increase of modulus of rupture and modular ratio (n).
2) The decrease of modulus of elasticity of fibrous concrete due to change in bond characteristics within the matrix.

These results can be obtained from table 5.12. The analysis of the results of (I_e) and (E_{ca}) and their effect on the stiffness of fibrous concrete are shown in table 6.14. If the increase of (I_e) is more significant than the decrease of E_c, the deflections will be less at service load for fibrous concrete. But when the decrease of (E_c) has more significant affect on the stiffness than the increase of (I_e), then the deflections at service load will be higher for fibrous concrete beams. Therefore the stiffness of fibrous concrete could decrease or increase depending on the properties and behavior of fibrous concrete under bending.

An important issue regarding the calculation of the effective moment of inertia (I_e) is, whether to use only the cracked moment of inertia of the section, or assume that parts of the beam are uncracked and include the gross moment of inertia in the calculations of (I_e).

Table 6.14

Effect of Modulus of Elasticity and Effective Moment of Inertia of Fibrous Concrete on Its Stiffness

(1) % Main Steel	(2) % Steel Fibers	(3) $\frac{M_{cr}}{M_a}$	(4) I_g term*	(5) % of Total I_e	(6) I_{cr} term*	(7) % of Total I_e	(8) I_e = (I_g term + I_{cr} term) in^4	(9) ** Ratio (1) for (I_e)	(10) E_c x10^6 psi	(11) ** Ratio (2) for (E_c)	(12) Ratio (1)x Ratio (2) (EI_e)
	0.0	0.41	15.34	25.9	43.95	74.1	59.28	1.00	3.97	1.00	1.00
0.67 (2#3)	0.8	0.54	33.92	44.5	42.39	55.5	76.31	1.28	3.67	0.92	1.17
	1.2	0.61	48.0	52.0	44.36	48.0	92.36	1.56	3.02	0.76	1.18
	0.0	0.26	3.61	4.7	72.95	95.3	76.56	1.00	3.97	1.00	1.00
1.21 (2#4)	0.8	0.34	8.02	9.7	74.97	90.3	83.00	1.08	3.67	0.92	0.99
	1.2	0.38	11.26	12.0	82.87	88.0	94.13	1.23	3.02	0.76	0.94
	0.0	0.24	3.04	3.1	95.81	96.9	98.85	1.00	3.97	1.00	1.00
1.89 (2#5)	0.8	0.32	6.76	6.4	99.25	93.6	106.00	1.07	3.67	0.92	0.98
	1.2	0.35	9.51	8.0	108.92	92.0	118.43	1.20	3.02	0.76	0.92

$$*I_e = \underbrace{\left(\frac{M_{cr}}{M_a}\right)^3 I_g}_{I_g \text{ term}} + \underbrace{\left[1 - \left(\frac{M_{cr}}{M_a}\right)^3\right] I_{cr}}_{I_{cr} \text{ term}}$$

** Ratio (1) = $\frac{\text{Effective moment of inertia of fibrous concrete}}{\text{Effective moment of inertia of plain concrete}}$

Ratio (2) = $\frac{\text{Modulus of elasticity of fibrous concrete}}{\text{Modulus of elasticity of plain concrete}}$

From columns (5) and (7) of table 6.14, it is apparent that as the percentage of steel fibers in the mix increases, the contribution of (I_g) (gross moment of inertia) to (I_e) (effective moment of inertia) increases and therefore, the contribution of (I_{cr}) (cracked moment of inertia) to (I_e) decreases. This indicates that the inclusion of fibers increases the length of the uncracked region and reduces the cracked portion of the beam, which means in fibrous concrete the gross moment of inertia is more important than in plain concrete. This was true in all cases where different main steel percentage was used.

Also from table 6.14, when low steel percentage (less than 1%) was used the effect of (I_g) was between 26 and 52 percent for zero and 1.2% steel fibers. As the main steel percentage (ρ) increased the ratio of $(\frac{M_{cr}}{M_a})$ decreased. Column (3) of table 6.14 shows the decrease of $(\frac{M_{cr}}{M_a})$ which reduces the effect of (I_g) on (I_e) to less than 12 percent.

From the preceding paragraph it can be concluded that when the ratio of $(\frac{M_{cr}}{M_a})$ is less than 0.40 or high steel percentage is used (> 1%), (I_g) will be much less significant. When low steel percentage is used the ratio $\frac{M_{cr}}{M_a}$ is higher, which results in less cracked regions along the member.

The increase of the effective moment of inertia of fibrous concrete is mainly caused by: a) the increase in modulus of rupture which increases the cracking moment and b) the increase of modular ratio (n) which increases the cracking moment of inertia (I_{cr}).

Therefore a modification of the ACI Code's equation for calculation of the effective moment of inertia is required when fibrous concrete is used. The modifications are as follows:

$$I_e = \left(\frac{M_{cr}}{M_a}\right)^3 I_g + \left[1 - \left(\frac{M_{cr}}{M_a}\right)^3\right] I_{cr} \quad \text{(plain concrete)}$$

1) Modification of (M_{cr}):

As mentioned in section 6.4, fibrous concrete has two modulus of ruptures.

1 - First modulus of rupture

$$f_{r1} = k_1 (7.5\sqrt{f_c'}) = (1 + 0.35\ \rho_s)\ 7.5\ \sqrt{f_c'} \qquad (6.3)$$

2 - Ultimate modulus of rupture

$$f_{ru} = k_2 (7.5\sqrt{f_c'}) = (1 + 0.58\ \rho_s)\ 7.5\ \sqrt{f_c'} \qquad (6.4)$$

The cracking moment calculation is based on the first modulus of rupture because in plain concrete, first and ultimate modulus ruptures are the same.

In fibrous concrete, the first cracking moment and ultimate cracking moments are different, therefore, either values could be used which could cause over or under estimation of deflections and therefore, an average value will be used.

$$M_{cr} = \frac{f_r\ I_g}{y_t} \quad (\rho_s = 0)$$

$$M_{cr}' = \frac{f_r'\ I_g}{y_t} = k.M_{cr} \quad (\rho_s > 0)$$

where: M_{cr} = cracking moment of plain concrete

M_{cr}' = cracking moment of fibrous concrete

$k = (1 + 0.5\ \rho_s)$ the factor that estimates M_{cr}' for fibrous concrete

(k) is the equation of the best fit line, using regression analysis through $\frac{f_{r'}}{f_r}$ and percentage of steel fibers (table D.9)

where: $f_r' = \frac{f_{rl} + f_{ru}}{2}$ for each case.

f_r = modulus of rupture for plain concrete $(7.5\sqrt{f_c'})$

Therefore:

$$M_{cr}' = (1 + 0.5\ \rho_s)\ M_{cr} = k\ M_{cr} \qquad (6.11)$$

2) Modification of (I_{cr}):

The cracking moment of inertia increases as the percentage of steel fiber increase. This is due to the increase in the modular ratio (n).

$$I_{cr} = \frac{b\overline{Kd}^3}{3} + n\ A_s\ (d - Kd^2)$$

where: $n = \frac{E_s}{E_c}$

The decrease in the modulus of elasticity of concrete when steel fibers are used, causes an increase of (n) which increases the cracking moment of inertia.

$$I_{cr}' = \lambda\ I_{cr} \qquad (6.12)$$

where $\lambda = (1 + 0.14\ \rho_s)$ from regression analysis, which is the best fit line through the data of $\frac{I_{cr}'}{I_{cr}}$ versus percent of steel fibers (Table D.10).

From the preceding discussion, the effective moment of inertia of fibrous concrete can be calculated as follows:

$$I_e' = \left(\frac{M_{cr}'}{M_a}\right)^3 I_g + \left[1 - \left(\frac{M_{cr}'}{M_a}\right)^3\right] I_{cr}' \qquad (6.13)$$

where: I_e' = effective moment of inertia of fibrous concrete

M_{cr}' = cracking moment of fibrous concrete

$$M_{cr}' = k.M_{cr} = (1 + 0.5\ \rho_s)\ M_{cr}$$

I_{cr}' = moment of inertia of a cracked section for fibrous concrete

$$I_{cr}' = \lambda\ I_{cr} = (1 + 0.14\ \rho_s)\ I_{cr}$$

M_{cr} = Cracking moment of plain concrete $\left(\frac{f_r\ I_g}{y_t}\right)$

I_{cr} = Moment of inertia of a cracked plain concrete section

$$I_{cr} = \frac{b\overline{Kd}^3}{3} + n\ A_s\ (d - Kd)^2$$

Table 6.15 shows a comparison between actual and the calculated effective moment of inertia and deflection using equation 6.13. The actual 'I_e' was calculated using actual deflections from testing and the measured modulus of elasticity.

$$I_{e_{actual}} = \frac{PL^3}{100\ E_c\ \Delta_{actual}}$$

where:

$\dot{P} = 0.6\ P_u$

L = span length

E_c = actual modulus of elasticity (psi) from testing

Also from table 6.14 (column 12) the ratio of $\frac{E_c I_e'}{E_c I_e}$ is calculated which represents the change in stiffness of concrete when steel fibers are used. When low steel percentage was used (< 1%) the increase in stiffness was about 18%, where in higher steel percentage it remained unchanged or even reduced in most cases. Therefore when low steel percentage is used the deflection could improve by using steel fibers.

The maximum deflections at failure for plain concrete ranged from 0.4 to about 1.0 inch, where the maximum deflection at failure for fibrous concrete ranged from 2 to 5 inches. Figure 6.19 show the deflection of fibrous concrete at failure. The high deflections at failure of fibrous concrete is another indication of the ductility and strain energy absorption capacity that fibrous concrete has.

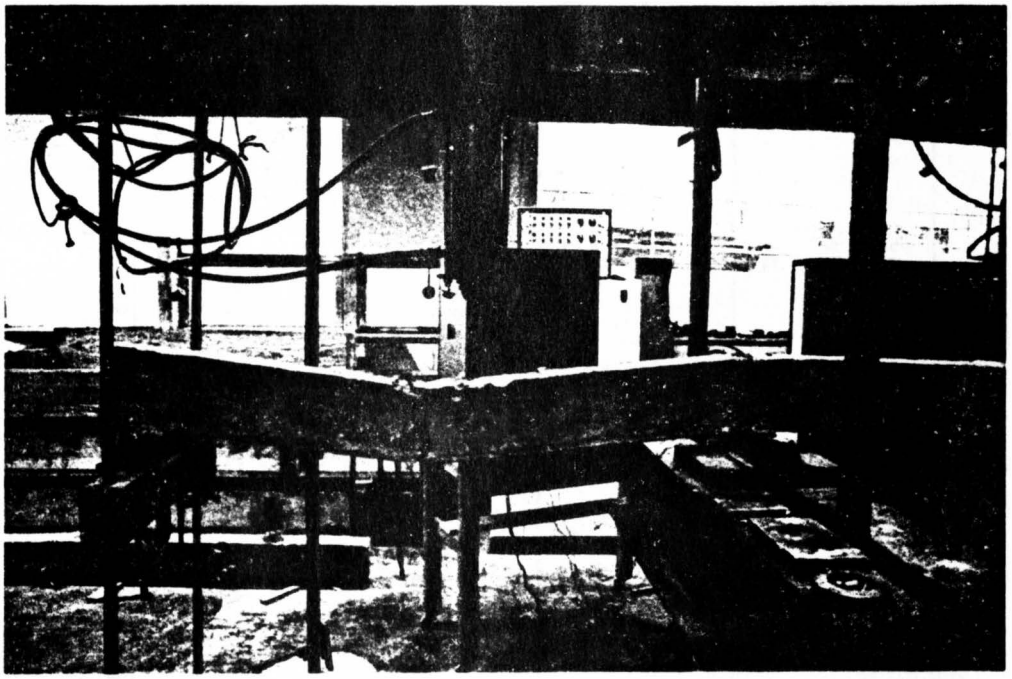

Figure 6.19 Deflection of Fibrous Concrete at Failure

Table 6.15

Comparison of Actual and Calculated Effective Moment of Inertia and Deflection Using Equation 6.13

% Main Steel	% Steel Fibers	Actual I_e in^4	Calculated I_e' using Equation 6.13	Actual Deflection $x10^{-3}$ in	Calculated Deflection Using I_e'	% Deviation from actual Deflection
	0.0	69	60.0	55	63	+14
0.67	0.8	77	84.0	54	50	- 7
	1.2	96	102.0	53	50	- 5
	0.0	87	76.5	71	77	+ 8
1.21	0.8	93	92.4	72	73	+ 1
	1.2	-	95.4	-	86	-
	0.0	89	98.0	73	67	- 8
1.89	0.8	107	112.0	66	64	- 3
	1.2	121	120.0	71	72	+ 1

6.7 Load Carrying Capacity

6.7.1 Ultimate Load Capacity

Table 5.13 shows the results of the actual and calculated yield and ultimate load capacity of the beams. In all cases the actual ultimate and yield loads were higher than expected. The reason for this increase is that in the ultimate moment capacity calculations the effect of steel fibers were not included for fibrous concrete. In the case of plain concrete, the calculated and actual yield loads had a deviation ranging from +16 to +24 percent (column 10 in table 5.13) which is expected in actual testing. For ultimate load the deviations ranged from +2 to +17 percent.

The load redistribution factors "r" and "r'" (experimental) are shown in table 5.13 columns 7 and 8. The experimental distribution factor "r'" ranged from 1.33 to 1.02. The highest values were obtained when the least percentage of main steel (0.67%) was used. Table 6.16 shows a summary of the load redistribution factor "r'".

It is obvious from table 6.16 that the smaller the steel percentage, the higher "r'" is. This means lower steel percentages provides more redistribution of the forces (19 to 33%). When main steel percentages of about 1.2% was used, 11 to 16% redistribution was obtained and when 'ρ' of close to 2 percent was used, "r'" reduced to less than 1.1 (less than 10 percent redistribution).

Table 6.16

Load Redistribution Factor

% Main Steel	% Steel Fibers	$r' = \frac{P_u'}{P_y'}$
0.67 (2#3)	0.0	1.33
	0.8	1.20
	1.2	1.19
1.21 (2#4)	0.0	1.11
	0.8	1.16
	1.2	-
1.89 (2#5)	0.0	1.08
	0.8	1.05
	1.2	1.02

From these results it can be stated that low steel percentage has results closer to what is expected and is recommended for higher redistributions. The ACI Code (section 8.4.3) requires that redistribution of negative moments shall be made only when the section, at which moment is reduced, is so designed that ρ for singly reinforced beam is not greater than 0.5 ρ_b.

where: $\rho_b = \frac{0.85\ \beta_1\ f_c'}{f_y} \quad \frac{87000}{87000 + f_y}$

Table 5.14 shows the increase in ultimate moment capacity of the section when steel fibers were used. When 0.67 percent main steel was used, the increase of ultimate moment capacity was 11 to 14 percent and when 1.21 percent main steel existed an increase of 5.6 percent was obtained. The result was similar when 1.89 percent main bars were used, an increase of 5 to 6 percent occurred. As it is seen from table 5.14 the increase in ultimate moment capacity with steel fibers is very insignificant and it is not a good method for moment capacity increase. But if steel fibers were to be used for moment capacity increase, the best results or the most effectiveness of steel fibers can be obtained when percent main reinforcement is less than 1%. This can be summarized in table 6.17.

Table 6.17

Ultimate Moment Capacity Increase

Using Steel Fibers

% Main Steel	Approximate % increase in moment capacity	remarks
$\rho < 1\%$	12	effective
$1\% < \rho < 2\%$	5.5	insignificant
$\rho > 2\%$	< 5	insignificant

6.7.2 Strains in Main Steel and Concrete

As explained in section (5.7.2) when steel fibers were used, the strains at service load were less than that of plain concrete.

Table 5.15 shows the actual results from testing at service load. From these results it can be noticed that:

1) At the negative moment section:
   a) Beams reinforced with 2#3 had strains of 1500, 1100, 1240 x 10^{-6} in/in for 0.0, 0.8, 1.2 percent steel fibers, the reduction in strains was 26 and 17 percent respectively.
   b) Beams reinforced with 2#4 had strains of 1820, 1560 x 10^{-6} in/in for 0.0 and 0.8 percent fiber, the percent reduction was 14 percent.
   c) Beams reinforced with 2#5 had strains of 1300, 1000, 1030 x 10^{-6} in/in for 0.0, 0.8, 1.2 percent steel fibers, the reduction was 23 and 21 percent.
2) At positive section
   a) Beams reinforced with 2#3 had strains of 1300, 1100, 1612 x 10^{-6} in/in for 0.0, 0.8 and 1.2 percent fiber with reductions of 15 and -24 percent respectively.
   b) Beams reinforced with 2#4 had strains of 1800 and 1355 x 10^{-6} in/in for 0.0 and 0.8 percent fibers, the reduction in strain was 24 percent respectively.
   c) Beams reinforced with 2#5 had strains of 1336, 1009, 1025 x 10^{-6} in/in for 0.0, 0.8 and 1.2 percent fibers, the reduction in strains was 25 and 24 percent respectively.

From the preceding it can be concluded that the best combination where the highest decrease of strains was achieved, was when 0.8 percent of steel fibers was added to the beams reinforced with 2#3 bars.

Concrete strains were also measured at service and ultimate loads. From table 5.16 it can be seen that at a given stress the strains of fibrous concrete are slightly higher than plain concrete. Similar results were obtained before in this research when testing cylinder for determination of modulus of elasticity of concrete, the strains of fibrous concrete were higher than strains in plain concrete causing reductions in modulus of elasticity.

The concrete strains at ultimate load or failure were also measured and they are explained as follows:

a) For beams reinforced with 2#3

The maximum strains in concrete compression zone varied from -2220 to -4920 x 10^{-6} in/in for 0.0 and 1.2 percent steel fibers, with an increase of 121 percent in ultimate compressive strains.

b) For beams reinforced with 2#4

The maximum strains in concrete compression zone varied from -2033 to -5800 x 10^{-6} in/in for 0.0 to 0.8 percent steel fibers, with an increase of 185 percent in the ultimate compressive strains.

c) For beams reinforced with 2#5

The maximum strains in concrete compression zone varied from -2775 to -5610 x 10^{-6} in/in for 0.0 to 0.8 percent steel fibers, with an increase of 102 percent in ultimate compressive strain.

Similar results were obtained by previous researchers[34,47] that ultimate strains of fibrous concrete are much higher than plain concrete. Musa[34] concluded that fibrous concrete can have maximum strains up to -6237 x 10^{-6} (in/in) and for plain concrete strains of -3055 x 10^{-6} in/in was obtained. Swamy and Al-Taan[47] concluded strains up to -6620 x 10^{-6} (in/in) for fibrous concrete and -5780 x 10^{-6} (in/in) for plain concrete can develop.

The main reason for higher strains is the ability of fibrous concrete to absorb the necessary strain energy for plastic deformation. This results in a very ductile failure where sudden crush of concrete can be avoided by the use of steel fibers. Figure (6.20) and (6.21) show different modes of failure for plain and fibrous concrete. It was seen in sections (6.5 and 6.6) that steel fibers improve the plastic deformation and increase the deflections at failure. Higher deflections will occur without any sudden failure because of the ability of fibrous concrete to absorb strain energy and take the necessary deformation for a ductile failure.

6.8 Cracks

There are two main crack characteristics to consider, maximum crack width and the spacing of the cracks. Tables 5.17 and 5.18

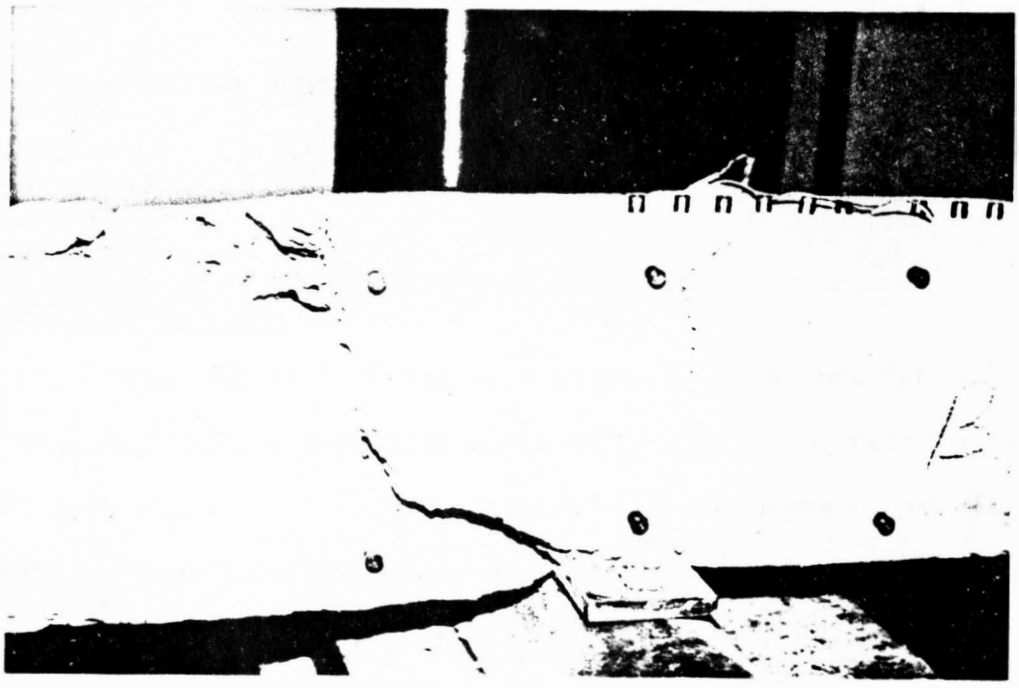

Figure 6.20 Failure of plain concrete

Figure 6.21 Failure of fibrous concrete

show the maximum crack width and crack spacings at a stress of about 60 percent of theyield strength of the main reinforcement or the assumed service load.

6.8.1 Crack Width

From tables 5.17 and 5.18 it can be seen that for all beams (2#3, 2#4, 2#5), the maximum crack width for plain concrete beams was much higher than that of fibrous concrete beams at service load with the same main reinforcement.

1) At middle support
   a) When 2#3 bars were used, the maximum cracks widths ranged from 82 to 55 x 10^{-4} inch for 0.0 to 1.2% steel fibers with a maximum decrease of 33 percent.
   b) When 2#4 bars were used, the maximum crack widths ranged from 105 to 80 x 10^{-4} (in) for 0.0 and 0.8% steel fibers with a decrease in crack width of 24 percent.
   c) When 2#5 bars were used, the maximum crack widths ranged from 117 to 68 x 10^{-4} (in) for 0.0 to 1.2% steel fibers with a decrease of 42 percent in the maximum crack width.
2) At midspan
   a) When 2#3 bars were used, the maximum crack widths ranged from 87 to 49 x 10^{-4} (inch) for 0.0 to 1.2% steel fibers with a percentage decrease of 44.

b) When 2#4 bars were used, the maximum crack widths ranged from 83 to 65 x 10^{-4} (in) for 0.0 to 0.8% steel fibers with a decrease of 21 percent.

c) When 2#5 bars were used crack widths ranged from 75 to 46 x 10^{-4} (in) for 0.0 to 1.2% steel fiber with a maximum decrease of 39 percent.

A statistical analysis using regression method was done for the maximum crack width data given in table 5.17. The actual readings were higher than the calculated values using Gregely-Lutz formula, except when 1.2% steel fibers was used. The best fitting line through the data points for $W/(0.076\ \beta_h.f_s\sqrt[3]{d_c.A_c})$ vs. % steel fibers was obtained with an intercept of 1.00 and slope of (-0.32), the 'F' value was 126 and the correlation coefficient was -0.946 (Table D.11). Therefore Gregely-Lutz formula could be modified to the form in equation 6.14, which the effect of steel fibers will be included in the formula. Gregely-Lutz formula which was adopted by the ACI Code slightly underestimates the crack widths. Equation 6.15 increases the crack width prediction by about 8 percent for plain concrete.

$$W = (1.00 - 0.32\ \rho_s)\ 0.076\ \beta_h.f_s\sqrt[3]{d_c.A_c} \qquad (6.14)$$

$$\text{or } W = (0.076 - 0.024\ \rho_s)\ \beta_h.f_s\ d_c.A_c \qquad (6.15)$$

where β_h, f_s, d_c and A_c are defined in section 5.8

Table 6.18 shows the actual and calculated values for maximum crack widths.

Table 6.18

Actual and Calculated Maximum Crack Widths at Midspan and Middle Support

Beam	% Steel Fibers	Actual Maximum Crack Width x 10^{-4} in	Calculated Maximum Crack Width Using Equation 6.15 x 10^{-4} in	% Deviation from Actual	Actual Maximum Crack Width x 10^{-4} in	Calculated Maximum Crack Width Using Equation 6.15 x 10^{-4} in	% Deviation from Actual
	0.0	87	74	-14	82	86	+ 5
2#3	0.8	57	56	- 2	60	65	+ 8
	1.2	49	46	- 6	55	54	- 2
	0.0	83	79	- 5	105	95	- 9
2#4	0.8	65	60	- 7	80	72	-10
	0.0	75	80	+ 7	117	95	-18
2#5	0.8	57	60	+ 5	107	72	-30
	1.2	46	50	+ 9	68	60	-11

6.8.2 Crack Spacings

Table 5.19 shows the maximum and minimum crack spacing at the middle support. It can be stated that:

a) Beams reinforced with 2#3 bars had maximum crack spacing ranging from 8 to 5 inches and minimum crack spacing 2 to 1.5 inches for 0 and 0.8% fibers.

b) Beams reinforced with 2#4 bars had maximum crack spacing of 5 to 4 inches and minimum spacing was about 2 inches for 0.0 and 0.8% steel fibers.

c) Beams reinforced with 2#5 bars had maximum crack spacing of 6 to 3 inches and minimum crack spacing of 1 inch for 0.0 to 0.8% fiber.

It is obvious that the inclusions of steel fibers reduces the spacing between the cracks because of better strain distribution. In most cases the minimum crack spacing or the closest distance between two consecutive cracks was betwen 1 to 2 inches. The maximum percentage for decrease of crack spacing was 50% when 2#5 bars and 0.8% steel fiber was used. A reduction of 37% was calculated for the case of 2#3 bars with 0.8% fibers.

When number of cracks at the middle support is considered, it is concluded from table (5.19) that when steel fibers are added to the mix, the number of cracks increase. Table (6.19) shows a summary of the number of cracks at service load and ultimate load for plain and fibrous concrete. This table represents the number of

cracks at the middle support and at midspan. The ratio of the number of cracks developed at service load to the total number of cracks at ultimate are also shown in table (6.19).

As it is shown in table (6.19) when steel fibers were present in the beams, between 45 to 66 percent of the cracks developed before service load and the rest started after the service load. It can be concluded that an average of about 55% of the cracks develop before the service load and 45% develop after the service load has been reached. On the other hand plain concrete develops about 80% of its cracks before service load. This means in the case of plain concrete two or three cracks start at lower loads and the same cracks lead up to failure. Figures (6.22) and (6.23) show the cracks for plain and fibrous concrete beams.

From the previous discussion it can be concluded that:

1) More cracks develop in fibrous concrete and the spacing between cracks are much smaller than that of plain concrete. This proves that the fibers distribute the strains more evenly in fibrous concrete. Henager and Doherty[25] also concluded that crack widths and crack spacings are smaller in fibrous concrete than plain concrete and also that first cracks develop at higher loads for fibrous concrete.

2) Crack widths were much smaller for fibrous concrete. At a given load, reductions up to 54 percent with 1.2

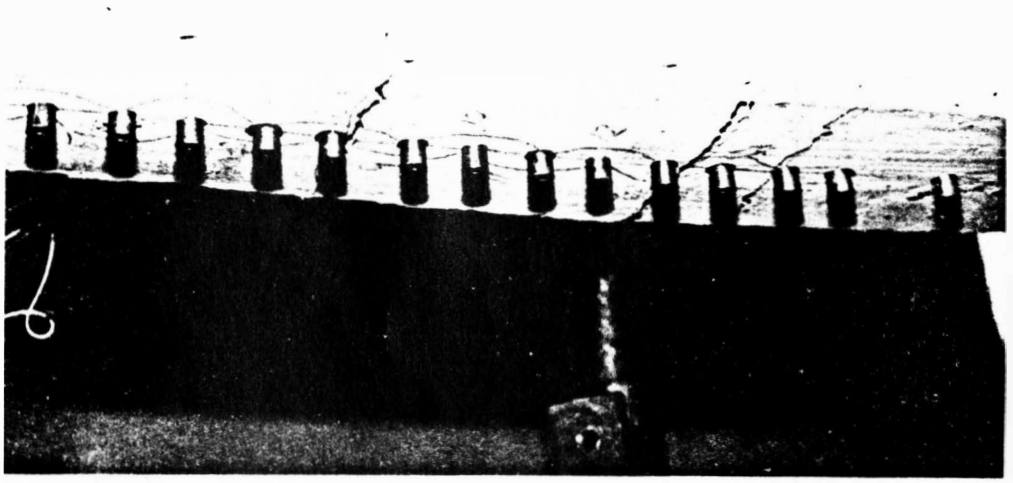

Figure 6.22 Cracks in plain concrete

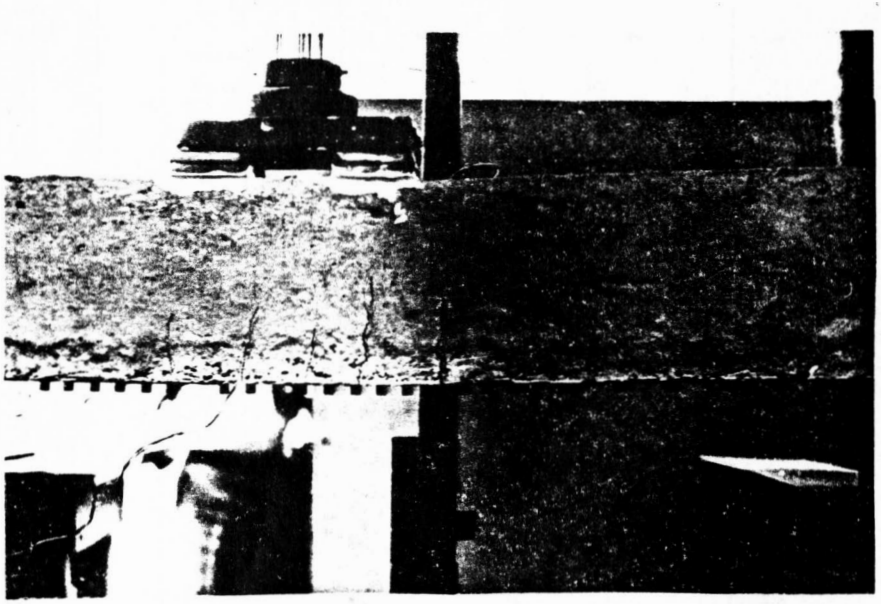

Figure 6.23 Cracks in fibrous concrete

Table 6.19

Number of Cracks at Service and Ultimate Loads

at Middle Support and Midspans

Beam	% Steel Fiber	At Middle Support Number of Cracks (Figure 3.17) At Service Load	At Ultimate	ratio*	At Midspan Number of Cracks (Figure 3.17) Service Load	Ultimate	ratio*
	0.0	4	6	66%	5	6	84%
2#3	0.8	3	5	60%	6	9	66%
	1.2	4	7	57%	4	8	50%
	0.0	3	4	75%	4	5	80%
2#4	0.8	3	7	43%	5	11	45%
	1.2	-	-	-	-	-	-
	0.0	3	4	75%	4	5	80%
2#5	0.8	4	7	57%	3	6	50%
	1.2	3	5	60%	4	7	57%

*ratio = $\frac{\text{Number of cracks at service load}}{\text{Total number of cracks at ultimate}}$

percent steel fiber was obtained. Similar results were obtained by previous researchers.[25,34]

3) When steel fibers were used, about 55% of the cracks developed at working loads and the cracks were better distributed than plain concrete cracks. Some started simultaneously and increased gradually, then more cracks started after service load. In the case of plain concrete, less cracks developed but the crack widths increased with higher intensity and were more critical. In all cases the cracks that developed at service loads, specially at the negative moment region, continued to grow and formed the plastic hinges.

6.9 Comparison of Some Results to Other Research

The effect of inclusion of steel fibers on some of the physical properties of concrete was tested. The results obtained in this research were somewhat similar to the results obtained by Musa.[34] The comparison of the conclusions are as follows:

1 - Modulus of elasticity

The modulus of elasticity of fibrous concrete is less that that of plain concrete. The equation obtained in this research is:

$$E_c = (33 - 7.6\ \rho_s)\ w^{1.5}\sqrt{f_c'} \qquad 4000 \leq f_c' \leq 5000$$

Musa[34] concluded that the decrease of the modulus of elasticity of fibrous concrete is as follows:

$$E_c = (33 - 6.7\ \rho_s)\ w^{1.5}\sqrt{f_c'} \quad 5000 \leq f_c' \leq 8000$$

The difference of the two equations is caused by the difference in the compressive strength of the concrete used. In high strength concrete, the bond strength between the fiber and cement are higher than normal strength concrete. This causes less reduction in strains, therefore there is less reduction in the modulus of elasticity.

Combining the data of both researches, equation 6.16 is suggested for calculating the modulus of elasticity of fibrous concrete for compressive strengths ranging from 4000 psi to 8000 psi.

$$E_c = (33 - 7.2\ \rho_s)\ w^{1.5}\sqrt{f_c'} \qquad (6.16)$$

2 - Split Cylinder Strength

The tensile strength of fibrous concrete for concrete compressive strength of 4000 psi to 5000 psi, can be calculated by the following equation obtained from this research.

$$f_{ct} = (6.7 + 2.3\ \rho_s)\ \sqrt{f_c'}$$

Musa[34] concluded the following equation for calculating the tensile strength of fibrous concrete for $5000 < f_c' < 8000$ psi.

$$f_{ct} = (6.7 + 4.4\ \rho_s)\ \sqrt{f_c'}$$

Combining the data of the two research projects, results into equation 6.17 for prediction of the tensile strength of fibrous concrete with f_c' ranging from 4000 psi to 8000 psi.

$$f_{ct} = (6.7 + 3.53\ \rho_s)\ \sqrt{f_c'} \qquad (6.17)$$

3 - Modulus of Rupture

Both research projects concluded that, when steel fibers are used, there are two stages of flexure failure: a) first modulus of rupture; b) ultimate modulus of rupture.

a) first modulus of rupture

The equation derived in this research is as follows:

$$f_{rl} = (7.5 + 2.6\ \rho_s)\ \sqrt{f_c'} \quad 4000 \leq f_c' \leq 5000 \text{ psi}$$

Musa[34] concluded a slightly different equation

$$f_{rl} = (7.5 + 3.4\ \rho_s)\ \sqrt{f_c'} \quad 5000 \leq f_c' \leq 8000 \text{ psi}$$

b) Ultimate modulus of rupture

The equation derived in this research is as follows:

$$f_{ru} = (7.5 + 4.35\ \rho_s)\ \sqrt{f_c'} \quad 4000 \leq f_c' \leq 5000 \text{ psi}$$

Musa[34] concluded the following:

$$f_{ru} = (7.5 + 6.1\ \rho_s)\sqrt{f_c'} \quad 5000 \leq f_c' \leq 8000 \text{ psi}$$

The difference between the conclusions of the two results are mainly caused by the difference in the compressive strength of the concrete used. In high

strength concrete, the fibers will be more effective in increasing the tensile strengths in bending than in normal strength concrete.

Combining the data of the two experiments, results into equations 6.18 and 6.19 to calculate the first and ultimate modulus of rupture of fibrous concrete for concrete compressive strength of 4000 psi to 8000 psi.

$$f_{r1} = (7.5 + 3.0\ \rho_s)\ \sqrt{f_c'} \qquad (6.18)$$

$$f_{ru} = (7.5 + 5.2\ \rho_s)\ \sqrt{f_c'} \qquad (6.19)$$

CHAPTER VII

CONCLUSIONS AND RECOMMENDATIONS

Based on the results of this experimental research project, a summary of the conclusions are presented in this chapter. The conclusions are divided into five sections: Physical Properties, Plastic Rotations, Deflection, Load Carrying Capacity and Cracks.

I. Physical Properties:

1) The compressive strength of fibrous concrete was 5 to 8 percent higher than plain concrete when 0.8 and 1.2 percent steel fibers was used. It is not recommended to use steel fibers to increase the compressive strength of concrete (section 6.1).

2) The modulus of elasticity of fibrous concrete was found to be 8 to 23 percent lower than plain concrete for 0.8 to 1.2 percent steel fibers. The main reason being the lower bond strength between fiber and cement mortar causing higher deformation and strains in compression. The following equation is recommended for calculating the modulus of elasticity of normal strength (4000 to 5000 psi) fibrous concrete (section 6.2).

$$E_c = (1 - 0.23\ \rho_s)\ 33\ w^{1.5}\sqrt{f_c'} \qquad (6.1)$$

3) Upon investigating the tensile strength of concrete, it is concluded that the split cylinder strength of fibrous concrete is much higher than that of plain

concrete. The following equation is recommended for calculation of the tensile strength of fibrous concrete (section 6.3)

$$f_{ct} = (1 + 0.34\ \rho_s)\ 6.7\sqrt{f_c'} \qquad (6.2)$$

4) The modulus of rupture of fibrous concrete was found to have two main stages:

a) First modulus of rupture, where the first crack starts to propagate, and it can be calculated by the following equation (section 6.4.1).

$$f_{rl} = (1 + 0.35\ \rho_s)\ 7.5\ \sqrt{f_c'} \qquad (6.3)$$

b) Ultimate modulus of rupture is when the specimens could not take any more stresses, and it is between 13 to 20 percent higher than first modulus of rupture for 0.8 to 1.2 percent steel fibers. The following equation was derived for the calculation of ultimate modulus of rupture for fibrous concrete (section 6.4.2).

$$f_{ru} = (1 + 0.58\ \rho_s)\ 7.5\ \sqrt{f_c'} \qquad (6.4)$$

II. Plastic Rotations:

The plastic rotation of fibrous concrete can be estimated within a reasonable range, if the following parameters are assumed correctly.

1) The length of the plastic hinge can be related to the effective depth of the section and the percentage of

main steel and steel fibers in the beam. The following equation can be used to estimate the length of the plastic hinge at a critical section (section 6.5.1).

$$H_L = (1.06 + 0.13\ \rho\rho_s).d \qquad (6.5)$$

2) The curvature distribution factor was calculated from investigating the rotations, and the recommended value is $\beta = 0.56$ for plain concrete, and for fibrous concrete the following is recommended (section 6.5.2).

$$\beta = 0.56 - 0.16\ \rho_s \qquad (6.6)$$

3) From the investigation of this research it is concluded that the plastic rotation capacity of fibrous concrete was substantially higher than that of plain concrete. The calculation of plastic rotations is usually too conservative compared to actual plastic rotation capacity of concrete, especially in fibrous concrete. The following equation is recommended for the estimation of plastic rotation of fibrous and plain concrete (section 6.5.3).

$$\theta_P = \gamma.\beta.\ \frac{0.003}{K_u} \qquad (6.9)$$

$$\text{or } \theta_P = (4.3 + 2.24\ \rho_s - 0.043\ f_y + 4.17\rho\rho_s).\beta\frac{0.003}{K_u}$$

where $\gamma = (4.3 + 2.24\ \rho_s - 0.043\ f_y + 4.17\ \rho\rho_s)$

The plastic rotation capacity of reinforced concrete is substantially improved by using steel fibers. It is also related to the percentage of main steel and the yield strength of the main bars. Low strength steel (less than 60 Ksi) is recommended for higher plastic rotation capacity.

The use of steel fibers is recommended in reinforced concrete structure especially in earthquake zone areas that seismic loadings are present and structures that could be introduced to dynamic and blast loading especially in military bases.

4) Ductility of reinforced concrete was estimated using the ratio of ultimate curvature to yield curvature. The superiority of fibrous concrete ductility is proven in this research. The ability to take inelastic deformation by fibrous concrete allowed the critical sections to rotate and deform inelastically without any sudden failure.

Steel fibers are recommended for ductility improvement and avoiding a catastrophic failure. The ductility of fibrous reinforced concrete can be estimated using the following equation (section 6.5.4).

$$\mu' = (1 + 3.8\ \rho_s)\ \mu \qquad (6.10)$$

III. Deflections

Deflection of reinforced concrete members is inversely proportional to the stiffness [$\Delta = f(\frac{1}{EI})$]; increase in stiffness reduces deflection while a decrease in stiffness increases deflection. The stiffness depends on two factors; 1 - Modulus of elasticity (E_c) and 2 - Effective moment of inertia (I_e).

From this research it was concluded that the modulus of elasticity decreases when steel fibers are added to the mix; therefore this decrease will increase the deflection at service load of fibrous concrete. It was also concluded that the effective moment of inertia of fibrous concrete is higher than that of plain concrete, due to the following:

a) increase in modulus of rupture which increases the cracking moment (M_{cr})

b) increase of the modular ratio (n) which increases the moment of inertia of a cracked section (I_{cr}).

If the increase of the effective moment of inertia (I_e) is more significant than the decrease of the modulus of elasticity (E_c), then deflections will be improved, but if the decrease of (E_c) is more signficant than the increase of (I_e), then there will be higher deflections at service load.

In this research the change of stiffness was insignificant, therefore, the inclusion of steel fibers did not have major effect on the deflections at service load. From the interpretation of the results, it can be concluded that the use of steel fibers could improve deflections when low main steel percentages are used. The following equation is recommended to calculate the effective moment of inertia of fibrous concrete.

$$I_e' = \left(\frac{M_{cr}'}{M_a}\right)^3 I_g + \left[1 - \left(\frac{M_{cr}'}{M_a}\right)^3\right] I_{cr}' \quad (6.13)$$

where: I_e' = effective moment of inertia of fibrous concrete

M_{cr}' = cracking moment of fibrous concrete

$= (1 + 0.5\ \rho_s)\ M_{cr}$

M_a = actual moment in the section

I_g = gross moment of inertia of the section neglecting the steel

I_{cr}' = moment of inertia of a cracked section in fibrous concrete

$= (1 + 0.14\ \rho_s)\ I_{cr}$

M_{cr} = cracking moment of plain concrete

I_{cr} = moment of inertia of a cracked, plain concrete section

The ACI Code formula can conservatively be used for fibrous concrete with main steel percentage > 1 to calculate deflection, using the stiffness of plain concrete, even though E_c and I_e change; the change in I_e and E_c counteract each other's effect on the stiffness.

IV. Ultimate Load Capacity (section 6.7)

1) The ultimate load capacity of fibrous concrete continuous beams was higher than that of plain concrete. The reduction in strains in the main steel, increases the yield load of the member.

2) Strain reductions in main steel were as high as 26 percent for 2#3 and 0.8 percent fibers at the negative moment section.

3) Strain reductions in main steel at the positive moment section were as high as 25% for 2#5 and 24 percent for 2#4 with 0.8 percent steel fibers (section 6.7.2).

4) Ultimate concrete strains were as higher as -5800 $x10^{-6}$ in/in for 2#4 and 0.8 percent steel fibers. For 2#5, ultimate concrete strains were about -5600 $x10^{-6}$ (in/in), where in plain concrete the ultimate concrete strains did not exceed -3000 $x10^{-6}$ (in/in).

5) In general, the ultimate moment capacity of fibrous concrete increased insignificantly. The most effective results were obtained when main steel percentage less than 1% was used, where the ultimate moment capacity increased by about 12 percent.

6) The ultimate moment capacity increased about 5 percent when $\rho > 1\%$ was used.

V. Cracks

1) Fibrous concrete beams had a better distribution of cracks, because the strains were more uniformly distributed.

2) Maximum crack spacing and the maximum crack widths were much smaller than that of plain concrete. Plain concrete beams had fewer but wider and critical cracks than identical beams containing steel fibers at service load.

3) Plain concrete develops about 80% of its cracks at working load. Fibrous concrete developes only about half of its cracks at working load.

4) The maximum and minimum crack spacings were 5 and 1.0 inches for fibrous concrete, and for plain concrete the maximum crack spacing was about 8 inches.

5) Fibrous concrete cracks at service load were smaller than plain concrete cracks. Maximum crack reductions of 54 and 44% were obtained when 2#3 and 1.2 percent steel was used at negative and positive moment section, respectively.

6) To calculate the crack widths for fibrous concrete the following equation is recommended (section 6.8.1).

$$W = (1 - 0.32\ \rho_s)\ 0.076\ \beta_h . f_s \sqrt[3]{d_c A_c} \quad (6.15)$$

BIBLIOGRAPHY

1. ACI Building Code Requirements for Reinforced Concrete, ACI 318-83.

2. ACI Committee 544, "Measurement of Properties of Fiber Reinforced Concrete", Journal American Concrete Institute, 75, No. 7, July 1978, pp. 283-289.

3. ACI Committee 544, "State-of-the-Art Report on Fiber Reinforced Concrete", Concrete International, Common Report, May 1982.

4. ACI Committee 544, "State-of-the Art Report on Fiber Reinforced Concrete", Journal American Concrete Institute, 70, No. 11, Nov. 1973, pp. 729-744.

5. Ali, Mir M. and Grierson, Donald E., "Reinforced Concrete Design for Strength and Deformability", ASCE Journal, Mechanics Division, Vol. 100, No. EM5, Oct. 1974, pp. 839-859.

6. Baker, A. L. L., "Limit-State Design of Reinforced Concrete", Cement and Concrete Association, London, 1970.

7. Baker, A. L. L., "The Ultimate Load Theory Applied to the Design of Reinforced and Prestressed Concrete Frames", Concrete Publications, London, England, 1956.

8. Beedle, Lynn S., "Plastic Design of Steel Frames", 1958.

9. Beckett, Derrick, "The Ultimate Load Design of Continuous Concrete Beams, published by Plenum Press, 1967, pp 65-78.

10. Berwanger, C., "Limit Design of Reinforced Concrete Continuous Beams", The Engineering Journal, May 1962, pp 42-49.

11. Burns, Ned H., and Siess, Chester P., "Plastic Hinging in Reinforced Concrete", ASCE Journal, Structural Division, Vol. 92, No. ST5, October 1966, pp 45-63.

12. Bishara, Alfred G. and Londot, Larry and Au, Peter and Sastry, Majety V., "Flexural Rotational Capacity of Spandrel Beams", ASCE Journal, Structural Division, Vol. 105, No. ST1, January 1979, pp 147-161.

13. British Standard Code of Practice CP110, 1972.

14. Chan, W. W. L., "The Rotation of Reinforced Concrete Plastic Hinges at Ultimate Load", Magazine of Concrete Research, Vol. 14, No. 41, July 1962, pp 63-72.

15. Chan, W. W. L., "The Ultimate Strength and Deformation of Plastic Hinges in Reinforced Concrete Frameworks", Magazine for Concrete Research, November 1955, pp 121-132.

16. Cohn, M. Z., "Limit Design Solutions for Concrete Structures" ASCE Journal, Structural Division, Vol. 93, No. ST1, February 1967, pp 37-57.

17. Cohn, M. Z., and Petca, V. A., "Moment Redistribution and Rotation Capacity of Plastic Hinges in Redundant Reinforced Concrete Beams", Indian Concrete Journal, August 1963, pp 282-290.

18. Cohn, M. Z., "Rotation Compatibility in the Limit Design of Reinforced Concrete Continuous Beams", Flexural Mechanics of Reinforced Concrete, Proceedings of the International Symposium, Miami, Fla., Nov. 10-12, 1964, pp 359-382.

19. Cohn, M. Z., and Ghosh, "The Flexural Ductility of Reinforced Concrete Sections, Vol. 33-11, 1972, pp 53-83..

20. Desay, Prakash and Sundara Raja Iyengar, K. T. and Reddy, K. Nagi, "Ductility of Reinforced Concrete Sections with Confined Compression Zones", Earthquake Engineering and Structural Dynamics, Vol. 4, 1975, pp 111-118.

21. Ernst, C. G., "A Brief for Limit Design", Transaction, ASCE Vol. 121, 1956, p 605.

22. Halvorsen, Grant T. and Kesler, Clyde E., "Moment-Curvature Relationships for Concrete Beams with Plain and Deformed Steel Fibers", ACI Journal, Technical paper, June 1979, pp 697-706.

23. Hassoun, Nadim, "Design of Reinforced Concrete Structures", 1984, (in printing).

24. Hassoun, Nadim, "Ultimate-load Design of Reinforced Concrete", A Practical Handbook, Printed by J. B. Shears & Sons, Ltd.

25. Henager, Charles H. and Doherty, Terrence J., "Analysis of Reinforced Fibrous Concrete Beams", ASCE Journal, Structural Division, Vol. 102, No. ST1, January 1976, pp 177-188.

26. ICE, Institution of Civil Engineers, London, V. 21, Feb. 1962, pp 400-422.

27. Kaushik, S. K. and Ramamurthy, L. N. and Kukreja, C. B., "Plasticity in Reinforced Concrete Continuous Beams with Parabolic Soffits", ACI Journal, September-October 1980, pp 369-377.

28. Kar, Jitendra, Pal, Anil, "Strength of Fiber Reinforced Concrete", Journal Structure Division, American Society of Civil Engineers, 98, No. ST5, May 1972, pp 1053-1068.

29. Kemp, A. R., "Ductility and Moment Redistribution in Reinforced Concrete Beams", The Civil Engineer in South Africa, May 1981, pp 175-181.

30. Kormeling, H. A. and Reinhardt, H. W. and Shah, S. P. "Static and Fatigue Properties of Concrete Beams Reinforced with Continuous Bars and with Fibers", ACI Journal, January-February 1980, pp 36-43.

31. Lenkei, P., "Local and Overall Specific Inelastic Rotation Capacities in Reinforced Concrete Beams", Acta Technica Academiae Scientiarum Hungarical, Tomus 79(3-4), 1974, pp 451-463.

32. McCormack, Jack C., "Design of Reinforced Concrete", Harper and Row Publishers, 1978.

33. Mattock, Alan H., "Rotational Capacity of Hinging Regions in Reinforced Concrete Beams", Flexural Mechanics of Reinforced Concrete, Proceedings of the International Symposium, Miami, Fla., November 10-12, 1964, pp 143-181.

34. Musa, Saadi, "The Effect of Steel Fibers on the Properties and Behavior of High Strength Reinforced Concrete Beams", M.S. Thesis, S.D.S.U., 1982.

35. Neville, Adam, "Fiber Reinforced Cement and Concrete", The Construction Press LTD, Rilem Symposium, 1975.

36. Noor, F. A., "Inelastic Behavior of Reinforced Concrete Frames", Magazine of Concrete Research, Vol. 28, No. 97, December 1976, pp 209-223.

37. Ramakrishnan, V. and Balakrishnan, S., "Elastic and Limit State Deformations of Reinforced Concrete Space Frames", Indian Concrete Journal, March 19?6, pp 85-91.

38. Richard, Rowland, Jr. and Lazara, Angel L., "Limit Analysis of a Reinforced Concrete Frame", ACI Journal, October 1971, pp 748-755.

39. Shaikh, M. F. and Mirza, M. S. and McCutcheon, J. O., "Limit Analysis of Reinforced Concrete Frames", Engineering Institute of Canada, Vol. 14, No. A-6, July 1971, pp I-VII.

40. Shah, Surendra P. and Rangan, B. Vijay, "Effects of Reinforcements on Ductility of Concrete", ASCE Journal, Structural Division, Vol. 96, No. ST6, June 1970, pp 1167-1183.

41. Shah, S. P. and Winter, George, "Inelastic Behavior and Fracture of Concrete", ACI Journal, September 1966, pp 925-930.

42. Snyder, M. J., and Lamkard, D. R., "Factors Affecting the Flexural Strength of Steel Fibrous Concrete", Journal of American Concrete Institute, 69, No. 2, Feb. 1972, pp 96-100.

43. Subrahmanyam, B. V., "Prediction of the Inelastic Behavior of One-way Continuous Slabs", ACI Journal, Technical Paper, pp 621-631.

44. Sawyer, H. A., "Elastic-Plastic Design of Single Span Beams and Frames", Proc. paper No. 551, ASCE, Vol. 81, Dec. 1955.

45. Scheaffer, Richard L., and McClave, James, "Statistics for Engineers", Published by PWS, 1982.

46. Swamy, R. N. and Mangat, P. S., "A Theory for the Flexural Strength of Steel Fiber Reinforced Concrete", Cement and Concrete Research, Vol. 4, 1974, pp 313-325.

47. Swamy, R. N. and AlTaan Saad, "Deformation and Ultimate Strength in Flexure of Reinforced Concrete Beams Made with Steel Fiber Concrete", Journal American Concrete Institute, Sept-Oct. 1981.

48. Swamy, R., and Al-Noori, K., "Flexural Properties of Steel Fiber Reinforced Concrete", Concrete (London), 9, No. 6, June 1975, pp 30-31.

49. Swamy, R. Narayan, Al-Taan, Saad A., and Ali, Sami A. R., "Steel Fibers for Controlling Cracking and Deflection", Concrete International, 1, No. 8, Aug. 1979, pp 41-49.

50. Velazco, K. Visalvanich and Shah, S. P., "Fracture Behavior and Analysis of Fiber Reinforced Concrete Beams", Cement and Concrete Research, Vol. 10, 1980, pp 41-51.

51. Wright, D. T. and Berwanger, C., "Limit Design of Reinforced Concrete Beams", ASCE Journal, Structural Division, Vol. 86, No. ST7, July 1960, pp 1-36.

APPENDIXES

APPENDIX A

Table A.1

Actual Rotation at the Critical Section Using

Method 1 $x10^{-4}$ Radians

Main Bars = 2#3 % Steel Fibers = 0.0 H_L = 8 inches

Load Kips	Moment Kip-in	ϕ_1	ϕ_2	ϕ	θ
1.05	11.70	0.05	0.05	0.10	0.8
2.10	23.37	0.10	0.10	0.20	1.6
3.15	35.00	0.15	0.17	0.32	2.6
4.20	46.75	0.20	0.94	1.14	9.1
5.25	58.43	0.28	2.66	2.94	23.5
6.30	70.12	0.46	3.78	4.24	33.9
7.35	81.81	0.66	5.59	6.25	50.0
8.40	93.49	1.17	6.76	7.93	63.4
9.45	105.18	1.84	8.74	10.58*	84.6*
10.50	-	1.92	11.56	13.48	107.9
11.55	-	2.00	25.60	27.60#	220.8#
12.60	-	4.95	30.50	35.45	284.0
13.00	-	13.90	24.00	47.90**	383.0**
13.40	-	-	-	-	-

* = first yield at middle support
\# = second yield at midspan
** = failure

Table A.2

Actual Rotation at the Critical Section Using

Method 1 $x10^{-4}$ Radians

Main Bars = 2#3 % Steel Fibers = 0.8 H_L = 6.5 inches

Load Kips	Moment Kip-in	ϕ_1	ϕ_2	ϕ	θ
1.05	11.8	.34	.28	.62	.03
2.10	23.6	.68	.57	1.25	8.13
3.15	35.4	1.02	.86	1.88	12.22
4.20	47.3	1.38	1.14	2.52	16.38
5.25	59.0	1.64	1.23	2.87	18.66
6.30	70.9	1.90	1.32	3.22	20.90
7.35	82.7	2.17	2.08	4.25	27.60
8.40	94.5	2.43	2.62	5.10	33.00
9.45	106.3	2.46	3.38	5.85	38.00
10.50	118.1	2.85	3.82	6.67*	43.40*
11.55	118.1	4.17	4.11	8.28	53.90
12.60	118.1	6.20	5.03	11.23#	73.00#
13.00	118.1	10.18	6.25	16.40	107.00
13.40	118.1	11.70	8.07	19.80	128.50
13.80	118.1	13.16	8.85	22.00	143.00
14.20	118.1	18.34	12.30	30.60	200.00
14.60	118.1	21.70	17.10	38.80	252.00
15.00	118.1	24.10	19.95	44.00	286.00
15.40	118.1	26.45	23.90	50.40	327.00
15.80	118.1	48.30	43.20	91.50	595.00
16.20	118.1	50.80	43.20	94.00	611.00
16.60	118.1	63.51	53.40	117.00	760.00
17.00	118.1	114.30	88.90	203.00**	1321.00**

* = first yield at middle support
\# = second yield at midspan
** = failure

Table A.3

Actual Rotation at the Critical Section Using

Method 1 $x10^{-4}$ Radians

Main Bars = 2#3 % Steel Fibers = 1.2 H_L = 7.5 inches

Load Kips	Moment Kip-in	ϕ_1	ϕ_2	ϕ	θ
1.05	11.8	0.20	.95	1.15	8.63
2.10	23.6	0.40	1.14	1.54	11.55
3.15	35.4	0.45	1.18	1.63	12.23
4.20	47.3	0.91	1.39	2.30	17.30
5.25	59.0	1.33	1.89	3.22	24.20
6.30	70.9	1.79	1.89	3.68	27.60
7.35	82.7	2.23	2.93	5.16	38.70
8.40	94.5	2.80	3.67	6.47	48.52
9.45	106.3	2.84	3.75	6.59	49.43
10.80	121.0	3.47	3.83	7.30*	54.80*
11.55	121.0	5.74	4.95	10.70	80.20
12.60	121.0	10.90	5.37	16.30#	122.00#
13.00	121.0	16.00	8.46	24.46	184.00
13.40	121.0	19.70	10.50	30.20	227.00
13.80	121.0	25.00	14.40	39.40	300.00
14.20	121.0	28.70	18.80	47.50	356.00
14.60	121.0	35.30	23.70	59.00	443.00
15.00	121.0	49.50	28.60	78.00	586.00
15.40	121.0	65.00	34.30	99.30	745.00
15.80	121.0	80.00	40.00	120.00	900.00
16.20	121.0	104.80	45.70	150.00	1129.00
16.60	121.0	198.30	66.00	264.30**	1982.00**

* = first yield at the middle support
\# = second yield at midspan
** = failure

Table A.4

Actual Rotations at the Critical Section Using

Method 1 x10^{-4} Radians

Main Bars = 2#4 % Steel Fibers = 0.0 H_L = 7 inches

Load Kips	Moment Kip-in	ϕ_1	ϕ_2	ϕ	θ
1.05	11.7	.13	.12	.25	1.75
2.10	23.4	.25	.24	.49	3.43
3.15	35.0	.38	.36	.74	5.20
4.20	46.8	.50	.48	.98	6.90
5.25	58.4	.63	.60	1.23	8.60
6.30	70.4	.76	.72	1.48	10.40
7.35	81.8	.88	.85	1.73	12.10
8.40	93.5	1.00	.90	1.90	13.30
9.45	105.2	1.12	1.10	2.22	15.50
10.50	117.0	1.37	1.20	2.57	18.00
11.55	128.6	1.78	1.43	3.21	22.50
12.60	140.2	2.12	1.53	3.65	26.00
13.65	152.2	2.78	1.95	4.73	33.00
14.70	163.6	3.38	2.10	5.48	38.00
15.75	175.3	4.00	2.30	6.30	44.00
16.80	187.0	4.25	3.50	7.75	54.00
17.85	199.0	4.95	4.30	9.25	65.00
18.90	210.4	5.60	5.00	10.60*	74.00*
19.95	210.4	16.30	14.90	31.20#	218.00#

* = first yield at middle support
# = second yield at midspan and failure

Table A.5

Actual Rotations at the Critical Section Using

Method 1 $x10^{-4}$ Radians

Main Bars = 2#4 % Steel Fibers = 0.8 H_L = 8 inches

Load Kips	Moment Kip-in	ϕ_1	ϕ_2	ϕ	θ
1.05	11.7	.13	.22	.35	2.8
2.10	23.4	.32	.44	.76	6.0
3.15	35.0	.69	.66	1.35	10.8
4.20	46.8	.88	.88	1.76	14.0
5.25	58.4	1.08	1.10	2.20	17.6
6.30	70.4	1.98	1.32	3.30	26.4
7.35	81.8	2.30	1.54	3.84	30.7
8.40	93.5	2.62	1.76	4.40	35.0
9.45	105.2	3.17	1.98	5.20	41.6
10.5	117.0	3.27	2.20	5.50	44.0
11.55	128.6	3.40	2.30	5.70	45.6
12.60	140.2	3.67	2.43	6.10	49.0
13.65	152.0	4.00	2.72	6.72	54.0
14.70	163.6	4.50	3.00	7.50	60.0
15.75	175.3	5.00	3.28	8.30	66.4
16.80	187.0	5.30	3.60	8.90	71.0
17.85	199.0	5.90	3.77	9.70	77.6
18.90	210.4	6.55	3.90	10.45*	83.6*
19.95	210.4	11.20	4.90	16.10	129.0
21.00	210.4	12.20	5.70	17.90	143.0
22.00	210.4	28.20	8.82	37.00#	296.0#
22.00	210.4	36.50	11.53	48.00	432.0
23.00	210.4	46.20	21.20	67.50	540.0
23.50	210.4	59.00	27.00	86.00	688.0
23.50	210.4	77.00	30.70	108.00**	864.0**

* = first yield at middle support
\# = second yield at midspan
** = failure

Table A.6

Actual Rotations at the Critical Section Using

Method 1 $x10^{-4}$ Radians

Main Bars = 2#5 % Steel Fiber = 0.0 H_L = 6.5 inches

Load Kips	Moment Kip-in	ϕ_1	ϕ_2	ϕ	θ
1.05	11.7	.03	.10	.13	.9
2.10	23.4	.10	.20	.30	2.0
3.15	35.0	.67	.30	.97	6.3
4.20	46.8	1.19	.40	1.59	10.4
5.25	58.4	1.96	.46	2.45	15.9
6.30	70.1	1.96	.59	2.55	16.6
7.35	81.80	2.01	.69	2.70	17.6
8.40	93.5	2.76	.78	3.54	23.0
9.45	105.2	2.82	.88	3.70	24.0
10.50	117.0	2.95	.97	3.92	25.5
11.55	128.6	3.12	1.08	4.20	27.3
12.60	140.2	3.31	1.17	4.50	29.3
13.65	152.0	3.90	1.27	5.17	33.6
14.70	163.6	4.04	1.37	5.40	35.1
15.75	175.3	4.26	1.46	5.72	37.2
16.80	187.0	4.39	1.56	5.95	38.7
17.85	199.0	4.63	1.66	6.30	41.0
18.90	210.4	4.70	1.76	6.46	42.0
19.95	222.0	4.90	1.86	6.76*	44.0*
21.00	222.0	6.80	2.50	9.30	60.5
21.00	222.0	13.90	2.63	16.50#	107.3#
23.10	222.0	26.90	16.40	43.30**	282.0**

* = first yield at middle support
\# = second yield at midspan
** = failure

Table A.7

Actual Rotations at the Critical Section Using

Method 1 x10^{-4} Radians

Main Bars = 2#5 % Steel Fiber = 0.8 H_L = 8 inches

Load Kips	Moment Kip-in	ϕ_1	ϕ_2	ϕ	θ
1.05	11.7	.17	.10	.27	2.16
2.10	23.4	.34	.19	.53	4.24
3.15	35.0	.51	.30	.81	6.50
4.20	46.8	.68	.38	1.06	8.50
5.25	58.4	.85	.49	1.34	10.70
6.30	70.1	1.02	.58	1.60	12.80
7.35	82.0	1.04	.68	1.72	13.80
8.40	93.5	1.48	1.30	2.78	22.00
9.45	105.2	1.75	1.47	3.20	25.60
10.50	117.0	2.09	1.90	4.00	32.00
11.55	128.6	2.36	2.15	4.51	36.00
12.60	140.2	2.83	2.54	5.37	43.00
13.65	152.0	3.00	2.64	5.64	45.00
14.70	163.6	3.37	2.81	6.20	49.60
15.75	175.3	3.62	2.90	6.52	52.00
16.80	187.0	4.12	3.05	7.17	57.00
17.85	199.0	4.24	3.32	7.56	60.50
18.90	210.4	4.61	3.63	8.24	66.00
19.95	222.0	5.34	3.96	9.30	74.40
21.00	236.0	5.60	4.39	10.00	80.00
21.50	236.0	6.94	4.56	11.50*	92.00*
21.50	236.0	9.50	5.10	14.60	117.00
22.00	236.0	14.56	6.11	20.70#	166.00#
22.00	236.0	15.15	8.27	23.40	187.00
22.00	236.0	15.30	9.73	25.00	200.00
23.00	236.0	16.65	12.70	29.35	235.00
23.00	236.0	17.10	14.00	31.10	248.00
23.00	236.0	18.33	17.20	35.50	284.00
24.00	236.0	20.00	20.30	40.30	322.00
24.00	236.0	22.50	27.10	49.60	397.00
24.00	236.0	33.00	38.80	71.80	575.00
24.00	236.0	45.00	76.00	121.00**	968.00**

* = first yield at middle support
\# = second yield at midspan
** = failure

Table A.8

Actual Rotation at the Critical Section Using

Method 1 x 10^{-4} Radians

Main Bars = 2#5 % Steel Fiber = 1.2 H_L = 9 inches

Load Kips	Moment Kip-in	ϕ_1	ϕ_2	ϕ	θ
1.05	11.7	.05	.10	.15	1.35
2.10	23.4	.10	.20	.30	2.70
3.15	35.0	.50	.29	.49	4.40
4.20	46.8	.62	.39	1.01	9.10
5.25	58.4	.80	.49	1.30	11.70
6.30	70.1	.88	.59	1.47	13.30
7.35	82.0	1.06	.69	1.75	15.80
8.40	93.5	1.22	.78	2.00	18.00
9.45	105.2	1.40	.88	2.30	20.70
10.50	117.0	1.55	.98	2.53	22.80
11.55	128.6	1.71	1.08	2.79	25.10
12.60	140.2	1.90	1.18	3.08	27.70
13.65	152.0	2.25	1.27	3.52	31.70
14.70	163.6	2.74	1.37	4.10	37.00
15.75	175.3	3.07	1.47	4.60	41.40
16.80	187.0	3.26	1.57	4.83	43.50
17.85	199.0	3.60	1.67	5.30	47.70
18.90	210.4	4.08	1.77	5.90	55.00
19.95	222.0	4.23	1.90	6.13	55.00
21.00	236.0	4.64	3.71	8.35*	75.00*
21.50	236.0	16.42	10.36	26.80	241.00
21.50	236.0	18.50	12.25	30.80#	277.00#
22.00	236.0	20.40	13.54	34.00	306.00
22.00	236.0	22.10	18.50	40.60	365.00
22.00	236.0	26.30	23.10	49.40	444.00
23.00	236.0	29.40	29.20	58.60	528.00
23.00	236.0	33.00	36.00	69.00	621.00
23.00	236.0	42.70	39.00	81.70	735.00
24.00	236.0	64.10	51.80	116.00	1044.00
24.00	236.0	97.00	77.65	174.70**	1566.00**

* = first yield at middle support
\# = second yield at midspan
** = failure

Table A.9

Strain and Curvature at Critical Sections-Method 2

Main Bars = 2#3 % Steel Fibers = 0.0 d = 6.56 inches

Load (Kips)	Moment (K-in)		μin/in Steel Strains			μin/in Concrete Strain			$x10^{-4}$ Curvature		
	negative	positive	negative	left	right	negative	left	right	negative	left	right
1.05	11.7	8.4	100	30	35	- 40	- 30	- 53	.21	.09	.13
2.10	23.4	16.8	244	71	79	- 105	- 85	- 125	.53	.24	.31
3.15	35.0	25.2	509	450	175	- 230	- 180	- 228	1.12	.96	.61
4.20	46.8	33.6	790	620	600	- 320	- 314	- 309	1.70	1.42	1.40
5.25	58.5	42.0	1063	1001	1050	- 480	- 430	- 375	2.40	2.20	2.20
6.30	70.2	50.4	1241	1100	1123	- 580	- 557	- 524	2.80	2.53	2.50
7.35	81.8	58.8	1492	1235	1350	- 722	- 667	- 654	3.40	2.90	3.10
8.40	93.5	67.2	1944	1740	1854	- 820	- 777	- 771	4.20	3.80	4.00
9.45	105.2	75.6	2200	2100	2151	-1020	- 900	- 892	5.00	4.50	4.60
10.50	105.2	84.0	-	2250	2400	-1233	-1059	-1020	-	5.04	5.20
11.55	105.2	92.4	-	-	2780	-1710	-1615	-1133	-	-	6.00
12.60	105.2	100.8	-	-	-	-2450	-1954	-2202	-	-	-
13.00	105.2	104.0	-	-	-	-2220	-2235	-2644	-	-	-

Table A.10

Strain and Curvature at Critical Sections-Method 2

Main Bars = 2#3 % Steel Fibers = 0.8 d = 6.56 inches

Load (Kips)	Moment (K-in)		μin/in Steel Strains			μin/in Concrete Strains			$x10^{-4}$ Curvature		
	negative	positive	negative	left	right	negative	left	right	negative	left	right
1.05	11.7	8.4	195	151.3	96	- 95	- 83	- 71	.44	.35	.25
2.10	23.4	16.8	390	303.0	192	- 170	- 167	- 142	.85	.71	.51
3.15	35.0	25.2	590	454.0	290	- 209	- 250	- 213	1.21	1.08	.77
4.20	46.8	33.6	781	605.0	382	- 333	- 333	- 285	1.70	1.42	1.01
5.25	58.5	42.0	932	727.0	472	- 460	- 498	- 445	2.20	1.90	1.40
6.30	70.2	50.4	1010	870.0	560	- 587	- 590	- 534	2.43	3.30	1.70
7.35	81.8	58.8	1096	1074.0	650	- 701	- 673	- 615	2.71	2.70	1.90
8.40	93.5	67.2	1340	1285.0	870	- 823	- 765	- 716	3.30	3.20	2.40
9.45	105.2	75.6	1630	1517.0	1080	- 972	- 850	- 784	4.00	3.60	2.85
10.50	116.9	84.0	2263	1800.0	1403	-1071	- 980	- 902	5.10	4.30	3.50
11.55	116.9	92.4	2765	2067.0	1600	-1170	-1101	- 978	6.00	4.90	3.90
12.60	116.9	100.8	-	2226.0	1940	-1224	-1262	-1080	-	5.30	4.60
13.13	116.9	105.0	-	-	-	-1292	-1532	-1180	-	-	-
14.18	116.9	114.0	-	-	-	-1330	-	-1317	-	-	-

Table A.11

Strain and Curvature at Critical Sections-Method 2

Main Bars = 2#3 % Steel Fibers = 1.2 d = 6.56 inches

Load (Kips)	Moment (K-in)		μin/in Steel Strains			μin/in Concrete Strains			$x10^{-4}$ Curvature		
	negative	positive	negative	left	right	negative	left	right	negative	left	right
1.05	11.7	8.4	42	121	70	- 10	- 32	- 31	.08	.23	.15
2.10	23.4	16.8	95	230	137	- 50	- 106	- 95	.22	.51	.35
3.15	35.0	25.0	277	520	570	- 170	- 209	- 230	.68	1.11	1.22
4.20	46.8	33.6	601	760	890	- 377	- 309	- 344	1.50	1.60	1.90
5.25	59.0	42.0	884	1045	1162	- 617	- 415	- 457	2.30	2.20	2.50
6.30	70.0	50.3	1164	1330	1486	- 875	- 510	- 578	3.30	2.80	3.10
7.35	82.0	59.0	1240	1540	1685	-1015	- 604	- 639	3.90	3.30	3.50
8.40	94.0	67.0	1851	1790	1948	-1211	- 714	- 742	4.70	3.80	4.10
9.45	105.0	76.0	2180	2000	2201	-1361	- 854	- 848	5.40	4.40	4.60
10.50	117.0	84.0	2590	2265	2520	-1582	-1030	-1002	6.40	5.00	5.40
11.55	129.0	92.4	2900	2467	2760	-1697	-1156	-1115	7.00	5.50	5.90
12.60	129.0	101.0	-	2705	2871	-1840	-1528	-1249	-	6.50	6.30
13.10	129.0	105.0	-	2760	2981	-2086	-1893	-1908	-	7.10	7.50
13.80	129.0	110.4	-	-	-	-3503	-2713	-	-	-	-
14.20	129.0	115.6	-	-	-	-4920	-3239	-	-	-	-

Table A.12

Strain and Curvature at Critical Sections-Method 2

Main Bars = 2#4 % Steel Fibers = 0.0 d = 6.5 inches

Load (Kips)	Moment (K-in)		μin/in Steel Strains			μin/in Concrete Strains			$x10^{-4}$ Curvature		
	negative	positive	negative	left	right	negative	left	right	negative	left	right
1.05	11.7	8.5	75	64	63	- 30	-	- 24	.16	-	.13
2.10	23.4	17.0	290	292	295	- 38	-	- 44	.50	-	.52
3.15	35.0	25.0	520	610	580	- 64	-	- 52	.90	-	.97
4.20	47.0	34.0	939	864	845	- 74	-	- 65	1.60	-	1.40
5.25	58.0	42.0	1205	1020	1500	- 155	-	- 138	2.10	-	2.52
6.30	70.4	50.0	1300	1180	1217	- 253	-	- 210	2.40	-	2.20
7.35	82.0	59.0	1420	1320	1331	- 320	-	- 282	2.70	-	2.50
8.40	94.0	67.0	1520	1461	1445	- 424	-	- 354	3.00	-	2.80
9.45	105.0	76.0	1650	1590	1600	- 520	-	- 470	3.40	-	3.20
10.50	117.0	84.0	1750	1744	1755	- 560	-	- 520	3.60	-	3.50
11.55	129.0	92.0	1890	1822	1795	- 884	-	- 810	4.11	-	3.90
12.60	140.0	101.0	2001	1950	1930	- 920	-	- 830	4.40	-	4.20
13.65	152.0	110.0	2100	2064	2075	- 980	-	- 854	4.65	-	4.50
14.70	164.0	118.0	2360	2265	2225	-1050	-	- 939	5.30	-	4.90
15.75	175.0	126.0	2458	2434	2377	-1080	-	-1060	5.40	-	5.30
16.80	187.0	135.0	2656	2564	2530	-1300	-	-1120	5.90	-	5.60
17.85	199.0	143.0	2845	2675	2639	-1654	-	-1350	6.90	-	6.10
18.90	210.0	151.0	-	2785	2745	-2033	-	-1900	-	-	7.20
19.95	210.0	160.0	-	-	2800	-	-	-	-	-	-

Table A.13

Strain and Curvature at Critical Sections-Method 2

Main Bars = 2#4 % Steel Fibers = 0.8 d = 6.5 inches

Load (Kips)	Moment (K-in)		μin/in Steel Strains			μin/in Concrete Strains			$x10^{-4}$ Curvature		
	negative	positive	negative	left	right	negative	left	right	negative	left	right
1.05	11.7	8.5	33	45	62	- 10	- 31	- 72	.07	.11	.2
2.10	23.4	17.0	52	78	132	- 40	- 101	- 161	.14	.28	.5
3.15	35.0	25.0	163	169	305	- 115	- 185	- 268	.42	.50	.9
4.20	47.0	34.0	451	243	430	- 230	- 266	- 380	1.04	.80	1.2
5.25	58.0	42.0	648	329	570	- 310	- 325	- 477	1.47	1.00	1.6
6.30	70.4	50.0	825	495	745	- 425	- 402	- 590	1.90	1.40	2.1
7.35	82.0	59.0	900	679	880	- 530	- 487	- 690	2.20	1.80	2.4
8.40	94.0	67.0	1110	804	1054	- 700	- 574	- 813	2.80	2.10	2.9
9.45	105.0	76.0	1240	950	1190	- 810	- 645	- 903	3.20	2.50	3.2
10.50	117.0	84.0	1347	1075	1300	- 850	- 706	-1014	3.40	2.80	3.6
11.55	129.0	92.0	1550	1230	1480	- 950	- 826	-1130	3.90	3.10	4.0
12.60	140.0	101.0	1650	1430	1604	-1100	- 909	-1257	4.30	3.60	4.4
13.65	152.0	110.0	1750	1520	1725	-1200	-1002	-1359	4.50	3.90	4.7
14.70	164.0	118.0	1825	1650	1850	-1420	-1073	-1455	5.00	4.20	5.1
15.75	175.0	126.0	1920	1843	2000	-1564	-1158	-1550	5.40	4.60	5.5
16.80	187.0	135.0	2150	1940	2140	-1700	-1239	-1687	5.90	4.90	5.9
17.85	199.0	143.0	2590	2030	2460	-1802	-1330	-1795	6.80	5.20	6.5
18.90	210.0	151.0	2640	2150	2530	-1900	-1422	-2023	7.00	5.50	7.0
19.95	222.0	160.0	2720	2300	2670	-2200	-1515	-2517	7.60	5.90	8.0
21.00	222.0	168.0	-	2410	2705	-3100	-1665	-1607	-	6.30	6.6
22.00	222.0	180.0	-	-	-	-4200	-1956	- 607	-	-	-
22.00	222.0	180.0	-	-	-	-5573	-2608	- 90	-	-	-
22.00	222.0	180.0	-	-	-	-5800	-3471	- 154	-	-	-

Table A.14

Strain and Curvature at Critical Sections-Method 2

Main Bars = 2#4 % Steel Fibers = 1.2 d = 6.5 inches

Load (Kips)	Moment (K-in)		μin/in Steel Strains			μin/in Concrete Strains			$x10^{-4}$ Curvature		
	negative	positive	negative	left	right	negative	left	right	negative	left	right
1.05	11.7	8.5	+ 6	95	132	- 9	-	- 30	.002	-	.2
2.10	23.4	17.5	16	225	280	- 14	-	- 70	.050	-	.5
3.15	35.0	25.0	25	335	408	- 35	-	- 167	.100	-	.9
4.20	47.0	34.0	37	445	520	- 70	-	- 256	.160	-	1.2
5.25	58.0	42.0	77	645	725	- 103	-	- 327	.270	-	1.6
6.30	70.0	50.0	106	870	993	- 229	-	- 495	.500	-	2.3
7.35	82.0	59.0	394	1190	1220	- 484	-	- 716	1.400	-	3.0
8.40	94.0	67.0	624	1180	1125	- 710	-	- 970	2.100	-	3.2
9.45	105.0	76.0	495	1360	1340	-1023	-	-1316	2.300	-	4.1
10.50	117.0	84.0	446	1525	1490	-1400	-	-1500	2.800	-	4.6
11.55	129.0	92.0	320	-	-	-1700	-	-1620	3.100	-	-
12.60	140.0	101.0	-	-	-	-	-	-	-	-	-

Table A.15

Strain and Curvature at Critical Sections-Method 2

Main Bars = 2#5 % Steel Fibers = 0.0 d = 6.44 inches

Load (Kips)	Moment (K-in)		μin/in Steel Strains			μin/in Concrete Strains			$x10^{-4}$ Curvature		
	negative	positive	negative	left	right	negative	left	right	negative	left	right
1.05	11.7	8.4	109	115	126	- 92	- 86	- 31	.3	.3	.2
2.10	23.4	16.8	150	202	276	- 184	- 112	- 65	.5	.5	.5
3.15	35.0	25.2	380	442	345	- 276	- 138	- 97	1.0	.9	.7
4.20	46.8	33.0	490	562	445	- 368	- 164	- 128	1.3	1.1	.9
5.25	59.0	42.0	580	656	570	- 460	- 190	- 160	1.6	1.3	1.1
6.30	70.0	50.0	680	739	585	- 552	- 218	- 186	1.9	1.4	1.2
7.35	82.0	59.0	782	840	606	- 644	- 255	- 204	2.2	1.7	1.3
8.40	94.0	67.0	1010	1021	950	- 736	- 338	- 330	2.7	2.1	2.0
9.45	105.0	76.0	1022	1151	1100	- 828	- 548	- 540	2.9	2.6	2.5
10.50	117.0	84.0	1039	1160	1244	- 920	- 650	- 610	3.0	2.8	2.9
11.55	129.0	92.4	1220	1270	1323	-1012	- 785	- 740	3.5	3.3	3.4
12.60	140.0	101.0	1340	1320	1430	-1100	- 923	- 900	3.8	3.5	3.6
13.65	152.0	110.0	1665	1521	5141	-1290	- 961	- 940	4.6	3.8	3.9
14.70	164.0	118.0	1810	1706	1711	-1400	- 999	-1080	5.0	4.2	4.3
15.75	175.0	126.0	1890	1806	1872	-1410	-1035	-1160	5.1	4.6	4.7
16.80	187.0	135.0	2030	1910	1996	-1410	-1135	-1180	5.3	4.7	4.9
17.85	199.0	143.0	2200	2013	2125	-1431	-1320	-1200	5.6	5.2	5.2
18.90	210.0	152.0	2430	2195	2320	-1452	-1343	-1240	6.0	5.5	5.5
19.95	222.0	160.0	2545	2307	2420	-1625	-1580	-1450	6.5	6.0	6.0
21.00	222.0	168.0	-	2330	2551	-1745	-2235	-1947	-	7.1	7.0
22.00	222.0	176.0	-	2406	2636	-	-2775	-2345	-	8.0	7.7
23.00	222.0	185.0	-	-	-	-	-	-	-	-	-

Table A.16

Strain and Curvature at Critical Sections-Method 2

Main Bars = 2#5 % Steel Fibers = 0.8 d = 6.44 inches

Load (Kips)	Moment (K-in)		μin/in Steel Strains			μin/in Concrete Strains			$x10^{-4}$ Curvature		
	negative	positive	negative	left	right	negative	left	right	negative	left	right
1.05	11.7	8.4	88	24	38	- 28	- 53	- 50	.2	.1	.13
2.10	23.4	17.0	176	81	131	- 78	- 119	- 125	.4	.3	.39
3.15	35.0	25.0	264	145	239	- 145	- 166	- 186	.6	.4	.70
4.20	47.0	33.0	352	262	348	- 290	- 239	- 266	1.0	.8	.95
5.25	59.0	42.0	440	361	444	- 375	- 300	- 300	1.3	1.0	1.20
6.30	70.0	50.0	528	450	541	- 510	- 400	- 375	1.6	1.3	1.40
7.35	82.0	59.0	616	510	637	- 590	- 440	- 420	1.9	1.4	1.60
8.40	94.0	67.0	704	650	750	- 790	- 522	- 503	2.3	1.8	1.90
9.45	105.0	76.0	792	734	830	- 905	- 585	- 550	2.6	2.0	2.10
10.50	117.0	84.0	888	815	913	-1080	- 666	- 605	3.1	2.2	2.40
11.55	129.0	92.0	970	905	1022	-1220	- 750	- 665	3.4	2.4	2.60
12.60	140.0	101.0	1035	995	1114	-1425	- 842	- 740	3.8	2.7	2.90
13.65	152.0	110.0	1102	1110	1244	-1600	- 947	- 804	4.2	3.2	3.20
14.70	164.0	118.0	1210	1201	1344	-1800	-1039	- 882	4.7	3.5	3.50
15.75	175.0	126.0	1360	1290	1457	-2000	-1145	- 950	5.2	3.8	3.70
16.80	187.0	135.0	1450	1365	1560	-2170	-1230	-1018	5.6	4.0	4.00
17.85	199.0	143.0	1527	1409	1677	-2390	-1348	-1094	6.1	4.3	4.30
18.90	210.0	152.0	1610	1510	1999	-2595	-1441	-1168	6.5	4.6	4.90
19.95	222.0	160.0	1750	1614	1900	-2792	-1552	-1244	7.1	4.9	4.90
21.00	233.0	168.0	1905	1710	2033	-3010	-1680	-1331	7.6	5.3	5.20
22.00	233.0	176.0	2200	1760	2160	-3350	-2360	-1438	8.6	6.3	5.60
23.00	233.0	185.0	-	1800	2148	-4142	-3760	-2090	-	8.6	6.60
24.00	233.0	205.0	-	1810	2150	-4450	-3200	-2300	-	7.8	6.90
24.00	233.0	205.0	-	1822	2160	-4720	-3066	-2428	-	7.6	7.10
24.00	233.0	205.0	-	-	2184	-5040	-2830	-2590	-	-	7.40
24.00	233.0	205.0	-	-	2200	-5364	-2670	-2832	-	-	7.80
24.00	233.0	205.0	-	-	2200	-5610	-2256	-3553	-	-	8.90

Table A.17

Strain and Curvature at Critical Sections-Method 2

Main Bars = 2#5 % Steel Fibers = 1.2 d = 6.44 inches

Load (Kips)	Moment (K-in)		μin/in Steel Strains			μin/in Concrete Strains			$x10^{-4}$ Curvature		
	negative	positive	negative	left	right	negative	left	right	negative	left	right
1.05	11.7	8.4	30	45	49	- 26	- 59	- 48	.09	.2	.2
2.10	23.0	17.0	59	89	97	- 51	- 118	- 96	.17	.3	.3
3.15	35.0	25.0	170	191	171	- 127	- 225	- 176	.50	.6	.5
4.20	47.0	33.0	280	293	244	- 202	- 333	- 256	.70	1.0	.8
5.25	59.0	42.0	385	388	372	- 306	- 439	- 335	1.10	1.3	1.1
6.30	70.0	50.0	490	482	499	- 410	- 544	- 414	1.40	1.6	1.4
7.35	82.0	59.0	585	581	604	- 573	- 654	- 489	1.80	1.9	1.7
8.40	94.0	67.0	680	681	709	- 735	- 764	- 563	2.20	2.2	2.0
9.45	105.0	76.0	790	775	807	- 891	- 879	- 653	2.60	2.6	2.3
10.50	117.0	84.0	891	871	905	-1047	- 994	- 742	3.00	2.9	2.6
11.55	129.0	92.0	990	965	996	-1196	-1101	- 822	3.40	3.2	2.8
12.60	140.0	101.0	1099	1056	1087	-1345	-1209	- 902	3.80	3.5	3.1
13.65	152.0	110.0	1197	1159	1185	-1517	-1342	-1000	4.20	3.9	3.4
14.70	164.0	118.0	1295	1262	1283	-1688	-1474	-1098	4.60	4.2	3.7
15.75	175.0	126.0	1385	1355	1377	-1840	-1600	-1203	5.00	4.6	4.0
16.80	187.0	135.0	1475	1456	1470	-1990	-1726	-1308	5.40	4.9	4.3
17.85	199.0	143.0	1493	1571	1570	-2160	-1855	-1416	5.70	5.3	4.6
18.90	210.0	152.0	1789	1715	1678	-2200	-2022	-1555	6.20	5.8	5.0
19.95	222.0	160.0	1872	1790	1783	-2267	-2155	-1680	6.40	6.1	5.4
21.00	233.0	168.9	1922	1885	1867	-2501	-2440	-1846	6.90	6.7	5.8
22.00	233.0	176.0	2140	1939	1893	-3200	-3690	-2590	8.30	8.7	7.0
22.00	233.0	185.0	-	2018	1985	-3900	-4928	-3400	-	9.4	8.4
22.00	233.0	185.0	-	2040	-	-4200	-3956	-3400	-	9.3	-
22.00	233.0	185.0	-	-	-	-4800	-4221	-4308	-	-	-

Table A.18

Strain and Curvature at Critical Sections-Method 2

Main Bars = 2#6 and 2#3 % Steel Fibers = 0.8 d = 6.4 inches

Load (Kips)	Moment (K-in)		μin/in Steel Strains			μin/in Concrete Strains			$x10^{-4}$ Curvature		
	negative	positive	negative	left	right	negative	left	right	negative	left	right
2.1	23.4	17	181	256	282	- 163	- 65	- 145	.5	.5	.7
4.2	47.0	33	290	406	438	- 327	- 129	- 295	1.0	.8	1.1
6.3	70.0	50	425	547	577	- 490	- 194	- 443	1.4	1.2	1.6
8.4	94.0	67	651	739	805	- 653	- 260	- 590	2.0	1.6	2.2
10.5	117.0	84	854	923	1005	- 816	- 324	- 737	2.6	2.6	2.7
12.6	140.0	100	1030	1080	1162	- 980	- 390	- 883	3.1	2.3	3.2
14.7	163.6	118	1330	1275	1376	-1130	- 452	-1035	3.8	2.7	3.8
16.8	187.0	134	1450	1390	1494	-1317	- 615	-1185	4.3	3.1	4.2
18.9	210.0	151	1580	1543	1653	-1492	- 780	-1314	4.8	3.6	4.6
21.0	233.0	168	1690	1675	1799	-1709	- 950	-1465	5.3	4.1	5.1
22.0	245.0	176	1840	1807	1924	-1834	-1091	-1587	5.7	4.5	5.5
23.0	256.0	184	1901	1847	1981	-1904	-1171	-1674	5.9	4.7	5.7
24.0	267.0	192	1981	1926	2063	-1985	-1283	-1778	6.2	5.0	6.0
25.0	278.0	200	2061	2000	2130	-2036	-1376	-1855	6.4	5.3	6.2
26.0	290.0	208	2126	2048	2185	-2080	-1448	-1920	6.6	5.5	6.4
27.0	300.0	216	2218	2104	2256	-2158	-1542	-2023	6.8	5.7	6.7
28.0	311.0	224	2290	2120	2343	-2238	-1680	-2145	7.1	5.9	7.0
29.0	323.0	232	2340	2293	2440	-2325	-1900	-2247	7.3	6.6	7.3
30.0	334.0	240	2440	2490	2353	-2560	-2100	-2512	7.8	7.2	7.6
32.0	356.0	256	2590	2503	2585	-2670	-2201	-2564	8.2	7.4	8.0
33.0	367.0	264	2805	2719	2734	-2803	-2510	-2773	8.8	8.2	8.6

APPENDIX B

Table B.1

Differential Level Readings (inches) $x10^{-3}$

Main Reinforcement 2#3

Load (Kips)	0% Steel Fibers Section				0.8 % Steel Fibers Section				1.2% Steel Fibers Section			
	1	2	3	4	1	2	3	4	1	2	3	4
0.0	0	0.0	0	0.0	0	0	0	0	0	0	0	0
2.1	20	12.5	8	12.5	25	12	12	29	21	16	12	25
4.2	41	21.0	25	29.0	46	38	33	50	41	29	29	33
6.3	66	41.0	38	50.0	54	50	41	58	58	54	45	58
8.4	88	58.0	58	75.0	67	63	54	95	79	63	54	79
10.5	208	125.0	108	138.0	83	79	91	112	100	71	75	100
11.55	291	163.0	175	242.0	125	92	100	129	146	120	145	225
12.60	558	275.0	196	313.0	188	121	116	163	233	163	188	296
14.70	-	-	-	-	291	179	129	188	262	195	229	366
15.50	-	-	-	-	380	208	212	312	316	204	329	515
16.00	-	-	-	-	513	304	275	433	479	304	404	675
16.80	-	-	-	-	1323	833	445	608	970	473	533	1079

Table B.2

Differential Level Readings (inches) $x10^{-3}$

Main Reinforcement 2#4

Load (Kips)	0% Steel Fibers Section				0.85 Steel Fibers Section				1.2% Steel Fibers Section			
	1	2	3	4	1	2	3	4	1	2	3	4
0.00	0	0	0	0	0	0	0.0	0	0	0	0	0
2.10	16	8	8	20	16	8	12.0	16	8	4	4	8
4.20	25	25	33	45	21	12	29.0	37	25	16	20	29
6.30	50	38	63	70	33	25	46.0	58	33	29	37	45
8.40	66	41	66	100	45	37	54.0	63	45	38	45	54
10.50	79	50	83	104	63	46	63.0	75	63	54	63	75
12.60	100	66	91	108	75	54	83.0	100	108	87	75	96
14.70	104	66	95	112	91	66	96.0	117	-	-	-	-
16.80	125	83	104	133	104	83	112.5	134	-	-	-	-
18.90	154	104	116	145	121	95	125.0	158	-	-	-	-
19.95	329	116	125	204	137	129	212.0	288	-	-	-	-
21.00	-	-	-	-	171	133	225.0	317	-	-	-	-
22.00	-	-	-	-	225	166	316.0	413	-	-	-	-
23.00	-	-	-	-	366	250	383.0	500	-	-	-	-
24.10	-	-	-	-	450	312	454.0	646	-	-	-	-
25.00	-	-	-	-	500	333	513	979	-	-	-	-

Table B.3

Differential Level Readings (inches) $x10^{-3}$

Main Reinforcement 2#5

Load (Kips)	0% Steel Fibers Section				0.8% Steel Fibers Section				1.2% Steel Fibers Section			
	1	2	3	4	1	2	3	4	1	2	3	4
0.00	0	0.0	0	0	0	0	0	0	0	0	0	0.0
2.10	20	12.5	13	21	16	8	8	13	8	4	6	16.0
4.20	45	25.0	25	29	33	29	20	25	46	21	20	29.0
6.30	54	33.0	38	50	41	33	38	46	54	33	29	50.0
8.40	63	41.0	50	58	54	41	41	50	79	38	38	62.5
10.50	75	58.0	66	66	79	54	50	63	87	38	50	75.0
12.60	83	75.0	88	88	83	67	63	71	96	50	54	88.0
14.70	88	79.0	88	96	96	71	75	88	104	54	66	100.0
16.80	92	83.0	91	96	108	79	79	96	121	54	75	116.0
18.90	129	113.0	100	116	121	87	87	113	129	58	75	125.0
19.95	175	154.0	125	142	125	91	95	125	146	91	83	133.0
21.00	225	188.0	150	180	133	100	100	129	163	92	125	150.0
22.00	250	192.0	158	213	145	108	105	145	262	116	229	283.0
23.10	348	213.0	163	400	208	166	129	175	375	216	316	412.0
24.15	-	-	-	-	383	330	167	246	671	408	458	750.0
25.20	-	-	-	-	721	354	266	330	1020	575	513	963.0

Table B.4

Actual Deflections $x10^{-3}$ inches

Main Bars 2#3

Load	0% Fiber			0.8% Fiber			1.2% Fiber		
(Kips)	left	right	average	left	right	average	left	right	average
1.05	7.0	8	8	9	9	9	8	8	8
2.10	12.5	14	13	16	15	15	16	16	16
3.15	23.0	20	22	25	23	24	24	26	25
4.20	32.0	29	30	34	32	33	32	36	34
5.25	43.0	37	40	43	40	42	41	45	43
6.30	53.0	47	50	56	52	54	50	56	53
7.35	63.0	58	60	63	58	60	58	66	62
8.40	75.0	66	70	73	68	70	70	77	74
9.45	85.0	80	83	82	78	80	79	88	83
10.50	105.0	92	99	93	88	90	91	101	96
11.55	133.0	125	130	104	98	101	103	115	109
12.60	438.0	493	466	121	116	119	131	156	144
13.65	-	-	-	154	121	138	191	204	198
14.70	-	-	-	283	138	210	275	420	347
15.75	-	-	-	365	177	269	513	802	645
16.80	-	-	-	1358	548	953	927	1121	1024
17.85	-	-	-	-	-	-	-	-	-
18.90	-	-	-	-	-	-	-	-	-
19.95	-	-	-	-	-	-	-	-	-
21.00	-	-	-	-	-	-	-	-	-
22.05	-	-	-	-	-	-	-	-	-
23.10	-	-	-	-	-	-	-	-	-
24.15	-	-	-	-	-	-	-	-	-
25.20	-	-	-	-	-	-	-	-	-

Table B.5

Actual Deflections $x10^{-3}$ inches

Main Bar 2#4

Loads (Kips)	0% Fiber			0.8% Fiber			1.2% Fiber		
	left	right	average	left	right	average	left	right	average
1.05	7	8	7	8	8	8	9	9	9
2.10	11	14	13	15	17	16	17	16	16
3.15	18	22	20	22	24	23	24	23	23
4.20	24	29	25	30	31	31	28	28	28
5.25	31	35	33	33	36	35	34	34	34
6.30	38	42	40	38	43	40	39	41	40
7.35	43	48	45	43	50	47	47	48	47
8.40	49	54	52	46	57	51	55	57	56
9.45	55	62	58	60	60	60	63	65	64
10.50	61	69	65	70	70	70	72	74	73
11.55	73	75	74	78	80	79	82	82	82
12.60	78	81	79	85	88	87	117	101	109
13.65	85	89	87	90	96	93	-	-	-
14.70	96	98	97	98	104	101	-	-	-
15.75	102	105	103	104	112	108	-	-	-
16.80	113	114	113	113	123	118	-	-	-
17.85	123	124	123	120	132	126	-	-	-
18.90	142	140	141	128	144	136	-	-	-
19.95	319	300	310	183	198	190	-	-	-
21.00	-	-	-	233	275	254	-	-	-
22.05	-	-	-	248	368	308	-	-	-
23.10	-	-	-	268	404	385	-	-	-
24.15	-	-	-	450	454	452	-	-	-
25.20	-	-	-	658	657	657	-	-	-

Table B.6

Actual Deflections $x10^{-3}$ inches

Main Bars 2#5

Load	0% Fibers			0.8% Fibers			1.2% Fibers		
(Kips)	left	right	average	left	right	average	left	right	average
1.05	8	8	8	8	8	8	7	9	8
2.10	17	17	17	15	16	16	14	18	16
3.15	24	23	23	21	23	22	23	25	24
4.20	29	28	28	28	29	28	31	33	32
5.25	35	33	34	33	35	34	37	39	38
6.30	41	40	40	38	41	39	43	45	44
7.35	46	45	45	43	48	45	49	52	51
8.40	53	50	51	48	52	50	54	58	56
9.45	59	58	58	53	57	55	61	64	62
10.50	67	67	67	61	64	62	66	68	67
11.55	74	74	74	65	69	67	69	73	71
12.60	82	79	81	73	77	75	77	82	80
13.65	87	84	85	79	83	81	85	88	86
14.70	96	92	94	86	90	88	90	94	92
15.75	103	99	101	91	95	93	99	101	100
16.80	114	108	111	98	103	101	103	106	104
17.85	120	113	116	104	108	106	113	116	115
18.90	130	122	126	113	102	107	121	123	122
19.95	150	129	140	120	122	121	129	132	131
21.00	186	138	162	128	130	129	136	140	138
22.05	233	170	201	142	136	142	273	278	276
23.10	522	414	469	178	148	163	354	389	372
24.15	-	-	-	363	220	292	671	475	573
25.20	-	-	-	741	610	676	1300	953	1126

Table B.7

Curvature and Deflection of 2#6 and 2#3 .8F

$\phi = \phi_1 + \phi_2$ (ϕ at middle support)

Load (Kips)	Moment (Kip-in)	Curvature 10^{-4}			Deflection $x10^{-3}$		
		ϕ_1 left side	ϕ_2 right	ϕ total	Δ left	Δ right	Δ ave.
1.05	11.7	.49	.63	1.12	14	16	15
2.10	23.0	.51	.72	1.23	32	34	33
3.15	35.0	.55	.76	1.31	46	48	47
4.20	47.0	.61	.84	1.45	58	62	60
5.25	58.0	.74	1.00	1.74	70	75	73
6.30	70.0	1.21	1.33	2.54	82	90	86
7.35	82.0	1.33	1.37	2.70	92	100	96
8.40	94.0	1.56	1.78	3.34	105	115	110
9.45	105.0	1.66	1.86	3.52	115	120	118
10.50	117.0	1.76	2.19	3.95	129	141	135
11.55	129.0	1.95	2.29	4.24	140	151	145
12.60	140.0	2.11	2.58	4.69	151	172	160
13.65	152.0	2.34	2.77	5.11	162	185	173
14.70	164.0	2.38	2.81	5.20	179	205	192
15.75	175.0	2.61	3.09	5.70	188	215	202
16.80	187.0	2.93	3.13	6.06	200	230	215
17.85	199.0	3.13	3.28	6.41	214	250	232
18.90	210.0	3.34	3.54	6.88	225	264	245
19.95	222.0	3.48	3.66	7.14	235	275	255
21.00	234.0	3.71	3.77	7.48	250	290	270
22.00	245.0	4.04	3.85	7.90	261	308	285
23.00	256.0	4.51	3.95	8.50	273	320	297
24.00	267.0	4.57	4.11	8.70	284	335	310
25.00	278.0	4.88	4.28	9.16	300	354	327
26.00	289.0	5.25	4.34	9.60	316	374	345
27.00	301.0	5.27	4.46	9.73	328	392	360
28.00	312.0	5.47	4.58	10.05	340	405	372
29.00	323.0	5.86	4.63	10.50	366	441	404
30.00	334.0	6.11	4.85	10.96	386	465	426
31.00	345.0	6.25	4.89	11.14	400	480	440
32.00	356.0	7.24	5.02	12.30	461	572	517
33.00	367.0	8.34	5.55	13.90	495	670	583
33.00	367.0	9.92	5.55	15.47	512	750	631

APPENDIX C

Table C.1

Crack Readings at Negative Section

Main Bars = 2#3 % Steel Fibers = 0.0 f_c' = 4584 psi

All readings are in 10^{-4} inches

Load (Kips)	P/P_u Ratio	Interval 1	2	3	4	5	6	7	8	9	10	11	12	13	14	15	16	17	18	19	20
0.00	0.00	0	0	0	0	0	0	0	0	0	0	0	0	0	0	0	0	0	0	-	-
2.10	0.17	0	3	9	0	2	0	4	0	2	0	18	23	0	0	0	-	2	7	-	-
4.20	0.33	0	0	4	2	1	8	10	0	-	-	45	48	-	-	-	0	6	4	-	-
6.30	0.50	-	-	-	67	-	30	39	-	-	-	127	120	-	-	-	-	85	11	-	-
8.40	0.67	-	-	-	134	-	38	39	-	-	-	203	200	-	-	-	-	142	22	-	-
10.50	0.83	-	-	-	136	-	43	46	-	-	-	418	405	-	-	-	-	163	73	-	-
11.55	0.91	-	-	-	182	-	-	-	-	-	-	1005	948	-	-	-	-	200	-	-	-
12.60	1.00	-	-	-	1170	-	-	-	-	-	-	2468	2451	-	-	-	-	570	-	-	-

Table C.2

Crack Readings at Negative Section

Main Bars = 2#3 % Steel Fibers = 0.8 f_c' = 4805 psi

All readings are in 10^{-4} inches

Load (Kips)	P/P_u Ratio	Interval 1	2	3	4	5	6	7	8	9	10	11	12	13	14	15	16	17	18	19	20
0.0	0.00	0	0	0	0	0	0	0	0	0	0	0	0	0	0	0	0	0	0	0	0
2.1	0.17	2	0	2	8	7	8	29	16	8	21	10	16	7	13	0	35	14	0	0	0
4.2	0.33	-	-	-	8	17	18	8	16	8	25	28	19	7	14	9	48	14	0	1	-
6.3	0.50	-	-	-	18	37	33	12	15	-	49	53	19	6	13	19	85	33	1	4	2
8.4	0.67	-	-	-	-	-	65	12	15	-	88	91	14	8	13	28	155	51	7	15	-
10.5	0.83	-	-	-	-	-	156	27	-	-	135	173	49	-	-	29	195	85	70	69	-
12.6	0.91	-	-	-	-	-	178	-	-	-	154	300	150	-	-	47	204	101	99	93	-
12.6	1.00	-	-	-	-	-	184	-	-	-	430	833	507	-	-	166	278	193	164	154	-

Table C.3

Crack Readings at Negative Section

Main Bars = 2#3 % Steel Fibers = 1.2 f_c' = 4927 psi

All readings are in 10^{-4} inches

Load (Kips)	P/P_u Ratio	Interval																			
		1	2	3	4	5	6	7	8	9	10	11	12	13	14	15	16	17	18	19	20
0.0	0.00	0	0	0	0	0	0	0	0	0	0	0	0	0	0	0	0	0	0	0	-
2.1	0.16	12	2	0	2	0	0	3	3	10	21	0	5	0	6	0	1	1	3	2	-
4.2	0.32	29	2	-	12	0	-	30	17	29	30	18	32	-	12	2	2	-	7	1	-
6.3	0.49	48	28	-	40	0	-	40	27	34	68	14	35	-	18	65	25	-	15	-	-
8.4	0.64	70	44	-	74	-	-	69	51	41	82	-	40	-	57	67	65	-	10	-	-
10.5	0.80	96	65	-	110	-	-	129	60	144	80	-	112	-	177	161	180	-	-	-	-
12.6	0.97	98	75	-	109	-	-	321	353	449	314	-	-	-	312	-	190	-	-	-	-
13.0	1.00	-	-	-	-	-	-	485	-	1032	-	-	-	-	500	-	-	-	-	-	-

Table C.4

Crack Readings at Negative Section

Main Bars = 2#4 % Steel Fibers = 0.0 f_c' = 4584 psi

All readings are in 10^{-4} inches

Load (Kips)	P/P_u Ratio	Interval																			
		1	2	3	4	5	6	7	8	9	10	11	12	13	14	15	16	17	18	19	20
0.0	0.00	0	0	0	0	0	0	0	0	0	0	0	0	0	0	0	0	0	0	0	0
2.1	0.10	1	0	1	2	0	2	1	4	2	7	5	4	5	3	12	0	0	15	38	9
4.2	0.20	0	-	1	2	5	3	3	8	6	10	8	2	2	0	16	-	-	53	44	10
6.3	0.30	-	-	-	-	-	-	25	8	61	12	6	8	11	12	19	-	-	80	90	15
8.4	0.42	-	-	-	-	-	-	69	15	101	8	6	7	-	-	-	-	-	90	95	43
10.5	0.52	-	-	-	-	-	-	125	32	181	-	-	-	-	-	-	-	-	205	219	69
12.6	0.60	-	-	-	-	-	-	134	-	226	-	-	-	-	-	-	-	-	268	302	97
14.7	0.70	-	-	-	-	-	-	224	-	285	-	-	-	-	-	-	-	-	341	347	114
16.0	0.80	-	-	-	-	-	-	241	-	335	-	-	-	-	-	-	-	-	365	362	200

Table C.5

Crack Readings at Negative Section

Main Bars = 2#4 % Steel Fibers = 0.8 f_c' = 4805 psi

All readings are in 10^{-4} inches

Load (Kips)	P/P_u Ratio	Interval 1	2	3	4	5	6	7	8	9	10	11	12	13	14	15	16	17	18	19	20
0.0	0.00	0	0	0	0	0	0	0	0	0	0	0	0	0	0	0	0	0	0	0	0
2.1	0.10	7	6	0	7	7	5	6	4	5	4	5	6	1	2	4	0	1	1	2	0
4.2	0.20	12	13	12	12	9	15	13	8	6	-	20	34	7	12	17	10	12	-	9	-
6.3	0.30	14	15	42	15	15	36	28	9	9	-	33	67	6	16	22	55	40	-	4	-
8.4	0.40	47	95	2	15	14	48	51	12	9	-	40	69	8	26	23	51	45	-	12	-
10.5	0.52	53	108	16	21	27	72	77	28	24	-	120	111	10	45	81	86	70	-	27	-
12.6	0.60	107	115	17	27	38	91	100	35	24	-	144	129	-	65	97	92	72	-	72	-
14.7	0.70	122	133	-	34	86	119	101	-	-	-	156	134	-	85	125	98	-	-	102	-
18.9	0.85	177	190	-	71	158	152	119	-	-	-	188	-	-	134	175	112	-	-	101	-
20.0	0.91	182	198	-	101	184	151	119	-	-	-	837	-	-	395	379	-	-	-	-	-

Table C.6

Crack Readings at Negative Section

Main Bars = 2#5 % Steel Fibers = 0.0 f_c' = 4584 psi

All readings are in 10^{-4} inches

Load (Kips)	P/P_u Ratio	Interval																			
		1	2	3	4	5	6	7	8	9	10	11	12	13	14	15	16	17	18	19	20
0.0	0.0	0	0	0	0	0	0	0	0	0	0	0	0	0	0	0	0	0	0	0	0
2.1	0.1	0	10	1	2	4	4	0	0	2	20	13	0	0	0	10	2	1	5	5	-
4.2	0.2	-	18	4	-	-	-	-	-	-	35	43	-	-	0	2	11	-	11	11	-
6.3	0.3	-	21	6	-	-	-	-	-	-	60	86	-	-	-	-	-	-	20	18	-
8.4	0.4	-	96	92	-	-	-	-	-	-	97	101	-	-	-	-	-	-	42	42	-
10.5	0.5	-	102	123	-	-	-	-	-	-	135	143	-	-	-	-	-	-	84	85	-
12.6	0.6	-	154	145	-	-	-	-	-	-	155	173	-	-	-	-	-	-	113	108	-
16.8	0.8	-	212	211	-	-	-	-	-	-	195	215	-	-	-	-	-	-	220	207	-
21.0	1.0	-	326	216	-	-	-	-	-	-	755	796	-	-	-	-	-	-	378	373	-

Table C.7

Crack Readings at Negative Section

Main Bars = 2#5 % Steel Fibers = 0.8 f_c' = 4805 psi

All readings are in 10^{-4} inches

Load (Kips)	P/P_u Ratio	Interval																			
		1	2	3	4	5	6	7	8	9	10	11	12	13	14	15	16	17	18	19	20
0.0	0.00	0	0	0	0	0	0	0	0	0	0	0	0	0	0	0	0	0	-	-	-
2.1	0.10	0	2	10	6	17	12	2	31	35	14	3	6	15	0	3	29	29	-	-	-
4.2	0.20	-	-	4	11	50	46	-	26	55	14	-	32	23	-	-	70	76	-	-	-
6.3	0.29	-	-	-	-	65	64	-	-	69	19	-	31	22	-	-	90	92	-	-	-
8.4	0.38	-	-	-	-	77	84	-	8	89	42	-	-	36	-	-	97	99	-	-	-
10.5	0.42	-	-	-	-	105	97	-	-	109	100	-	-	15	-	-	122	119	-	-	-
12.6	0.57	-	-	-	-	125	127	-	-	115	115	-	-	40	-	-	131	124	-	-	-
16.8	0.76	-	-	-	-	160	169	-	-	129	134	-	-	180	-	-	329	319	-	-	-
22.0	1.00	-	-	-	-	200	205	-	-	398	462	-	-	361	-	-	420	431	-	-	-

Table C.8

Crack Readings at Negative Section

Main Bars = 2#5 % Steel Fibers = 1.2 f_c' = 4927 psi

All readings are in 10^{-4} inches

Load (Kips)	P/P_u Ratio	Interval																			
		1	2	3	4	5	6	7	8	9	10	11	12	13	14	15	16	17	18	19	20
0.0	0.00	0	0	0	0	0	0	0	0	0	0	0	0	0	0	0	0	0	0	0	0
2.1	0.10	0	1	3	2	4	10	4	2	1	0	0	1	1	2	-	0	15	0	-	-
4.2	0.20	-	-	0	9	9	2	19	13	0	-	-	6	20	2	1	0	22	-	-	-
6.3	0.29	-	-	1	8	20	-1	41	41	-	-	-	26	48	0	-	7	30	-	-	-
8.4	0.38	-	-	-	44	53	-	52	48	-	-	-	43	63	-	-	40	55	-	-	-
10.5	0.47	-	-	-	69	97	-	75	72	-	-	-	64	78	-	-	73	82	-	-	-
12.6	0.57	-	-	-	95	121	-	86	83	-	-	-	79	93	-	-	100	110	-	-	-
16.8	0.76	-	-	-	149	154	-	117	126	-	-	-	114	131	-	-	160	168	-	-	-
22.0	1.00	-	-	-	541	1206	-	774	763	-	-	-	1300	1298	-	-	-	244	-	-	-

Table C.9

Crack Readings at Negative Section

Main Bars = 2#6 and 2#3 % Steel Fibers = 0.8 f_c' = 5100 psi

All readings are in 10^{-4} inches

Load (Kips)	P/P_u Ratio	Interval																			
		1	2	3	4	5	6	7	8	9	10	11	12	13	14	15	16	17	18	19	20
0.0	0.00	0	0	0	0	0	0	0	0	0	0	0	0	0	0	0	0	0	0	0	0
4.2	0.12	3	7	6	9	0	18	23	1	0	0	28	45	0	0	21	25	1	-	-	-
8.4	0.24	10	16	1	0	-	50	43	-	-	-	34	54	-	-	25	22	-	-	-	-
12.6	0.36	42	3	-	-	-	59	63	-	-	-	59	84	-	-	72	70	-	-	-	-
16.8	0.48	62	-	46	-	-	91	103	-	-	-	95	-	-	-	102	97	-	-	-	-
21.0	0.60	92	-	66	-	-	122	138	-	-	-	129	-	-	-	136	122	-	-	-	-
24.0	0.68	113	-	86	-	-	145	163	-	-	-	149	-	-	-	159	148	-	-	-	-

Table C.10

Crack Readings at Positive Section

Main Bars = 2#3 % Steel Fibers = 0.0 f_c' = 4584 psi

All readings are in 10^{-4} inches

Load (Kips)	P/P_u Ratio	Interval																			
		1	2	3	4	5	6	7	8	9	10	11	12	13	14	15	16	17	18	19	20
0.00	0.00	0	0	0	0	0	0	0	0	0	0	0	0	0	0	0	0	0	-	-	-
2.10	0.17	4	0	1	0	6	8	0	1	0	25	20	4	0	0	3	5	12	-	-	-
4.20	0.33	20	10	2	0	40	40	1	0	-	65	70	31	1	0	9	2	2	-	-	-
6.30	0.50	67	39	-	-	65	75	-	-	-	124	106	52	0	0	70	-	47	-	-	-
8.40	0.67	92	75	-	-	112	112	-	-	-	160	142	69	-	-	120	-	68	-	-	-
10.50	0.83	117	103	-	-	148	155	-	-	-	225	220	-	-	-	180	-	79	-	-	-
11.55	0.91	137	123	-	-	313	310	-	-	-	830	892	132	-	-	-	-	-	-	-	-
12.60	1.00	159	135	-	-	463	463	-	-	-	1154	-	630	-	-	204	-	-	-	-	-

Table C.11

Crack Readings at Positive Section

Main Bars = 2#3 % Steel Fibers = 0.8 f_c' = 4805 psi

All readings are in 10^{-4} inches

Load (Kips)	P/P_u Ratio	Interval 1	2	3	4	5	6	7	8	9	10	11	12	13	14	15	16	17	18	19	20
0.0	0.00	0	0	0	0	0	0	0	0	0	0	0	0	0	0	0	0	0	0	0	0
2.1	0.17	0	0	20	12	6	0	20	16	0	0	0	20	12	10	-	-	5	0	12	0
4.2	0.33	0	1	37	35	17	-	52	35	-	0	-	42	32	31	-	-	16	2	23	0
6.3	0.50	-	-	47	46	33	-	82	67	-	-	-	92	62	44	-	-	28	10	29	-
8.4	0.67	-	-	77	87	32	-	201	94	-	-	-	98	83	58	35	-	40	22	33	-
10.5	0.83	-	-	103	150	-	-	251	95	-	-	-	230	110	173	35	-	55	22	63	-
12.6	0.91	-	-	-	-	-	-	-	-	-	-	-	-	-	-	-	-	-	-	-	-
12.6	1.00	-	-	117	153	-	-	290	156	-	-	-	232	132	298	41	-	52	37	93	-

Table C.12

Crack Readings at Positive Section

Main Bars = 2#3 % Steel Fibers = 1.2 f_c' = 4927 psi

All readings are in 10^{-4} inches

Load (Kips)	P/P_u Ratio	Interval																			
		1	2	3	4	5	6	7	8	9	10	11	12	13	14	15	16	17	18	19	20
0.0	0.00	0	0	0	0	0	0	0	0	0	0	0	0	0	-	-	-	-	-	-	-
2.1	0.16	2	10	0	35	17	7	0	2	15	10	15	1	0	-	-	-	-	-	-	-
4.2	0.32	10	12	-	58	37	43	-	48	25	5	20	1	-	-	-	-	-	-	-	-
6.3	0.49	22	35	-	62	39	50	-	65	45	4	41	-	-	-	-	-	-	-	-	-
8.4	0.65	44	64	-	85	41	88	-	72	74	16	80	-	-	-	-	-	-	-	-	-
10.5	0.82	85	93	-	109	81	90	-	90	125	-	80	-	-	-	-	-	-	-	-	-
13.0	1.00	85	96	-	248	201	116	-	121	126	-	91	-	-	-	-	-	-	-	-	-

Table C.13

Crack Readings at Positive Section

Main Bars = 2#4 % Steel Fibers = 0.0 f_c' = 4584 psi

All readings are in 10^{-4} inches

Load (Kips)	P/Pu Ratio	Interval																			
		1	2	3	4	5	6	7	8	9	10	11	12	13	14	15	16	17	18	19	20
0.0	.00	0	0	0	0	0	0	0	0	0	0	0	0	0	0	0	0	0	0	0	0
2.1	.10	1	-1	21	25	29	0	2	32	2	-	10	30	-	11	25	0	12	9	0	5
4.2	.20	0	-	40	26	29	-	-	59	-	-	5	30	-	42	30	-	29	-	-	15
6.3	.30	-	-	65	58	31	-	-	65	-	-	6	32	-	63	43	-	34	-	-	16
8.4	.42	-	-	74	10	32	-	-	80	-	-	-	55	-	65	59	-	38	-	-	21
10.5	.52	-	-	87	-	37	-	-	118	-	-	-	81	-	73	77	-	44	-	-	26
12.6	.60	-	-	93	-	60	-	-	137	-	-	-	87	-	74	78	-	71	-	-	46
14.7	.70	-	-	111	-	74	-	-	162	-	-	-	170	-	89	92	-	94	-	-	64
16.0	.80	-	-	123	-	106	-	-	180	-	-	-	279	-	111	97	-	125	-	-	73

Table C.14

Crack Readings at Positive Section

Main Bars = 2#4 % Steel Fibers = 0.8 f_c' = 4805 psi

All readings are in 10^{-4} inches

Load (Kips)	P/P_u Ratio	Interval																			
		1	2	3	4	5	6	7	8	9	10	11	12	13	14	15	16	17	18	19	20
0.0	0.00	0	0	0	0	0	0	0	0	0	0	0	0	0	-	-	-	-	-	-	-
2.1	0.10	0	1	10	0	1	0	1	5	1	6	1	0	0	-	-	-	-	-	-	-
4.2	0.20	0	0	20	-	37	-	0	37	-	15	5	1	1	-	-	-	-	-	-	-
6.3	0.30	-	25	34	-	60	-	-	50	-	40	-	17	0	-	-	-	-	-	-	-
8.4	0.40	-	55	64	-	62	-	-	58	-	60	-	29	-	-	-	-	-	-	-	-
10.5	0.52	-	69	78	-	85	-	-	76	-	93	-	29	-	-	-	-	-	-	-	-
12.6	0.60	-	107	114	-	130	-	-	106	-	108	-	44	-	-	-	-	-	-	-	-
14.7	0.70	-	132	127	-	154	-	-	111	-	114	-	49	-	-	-	-	-	-	-	-
18.9	0.85	-	235	235	-	331	-	-	-	-	242	-	155	-	-	-	-	-	-	-	-
20.0	0.91	-	260	230	-	335	-	-	-	-	244	-	-	-	-	-	-	-	-	-	-

Table C.15

Crack Readings at Positive Section

Main Bars = 2#5 % Steel Fibers = 0.0 f_c' = 4584 psi

All readings are in 10^{-4} inches

Load (Kips)	P/P_u Ratio	Interval																			
		1	2	3	4	5	6	7	8	9	10	11	12	13	14	15	16	17	18	19	20
0.0	0.0	0	0	0	0	0	0	0	0	0	0	0	0	0	0	0	0	0	0	0	0
2.1	0.1	7	7	1	3	0	2	0	9	4	5	5	1	0	0	0	10	1	5	-	-
4.2	0.2	20	17	1	8	1	1	1	16	24	1	10	10	-	-	-	21	-	10	-	-
6.3	0.3	42	29	0	31	36	1	0	53	56	-	21	16	-	-	-	32	-	30	-	-
8.4	0.4	50	39	-	43	49	-	-	58	64	-	27	26	-	-	-	40	-	30	-	-
10.5	0.5	67	74	-	57	61	-	-	82	75	-	45	49	-	-	-	55	-	35	-	-
12.6	0.6	110	94	-	74	70	-	-	84	81	-	65	69	-	-	-	63	-	42	-	-
16.8	0.8	125	116	-	89	98	-	-	104	106	-	90	86	-	-	-	86	-	77	-	-
21.0	1.0	227	192	-	105	110	-	-	494	501	-	166	166	-	-	-	185	-	109	-	-

Table C.16

Crack Readings at Positive Section

Main Bars = 2#5 % Steel Fibers = 0.8 f_c' = 4805 psi

All readings are in 10^{-4} inches

Load (Kips)	P/P_u Ratio	Interval																			
		1	2	3	4	5	6	7	8	9	10	11	12	13	14	15	16	17	18	19	20
0.0	0.00	0	0	0	0	0	0	0	0	0	0	0	0	0	-	-	-	-	-	-	-
2.1	0.10	0	1	5	12	7	2	1	0	0	-1	20	0	0	-	-	-	-	-	-	-
4.2	0.20	31	25	20	30	12	18	12	5	15	-	30	35	1	-	-	-	-	-	-	-
6.3	0.29	35	29	30	41	32	30	21	12	19	-	38	42	-	-	-	-	-	-	-	-
8.4	0.38	42	35	36	48	38	36	25	18	25	-	42	45	-	-	-	-	-	-	-	-
10.5	0.42	80	85	80	66	74	72	70	75	76	-	124	94	-	-	-	-	-	-	-	-
12.6	0.57	142	129	128	-	141	83	79	85	110	-	134	105	-	-	-	-	-	-	-	-
16.8	0.76	140	132	135	-	141	-	-	89	122	-	184	169	-	-	-	-	-	-	-	-
22.0	1.00	135	130	180	-	148	-	-	169	138	-	189	232	-	-	-	-	-	-	-	-

Table C.17

Crack Readings at Positive Section

Main Bars = 2#5 % Steel Fibers = 1.2 f_c' = 4927 psi

All readings are in 10^{-4} inches

Load (Kips)	P/P_u Ratio	Interval																			
		1	2	3	4	5	6	7	8	9	10	11	12	13	14	15	16	17	18	19	20
0.0	0.00	0	0	0	0	0	0	0	0	0	0	0	0	0	0	0	0	0	0	-	-
2.1	0.10	1	10	2	2	0	0	11	5	7	1	12	1	39	50	1	4	5	2	-	-
4.2	0.20	0	17	12	9	10	0	28	28	10	1	13	0	48	55	1	4	3	10	-	-
6.3	0.29	-	15	15	15	5	1	33	35	2	4	23	5	48	60	8	11	-	-	-	-
8.4	0.38	-	19	30	23	-	1	53	55	-	4	33	20	61	67	9	33	-	-	-	-
10.5	0.42	-	46	53	40	-	4	66	67	-	5	56	48	72	85	-	50	-	-	-	-
12.6	0.57	-	54	70	63	-	22	83	110	-	7	73	64	83	95	-	55	-	-	-	-
16.8	0.76	-	68	78	77	-	209	232	111	-	148	143	165	83	96	-	60	-	-	-	-
22.0	1.00	-	127	134	140	-	244	296	-	-	234	248	198	118	-	19	65	-	-	-	-

Table C.18

Crack Readings at Positive Section

Main Bars = 2#6 and 2#3 % Steel Fibers = 0.8 f_c' = 5100 psi

All readings are in 10^{-4} inches

Load (Kips)	P/P_u Ratio	Interval																			
		1	2	3	4	5	6	7	8	9	10	11	12	13	14	15	16	17	18	19	20
0.0	0.00	0	0	0	0	0	0	0	0	0	0	0	0	0	-	-	-	-	-	-	-
4.2	0.12	10	4	1	9	16	0	17	1	0	12	0	1	0	-	-	-	-	-	-	-
8.4	0.24	1	2	-	19	25	-	47	-	-	31	-	-	-	-	-	-	-	-	-	-
12.6	0.36	-	72	-	-	47	-	67	-	-	-	-	-	-	-	-	-	-	-	-	-
16.8	0.48	-	-	-	60	71	-	98	-	-	-	-	-	-	-	-	-	-	-	-	-
21.0	0.60	-	-	-	100	161	-	194	-	-	166	-	-	-	-	-	-	-	-	-	-
24.0	0.68	-	-	-	-	-	-	-	-	-	-	-	-	-	-	-	-	-	-	-	-

APPENDIX D

Table D.1

Statistical Analysis for Modulus of Elasticity

STEP 1 VARIABLE X1 ENTERED R SQUARE = 0.84813230 C(P) = 2.00000000

	DF	SUM OF SQUARES	MEAN SQUARE	F	PROB>F
REGRESSION	1	0.09957073	0.09957073	27.92	0.0032
ERROR	5	0.01782927	0.00356585		
TOTAL	6	0.11740000			

	B VALUE	STD ERROR	TYPE II SS	F	PROB>F
INTERCEPT	1.00170732				
X1	-0.23048780	0.04361781	0.09957073	27.92	0.0032

THE ABOVE MODEL IS THE BEST 1 VARIABLE MODEL FOUND.

Table D.2

Statistical Analysis for Split Cylinder Strength

STEP 1 VARIABLE X1 ENTERED R SQUARE = 0.99595262 C(P) = 2.00000000

	DF	SUM OF SQUARES	MEAN SQUARE	F	PROB>F
REGRESSION	1	3.88268810	3.88268810	246.07	0.0405
ERROR	1	0.01577857	0.01577857		
TOTAL	2	3.89846667			

	B VALUE	STD ERROR	TYPE II SS	F	PROB>F
INTERCEPT	6.66642857				
X1	2.28035714	0.14536855	3.88268810	246.07	0.0405

THE ABOVE MODEL IS THE BEST 1 VARIABLE MODEL FOUND.

Table D.3

Statistical Analysis for First Modulus of Rupture

STEP 1 VARIABLE X1 ENTERED R SQUARE = 0.99066582 C(P) = 2.00000000

	DF	SUM OF SQUARES	MEAN SQUARE	F	PROB>F
REGRESSION	1	7.32161481	7.32161481	212.27	0.0047
ERROR	2	0.06898519	0.03449259		
TOTAL	3	7.39060000			

	B VALUE	STD ERROR	TYPE II SS	F	PROB>F
INTERCEPT	7.56814815				
X1	2.60370370	0.17871090	7.32161481	212.27	0.0047

THE ABOVE MODEL IS THE BEST 1 VARIABLE MODEL FOUND.

Table D.4

Statistical Analysis for Ultimate Modulus of Rupture

STEP 1 VARIABLE X1 ENTERED R SQUARE = 0.99628002 C(P) = 2.00000000

	DF	SUM OF SQUARES	MEAN SQUARE	F	PROB>F
REGRESSION	1	20.42760093	20.42760093	535.64	0.0019
ERROR	2	0.07627407	0.03813704		
TOTAL	3	20.50387500			

	B VALUE	STD ERROR	TYPE II SS	F	PROB>F
INTERCEPT	7.55296296				
X1	4.34907407	0.18791506	20.42760093	535.64	0.0019

THE ABOVE MODEL IS THE BEST 1 VARIABLE MODEL FOUND.

Table D.5

Statistical Analysis of Plastic Hinge Length

STEP 1 VARIABLE X3 ENTERED R SQUARE = 0.59970051 C(P) = 5.37914547

	DF	SUM OF SQUARES	MEAN SQUARE	F	PROB>F
REGRESSION	1	0.07541234	0.07541234	8.99	0.0241
ERROR	6	0.05033766	0.00838961		
TOTAL	7	0.12575000			

	B VALUE	STD ERROR	TYPE II SS	F	PROB>F
INTERCEPT	1.06577189				
X3	0.12710659	0.04239530	0.07541234	8.99	0.0241

THE ABOVE MODEL IS THE BEST 1 VARIABLE MODEL FOUND.

STEP 2 VARIABLE X2 ENTERED R SQUARE = 0.67742119 C(P) = 5.55812500

	DF	SUM OF SQUARES	MEAN SQUARE	F	PROB>F
REGRESSION	2	0.08518571	0.04259286	5.25	0.0591
ERROR	5	0.04056429	0.00811286		
TOTAL	7	0.12575000			

	B VALUE	STD ERROR	TYPE II SS	F	PROB>F
INTERCEPT	1.09067194				
X2	-0.12378638	0.11278140	0.00977338	1.20	0.3224
X3	0.19198408	0.07233275	0.05715238	7.04	0.0452

THE ABOVE MODEL IS THE BEST 2 VARIABLE MODEL FOUND.

STEP 3 VARIABLE X1 ENTERED R SQUARE = 0.82928104 C(P) = 4.00000000

	DF	SUM OF SQUARES	MEAN SQUARE	F	PROB>F
REGRESSION	3	0.10428209	0.03476070	6.48	0.0514
ERROR	4	0.02146791	0.00536698		
TOTAL	7	0.12575000			

	B VALUE	STD ERROR	TYPE II SS	F	PROB>F
INTERCEPT	1.28430570				
X1	-0.15403007	0.08165728	0.01909638	3.56	0.1323
X2	-0.31031843	0.13488274	0.02840744	5.29	0.0829
X3	0.34014234	0.09813469	0.06447718	12.01	0.0257

Table D.6

Statistical Analysis of Curvature Distribution Factor

STEP 1 VARIABLE X1 ENTERED R SQUARE = 0.91563967 C(P) = 2.00000000

	DF	SUM OF SQUARES	MEAN SQUARE	F	PROB>F
REGRESSION	1	0.05200833	0.05200833	65.12	0.0002
ERROR	6	0.00479167	0.00079861		
TOTAL	7	0.05680000			

	B VALUE	STD ERROR	TYPE II SS	F	PROB>F
INTERCEPT	0.55875000				
X1	-0.16458333	0.02039469	0.05200833	65.12	0.0002

THE ABOVE MODEL IS THE BEST 1 VARIABLE MODEL FOUND.

Table D.7

Statistical Analysis for Plastic Rotation Coefficient

STEP 1 VARIABLE X4 ENTERED R SQUARE = 0.96666899 C(P) = 0.11950736

	DF	SUM OF SQUARES	MEAN SQUARE	F	PROB>F
REGRESSION	1	144.27804098	144.27804098	174.01	0.0001
ERROR	6	4.97474652	0.82912442		
TOTAL	7	149.25278750			

	B VALUE	STD ERROR	TYPE II SS	F	PROB>F
INTERCEPT	1.91536099				
X4	5.55964390	0.42146034	144.27804098	174.01	0.0001

THE ABOVE MODEL IS THE BEST 1 VARIABLE MODEL FOUND.

STEP 2 VARIABLE X2 ENTERED R SQUARE = 0.97940004 C(P) = 0.54602782

	DF	SUM OF SQUARES	MEAN SQUARE	F	PROB>F
REGRESSION	2	146.17818612	73.08909306	118.86	0.0001
ERROR	5	3.07460138	0.61492028		
TOTAL	7	149.25278750			

	B VALUE	STD ERROR	TYPE II SS	F	PROB>F
INTERCEPT	1.56816759				
X2	1.72601264	0.98188357	1.90014514	3.09	0.1391
X4	4.65502605	0.62973447	33.60068404	54.64	0.0007

THE ABOVE MODEL IS THE BEST 2 VARIABLE MODEL FOUND.

STEP 3 VARIABLE X3 ENTERED R SQUARE = 0.98310765 C(P) = 2.08779074

	DF	SUM OF SQUARES	MEAN SQUARE	F	PROB>F
REGRESSION	3	146.73155648	48.91051883	77.60	0.0005
ERROR	4	2.52123102	0.63030775		
TOTAL	7	149.25278750			

	B VALUE	STD ERROR	TYPE II SS	F	PROB>F
INTERCEPT	4.30299287				
X2	2.24195066	1.13640760	2.45321996	3.89	0.1198
X3	-0.04309509	0.04599347	0.55337036	0.88	0.4018
X4	4.16554868	0.82424996	16.09827001	25.54	0.0072

THE ABOVE MODEL IS THE BEST 3 VARIABLE MODEL FOUND.

Table D.7 (Continued)

Statistical Analysis for Plastic Rotation Coefficient

STEP 4 VARIABLE X6 ENTERED R SQUARE = 0.98368335 C(P) = 4.01663718

	DF	SUM OF SQUARES	MEAN SQUARE	F	PROB>F
REGRESSION	4	146.81748204	36.70437051	45.22	0.0052
ERROR	3	2.43530546	0.81176849		
TOTAL	7	149.25278750			

	B VALUE	STD ERROR	TYPE II SS	F	PROB>F
INTERCEPT	3.57301911				
X2	2.58726925	1.67025772	1.94781840	2.40	0.2191
X3	-0.03981012	0.05316346	0.45519004	0.56	0.5083
X4	3.91723539	1.20726844	8.54641219	10.53	0.0477
X6	0.00678210	0.02084582	0.08592556	0.11	0.7663

THE ABOVE MODEL IS THE BEST 4 VARIABLE MODEL FOUND.

STEP 5 VARIABLE X5 ENTERED R SQUARE = 0.98381796 C(P) = 6.00000000

	DF	SUM OF SQUARES	MEAN SQUARE	F	PROB>F
REGRESSION	5	146.83757321	29.36751464	24.32	0.0400
ERROR	2	2.41521429	1.20760714		
TOTAL	7	149.25278750			

	B VALUE	STD ERROR	TYPE II SS	F	PROB>F
INTERCEPT	2.93612886				
X2	4.46694468	14.71450547	0.11128983	0.09	0.7901
X3	-0.03213270	0.08801926	0.16094030	0.13	0.7501
X4	3.62476469	2.70363705	2.17064366	1.80	0.3120
X5	-0.02468887	0.19140860	0.02009117	0.02	0.9092
X6	0.00890808	0.03030038	0.10437525	0.09	0.7965

THE ABOVE MODEL IS THE BEST 5 VARIABLE MODEL FOUND.

NO FURTHER IMPROVEMENT IN R-SQUARE IS POSSIBLE.

The three variable model was chosen because it has the most realistic parameters included (ρ_s, ρ, f_y), since all of these have an effect on the rotation capacity.

Table D.8

Statistical Analysis for Ductility Index

STEP 1 VARIABLE X1 ENTERED R SQUARE = 0.52403538 C(P) = 2.00000000

	DF	SUM OF SQUARES	MEAN SQUARE	F	PROB>F
REGRESSION	1	28.06020833	28.06020833	6.61	0.0423
ERROR	6	25.48619167	4.24769861		
TOTAL	7	53.54640000			

	B VALUE	STD ERROR	TYPE II SS	F	PROB>F
INTERCEPT	0.98125000				
X1	3.82291667	1.48739471	28.06020833	6.61	0.0423

THE ABOVE MODEL IS THE BEST 1 VARIABLE MODEL FOUND.

Table D.9

Statistical Analysis for Cracking Moment

STEP 1 VARIABLE X1 ENTERED R SQUARE = 0.99906442 C(P) = 2.00000000

	DF	SUM OF SQUARES	MEAN SQUARE	F	PROB>F
REGRESSION	1	0.19068810	0.19068810	1067.85	0.0195
ERROR	1	0.00017857	0.00017857		
TOTAL	2	0.19086667			

	B VALUE	STD ERROR	TYPE II SS	F	PROB>F
INTERCEPT	0.99642857				
X1	0.50535714	0.01546474	0.19068810	1067.85	0.0195

THE ABOVE MODEL IS THE BEST 1 VARIABLE MODEL FOUND.

Table D.10

Statistical Analysis for Cracked Moment of Inertia

STEP 1 VARIABLE X1 ENTERED R SQUARE = 0.82404268 C(P) = 2.00000000

	DF	SUM OF SQUARES	MEAN SQUARE	F	PROB>F
REGRESSION	1	0.04609603	0.04609603	32.78	0.0007
ERROR	7	0.00984286	0.00140612		
TOTAL	8	0.05593889			

	B VALUE	STD ERROR	TYPE II SS	F	PROB>F
INTERCEPT	0.98547619				
X1	0.14345238	0.02505461	0.04609603	32.78	0.0007

THE ABOVE MODEL IS THE BEST 1 VARIABLE MODEL FOUND.

Table D.11

Statistical Analysis for Crack Width Estimation

STEP 1 VARIABLE X2 ENTERED R SQUARE = 0.90033626 C(P) = 1.46322755

	DF	SUM OF SQUARES	MEAN SQUARE	F	PROB>F
REGRESSION	1	0.39270417	0.39270417	126.47	0.0001
ERROR	14	0.04347083	0.00310506		
TOTAL	15	0.43617500			

	B VALUE	STD ERROR	TYPE II SS	F	PROB>F
INTERCEPT	1.00562500				
X2	-0.31979167	0.02843606	0.39270417	126.47	0.0001

THE ABOVE MODEL IS THE BEST 1 VARIABLE MODEL FOUND.

STEP 2 VARIABLE X1 ENTERED R SQUARE = 0.91100305 C(P) = 2.02228788

	DF	SUM OF SQUARES	MEAN SQUARE	F	PROB>F
REGRESSION	2	0.39735675	0.19867838	66.54	0.0001
ERROR	13	0.03881825	0.00298602		
TOTAL	15	0.43617500			

	B VALUE	STD ERROR	TYPE II SS	F	PROB>F
INTERCEPT	0.96521734				
X1	0.03222944	0.02581973	0.00465259	1.56	0.2340
X2	-0.32026168	0.02788819	0.39378757	131.88	0.0001

THE ABOVE MODEL IS THE BEST 2 VARIABLE MODEL FOUND.

STEP 3 VARIABLE X3 ENTERED R SQUARE = 0.91116804 C(P) = 4.00000000

	DF	SUM OF SQUARES	MEAN SQUARE	F	PROB>F
REGRESSION	3	0.39742872	0.13247624	41.03	0.0001
ERROR	12	0.03874628	0.00322886		
TOTAL	15	0.43617500			

	B VALUE	STD ERROR	TYPE II SS	F	PROB>F
INTERCEPT	0.97195477				
X1	0.02687805	0.04478571	0.00116296	0.36	0.5596
X2	-0.33042193	0.07397771	0.06441466	19.95	0.0008
X3	0.00803529	0.05382290	0.00007196	0.02	0.8838

THE ABOVE MODEL IS THE BEST 3 VARIABLE MODEL FOUND.

The one variable model is chosen because R square for two or three variable model is not significantly higher than that of one variable model.

APPENDIX E

Table E.1

Calibration of Ram vs. Testing Machine

Observation	Ram Pressure (psi)	Average Machine Load Jack (1) (lbs)	Average Machine Load Jack (2)	% error
1	0	0	0	0
2	100	1,018	990	%2.80
3	200	2,044	1,925	%6.10
4	300	3,034	3,070	%1.18
5	400	3,956	3,924	%0.80
6	500	4,972	5,097	%2.50
7	600	6,016	6,092	%1.20
8	700	7,054	7,150	%1.35
9	800	8,128	8,139	%0.13
10	900	9,160	9,130	%0.32
11	1000	10,230	10,278	%0.47
12	1100	11,290	11,230	%0.53
13	1200	12,420	12,330	%0.73
14	1300	13,430	13,300	%0.97
15	1400	14,480	14,383	%0.67
16	1500	15,530	15,483	%0.30
17	1600	16,630	16,470	%0.97
18	1700	17,720	17,500	%1.25
19	1800	18,860	18,673	%1.00
20	1900	19,940	19,675	%1.34
21	2000	20,810	20,708	%0.49
22	2500	25,920	25,678	%0.94
23	3000	31,280	31,000	%0.90
24	3500	36,800	36,290	%1.40
25	4000	42,280	41,480	%1.92
26	4500	47,446	46,773	%1.43
27	5000	52,700	52,130	%1.09

Figure E.1

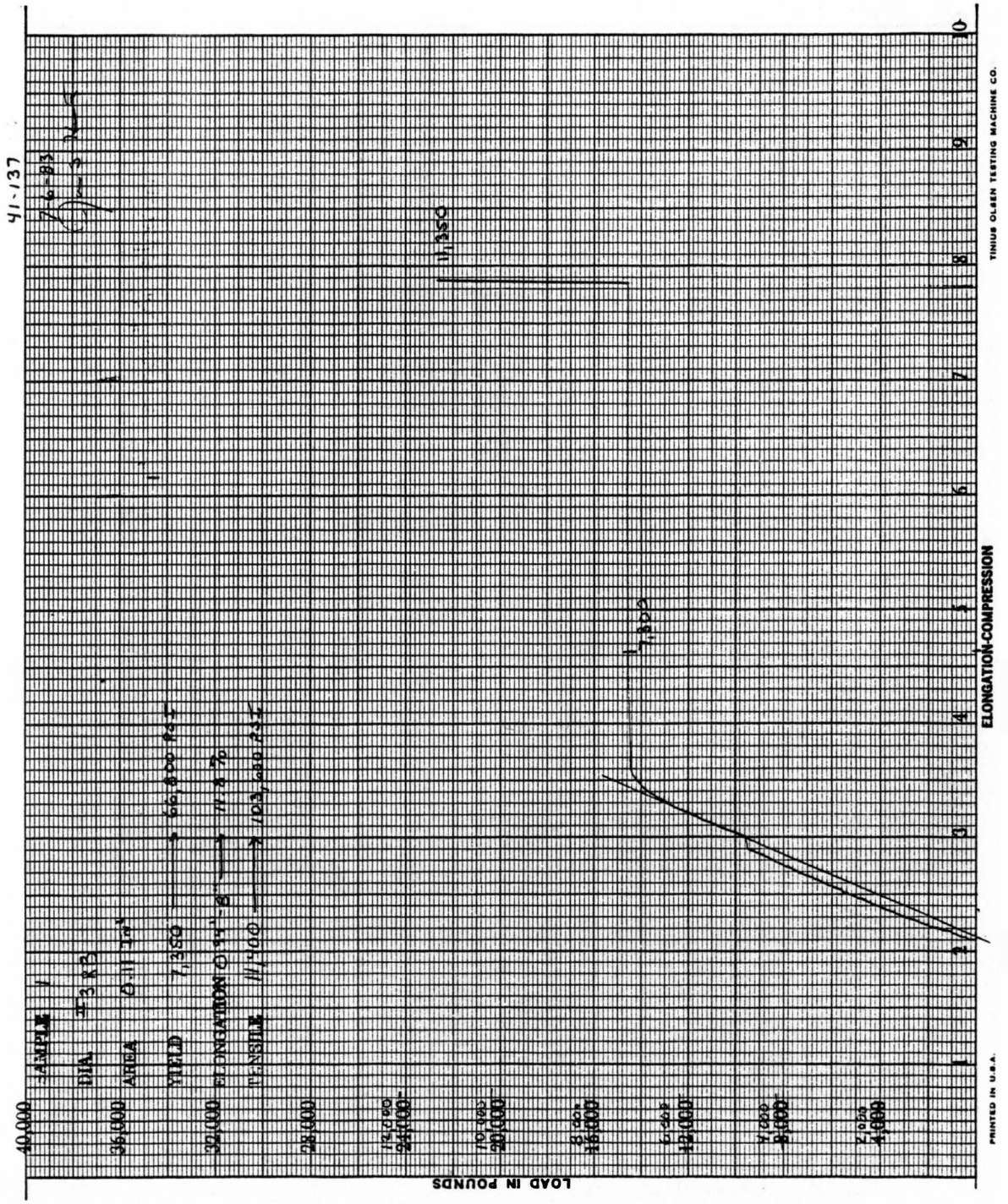
41-137
7-6-83
SAMPLE
DIA. .353
AREA .0117 in²
YIELD 7,350 → 66,000 PSI
ELONGATION @ 34"-8 → 11 %
TENSILE 11,700 → 103,000 PSI
11,350
7,300
LOAD IN POUNDS
40,000
36,000
32,000
28,000
24,000
20,000
16,000
12,000
8,000
4,000
ELONGATION-COMPRESSION
TINIUS OLSEN TESTING MACHINE CO.
PRINTED IN U.S.A.

Figure E.2

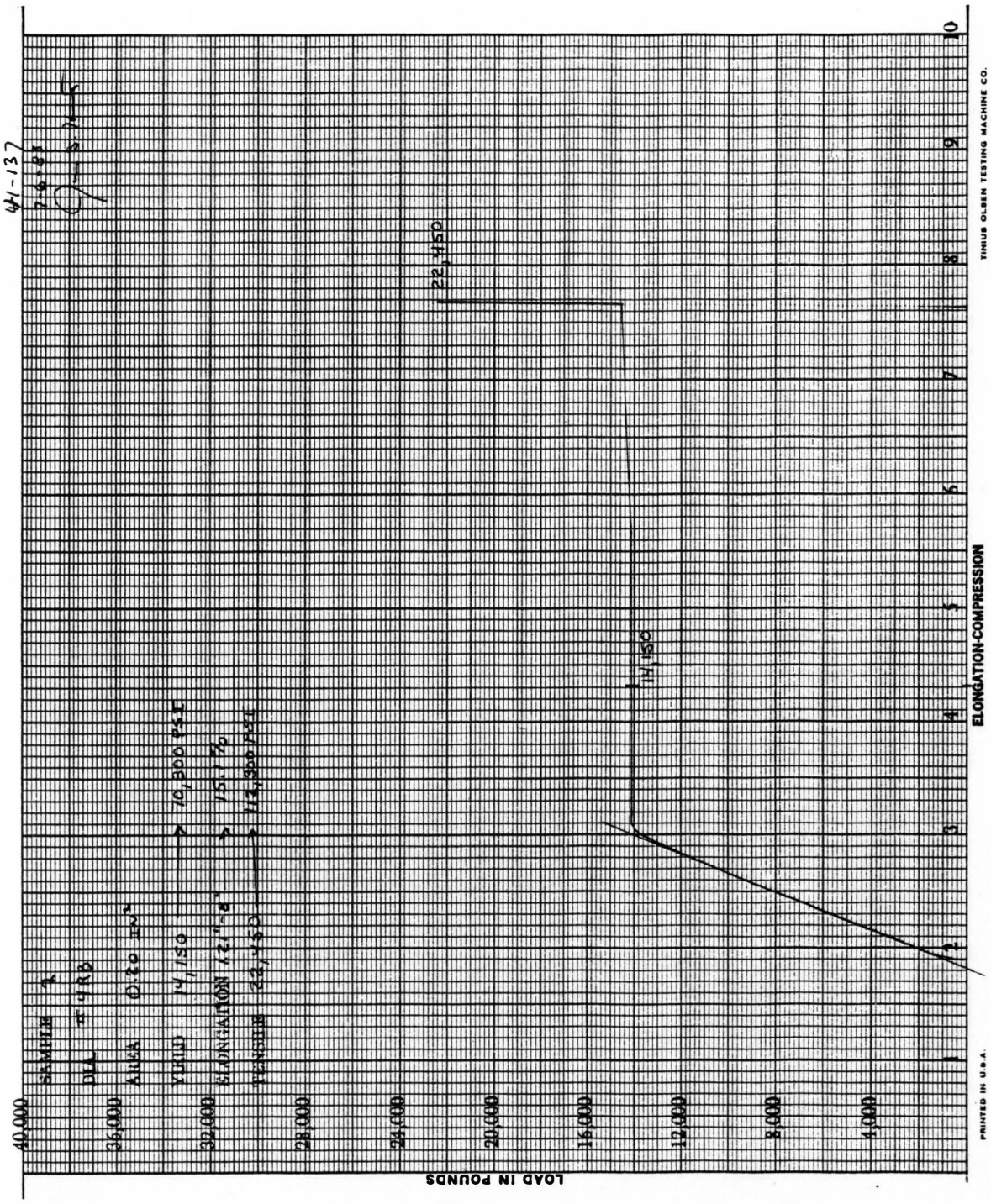
LOAD IN POUNDS
40,000
36,000
32,000
28,000
24,000
20,000
16,000
12,000
8,000
4,000
1
2
3
4
5
6
7
8
9
10
22,450
14,150
ELONGATION-COMPRESSION
TINIUS OLSEN TESTING MACHINE CO.
PRINTED IN U.S.A.

Figure E.3

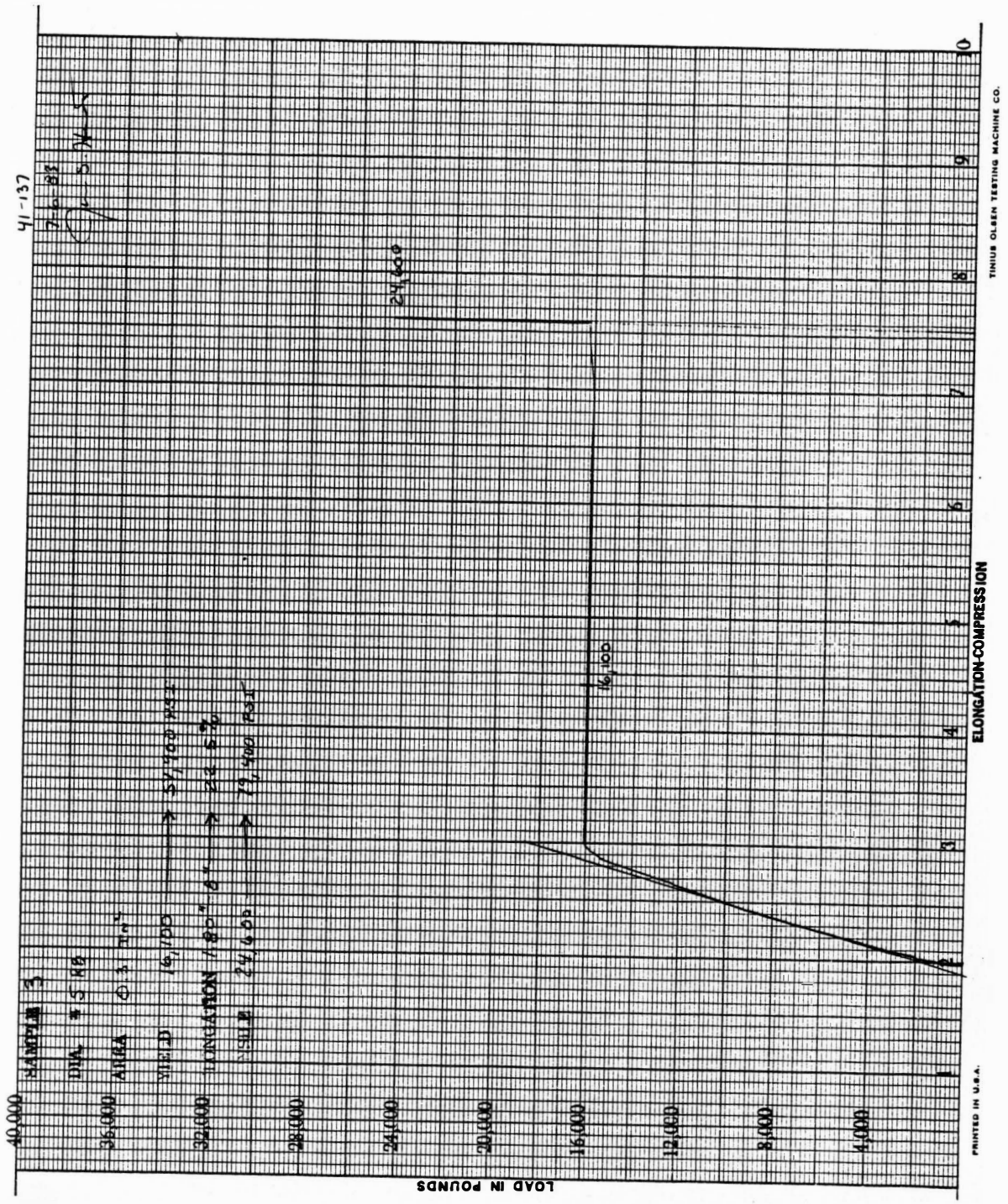
41-137
7-6-88
SAMPLE #3
DIA. #5 RB
AREA Φ .3 π=
YIELD 16,100 → 37,100 PSI
ELONGATION .180" Δ" → 23.5%
RSLT 24,600 → 79,400 PSI
24,600
16,100
40,000
36,000
32,000
28,000
24,000
20,000
16,000
12,000
8,000
4,000
LOAD IN POUNDS
ELONGATION-COMPRESSION
TINIUS OLSEN TESTING MACHINE CO.
PRINTED IN U.S.A.